ADSORPTION AND MASS TRANSFER IN SOLID CATALYSTS AND ADSORBENTS

A THESIS
SUBMITTED TO THE
UNIVERSITY OF POONA
FOR THE DEGREE OF
DOCTOR OF PHILOSOPHY
(IN CHEMISTRY)

BY
S. MAYADEVI
M. Tech.

CHEMICAL ENGINEERING DIVISION
NATIONAL CHEMICAL LABORATORY
PUNE-411 008 (INDIA)

AUGUST 1991

CONTENTS

ABSTRACT

ABSTRACT

Many industrial processes, including catalytic processes and adsorption separation processes, involve gas-solid contacting. An understanding of the adsorption and mass transport between the fluid and solid particles is essential for the design and analysis of such processes.

The investigation for the PhD thesis was undertaken with the following objectives.

1. To study the influence of coke deposition on inter-crystalline mass transfer and catalytic properties of Pt.H-ZSM-5. Al_2O_3 catalyst.
2. To study the sorption of CO_2, CH_4, C_2H_6, C_2H_4 and H_2O in medium and large pore zeolites.
3. To study the adsorption of O_2 and N_2 on $AlPO_4$-5 and SAPO-5 at moderate pressures.
4. To study the effective intraparticle mass transfer of O_2, CO_2, CH_4 and C_2H_4 in macroporous low surface area inert spherical support.
5. To study the step-wise thermal desorption of CO_2 on synthetic zeolites.

The thesis has been divided into six chapters.

Chapter 1 Summary and Conclusions

The first chapter gives a brief introduction to the thesis. This chapter also discusses the objectives, scope and the summary and conclusions of the present work.

Chapter 2 The influence of coke deposition on intercrystalline mass transfer and catalytic properties of Pt.H-ZSM-5.Al_2O_3 catalyst

Three batches of coked Pt.H-ZSM-5.Al_2O_3 catalysts with different extents of coke deposition were prepared by carrying out cumene crackig reaction over it at 673K for different periods of time. A comparative study has been conducted on these coked catalysts and fresh Pt.H-ZSM-5.Al_2O_3 to find out the influence of coke deposition on the inter-crystalline mass transfer and catalytic properties. The catalysts were analyzed for their carbon content and characterized for their surface area and porosity. Thermogravimetric analysis and spectroscopic analyses by XPS and NMR were also carried out on the catalyst samples as an effort to characterize the nature of the coke. The acidity distribution in the catalyst samples were determined by the step-wise thermal desorption of pyridine from 353 to 673K. The effect of coking on the heat of sorption and the effective inter-crystalline diffusivity under reaction condions of the catalyst samples was determined by gc pulse technique using iso-octane (which does not penetrate the zeolite channels) as probe molecule and compared with the effect due to pyridine poisoning. The influence of coking on the catalytic activity and product selectivity in o-xylene isomerization, iso-octane cracking and methanol-to-aromatics conversion reactions was investigated by carrying out these reactions on the fresh and coked catalysts in a pulse micro reactor.

Chapter 3 Sorption of Methane, Ethane, Ethylene, Carbon Dioxide and Water in Medium and Large Pore Zeolites

In this chapter, X, Y, L, mordenite, ZSM-5 and ZSM-8 type zeolites, their various cation exchanged forms, silicalite, $AlPO_4$-5 and SAPO-5 have been evaluated for their sorption of CH_4, C_2H_6, C_2H_4, CO_2 and H_2O. The initial heat of sorption and the adsorption equilibrium constant of the hydrocarbons, CO_2 and H_2O on these adsorbents in the temperature range 313 to 523K have been determined by the gc pulse technique.

A novel gravimetric method has been developed for measuring adsorption isotherms at low pressures (0-200 kPa) and isotherm data for the above adsorbates on selected adsorbents in the temperature range 305-353K were collected by the above method. The isosteric heat of sorption at different surface coverages has been obtained from the adsorption isotherms by means of the Clausius-Clapeyron equation. Standard models with increasing complexity have been tried for fitting the isotherm data. Parameter values for simpler models like Langmuir, Freundlich and Dubinin-Polanyi were estimated by linear regression analysis using a programmable calculator. Marquardt's method for multivariable non-linear regression has been used for parameter estimation of more complex models and was carried out on an IBM PC-XT. The model selection has been made based on the regression coefficient, percentage deviation of the quantity adsorbed and also on the simplicity of the model.

Chapter 4 Adsorption of Oxygen and Nitrogen on $AlPO_4$-5 and SAPO-5 at Moderate Pressure Using a Simple Volumetric Adsorption/Desorption Apparatus

The adsorption isotherms of oxygen and nitrogen on $AlPO_4$-5 and SAPO-5 at 309-329K and 500-3000 kPa have been collected volumetrically by adsorbing the gas on the adsorbent at the required pressure and measuring the quantity of the desorbed gas. Two new, simple methods have been developed for the measurement of adsorption isotherms at moderate pressures. In the first method, the adsorbed gases were desorbed to a constant volume pre-evacuated desorber and the amount of gas desorbed was calculated from the increase in pressure of the desorber. In the second method, the volume of the desorbed gas at atmospheric pressure was determined from the quantity of water displaced, using a constant pressure gas collector. The reliability of the method was tested by collecting data on the adsorption of nitrogen and oxygen on sodium mordenite and comparing with published results.

Sips' equation was found to give the best fit for the adsorption data of oxygen and nitrogen on both $AlPO_4$-5 and SAPO-5. The model parameters of the Sips' isotherm have been estimated by the Marquardt's method for multivariable non-linear regression.

Chapter 5 Intraparticle Mass Transfer of O_2, CO_2, CH_4 and C_2H_4 in Macroporous Low Surface Area Inert Spherical Support

In this chapter, the effective diffusivity and tortuosity factors of commercial spherical macroporous silicon carbide pellets (pore dia. 12-370 μm) for the diffusion of

ethylene (N_2), methane (N_2), carbon dioxide (N_2) and oxygen (He) at 423-573K have been determined by gc pulse technique using a single pellet string column (the carrier gas used is given in brackets). The chromatographic data collected has been analyzed by the method of moments. GC pulse experiments conducted for detecting the occurrence of adsorption indicated that there was no irreversible or reversible adsorption of any of the diffusing species on the silicon carbide pellets at 423-573K. Hence the equations applicable for an inert porous solid or a non-adsorbing sample have been used for the evaluation of the mass transfer parameters.

Chapter 6 Step-wise Thermal Desorption of Carbon Dioxide on Synthetic Zeolites

This chapter discusses the chemisorption of CO_2 and STD of CO_2 have been carried out on a large number of synthetic zeolites (viz. Na-H-ZSM-8, H-ZSM-8, MgO.H-ZSM-8, H-Na-ZSM-5, NaM, HM, NaY, CeNaY (Ce^{+3} exchange 33%), CeNaY (Ce^{+3}exchange 72%), deammoniated NH_4Y, NaX, KL, HKL, silicalite, $AlPO_4$-5 and SAPO-5) for evaluating the basicity and base strength distribution on the zeolites and also to know the regenerability of the zeolite, if used in the adsorptive separation of gases containing carbon dioxide. The step-wise thermal desorption of carbon dioxide on the zeolites have been carried out by saturating the zeolite with pure carbon dioxide gas at 323K and desorbing it from 323 to 1173K in a number of temperature steps. During each step, the carbon dioxide desorbed was adsorbed in a

solution of barium hydroxide and measured quantitatively by gravimetric estimation of the barium carbonate formed.

A comparative study has been made on the temperature dependence of chemisorption and the step-wise thermal desorption of carbon dioxide on the various synthetic zeolites.

CHAPTER - 1

SUMMARY AND CONCLUSIONS

1 SUMMARY AND CONCLUSIONS

1.1 INTRODUCTION

Many industrial processes, including catalytic processes and adsorption separation processes, involve gas-solid contacting. An understanding of the adsorption and mass transport between the fluid and solid particles is essential for the design and analysis of such processes.

Low surface area macroporous inert supports are commonly used as catalyst supports for a number of hydrocarbon conversion reactions. Effective diffusion coefficients are usually used for characterization of diffusional mass transport inside porous catalysts and adsorbents. The knowledge of effective intraparticle diffusivities of reactants and products in porous catalysts is essential for predicting the effects of intraparticle mass transfer on the reaction rate, and also in the design of catalytic reactors. A knowledge of mass transfer rates at ambient conditions is seldom required, and it is desirable to measure the effective diffusivity under actual reaction conditions or atleast at temperatures at which the catalytic process occurs.

Zeolites are materials which have great industrial potential due to their capacities to sorb gases, vapors and liquids, to catalyze reactions and to act as cation exchangers. They find industrial application in a number of hydrocarbon conversion reactions and as adsorbents and ion exchangers in

many separation/purification processes.

The information on catalyst deactivation due to the accumulation of adsorbed fouling material like coke or carbonaceous matter on the catalyst surface is of commercial importance, since the deactivation of catalyst governs, in many ways, the economic design and operation of catalytic reactors. Because of its importance, the fouling of catalyst pellets has been widely investigated, both experimentally and theoretically. Most of these studies have been on the factors affecting deactivation/coking and regeneration of catalysts, on the characterization of the coke deposits and on the deactivation kinetics. Influence of coking on intraparticle mass transfer and catalytic properties, particularly for zeolite catalysts has not been thoroughly investigated so far.

With the escalation of energy prices and demand for cleaner environment, adsorption separation and purification processes are becoming increasingly viable economically and gaining more and more importance for the separation of closely boiling liquids, azeotropes and gases. The search for a suitable adsorbent is generally the first step in the development of an adsorption separation process. It is often necessary to screen a range of possible adsorbents and the information about heat of sorption and the equilibrium sorption capacity at various temperatures and pressures are required for this preliminary screening.

Zeolites have extensive commercial application in a large number of purification and separation processes. There is a large amount of data available in literature on the sorption

of hydrocarbons in zeolites. However, the data for the adsorption of methane, ethane, ethylene and carbon dioxide are available only for selected zeolites. More over, from the data available, it is not possible to make a direct comparison of the zeolites for their sorption properties for these gases. The sorption of the light hydrocarbon gases and carbon dioxide are of special interest as they form the product of the newly emerging process of direct methane conversion to higher hydrocarbons. The sorption properties of zeolites for light hydrocarbon gases are also of interest from the point of separation of natural gas components.

1.2 OBJECTIVES

Taking into consideration the above aspects, the investigation for the PhD thesis was undertaken with the following objectives.

1. To study the influence of coke deposition on inter-crystalline mass transfer and catalytic properties of Pt.H-ZSM-5. Al_2O_3 catalyst.
2. To study the sorption of CO_2, CH_4, C_2H_6, C_2H_4 and H_2O in medium and large pore zeolites.
3. To study the adsorption of O_2 and N_2 on $AlPO_4$-5 and SAPO-5 at moderate pressures.
4. To study the effective intraparticle mass transfer of O_2, CO_2, CH_4 and C_2H_4 in macroporous low surface area inert spherical support.
5. To study the step-wise thermal desorption of CO_2 on

synthetic zeolites.

1.3 SUMMARY AND CONCLUSIONS

The influence of coke deposition on inter-crystalline mass transfer and catalytic properties of Pt.H-ZSM-5.Al_2O_3 catalyst is studied in **Chapter 2**. Three batches of coked Pt.H-ZSM-5.Al_2O_3 catalysts with different extents of coke deposition were prepared by carrying out cumene crackig reaction over it at 673K for different periods of time. A comparative study has been conducted on these coked catalysts and fresh Pt.H-ZSM-5.Al_2O_3 to find out the influence of coke deposition on the inter-crystalline mass transfer and catalytic properties. The catalysts were analyzed for their carbon content and characterized for their surface area and porosity. Thermogravimetric analysis and spectroscopic analyses by XPS and NMR were also carried out on the catalyst samples as an effort to characterize the nature of the coke. The acidity distribution in the catalyst samples were determined by the step-wise thermal desorption of pyridine from 353 to 673K. The effect of coking on the heat of sorption and the effective inter-crystalline diffusivity under reaction condions of the catalyst samples was determined by gc pulse technique using iso-octane (which does not penetrate the zeolite channels) as probe molecule and compared with the effect due to pyridine poisoning. The influence of coking on the catalytic activity and product selectivity in o-xylene isomerization, iso-octane cracking and methanol-to-aromatics conversion reactions was investigated by carrying out these reactions on the fresh and coked catalysts in

a pulse micro reactor.

The following conclusions have been drawn from the investigations.

1. The poisoning of the Pt.H-ZSM-5.Al_2O_3 with pyridine (by its chemisorption at 523 K) causes a very significant decrease in the adsorption equilibrium constant and heat of adsorption of iso-octane, but a large increase in its effective diffusivity in the meso- and macro- pores of the catalyst.

2. The coke deposited on the catalyst is composed of condensed aromatics, methyl substituted aromatics and methyl substituted aliphatics. The ratio of aliphatic to aromatic coke increases with increase in the extent of coke deposition on the catalyst. The condensed aromatics are expected to be located in the meso- and macro- pores whereas methyl aromatics and aliphatics are expected to be located in the zeolite channels as strongly sorbed or occluded hydrocarbon species.

3. The acidity and acid strength distribution on the catalyst are strongly influenced due to the coke deposition. The strong acid sites (measured in terms of pyridine chemisorbed at 673 K) are decreased markedly whereas the weaker acid sites (measured in terms of pyridine chemisorbed at < 573 K) are increased due to the coke deposition; the increase in the weaker sites is larger for the larger coke deposition.

4. The coke deposition causes an increase in the adsorption equilibrium constant and heat of adsorption of iso-octane indicating creation of new sites in the meso- and macro-pores for adsorption of iso-octane due to the coking of the catalyst.

5. The effective intercrystalline diffusivity of iso-octane in the coked catalysts is decreased depending upon the extent of coke deposition.

6. The catalytic activity/selectivity in the iso-octane cracking, o-xylene isomerization and methanol-to-aromatics conversion reactions is strongly influenced by the coke deposition. When the extent of coke on the catalyst is increased, (i) the iso-octane cracking activity is decreased due to deactivation of intercrystalline strong acid sites, (ii) the xylene isomerization activity is initially increased (for lower coke deposition) and then decreased (for higher coke deposition) due to creation of new active sites on coke and the increased mass transfer resistance, and the p-selectivity is decreased because of the occurrence of part of the isomerization reaction on the newly created active sites on the intercrystalline coke and (iii) the extent of aromatization and p-selectivity in the methanol-to-aromatics conversion is decreased due to the deactivation of strong acid sites and the occurrence of xylene isomerization on the new active sites present on the intercrystalline coke respectively.

In **Chapter** 3, X, Y, L, mordenite, ZSM-5 and ZSM-8 type zeolites, their various cation exchanged forms, silicalite, $AlPO_4$-5 and SAPO-5 have been evaluated for their sorption of CH_4, C_2H_6, C_2H_4, CO_2 and H_2O. The initial heat of sorption and the adsorption equilibrium constant of the hydrocarbons, CO_2 and H_2O on these adsorbents in the temperature

range 313 to 523K have been determined by the gc pulse technique.

A novel gravimetric method has been developed for measuring adsorption isotherms at low pressures (0-200 kPa) and isotherm data for the above adsorbates on selected adsorbents in the temperature range 305-353K were collected by the above method. The isosteric heat of sorption at different surface coverages has been obtained from the adsorption isotherms by means of the Clausius-Clapeyron equation. Standard models with increasing complexity have been tried for fitting the isotherm data. Parameter values for simpler models like Langmuir, Freundlich and Dubinin-Polanyi were estimated by linear regression analysis using a programmable calculator. Marquardt's method for multivariable non-linear regression has been used for parameter estimation of more complex models and was carried out on an IBM PC-XT. The model selection has been made based on the regression coefficient, percentage deviation of the quantity adsorbed and also on the simplicity of the model.

In general, it has been observed that the Dubinin-Polanyi model gives a good fit for the sorption of methane, ethane and ethylene in most of the adsorbents studied. This is to be expected as the theory for this model is based on pore volume filling, which is the mechanism of sorption in zeolites and is considered to represent well the equilibrium adsorption of non-polar molecules on many adsorbents. Langmuir model fits the equilibrium sorption data of CO_2 on the adsorbents except $AlPO_4$-5 and SAPO-5. Langmuir model also gives a good fit for the

sorption isotherms of C_2H_4 on NaY, NaM, Silicalite and that of C_2H_6 on NaM. Freundlich model gives a reasonably good fit for the sorption of all the gases on silicalite except ethylene for which Langmuir is the best fitting model. Only Dubinin-Astakhov model represent well the adsorption of ethane on NaY and ethylene on NaX.

The heat of sorption at zero coverage is a measure of the sorbate-sorbent interaction and can be taken as indicative of the ease of regeneration of the adsorbent in terms of the energy input required for the adsorptive separation process. The comparison of the zeolites for the heat of sorption of the various sorbates, determined by the gc pulse technique reveals that $AlPO_4$-5 and silicalite have the lowest heat of sorption for almost all the sorbates. So, from the point of view of the cost of regeneration, $AlPO_4$-5 and silicalite can be considered as the most preferred adsorbents. The other possible choices with respect to lower heat of sorption are NaY, NaX and KL.

The relative thermodynamic equilibrium constants or the retention volume per unit volume of adsorbent (relative to methane) obtained from the gc pulse data may be taken as a rough measure of the separation factor (with respect to methane). A high value of the relative equilibrium constant is indicative of a high separation factor. At 303 K, all the sorbents are having a relative equilibrium constant value (with respect to methane) >> 1 which implies that a good separation of methane from the other sorbates is possible.

Among the adsorbents, NaM, NaY, NaX, Na-H-ZSM-8, CeNaY and KL are having the relative values of equilibrium constant

(at 303 K) very much greater than unity. However, acidic zeolites like HM, HKL, HY, CeNaY, H-ZSM-8, Na-H-ZSM-8, H-ZSM-5, H-Na-ZSM-5 are not suitable for use as adsorbents due to their reactivity towards ethylene and ethane and may be eliminated.

The data from the gc pulse method give the values of heat of sorption and sorption equilibrium constant at near zero coverage and hence can be taken only as indicative of the sorption behavior. The separation factor is dependent on temperature, pressure and also may be affected by the presence of other sorbates. For determining the true performance of these selected sorbents (viz. $AlPO_4$-5, SAPO-5, NaY, NaX, KL and NaM) detailed experimentation under actual conditions of operation are therefore required.

Chapter 4 presents the adsorption of oxygen and nitrogen on $AlPO_4$-5 and SAPO-5 at moderate pressures. The adsorption isotherms of oxygen and nitrogen on AlPO-5 and SAPO-5 at 309-329K and 500-3000 kPa have been collected volumetrically by adsorbing the gas on the adsorbent at the required pressure and measuring the quantity of the desorbed gas. Two new, simple methods have been developed for the measurement of adsorption isotherms at moderate pressures. In the first method, the adsorbed gases were desorbed to a constant volume pre-evacuated desorber and the amount of gas desorbed was calculated from the increase in pressure of the desorber. In the second method, the volume of the desorbed gas at atmospheric pressure was determined from the quantity of water displaced, using a constant pressure gas collector. The reliability of the method

was tested by collecting data on the adsorption of nitrogen and oxygen on sodium mordenite and comparing with published results.

Sips' equation was found to give the best fit for the adsorption data of oxygen and nitrogen on both $AlPO_4$-5 and SAPO-5. The model parameters of the Sips' isotherm have been estimated by the Marquardt's method for multivariable non-linear regression.

Intraparticle mass transfer of O_2, CO_2, CH_4 and C_2H_4 in macroporous low surface area inert spherical support have been studied in **Chapter 5**. The effective diffusivity and tortuosity factors of commercial spherical macroporous silicon carbide pellets (pore dia. 12-370 μm) for the diffusion of ethylene (N_2), methane (N_2), carbon dioxide (N_2) and oxygen (He) at 423-573K have been determined by gc pulse technique using a single pellet string column (the carrier gas used is given in brackets). The chromatographic data collected has been analyzed by the method of moments. GC pulse experiments conducted for detecting the occurrence of adsorption indicated that there was no irreversible or reversible adsorption of any of the diffusing species on the silicon carbide pellets at 423-573K. Hence the equations applicable for an inert porous solid or a non-adsorbing sample have been used for the evaluation of the mass transfer parameters.

Under the experimental conditions, the pore diffusion mechanism was found to be in the bulk diffusion regime. The effective diffusivity of all the diffusing species showed a mild temperature dependence. The internal tortuosity factor of the silicon carbide pellets for all the diffusing species was found

to be much larger than the theoretical value of τ = 3. The average values of τ for the diffusion of methane(N_2), ethylene(N_2), carbon dioxide(N_2) and oxygen(He) were found to be 16.1, 13.3, 17.6 and 33.8 respectively. Commercial silicon carbide pellets are highly sintered material. The observed high value of tortuosity factor is due to the presence of dead end pores and pore constrictions in the sintered support material. The wide difference between the τ value of oxygen and that of the other gases may be attributed to the different carrier gases used for the gc pulse experiments and also to the presence of smaller diameter (<0.012 μm) pores (which are likely to be the pore constrictions formed during the sintering of the silicon carbide pellets) occupying about 6% of the total pore volume; these smaller diameter pores may contribute to the mass transfer in the pellets by Knudsen diffusion which has not been considered for the calculation of .

In **Chapter 6** the chemisorption of CO_2 and STD of CO_2 have been carried out on a large number of synthetic zeolites (viz. Na-H-ZSM-8, H-ZSM-8, MgO.H-ZSM-8, H-Na-ZSM-5, NaM, HM, NaY, CeNaY (Ce^{+3} exchange 33%), CeNaY (Ce^{+3}exchange 72%), deammoniated NH_4Y, NaX, KL, HKL, silicalite, $AlPO_4$-5 and SAPO-5) for evaluating the basicity and base strength distribution on the zeolites and also to know the regenerability of the zeolite, if used in the adsorptive separation of gases containing carbon dioxide. The step-wise thermal desorption of carbon dioxide on the zeolites have been carried out by saturating the zeolite with pure carbon dioxide gas at 323K and desorbing it from 323

to 1173K in a number of temperature steps. During each step, the carbon dioxide desorbed was adsorbed in a solution of barium hydroxide and measured quantitatively by gravimetric estimation of the barium carbonate formed.

A comparative study has been made on the temperature dependence of chemisorption and the step-wise thermal desorption of carbon dioxide on the various synthetic zeolites in different cation exchanged forms. The STD and chemisorption of CO_2 on zeolites show that the zeolites differ widely in their basicity. All the zeolites have broad base strength distribution and it is strongly influenced by Na or alkali metal content of the zeolite and also its Al content or the Si/Al ratio. In general, the alkali metal and cerium cation exchanged form of the zeolite have more number of basic sites (as given by CO_2 chemisorption) compared to their H-form. However, the concentration of the cation in the zeolite do not have one to one correspondence to the total basicity in the zeolites obtained from CO_2 chemisorption. For example, NaM, which gives the maximum CO_2 chemisorption is not the one that has the highest Al^{+3} or Na^{+} concentration. This clearly shows that not only the chemical environment, but also the structure plays a role in the basicity of the zeolite.

CHAPTER - 2

INFLUENCE OF COKE DEPOSITION ON INTERCRYSTALLINE MASS TRANSFER AND CATALYTIC PROPERTIES OF Pt.H–ZSM–5.Al_2O_3 CATALYST

2 INFLUENCE OF COKE DEPOSITION ON INTERCRYSTALLINE MASS TRANSFER AND CATALYTIC PROPERTIES OF Pt.H-ZSM-5.Al_2O_3 CATALYST

2.1 INTRODUCTION

ZSM-5 type zeolites have gained tremendous importance as commercial catalysts in methanol-to-hydrocarbon conversion processes [1-3] and also on a number of hydrocarbon alkylation and conversion processes for the manufacture of p-xylene, ethylbenzene, p-ethyltoluene, diethylbenzene etc. [3,4].

It is common practice that when zeolites are used as catalysts, particularly in packed bed reactors, these are used in the form of pellets or extrudates which consist of zeolite crystallites bounded by a binder. Though zeolite crystals are microporous, the pelletization or extrudation gives rise to intercrystalline pore system having larger pore diameter. These intercrystalline pores are commonly called as macropores. In commercial zeolite catalyst, in order to minimize intracrystalline mass transfer resistance, small size (< 1 μm) zeolite crystals are employed. The diffusivities of reactants and products for the intercrystalline mass transfer are very much higher than those for intracrystalline mass transfer but the diffusion path for intercrystalline mass transfer is very much longer [because of the larger particle or pellet size (> 1.5 mm) of the zeolite catalyst] than that for the intracrystalline mass transfer. Therefore, the intercrystalline mass transfer resistance cannot be neglected and it is obviously necessary to know the relative importance of the micropore

(intracrystalline) and macropore (intercrystalline) diffusion resistances. The importance of both micro- and macro- pore diffusion in pelleted zeolite catalysts has been emphasized in the review by Palekar and Rajadhyaksha [5].

In the conversion of dimethyl ether to hydrocarbons on ZSM-5 at 600 K, Riekert and coworkers [6,7] observed that intercrystalline mass transfer affects catalytic activity and selectivity of the zeolite pellets when dia. > 2 mm are used, whereas intracrystalline mass transfer does not seem to be important with respect to catalytic activity and selectivity of the zeolite at < 600 K.

Recently Choudhary and Akolekar [7a] have reported that the activity and selectivity of Pt.H-ZSM-5.Al_2O_3 catalyst in the o-xylene isomerization, iso-octane cracking and methanol-to-aromatics conversion reactions are strongly influenced by the intracrystalline mass transfer.

Carbonaceous deposits called coke are inevitable by-products in many acid catalyzed hydrocarbon reactions viz. cracking, isomerization, alkylation etc.. Though low coke yields are observed for molecular shape selective zeolites like ZSM-5, coke deposition on the intercrystalline spaces and pore blockage effects may play a non-negligible role in certain hydrocarbon reactions [8]. Such coke deposition can influence the intercrystalline mass transfer of the reactants and products through the macropores and change the catalyst selectivity. Most of the studies on coking have been on the factors affecting coking and regeneration of catalysts, on the characterization of

coke deposits and on the deactivation kinetics [8a]. Influence of coking on intraparticle mass transfer and catalytic properties, particularly for zeolite catalysts have not been thoroughly investigated so far. It is therefore very interesting to investigate the influence of coking on intercrystalline mass transfer and catalytic properties of the ZSM-5 type catalyst.

In the present investigation, the influence of coking on intercrystalline mass transfer and catalytic activity and selectivity in iso-octane cracking, o-xylene isomerization and methanol-to-aromatics conversion over Pt.H-ZSM-5.Al_2O_3 catalyst have been studied by carrying out the reactions on the catalyst with different extents of coke deposition, in a pulse microreactor. The effect of coking on the heat of adsorption and the effective intercrystalline diffusivity under reaction conditions of the catalyst samples was determined by gc pulse technique using iso-octane (which does not penetrate the zeolite channels) as the probe molecule.

2.2 EXPERIMENTAL

2.2.1 Chemicals and Gases

The following chemicals and gases have been used.

Hydrogen : High purity (IOLAR - I, obtained from Indian Oxygen Ltd., Bombay) passed over molecular sieves (3A) to remove traces of moisture.

Nitrogen : IOLAR - II, obtained from Indian Oxygen Ltd., Bombay.

Methanol : BDH, AR.

Iso-octane : Fluka, puriss.

n-Hexane : Fluka, puriss.

o-Xylene : Fluka, puriss.

Pyridine : Sarabhai Merck, GR.

2.2.2 Catalyst

The catalyst Pt.H-ZSM-5.Al_2O_3 (0.1 wt % Pt., 50 wt % Al_2O_3) in the form of extrudates of dia.: 0.16 cm was provided by Dr. P. Ratnasamy (National Chemical Laboratory, Pune-8). The properties of the catalyst and the ZSM-5 zeolite used therein are given in Table 2.1.

The catalyst (particle size 0.16cm) was calcined in static air at 773 K for 4 h. For obtaining catalysts coked to different extents, the following procedure was used.

The catalyst (about 10 g in each batch) was heated in a reactor at 673 K for two hours in a flow of nitrogen (flow rate: 1.5 $l.min^{-1}$). Then nitrogen at high flow rate (flow rate: 2.0 $l.min^{-1}$) bubbled through a saturator containing cumene at 296 K was passed over the catalyst. The catalyst was exposed to this nitrogen saturated with cumene to different periods of time (2h, 8h, 28h) at 673 K to get samples coked to different extents. After coking, each batch of catalyst was kept at 673 K for 1 h to remove the volatiles and then cooled to room temperature in a flow of oxygen-free nitrogen (flow rate: 1.5 $l.min^{-1}$).

The catalyst poisoned with pyridine was prepared *in situ* by passing H_2 saturated with pyridine (in a saturator) continuously (flow rate: 30 $cm^3.min^{-1}$) through the column containing fresh Pt.H-ZSM-5.Al_2O_3 at 473 K for 2 h. The

Table 2.1

Properties of the Pt.H-ZSM-5.Al_2O_3 catalyst

Catalyst form	:	Extrudates (dia.: 0.16 cm)
Catalyst composition	:	Pt. (0.1 wt. %), H-ZSM-5 (50 wt. %) and Al_2O_3 (50 wt. %)
Crystal size of the H-ZSM-5	:	0.2 - 0.3 μm
Si/Al ratio of the H-ZSM-5	:	70
Bulk density of the catalyst	:	0.62 $g.cm^{-3}$

temperature was then raised and kept at 523 K for 1 h and brought back to the temperature of the experiment (473 K).

2.2.3 Catalyst Characterization

2.2.3.1 Measurement of Surface Area

The surface area of the fresh and coked catalysts were measured by dynamic N_2 adsorption/desorption method at liquid nitrogen temperature (78 K) and N_2 concentration of 30 mole % (balance helium) using a Quantasorb Surface Area Meter (Quantachrome Corp.,U.S.A.).

2.2.3.2 Measurement of Pore Size Distribution

The pore size distribution of the catalyst was measured by mercury porosimetry using an Autoscan-60 Porosimeter (Quantachrome Corp.,U.S.A.) by varying the pressure in the porosimeter from 0-60,000 psig.

2.2.3.3 Estimation of Carbon

The carbon content of the different coked catalysts was measured gravimetrically by burning the carbon and trapping the CO_2 formed in saturated $Ba(OH)_2$ solution.

A known quantity of the catalyst was heated gradually in a quartz reactor to 723 K in a flow of air (50 $cm^3.min^{-1}$) and the outcoming gases were passed through a series of bubblers containing saturated $Ba(OH)_2$ solution. The CO_2 present in the air, if any, was removed by bubbling through saturated NaOH solution before its entry to the reactor. The heating was continued till the outcoming gases from the reactor showed the

absence of CO_2 i.e. no precipitate formation when bubbled through freshly prepared $Ba(OH)_2$ solution. When the oxidation was complete, the solutions were filtered through a previously weighed Whatman 41 filter paper, washed till the filtrate was neutral to litmus, dried in an oven at 373 K until a constant weight was obtained. The amount of carbon present in the catalyst was calculated from the weight of the $BaCO_3$.

2.2.3.4 X-ray Photoelectron Spectroscopy (XPS)

Surface analysis of the fresh and coked Pt.H-ZSM-5.Al_2O_3 was carried out by XPS using a VG-Scientific ESCA-3 MK II electron spectrometer.

2.2.3.5 TG / DTG

The thermal analysis data on the catalyst samples were obtained by using an automatic NETSCH STA 409 model (Netzsch Geratebau GmbH) thermal analyzer under the following experimental conditions.

Sample size : 50 mg

Temperature range : 303 - 1273 K

Linear heating rate : 10 $K.min^{-1}$

Atmosphere : Air (flow rate: 100 $cm^3.min^{-1}$)

2.2.3.6 NMR

The nature of the coke on the catalyst samples was studied by solid state ^{13}C (CP/MAS) nuclear magnetic resonance spectroscopy at 75.47 M Hz on a Bruker MSL 300 FT-NMR spectrometer with a contact time of 4 s and a spinning speed of 4.1 k Hz. Dipolar dephasing technique (dephasing delay 40 μ s)

was employed to distinguish quarternary and methyl carbon. 10,000-17,000 spectra were accumulated before Fourier transformation. The chemical shifts were measured with respect to adamentane CH carbon taken as 37.8 ppm.

2.2.4 Measurement of Acidity Distribution

The acidity distribution on the catalysts was determined by gc adsorption/desorption methods [9,10] using pyridine as an acid probe.

Gas chromatographic adsorption/desorption data were collected using a Perkin-Elmer Sigma 3B GC fitted with a flame ionization detector. Nitrogen, passed over activated molecular sieves to remove traces of moisture, was used as the carrier gas. The flow rate was about 10 cm^3 (NTP).min^{-1} in all the experiments.

A 15 cm long gc column was prepared by packing about 0.3 g of the catalyst (particle size: 0.2 mm) in a stainless steel tube (3 mm o.d.). In order to minimize the dead volume, one end of the column was directly connected to the detector and the other end to the injector through a 50 cm long stainless steel capillary (about 1.5 mm o.d. and 0.7 mm i.d.), which acted as a pre-heater. The catalyst was calcined in situ by heating it in a flow of nitrogen from 353-673 K at a linear heating rate of 10 K.min^{-1} and further at 673 K for 2 h.

Measurement of Irreversible Adsorption of Pyridine at 673 K

The irreversible adsorption (or chemisorption) of pyridine in the catalyst was measured by the gc pulse method [9] based on TPD under chromatographic conditions.

The initial temperature chosen for the TPD was 353 K. After calcination of the catalyst, the GC oven temperature was decreased to 353 K and a known amount of pyridine was injected into the catalyst column. After allowing 1 min for the redistribution of the adsorbed species in the column, the TPD was started at a linear heating rate of 10 $K.min^{-1}$ in the flow of nitrogen. The final temperature chosen for the TPD (or, the temperature at which the irreversible adsorption of the adsorbate was to be measured) was 673 K. After the final temperature was reached, the desorption of the reversibly adsorbed species was allowed to continue for a further period of 60 min isothermally at that temperature. At the end of the TPD, the zeolite retained only the adsorbate irreversibly adsorbed at 673 K.

After recording the first TPD chromatogram, the GC oven temperature was reduced to 353 K and the procedure was repeated to obtain the second TPD chromatogram by injecting the same amount of adsorbate.

The amount of pyridine irreversibly adsorbed was calculated from the expression

$$q_i = (A^* / s) / M \qquad (2.1)$$

where A^* is the difference between the areas of the two chromatograms obtained by the superimposition of the two chromatograms and cutting and weighing, s is the detector sensitivity ($area.mol^{-1}$) and M is the mass of the catalyst.

The irreversible adsorption (or chemisorption) in the present study is defined as the amount of adsorbate retained by the presaturated catalyst after it was swept with pure nitrogen at the temperature of chemisorption for 60 min.

Measurement of Stepwise Thermal Desorption (STD) of Pyridine

After the in situ pretreatment, the zeolite was saturated with pyridine at 373 K by injecting a number of pulses of pyridine and the reversibly adsorbed pyridine at this temperature was desorbed in the flow of nitrogen. The species adsorbed irreversibly at 373 K was thermally desorbed in the flow of nitrogen (flow rate: 10 $cm^3.min^{-1}$) by heating the catalyst from 373 to 673 K in six steps. The temperature in each step was raised at a linear rate of 10 $K.min^{-1}$. After the maximum temperature of a step was reached, it was maintained for a period of 60 min to desorb the pyridine reversibly adsorbed in the catalyst at that temperature. The adsorbate desorbed in each step was measured quantitatively by the FID. The amount of adsorbate desorbed (q_d) in a step due to increase in the temperature from T_1 to T_2 is given by the expression

$$[q_d]_{T_1}^{T_2} = A_d \,/\, (s.M) \qquad (2.2)$$

where A_d is the area under the desorption chromatogram.

The amount of pyridine irreversibly adsorbed (or chemisorbed) at different temperatures [$q_{i(T)}$] was calculated from the STD data as follows:

$$q_{i(T)} = q_{i(673K)} + [q_d]_T^{673} \qquad (2.3)$$

The amount of pyridine irreversibly adsorbed at 673 K, [$q_{i(673\ K)}$] was determined as discussed in the earlier section.

2.2.5 Measurement of Heat of Adsorption

The heat of adsorption of iso-octane in fresh, coked and pyridine poisoned catalyst was determined from the gc pulse retention data obtained at different temperatures using the relation [11]

$$\log V_R = a - (\Delta H / 2.303R)\ 1 / T \qquad (2.4)$$

where V_R is the retention volume of the adsorbate, which is equal to $(t_m - t_d).V$; t_m and t_d are the retention time for the adsorbate and the non-adsorbate respectively, V is the carrier gas flow rate (corrected to column conditions), H is the heat of adsorption, R is the gas constant, T is the temperature and a is a constant. The heat of adsorption H is calculated from the slope of the linear plots of log V_R versus 1/T.

The schematic diagram of the experimental setup used for the measurement of heat of adsorption and diffusivity of iso-octane is given in Fig. 2.1. Perkin-Elmer Sigma 3B GC with FID detector was used for carrying out the experiments. The catalyst packed in a stainless steel tube (length: 53cm, i.d.: 0.547 cm) was fitted inside the GC oven. Hydrogen was used as the carrier gas and its flow rate was controlled by a differential flow control valve (range 0-200 $cm^3.min^{-1}$) at a constant inlet pressure of 52 psig. Hydrogen, bubbled through a saturator containing iso-octane and diluted to 1.5 % (volume), was used as the sample (injection volume: 0.3 cm^3). Part of the

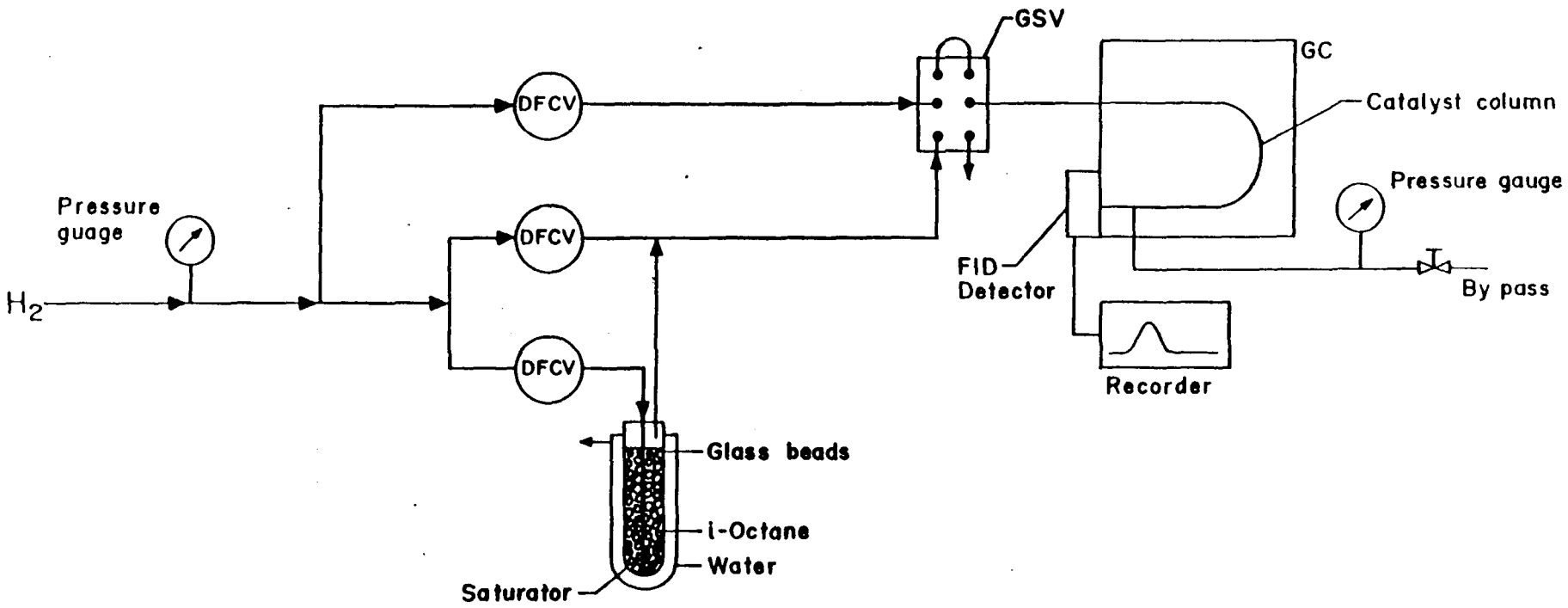

FIG. 2·1 : EXPERIMENTAL SET UP FOR THE MEASUREMENT OF HEAT OF SORPTION AND DIFFUSIVITY [Length of column : 53 cm, i.d. : 0·547 cm]

outlet gas from the column was bled off at constant pressure before passing it to the detector.

2.2.6 Measurement of Effective Diffusivity

The effective pore diffusivity of iso-octane in the fresh, pyridine poisoned and coked samples of Pt.H-ZSM-5.Al_2O_3 catalyst was determined by measuring the gc pulse broadening of iso-octane at various flow velocities by the method of HETP using the van Deemter equation [12].

$$HETP = A + B/v + Cv \qquad (2.5)$$

v is the linear gas velocity through the chromatographic column and A, B, C are the constants representing eddy diffusion, molecular diffusion and resistance to mass transfer respectively. The Height Equivalent of a Theoretical Plate, HETP was measured from the chromatogram using the expression [13]

$$HETP = (L/16) (y/x)^2 \qquad (2.6)$$

L is the length of the column, y is the length of the base line cut by the two tangents of the chromatogram at its points of inflection and x is the distance from the injection to the peak maximum.

The mass transfer term C was obtained from the linear plots of HETP versus v at high linear gas velocities (15 to 100 $cm.s^{-1}$). The effective pore diffusivity, D_p was estimated from the C term using the following relationships.

$$C = (F_1 d_p^2 K) / [2 \pi^2 F_2 D_p (1 + K F_1 / F_2)^2] \qquad (2.7)$$

$$C = F_1 F_2 [1+(1-\epsilon) / \epsilon K] d_p^2 / 30 D_p[1+F_2(1-\epsilon) / \epsilon K]^2 \quad (2.8)$$

Equation (2.7) is the original expression (neglecting the external diffusion in the packed column) suggested by van Deemter et al. [12] for the case of an ion-exchanged resin. Equation (2.8) was derived by Hawkes [14] using the Gidding's theory of non-equilibrium chromatography [15]. F_1, F_2 are the void and solid fractions in the packing; is the porosity of the catalyst and d_p is the average particle diameter. The distribution coefficient K was obtained from the expression [16]

$$K = 1 / [\epsilon + (t_m - t_d) v F_1 / F_2 L] \quad (2.9)$$

t_m, t_d are the retention times of the adsorbate and the non-adsorbate respectively and L is the length of the packed column. The apparent adsorption equilibrium constant K_n was determined from the relation [17]

$$K_n = (t_m - t_d) v F_1 / L \quad (2.10)$$

2.2.7 Measurement of Catalytic Activity and Selectivity

The catalytic activity and selectivity of the zeolites in the iso-octane cracking, o-xylene isomerization and methanol-to-aromatics conversion reactions were determined using a pulse microreactor (o.d.: 0.6 cm, i.d.: 0.4 cm, length: 22 cm) connected to a GC with FID. The microreactor was made of stainless steel and consisted of a tube with the catalyst held between quartz wool plugs and an injection port. The temperature of the catalyst (measured by a thermocouple kept in the catalyst

bed) and that of the injection port could be varied independently. A part of the reactor effluents could be by-passed with the help of a needle valve before allowing the effluents to enter the analytical column.

The catalyst in the microreactor was heated at 673 K in a flow of H_2 for 1 h. The activity of the catalyst was determined using H_2 as the carrier gas by injecting a known amount of the reactant into the microreactor at the desired reaction conditions and analyzing the reaction products with the GC (provided with FID and calculating integrator).

The products of all reactions were analyzed at the following conditions:

Analytical column	:	Bentone - 34 (5%) and dinonyl phthalate (5%) on chromasorb-w (3 mm x 9 m)
H_2 flow rate	:	20 $cm^3.min^{-1}$
Column temperature	:	Programmed from 323 to 423 K at a heating rate of 10 $K.min^{-1}$, the initial and final temperatures were held for 10 and 30 min respectively.

The following reaction conditions were employed for the measurement of catalytic activity and selectivity of the fresh and coked catalysts in the iso-octane cracking, o-xylene isomerization and methanol-to-aromatics conversion reactions.

Amount of catalyst	:	0.2 g
Catalyst particle size	:	0.16 cm
H_2 flow rate	:	80 $cm^3.min^{-1}$
Reaction temperature	:	673 K

Pressure : 203 kPa

Pulse size : 2.0 µl

2.3 RESULTS AND DISCUSSION

2.3.1 Characterization of Fresh and Coked Pt.H-ZSM-5.Al_2O_3 Catalyst

2.3.1.1 Surface Area and Pore Size Distribution

The surface area of the different catalyst samples were measured by nitrogen adsorption and mercury porosimetry, and the mercury penetration data (volume) are given in Table 2.2. Table 2.2 also gives the carbon content of the catalyst coked to different extents.

The pore size distribution of the fresh and coked (2.1 % carbon) catalysts and the variation of dV_p/d_p (where V_p is the volume filled with mercury at pressure P) with logarithm of pore radius are given in Fig. 2.2.

The catalyst which is in the form of extrudates, contains crystallites (0.2-0.3 μm) of the zeolite and particles of high surface area (about 200 $m^2.g^{-1}$) alumina. It is therefore expected to contain three distinct pore systems: (i) the intracrystalline pores (micropores of dia.: 0.6 nm) in the zeolite, (ii) the intraparticle pores in the alumina particles (mesopores), and (iii) the intercrystalline and inter-alumina particles pores (macropores). The non-zeolitic pores of the catalyst (which comprise of intraparticle pores in the alumina and interparticle and intercrystalline pores) are expected to have a bimodal pore size distribution and indeed it is observed as shown in Fig. 2.2b. The mesopores [r_p (average) 7.0 nm] are

Table 2.2

The carbon content and surface area of fresh and coked Pt.H-ZSM-5.Al_2O_3

Catalyst	wt. % of carbon	Vol. of Hg. intruded ($cm^3.g^{-1}$)	Surface Area	
			N_2 adsorption ($m^2.g^{-1}$)	Hg. porosimetry ($m^2.g^{-1}$)
Fresh (uncoked) catalyst	0.0	0.49	381	133
Coked catalyst (I)	0.3	0.47	361	122
Coked catalyst (II)	0.4	0.48	368	124
Coked catalyst (III)	2.1	0.47	361	122

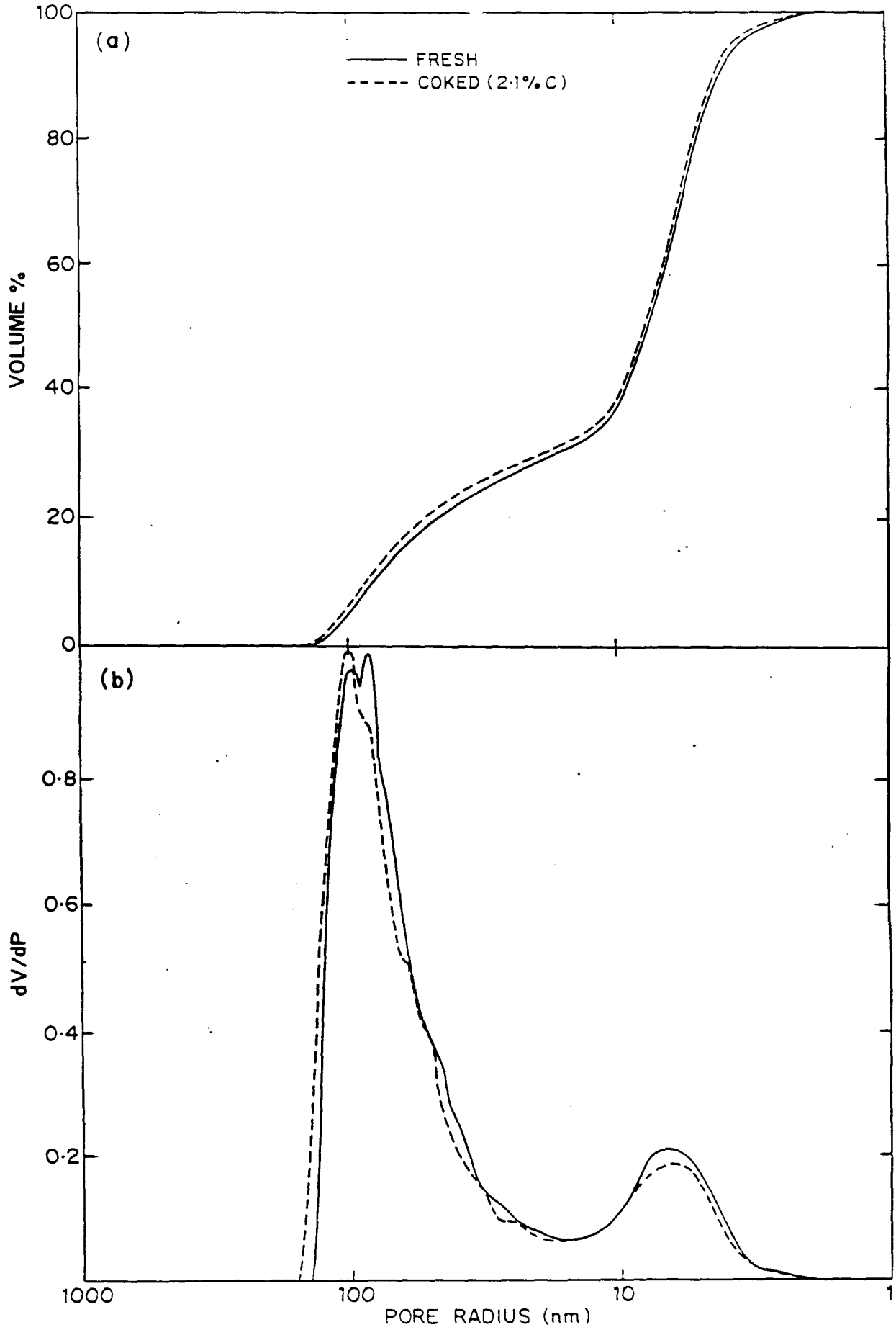

FIG.2·2: INFLUENCE OF COKING ON PORE SIZE DISTRIBUTION OF Pt. H-ZSM-5 Al_2O_3

expected to be present in the fine particles of alumina. The macropores are expected to be the voids in the zeolite crystallites and the alumina particles in the extrudates of the catalyst.

The results (Table 2.2) show a small decrease in the surface area of the catalyst due to coking. The results of the pore size distribution reveal that there is no significant change in the pore size distribution of the zeolite catalyst due to coking (Fig. 2.2) The decrease in the pore volume due to coking as measured by the mercury porosimetry (Table 2.2) is also very small.

2.3.1.2 Acidity Distribution

The acidity distribution of the catalyst samples have been measured by temperature programmed desorption (TPD) and stepwise thermal desorption (STD) of pyridine.

Temperature dependence of the chemisorption of pyridine on the fresh and coked Pt.H-ZSM-5.Al_2O_3 is shown in Fig. 2.3a. The site energy or acid strength distribution obtained by the STD of pyridine on the catalyst samples is presented in Fig. 2.3b. The numerical data on the chemisorption and STD of pyridine on the catalyst samples are given in Appendices 2.1 and 2.2 respectively.

It may be noted that the catalysts show a wide variation in the acid strength distribution. The acid strength distribution changes considerably with the degree of coking. It is interesting to note that pyridine chemisorption at lower temperatures (< 573 K) is increased with increasing coke

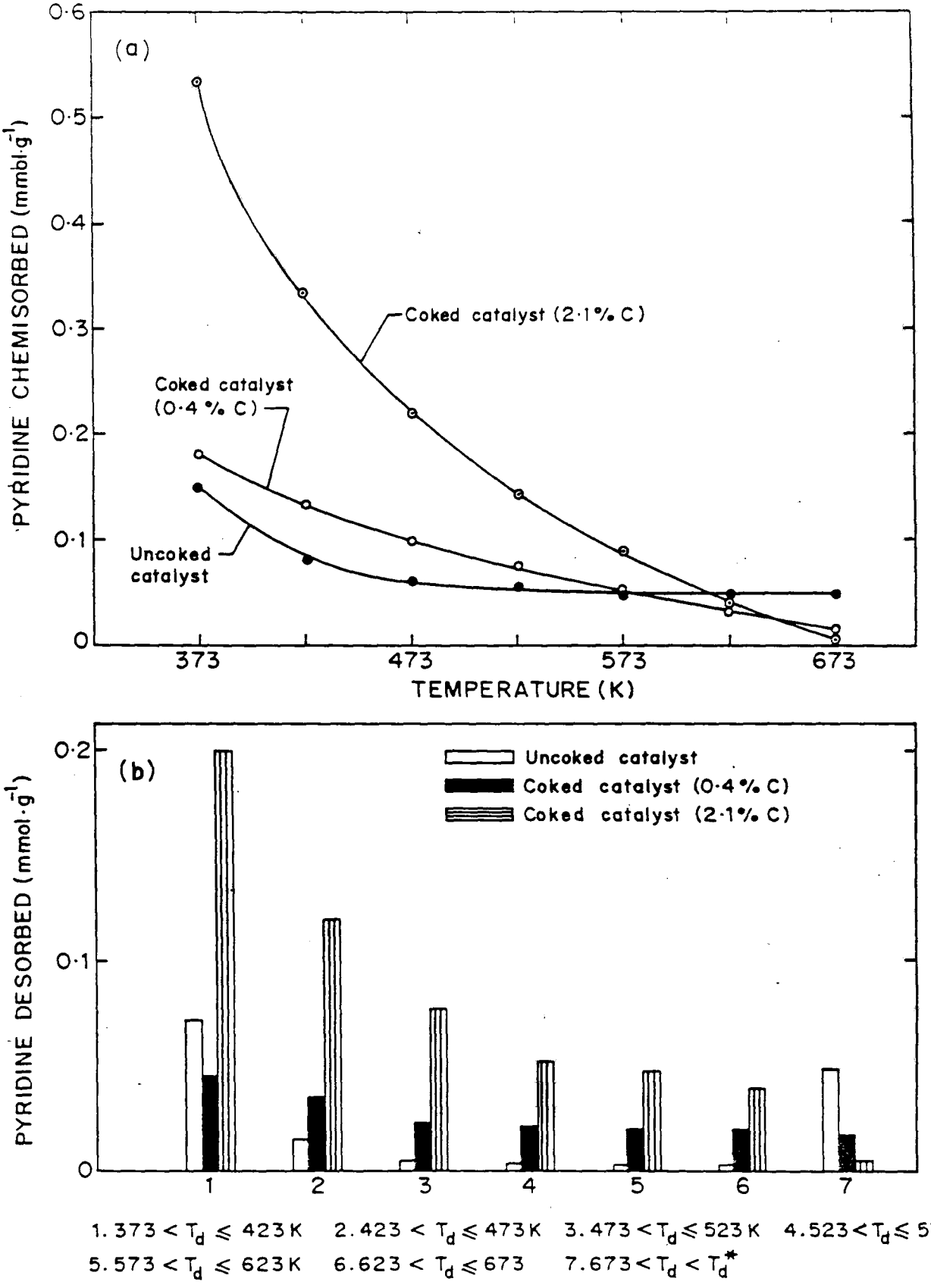

FIG. 2·3 : (a) TEMPERATURE DEPENDENCE OF CHEMISORPTION OF PYRIDINE ON Pt·H-ZSM-5·Al_2O_3 CATALYST COKED TO DIFFERENT EXTENTS

(b) ACID STRENGTH DISTRIBUTION OF THE CATALYST COKED TO DIFFERENT EXTENTS

deposition. At higher temperatures (> 650 K), it is decreased with increasing coke deposition (Fig. 2.3a). The results indicate the creation of weaker acid centers due to the coke deposition. The newly created weak acid centers are expected to be on the coke itself.

2.3.1.3 Thermal Analysis

The thermogravimetric analysis of the fresh and the coked catalysts are given in Fig. 2.4. Figures 2.4a and 2.4b give the TG and DTG data for the catalyst with 2.1 % and 0.4 % carbon, while Fig. 2.4c gives that for the uncoked catalyst.

The DTG curve in Fig. 2.4c shows a single peak at 373 K due to the desorption of physically adsorbed water from the catalyst. The DTG curve in Figs. 2.4a and b show a peak at 373 K due to the desorption of water from the coked catalysts and a smaller peak at higher temperature (> 730 K). This second peak for the coked catalysts is due to the burning of coke on the catalyst.

For the coked catalyst with 0.4 % carbon, the DTG peak is at 739 K whereas that for the coked catalyst with 2.1 % carbon is observed at 823 K. This reveals that the removal of coke by its combustion from the catalyst with 2.1 % carbon occurs at higher temperature. This leads to the conclusion that the nature and/or location of the coke in the two coked catalysts is somewhat different.

2.3.1.4 XPS

The carbon (1s) spectra of fresh and coked Pt.H-ZSM-5.Al_2O_3 catalysts are given in Fig. 2.5. The C (1s) spectrum for

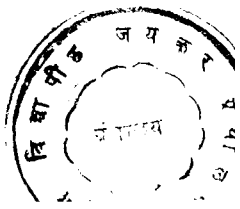

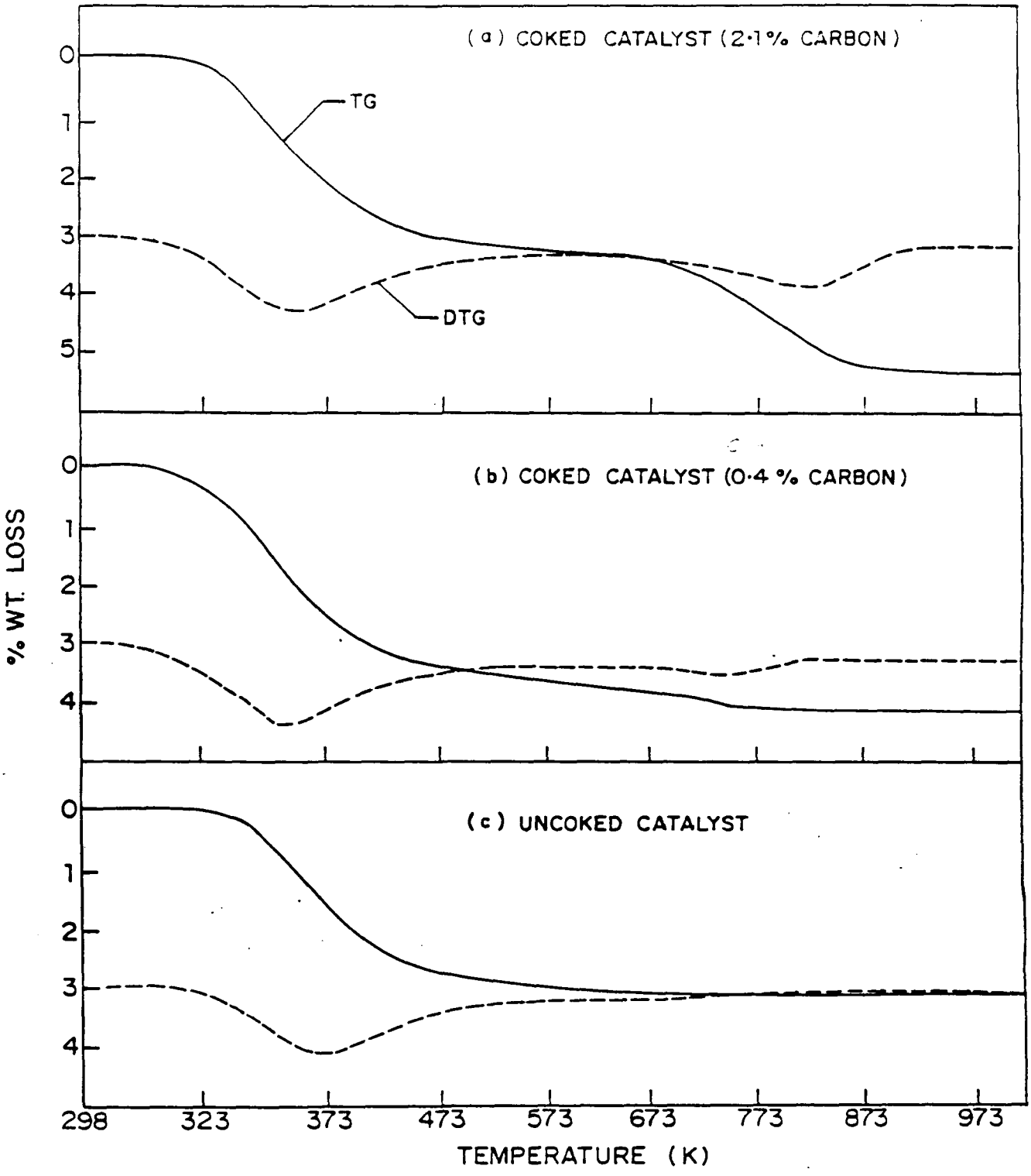

FIG. 2·4 : TG / DTG CURVES FOR Pt-HZSM-5-Al_2O_3 COKED TO DIFFERENT EXTENTS

9136

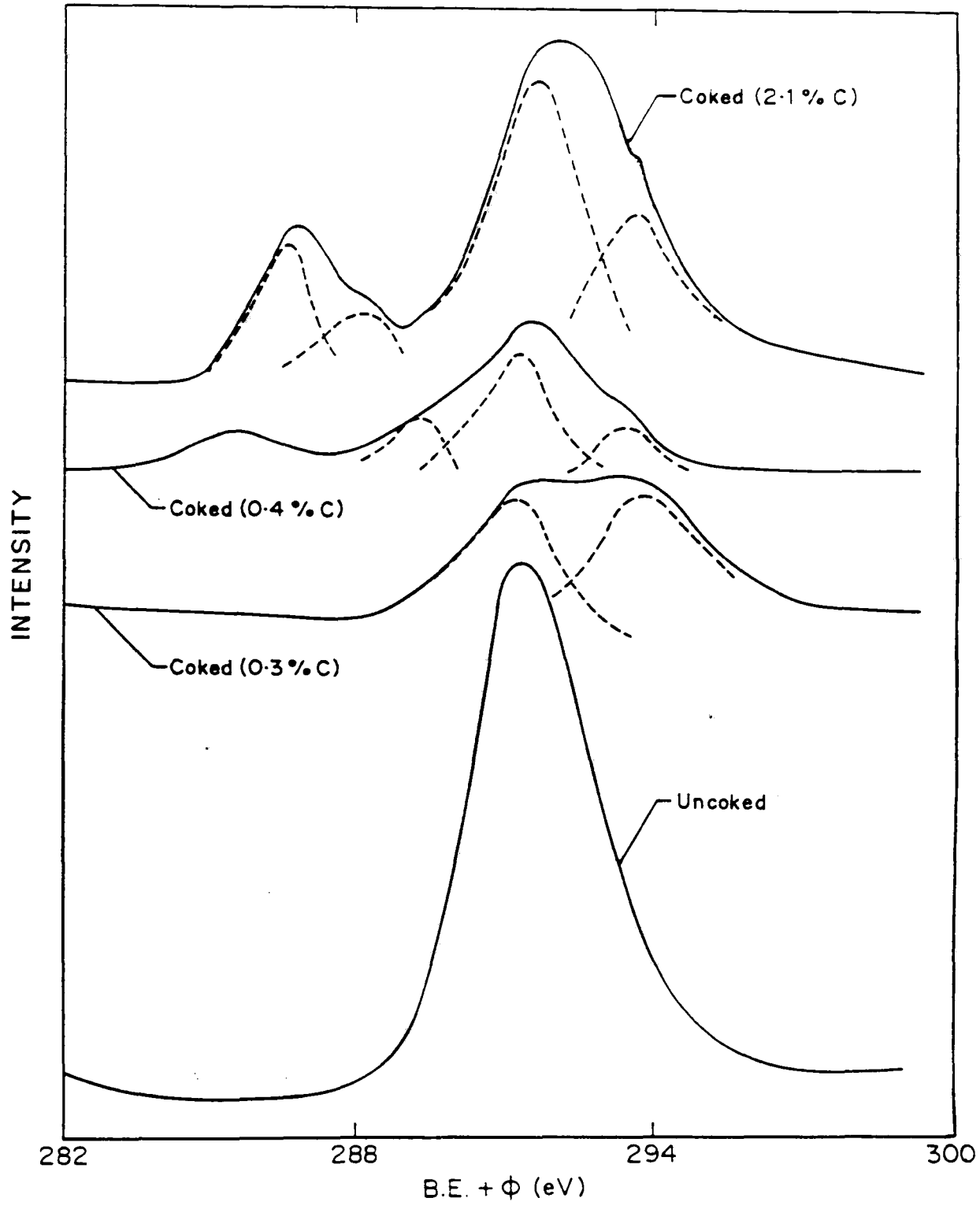

FIG.2·5 : C(1s) SPECTRA OF Pt. H-ZSM-5 • Al_2O_3 CATALYST COKED TO DIFFERENT EXTENTS (B.E. = Electron binding energy ; Φ = WORK FUNCTION)

the fresh catalyst is a single sharp peak at 291 eV due to the presence of residual carbon compounds in the spectrometer. For the coked catalyst samples, the C (1s) spectrum shows broad and multiple peaks with humps (Fig. 2.5). The comparison of C (1s) spectra of the catalyst coked to different extents reveals that carbon exists in different forms in the coked catalyst and the nature of the coke on the catalyst changes with the extent of coke deposition.

2.3.1.5 NMR

The ^{13}C (CP/MAS) spectra of Pt.H-ZSM-5.Al_2O_3 catalyst coked to different extents are shown in Fig. 2.6. The results indicate that the n.m.r. visible coke is composed of methyl substituted aromatics, long chain methyl substituted aliphatics and condensed aromatics.

The ^{13}C (CP/MAS) spectrum of the catalyst with 0.4 % carbon (Fig. 2.6a) exhibits three distinct resonances in the range 30-150 ppm which are assigned to (i) secondary, tertiary and quarternary aliphatic carbons (δ = 30-50 ppm), (ii) aromatic CH groups (δ = 127 ppm) and (iii) substituted aromatic carbons, bridged carbons in condensed aromatics or olefinic CH groups (δ = 141 ppm) [18, 19]. Fig. 2.6b gives the spectrum of the same catalyst sample taken with a dipolar dephasing of 40 μs. Dipolar dephasing technique detects only non-protonated and methyl carbons. The spectrum shows two signals in the region of non-protonated aromatic carbons (100-150 ppm) while the methyl carbons are absent or negligible. On comparison with Fig. 2.6a, the signal at 127 ppm is assigned to non-protonated aromatic

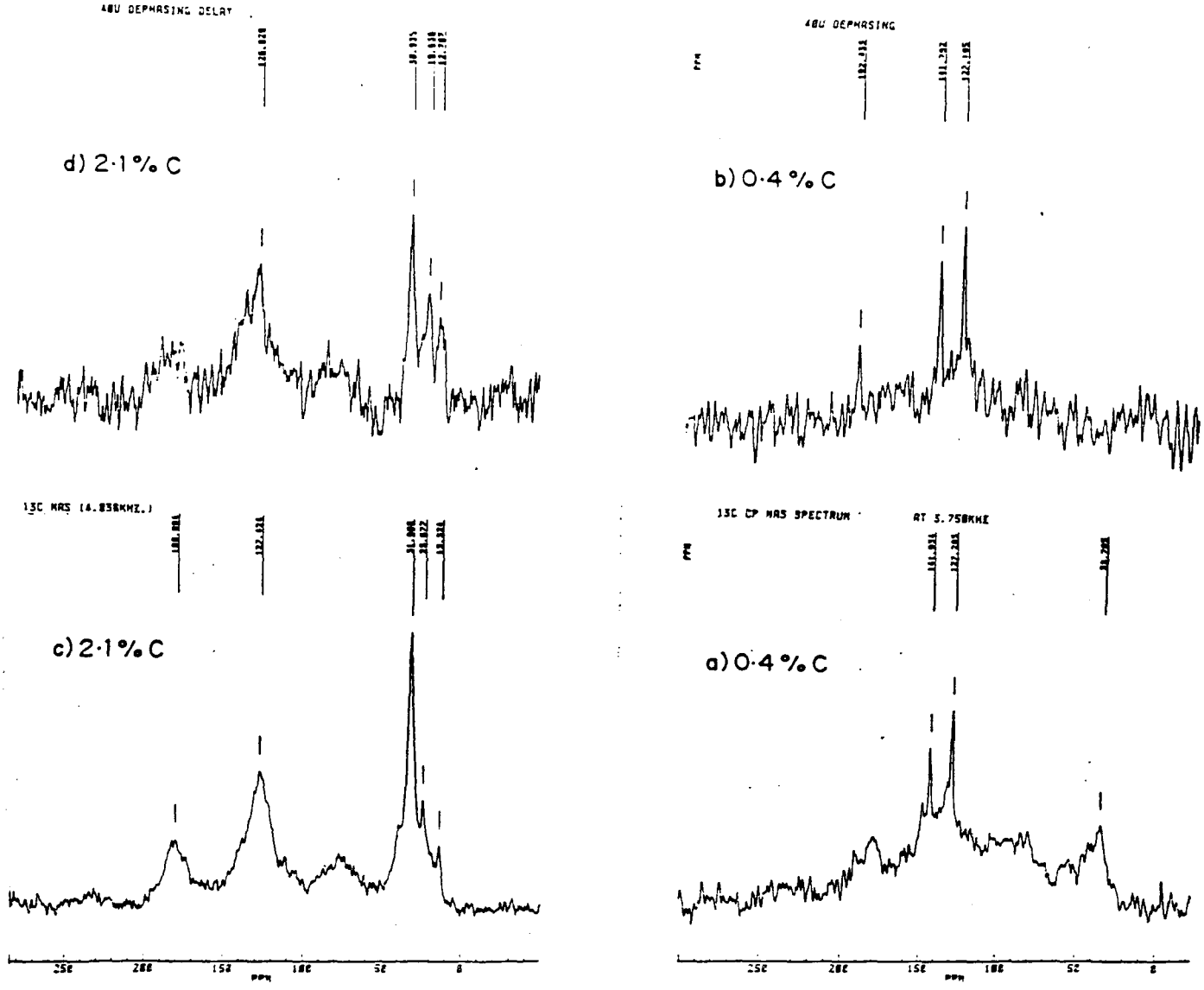

FIG. 2·6: ^{13}C(CP/MAS) SPECTRA OF Pt·H-ZSM-5·Al_2O_3 CATALYST COKED TO DIFFERENT EXTENTS

carbons and that at 141 ppm is assigned to bridged carbon in condensed aromatics [18]. The signal at 192 ppm is due to spinning side bands. This result suggests that a significant portion of the aromatics on the catalytic surface may be polycyclic or polycondensed aromatics.

The ^{13}C (CP/MAS) n.m.r. spectrum of the catalyst containing 2.1 % carbon (Fig. 2.6c) gives three signals in the aliphatic range and one signal at 127 ppm in the aromatic range. The signal at 180 ppm is due to spinning side bands. In the aliphatic range, methyl groups attached to secondary carbons (13 ppm), CH_2-groups linked methyl groups (23 ppm) and other types of paraffinic CH_2-groups and/or quarternary carbon atoms (30-32 ppm) are detected. Figure 2.6d gives the dipolar dephased spectrum of the same catalyst. The three distinct resonances in the aliphatic range are assigned to (i) methyl groups linked to secondary carbon atoms (13 ppm), (ii) methyl groups linked to aromatics (19 ppm) and (iii) methyl groups linked to aliphatic quarternary carbon (30 ppm). The signal at 127 ppm is assigned to aromatic quarternary carbon and the signal for bridged aromatic carbon is very weak. The spectrum shows a significant amount of aliphatic carbons due to methyl and methylene (CH_2) groups suggesting that the coke consists mainly of methyl substituted aromatics and long chain aliphatics.

Comparison of the spectra for the two coked catalyst samples shows that with the increase in the extent of coke deposition from 0.4 to 2.1 %, (i) there is an increase in the aliphatic carbon content of the coke from 13.3 to 30.0 % and a

corresponding decrease in the aromatic carbon from 86.7 to 70.0 %, (ii) there is a decrease in the signal intensity due to bridged carbon in condensed aromatics. This observation is in accordance with the hypothesis that, on all zeolites, coke formation occurs via olegomerization of olefinic cracking products followed by cyclization of the olegomers, transformation through monoaromatics, alkylation of these monoaromatics, then cyclization and hydrogen transfer to give biaromatics, triaromatics etc. [8a].

The polyaromatic or condensed aromatic coke observed on both the catalyst samples is expected to be present only in the meso- and macro- pores as the formation of polyaromatics is not favoured in the channels of ZSM-5 because of restricted transition state molecular shape selectivity of the zeolite [20, 8]. The aliphatic carbon of the coke is expected to be located in the zeolite channels in the form of strongly sorbed or occluded long chain hydrocarbons and highly alkylated benzenes or polyalkylated benzenes. Earlier studies on pentasil zeolites [21, 22] have indicated the zeolite deactivation in the cumene cracking reaction due to strongly sorbed or occluded hydrocarbons in the zeolite channels. It has also been observed earlier [23-25] that when ZSM-5 zeolite contains a very few strong acid sites or in their absence, the retention of hydrocarbons (mostly in the form of long chain hydrocarbons) in the zeolite channels is favoured during the conversion of alcohols or olefins.

2.3.2 Influence of Poisoning

It has been reported [26] that the poisoning of Pt.H-ZSM-5.Al_2O_3 catalyst with pyridine (which can penetrate the macro-, meso- and micro- pores of the catalyst) results in a drastic decrease in its activity towards o-xylene isomerization and iso-octane cracking reactions. In this study, the influence of poisoning of Pt.H-ZSM-5Al_2O_3 with pyridine (by its chemisorption at 523 K) on the heat of adsorption and diffusion of iso-octane in the catalyst has been investigated. The results reflect the influence of poisoning of the active sites present in the macro- and meso- pores only, as iso-octane cannot penetrate the micropores (intracrystalline pores of ZSM-5) of the catalyst even at 673 K [21].

2.3.2.1 Heat of Adsorption of Iso-octane on Poisoned catalyst

The heats of adsorption of iso-octane on fresh and poisoned (with pyridine) Pt.H-ZSM-5.Al_2O_3 catalysts were estimated from the gc pulse data using Equation (2.4). Plots of logarithm of retention volume versus reciprocal column temperature for the estimation of heat of adsorption of iso-octane at 473 K on these catalysts are given in Fig. 2.7. The values of heat of adsorption of iso-octane on the fresh and poisoned catalysts are given in Table 2.3. The heat of adsorption of iso-octane on the poisoned catalyst is much less than that on the fresh catalyst. This reveals that the stronger sites involved in the adsorption of iso-octane on the catalyst are blocked due to pyridine poisoning (i.e. due to the chemisorption of pyridine at 523 K).

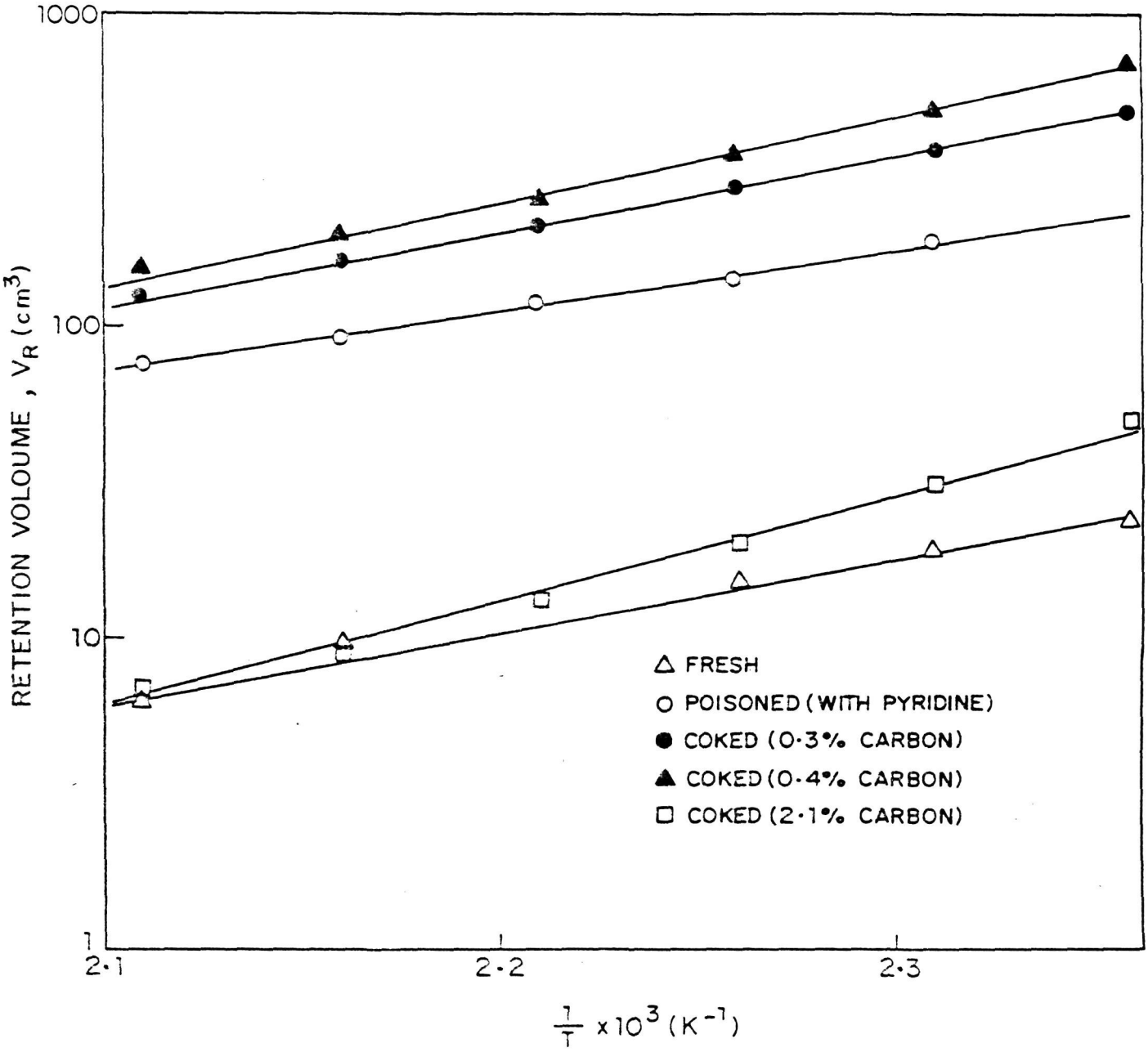

FIG.2·7: PLOTS OF RETENTION VOLUME vs $\frac{1}{T}$ FOR POISONED AND COKED CATALYSTS FOR THE CALCULATION OF HEAT OF SORPTION OF ISO-OCTANE AT 473 K

Table 2.3

Influence of poisoning and coking on adsorption and mass transfer of iso-octane in Pt.H-ZSM-5.Al_2O_3

Catalyst	Mass transfer term(at 473 K) C	Distribution coefficient K	Apparent equil. constant K_n	Heat of adsorption ($kJ.mol^{-1}$)	Pore diffusivity (Eqn. 2.7)	Pore diffusivity (Eqn. 2.8)
Fresh	0.088	0.075	7.22	47.2	2.94	2.47
Poisoned (with pyridine)	0.051	0.115	4.60	37.2	7.29	5.44
Coked (0.3 % C)	0.093	0.060	9.74	48.1	2.00	1.61
Coked (0.4 % C)	0.109	0.050	11.44	53.1	1.51	1.23
Coked (2.1 % C)	0.104	0.018	33.05	65.2	0.58	0.50

2.3.2.2 Diffusion and Mass Transfer of Iso-octane in the Poisoned Catalyst

The mass transfer term C, and the intraparticle diffusivity D_p for iso-octane on the fresh and poisoned Pt.H-ZSM-5.Al_2O_3 Have been estimated using Equations (2.5) - (2.8). Plots of HETP versus linear gas velocity, v, for the estimation of the mass transfer term, C, are given in Figs. 2.8 and 2.9. Table 2.3 gives the values of the mass transfer term (C), distribution coefficient (K), apparent equilibrium constant (K_n) and effective pore diffusivity (D_p) for the fresh and poisoned catalysts at 473 K.

The mass transfer term and the apparent adsorption equilibrium constant are decreased due to poisoning whereas the distribution coefficient and the intraparticle diffusivity of iso-octane on the catalyst are increased due to poisoning. The decrease in the adsorption equilibrium constant is due to the decrease in the available adsorption sites due to the poisoning.

On poisoning, the acid sites that are involved in the chemisorption of pyridine at 523 K are blocked by pyridine and hence the number of sites available for the adsorption of iso-octane is reduced considerably. Also, the sites available for the adsorption of iso-octane are weaker. This results in a decrease in the heat of adsorption and also a decrease in the apparent equilibrium constant for the adsorption of iso-octane on the poisoned catalyst.

Generally, diffusion in porous adsorbent is retarded due to adsorption on the pore walls and is enhanced because of surface diffusion in the adsorbed phase. The observed large

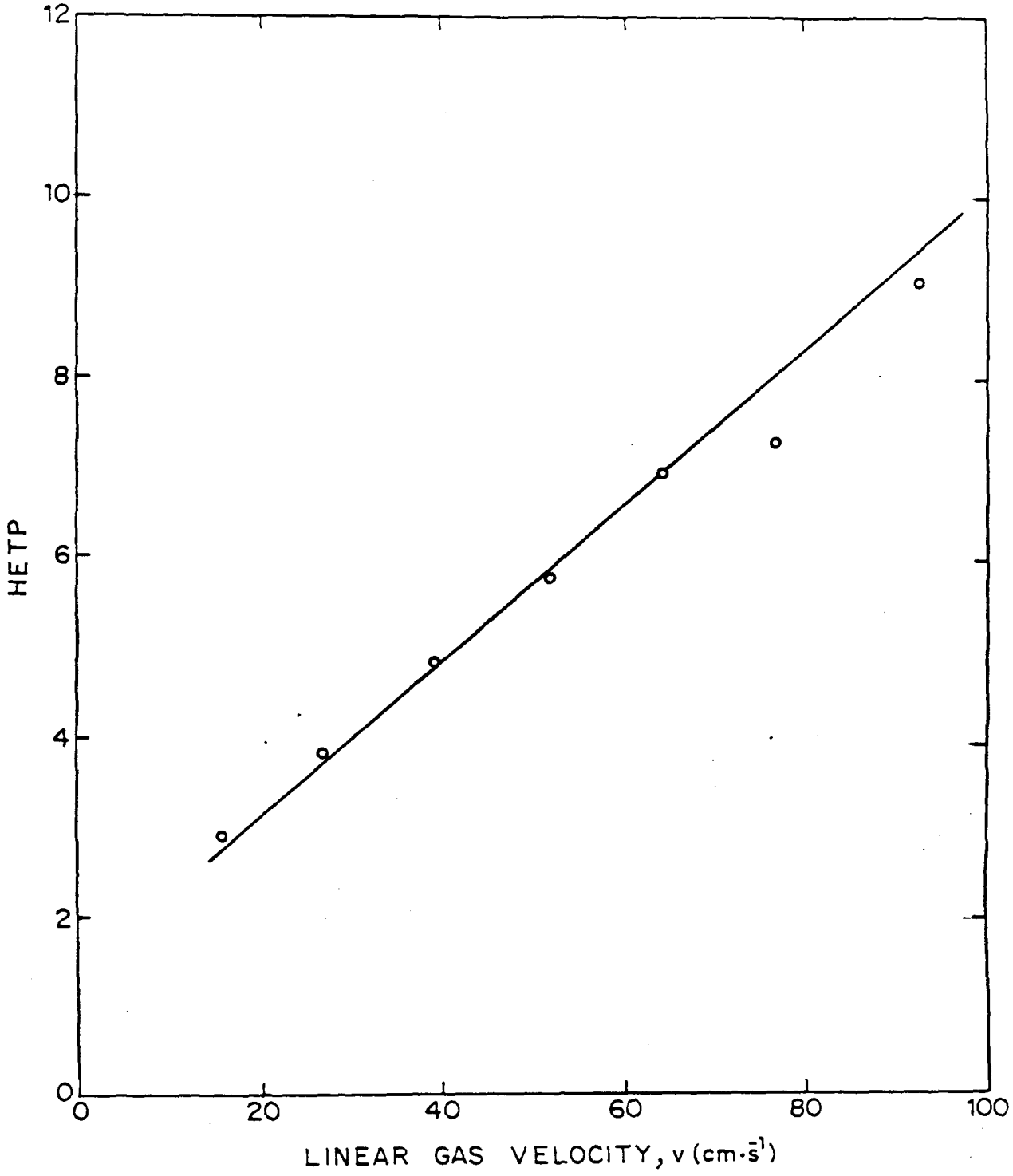

FIG. 2·8 : PLOT OF HETP vs v FOR THE CALCULATION OF MASS TRANSFER TERM C OF ISO-OCTANE ON Pt. H-ZSM-5·Al_2O_3 CATALYST AT 473K

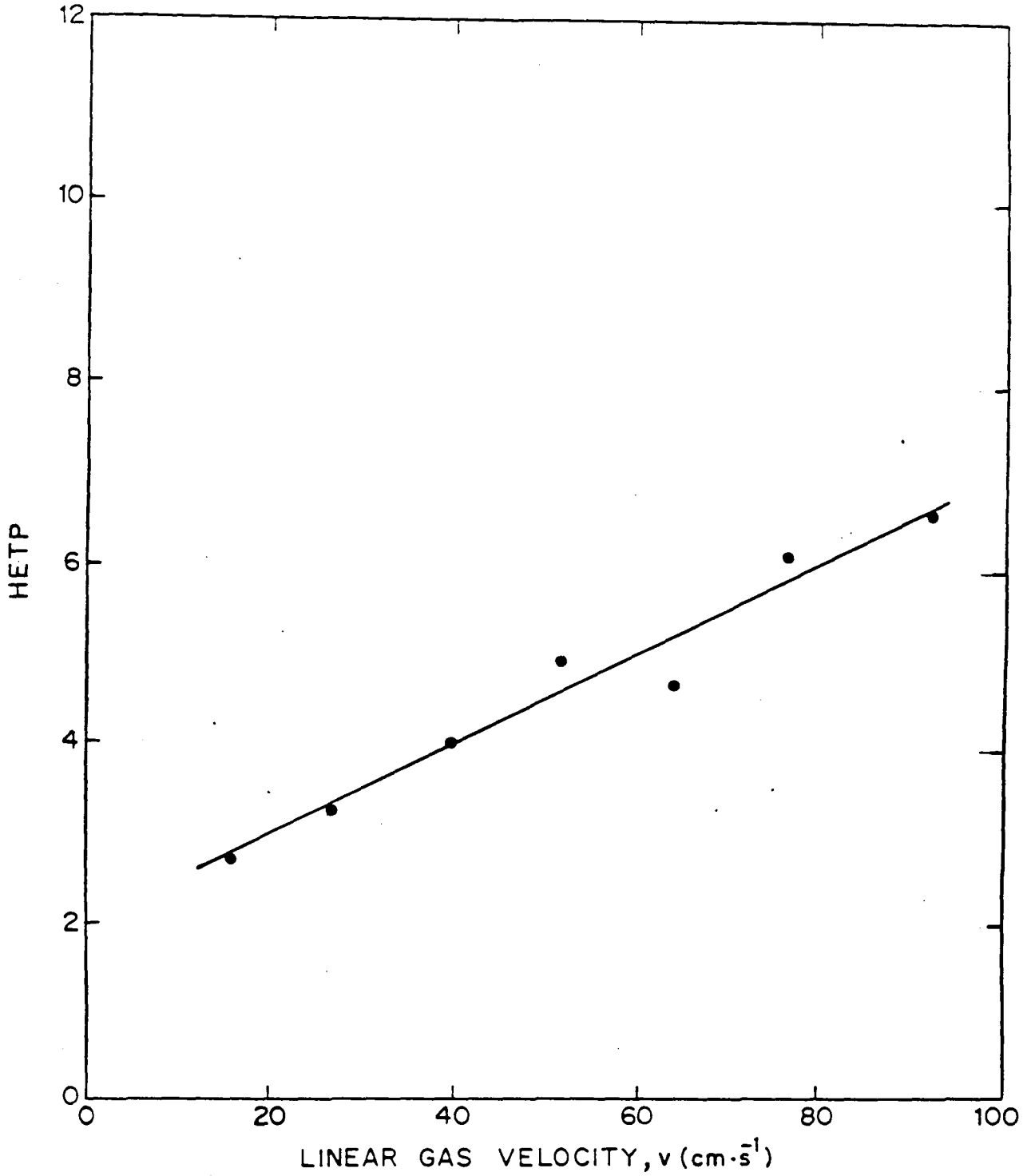

FIG.2·9: PLOT OF HETP vs v FOR THE CALCULATION OF MASS TRANSFER TERM C OF ISO-OCTANE ON Pt. H-ZSM-5·Al_2C_3 POISENED WITH PYRIDINE AT 473K

increase in the diffusivity of iso-octane in the catalyst due to the poisoning is mostly because of the decreased adsorption of iso-octane and may also be, to some extent, due to an increase in the surface diffusion because of the decrease in the energy (or heat) of adsorption, which is expected to increase the mobility of adsorbed iso-octane molecules.

2.3.3 Influence of coking

In this section the influence of coking on the heat of adsorption and diffusion of iso-octane in the meso- and macro-pores of the catalyst and on the activity of the catalyst in the iso-octane cracking, o-xylene isomerization and methanol-to-aromatics conversion reactions has been discussed.

2.3.3.1 Heat of Adsorption of Iso-octane on Coked Catalyst

The heat of adsorption of iso-octane on Pt.H-ZSM-5.Al_2O_3 catalyst coked to different extents has been estimated from the slope of the plots of log (V_R) versus $1/T_c$ where V_R is the corrected retention volume and T_c, the column temperature. These plots for the catalyst coked to different extents are shown in Fig. 2.7. The values of heat of adsorption of iso-octane on the catalyst with different extents of coke deposition are included in Table 2.3. The results (Table 2.3) reveal that the heat of adsorption and adsorption equilibrium constant of iso-octane on the catalyst increase with increasing the carbon content of the catalyst. This is expected mostly because of the creation of additional sites on the catalyst for the adsorption of iso-octane, due to the coke deposition. This is very much

consistent with observed large increase in the sites for pyridine chemisorption at < 573 K, due to coking.

2.3.3.2 Diffusion and Mass Transfer of Iso-octane in Coked Catalyst

The mass transfer term C has been estimated from the slopes of the linear plots of HETP versus linear gas velocity according to Equation (2.5). These plots for the catalyst with different extents of coke deposition are given in Figs. 2.10-2.12. The effective pore (meso- and macro-) diffusivity, D_p, at 473 K has been estimated from the mass transfer term using Equations (2.7) and (2.8). Values of the mass transfer term, distribution coefficient, apparent equilibrium constant and effective pore diffusivity are included in Table 2.3. It is observed that the mass transfer term and the apparent equilibrium constant increase with increasing the carbon content, while the distribution coefficient and effective pore diffusivity decrease with increasing the coke content of the catalyst. There are two factors contributing to the observed decrease in the effective pore diffusivity.

(i) The coke provides a large number of additional sites on the catalyst for the adsorption of iso-octane. This is indicated by the increase in the equilibrium constant and heat of adsorption of iso-octane. The increased adsorption of iso-octane is expected to cause retardation in the diffusion of iso-octane in the meso- and macro- pores of the catalyst. Thus the increased adsorption and heat of adsorption of iso-octane due to coking causes a decrease in the effective diffusivity. The

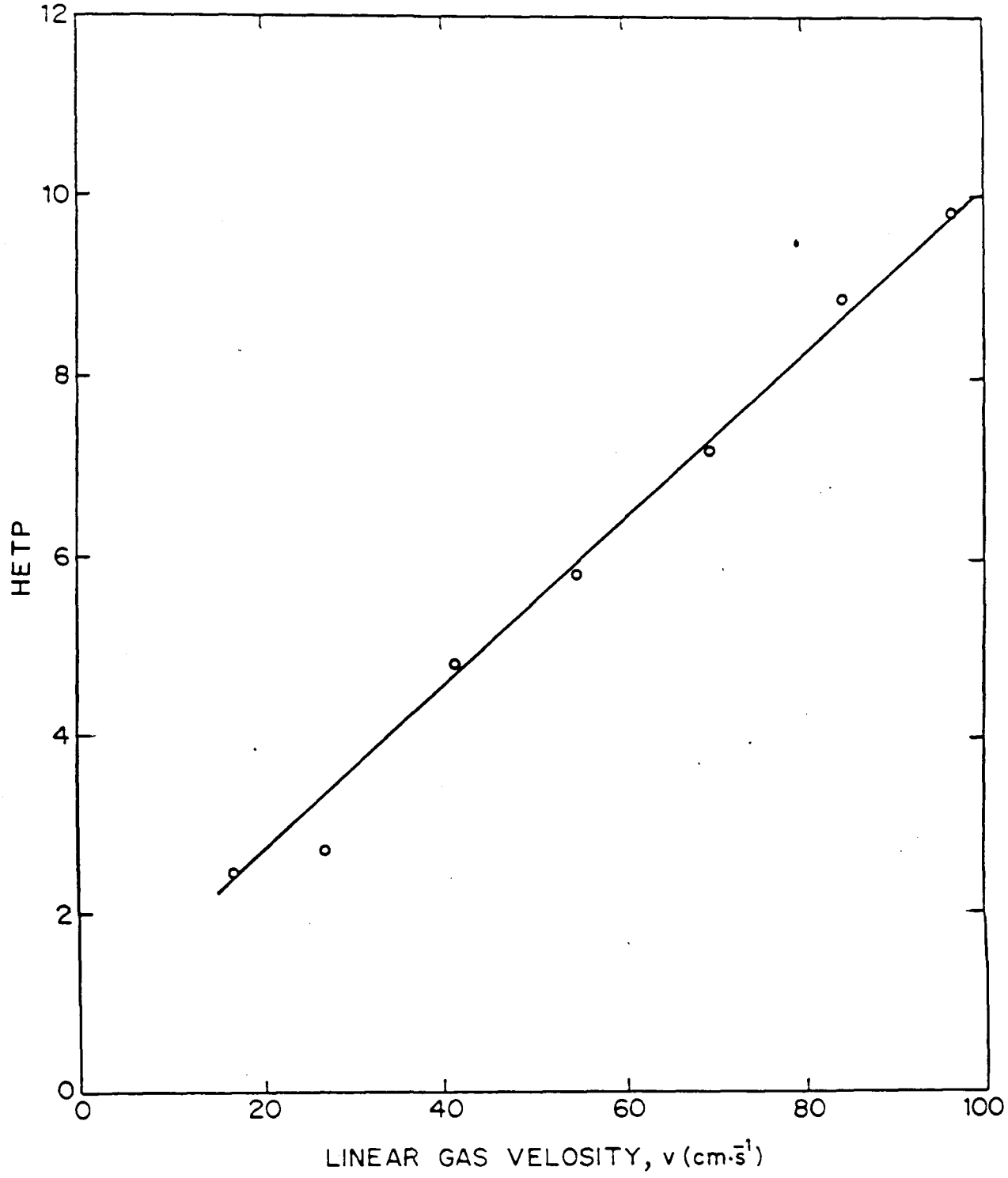

FIG.2·10: PLOT OF HETP vs v FOR THE CALCULATION OF MASS TRANSFER TERM C IN ISO-OCTANE ON Pt. H-ZSM-5 · Al_2O_3 (0·3 % C) AT 473K

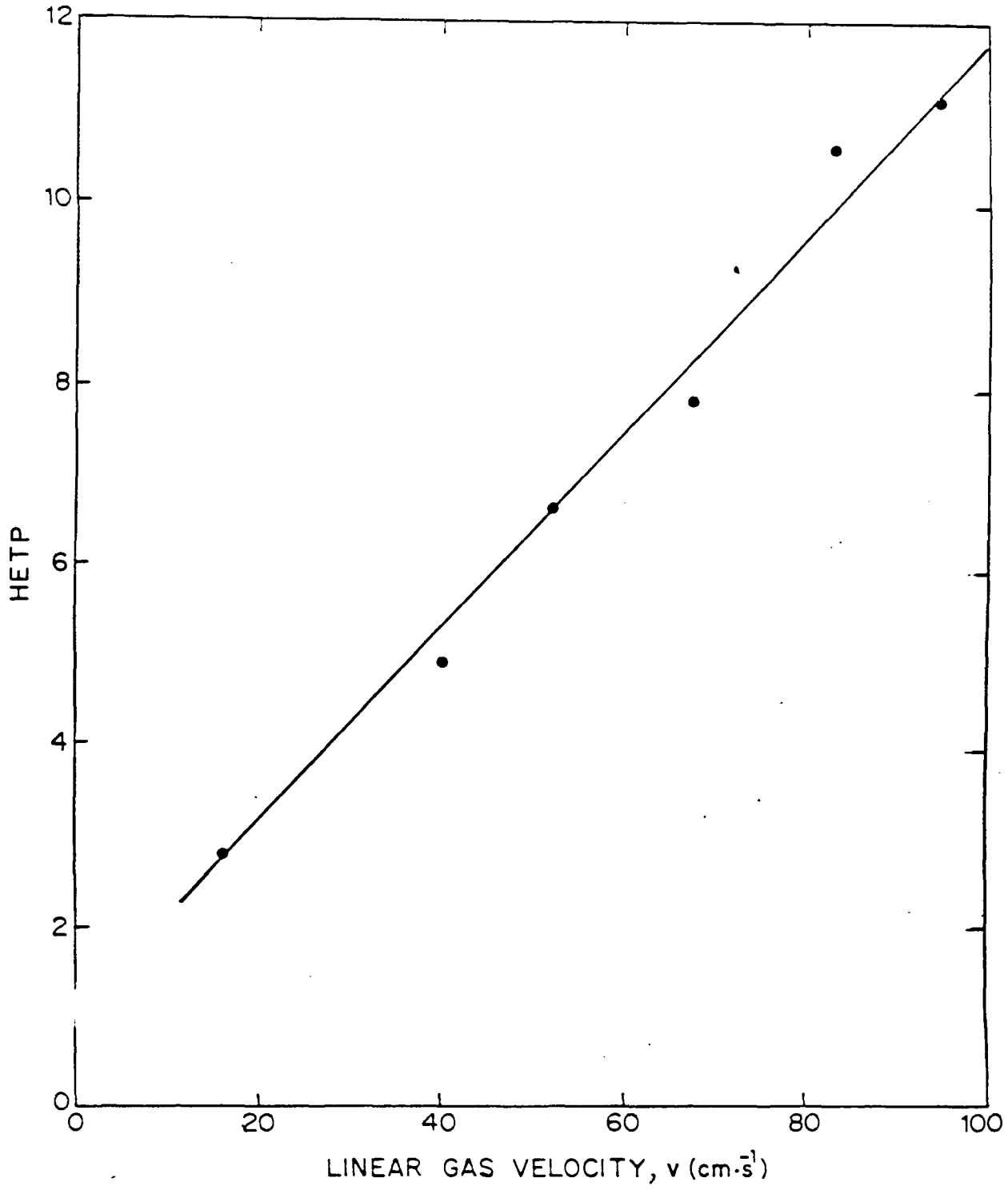

FIG.2·11: PLOT OF HEPT vs v FOR THE CALCULATION OF MASS TRANSFER TERM C OF ISO-OCTANE ON COKED Pt.H-ZSM-5·Al_2O_3 (0·4% C) AT 473 K

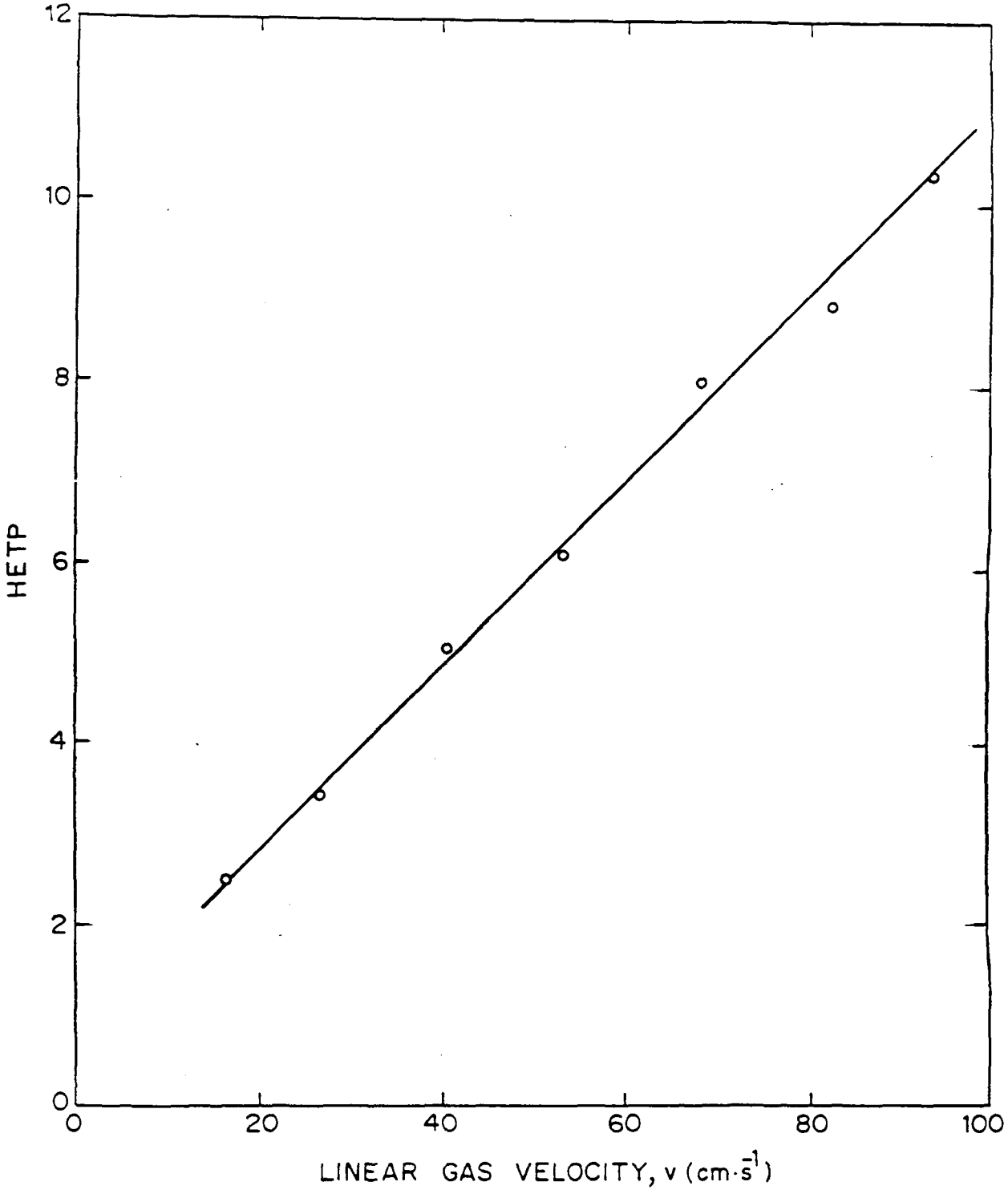

FIG.2·12: PLOT OF HETP vs v FOR THE CALCULATION OF MASS TRANSFER TERM C OF ISO-OCTANE ON COKED Pt. H-ZSM-5·Al_2O_3 (2·1% C) AT 473K

increased heat of adsorption is also expected to cause a decrease in the surface diffusivity of adsorbed iso-octane.

(ii) Coke deposited on the pore mouths, particularly of the mesopores, may offer some resistance to the diffusion of iso-octane in the catalyst, particularly in that coked to the largest extent. However, the comparison between the pore size distribution of the fresh and the coked (with 2.1 % carbon) catalysts show only a small effect of coking on the pore size distribution.

2.3.3.3 Catalytic Activity of Coked Catalyst

In order to find out the influence of coking on the catalytic activity and selectivity (or product distribution) of the Pt.H-ZSM-5.Al_2O_3 catalyst, the iso-octane cracking, o-xylene isomerization and methanol-to-aromatics conversion, which are acid catalyzed reactions, have been carried out, over the catalyst coked to different extents, in a pulse microreactor at 673 K.

Iso-octane Cracking

The data on the activity and selectivity in the iso-octane cracking over the catalyst coked to different extents are presented in Table 2.4. The iso-octane cracking activity decreases with increase in the extent of coke in the catalyst.

The iso-octane molecule, because of their bulkier size (critical molecular size = 0.7 nm) cannot penetrate the channels of the ZSM-5 zeolite (micropores) even at 673 K. Hence, the cracking reaction occurs only on the alumina and external

Table 2.4

Data on cracking of iso-octane over Pt.H-ZSM-5.Al_2O_3 coked to different extents

Reaction conditions: Amount of catalyst, 0.2g; H_2 flow rate, 8 $cm^3.min^{-1}$; pulse size, 2 µl; pressure, 205 kPa; temperature, 673 K.

	Fresh catalyst	Coked catalyst		
		0.3 % C	0.4 % C	2.1 % C
Conversion of iso-octane	44.0	14.0	10.8	9.9
Distribution of hydrocarbons (wt %)				
Iso-octane	56.0	86.0	89.2	90.1
Aliphatics	42.6	11.5	8.3	7.0
Aromatics	1.4	2.5	2.5	2.9
Total	**100.0**	**100.0**	**100.0**	**100.0**
Aromatics / Aliphatics (wt./wt.)	0.03	0.22	0.30	0.41

surface of the zeolite crystallites. It is well established [21,27] that the iso-octane cracking occurs essentially on strong acid sites. The decrease in the iso-octane cracking activity of the catalyst with increasing the extent of coke is due to the fact that the stronger acid sites (in the meso- and macro- pores) accessible for iso-octane are blocked by the coke. The decrease in the iso-octane cracking activity is very much consistent with the decrease in the strong acid sites (measured in terms of the chemisorption of pyridine at 673 K, Fig. 2.3) due to the coking. The increased resistance for the diffusion of iso-octane due to the coke deposition may also be responsible, to some extent, for the decreased iso-octane cracking activity by making the reaction diffusion controlled, particularly for the case of the highly coked catalyst. However this has not been confirmed in the present study by using the coked catalyst of different particle sizes. The results (Table 2.4) also show that the formation of aromatics relative to aliphatics (other than iso-octane) is increased with increasing the extent of coke. This may be due to the increased resistance to interparticle mass transfer due to coking. The aromatization of the iso-octane cracking products in the zeolite channels is expected to be favoured when the intercrystalline or particle mass transfer resistance is increased.

O-xylene Isomerization

The results of o-xylene isomerization at 673 K over the Pt.H-ZSM-5.Al_2O_3 catalyst coked to different extents are given in Table 2.5.

Table 2.5
Data on activity and product distribution in o-xylene isomerization over Pt.H-ZSM-5.Al_2O_3 coked to different extents

Reaction conditions: Amount of catalyst, 0.2g; H_2 flow rate, 80 $cm^3.min^{-1}$; pulse size, 2 µl; pressure, 205 kPa; temperature, 673 K.

	Fresh catalyst	Coked catalyst		
		0.3 % C	0.4 % C	2.1 % C
Conversion of o-xylene	32.0	34.6	41.9	22.8
Distribution of hydrocarbons (wt %)				
Aliphatics	0.5	1.4	5.4	0.8
Benzene	0.1	0.2	0.8	0.1
Toluene	0.9	1.2	3.0	0.6
p-Xylene	13.8	12.9	13.1	7.7
m-Xylene	15.9	18.2	17.7	13.1
o-Xylene	68.6	65.4	58.1	77.2
C_9^+ Aromatics	0.2	0.7	1.9	0.5
Total	**100.0**	**100.0**	**100.0**	**100.0**
p-X/m-X	0.86	0.71	0.74	0.59
Isomerization selectivity	95.3	89.9	73.5	91.2

The catalyst activity (i.e. conversion of o-xylene) passes through a maximum with the increase in the extent of coke deposition. The p- to m- xylene ratio for the coked catalysts is lower than that for the fresh catalyst. The isomerization selectivity is also decreased due to the coke deposition.

Both the beneficial and detrimental effects of coke deposition are reflected in the isomerization activity presented in Table 2.5. It has been reported [21] that the isomerization of o-xylene occurs also on the weak acid sites of the zeolites. In the present case, the formation of a large number of weaker acid sites due to coking has already been established by the pyridine chemisorption studies (Fig. 2.3). These weaker catalytically active centers present in the coke deposits are responsible for the enhancement in the isomerization activity of the catalyst due to coking at lower level of coke deposition (i.e. 0.3 or 0.4 wt.% carbon) on the catalyst. However when the extent of coke deposition is increased to 2.1% carbon, the catalytic activity of the coked catalyst is decreased below that of the fresh one.

In the earlier studies, an increase in the catalytic activity due to coke deposition has been observed for the hydrocarbon conversion reactions on $AlPO_4$-5 [22]. Also, earlier studies on zeolites [8] have indicated the possibility of existence of carbonium ion type active sites on coke, which can have both detrimental and beneficial effects on catalytic processes.

The decrease in the catalytic activity at the higher level of coke deposition (2.1 % carbon) on the catalyst is mostly because of two reasons.

(i) Because of blockage of some of the zeolite channels by strongly sorbed or occluded hydrocarbon molecules (this is supported by n.m.r. studies), thus making some of the active sites unavailable/inaccessible to o-xylene.

(ii) Because of an increase in the intracrystalline mass transfer resistance for o-xylene in the zeolite due to blockage of the zeolite channels due to strongly sorbed or occluded hydrocarbons, and deposition of coke on the external surface of zeolite crystallites, thus blocking partially or completely the channel openings.

The results (Table 2.5) show a decrease in the p-xylene to m-xylene ratio (i.e. in the shape selectivity) due to the coke deposition on the catalyst. This is to be expected because, the isomerization reaction, to an appreciable extent , occurs also on the active sites created due to coke deposition in the meso- and macro- pores of the catalyst.

Methanol-to-Aromatics Conversion

The influence of coke deposition on the formation of aromatics and their distribution in the conversion of methanol-to-aromatics on the catalyst at 673 K is shown in Table 2.6. It is very interesting to note that the aromatization in the methanol conversion is strongly influenced by the coking; the extent of aromatization decreases drastically with increase in the coke deposition. The distribution of aromatics formed in the

Table 2.6

Data on activity and product distribution in methanol-to-aromatics conversion on Pt.H-ZSM-5.Al_2O_3 coked to different extents

Reaction conditions: Amount of catalyst, 0.2 g; H_2 flow rate, 80 $cm^3.min^{-1}$; pulse size, 2 µl; pressure, 205 kPa; temperature, 673 K.

	Fresh catalyst	Coked catalyst		
		0.3 % C	0.4 % C	2.1 % C
Conversion of mehtanol (%)	100	100	100	100
Concentration of aromatics in the hydrocarbons(%)	21.0	12.0	10.7	5.2
Distribution of aromatics (wt. %)				
Benzene	2.1	5.0	11.2	11.7
Toluene	9.1	7.5	9.3	19.4
Ethyl benzene	2.9	1.7	1.9	3.9
p-Xylene	16.9	18.3	15.0	12.6
m-Xylene	19.0	21.7	18.7	17.9
o-Xylene	15.0	13.3	15.0	15.1
(Total xylenes)	(50.9)	(53.3)	(48.7)	(45.6)
C_9^+ Aromatics	35.0	32.5	28.9	19.4
Total	**100.0**	**100.0**	**100.0**	**100.0**
p-X/m-X	0.89	0.84	0.80	0.70

methanol conversion reaction is also strongly influenced by the coking. Also, the p-xylene/m-xylene ratio is decreased with increasing the coke deposition.

The large decrease in the aromatization activity of the catalyst due to the coking is attributed to the decrease in the strong acid sites (measured in terms of chemisorption of pyridine at 673 K) due to the coke deposition. The aromatization reaction occurs on strong acid sites [21,23,24] and therefore the weaker acid sites created due to the coke deposition in the meso- and macro- pores of the catalyst are not active in the aromatization. However, on these weaker sites xylene isomerization can occur, which leads to a decrease in the p-xylene/m-xylene ratio in the products for the coked catalysts.

2.4 CONCLUSIONS

The following conclusions have been drawn from the present investigation.

1. The poisoning of the Pt.H-ZSM-5.Al_2O_3 with pyridine (by its chemisorption at 523 K) causes a very significant decrease in the adsorption equilibrium constant and heat of adsorption of iso-octane, but a large increase in its effective diffusivity in the meso- and macro- pores of the catalyst.

2. The coke deposited on the catalyst is composed of condensed aromatics, methyl substituted aromatics and methyl substituted aliphatics. The ratio of aliphatic to aromatic coke increases with increase in the extent of coke deposition on the catalyst. The condensed aromatics are expected to be located in the meso- and macro- pores whereas methyl aromatics and

aliphatics are expected to be located in the zeolite channels as strongly sorbed or occluded hydrocarbon species.

3. The acidity and acid strength distribution on the catalyst are strongly influenced due to the coke deposition. The strong acid sites (measured in terms of pyridine chemisorbed at 673 K) are decreased markedly whereas the weaker acid sites (measured in terms of pyridine chemisorbed at < 573 K) are increased due to the coke deposition; the increase in the weaker sites is larger for the larger coke deposition.

4. The coke deposition causes an increase in the adsorption equilibrium constant and heat of adsorption of iso-octane indicating creation of new sites in the meso- and macro-pores for adsorption of iso-octane due to the coking of the catalyst.

5. The effective intercrystalline diffusivity of iso-octane in the coked catalysts is decreased depending upon the extent of coke deposition.

6. The catalytic activity/selectivity in the iso-octane cracking, o-xylene isomerization and methanol-to-aromatics conversion reactions is strongly influenced by the coke deposition. When the extent of coke on the catalyst is increased, (i) the iso-octane cracking activity is decreased due to deactivation of intercrystalline strong acid sites, (ii) the xylene isomerization activity is initially increased (for lower coke deposition) and then decreased (for higher coke deposition) due to creation of new active sites on coke and the increased mass transfer resistance, and the p-selectivity is

decreased because of the occurrence of part of the isomerization reaction on the newly created active sites on the intercrystalline coke and (iii) the extent of aromatization and p-selectivity in the methanol-to-aromatics conversion is decreased due to the deactivation of strong acid sites and the occurrence of xylene isomerization on the new active sites present on the intercrystalline coke respectively.

REFERENCES

1. Chang, C.D., Catal. Rev. Sci. Eng., **25**, 1 (1983)
2. Chang, C.D., Catal. Rev. Sci. Eng., **26**, 323 (1984)
3. Scott, J. (Ed.), 'Zeolite Technology and Applications - Recent Advances', Noyes Data Corp., NJ, (1980)
4. Kaeding, W.W., Barik, G.C. and Wu, M.M., Catal. Rev. Sci. Eng., **26**, 597 (1984)
5. Palekar, M.G. and Rajadhyaksha, R.A., Catal. Rev. Sci. Eng., **28**, 371 (1986)
6. Doelle, H.J., Heering, J., Riekert, L. and Marosi, L., J. Catal., **71**, 27 (1980)
7. Heering, J., Kotter, M. and Riekert, L., Chem. Eng. Sci.,**37**, 581 (1982)

7a. Choudhary, V.R. and Akolekar, D.B., J.Catal., **116**, 130 (1989)

8. Derouane, E.G., 'Catalysis by Acids and Bases', Ed. B.Imelik et al., Elsevier Science Publishers B.V., Amsterdam., 221 (1985)

8a. Guisnet, M. and Magnoux, P., Appl. Catal., **54**, 1 (1989)

9. Choudhary, V.R. and Nayak, V.S., Appl. Catal., **4**, 31 (1982)
10. Choudhary, V.R., J. Chromatogr., **268**, 207 (1983)
11. Choudhary, V.R. and Doraiswamy, L.K., Ind. Eng. Chem. Prod. Res. Dev., **10**, 218 (1971)
12. Van Deemter, J.J., Zuiderweg, F.J. and Kinkenberg, A., Chem. Eng. Sci., **5**, 271 (1956)

13. Mc Nair, H.M. and Bonelli, E.J., 'Basic Gas Chromatography', Varian Instruments Division, California (1969)

14. Hawkes, S.J., J. Chromatog., **68**, 1 (1972)

15. Gidding, J.C., Dynamics of Chromatography, Marcel Dekker, N.Y., (1965)

16. Eberly (Jr.), P.E., Ind. Eng. Chem. Fundam., **8**, 25 (1969)

17. Eberly (Jr.), P.E. and Spencer, E.M., Trans. Faraday Soc., **56**, 289 (1961)

18. Weitkamp, J. and Maxiner, S., Zeolites, **7**, 6 (1987)

19. Carlton, L., Copperthwaite, R.G., Hutchings, G.J. and Reynhardt, E.C., J. Chem. Soc. Chem. Commun., 1008 (1986)

20. Dejaifve, P., Auroux, A., Gravelle, P.C., Vedrine, J.C., Gabelica, Z. and Derouane, E.G., J. Catal., **70**, 123 (1981)

21. Choudhary, V.R. and Akolekar, D.B., J. Catal., **125**, 143 (1990)

22. Nayak, V.S. and Choudhary, V.R., J. Catal., **105**, 416(1987)

23. Nayak, V.S. and Choudhary, V.R., J. Catal., **81**, 26 (1983)

24. Nayak, V.S. and Choudhary, V.R., Appl. Catal., **9**, 251 (1984)

25. Choudhary, V.R., and Nayak, V.S., Zeolites, **5**, 325 (1985)

26. Akolekar, D.B., 'Sorption, Diffusion and Catalytic Reactions on Zeolites and Zeolite - like Materials.', PhD thesis, Univ. Poona, Pune. (1987)

27. Choudhary, V.R., Zeolites, **7**, 272 (1987)

Appendix 2.1

Data on irreversible adsorption of pyridine on fresh and coked Pt.H-ZSM-5.Al_2O_3

Catalyst	Amount of pyridine adsorbed irreversibly, q_i ($mmol.g^{-1}$)						
	373 K	423 K	473 K	523 K	573 K	623 K	673 K
Fresh	0.150	0.076	0.062	0.056	0.053	0.050	0.048
Coked (0.3 % C)	0.378	0.268	0.201	0.155	0.129	0.097	0.087
Coked (0.4 % C)	0.177	0.132	0.098	0.075	0.054	0.035	0.015
Coked (2.1 % C)	0.540	0.340	0.223	0.145	0.093	0.045	0.006

Appendix 2.2

Data on STD of pyridine on fresh and coked Pt.H-ZSM-5.Al_2O_3

Catalyst	Amount of pyridine desorbed, q_d ($mmol.g^{-1}$)						
	373-423 K	423-473 K	473-523 K	523-573 K	573-623 K	623-673 K	> 673 K
Fresh	0.074	0.014	0.006	0.004	0.002	0.002	0.048
Coked (0.3 % C)	0.110	0.067	0.046	0.026	0.032	0.010	0.087
Coked (0.4 % C)	0.045	0.034	0.023	0.021	0.019	0.020	0.015
Coked (2.1 % C)	0.200	0.120	0.078	0.052	0.048	0.039	0.006

CHAPTER - 3

SORPTION OF METHANE, ETHANE, ETHYLENE, CARBON DIOXIDE AND WATER IN MEDIUM AND LARGE PORE ZEOLITES

3 SORPTION OF METHANE, ETHANE, ETHYLENE, CARBON DIOXIDE AND WATER IN MEDIUM AND LARGE PORE ZEOLITES

3.1 INTRODUCTION

3.1.1 Objectives/Scope

Natural gas is among the largest of the World's primary energy resources today. Natural gas finds widespread application in various sectors over and above its primary use for meeting energy needs of the industrial, commercial and domestic sectors. These are in the areas of feed stock for fertilizers, petrochemical and non-petrochemical industries, power generation and transport fuel. Depending upon the quality and specific application/use, several purification and separation operations are required to be performed on natural gas. These involve absorption, cryogenic distillation, extraction, centrifugal separation, condensation, adsorption etc. Many of these processes are highly energy intensive, and with escalating energy costs, there is a need to look for energy efficient alternatives. Although adsorption separation process is not yet commonly used for the separation of natural gas components, it has a high potential for separating the hydrocarbons in an energy efficient manner.

Recently (since 1985), extensive efforts have been put world wide for developing energy efficient and commercially feasible processes for indirect or direct conversion of methane to value added chemicals like ethylene and propylene (which are the key stones to petrochemical industry), and also for easily transportable and value added products such as methanol and

liquid hydrocarbon fuels (gasoline, middle distillates and diesel). In the oxidative coupling of methane, the products ethane and ethylene have to be separated before they can be used as industrial feed stocks. As the concentration of C_2 hydrocarbons in the product stream is low, conventional methods of separation (for example cryogenic methods) are not economic. Here again, adsorption processes can be used as a commercially viable separation method due to its highly selective nature and energy efficient operation.

In recent years, adsorptive separation processes, particularly involving the use of zeolites have been gaining more and more importance. It is possible to separate individual natural gas components very efficiently using pressure swing adsorption (PSA) or temperature swing adsorption (TSA) or combined pressure swing and temperature swing methods. These are also expected to be less energy intensive. Hence there is a need for the development of commercial processes for the separation of C_2 hydrocarbons from natural gas and also from the product stream of oxidative coupling of methane based on adsorption technology. The search for a suitable adsorbent is the first step in the development of any adsorption separation process. It is often necessary to screen a range of possible adsorbents and the information about the equilibrium sorption capacity at various temperatures and pressures and the adsorption isotherm data are required for this preliminary screening. The data on heat of sorption is also important as it indicates the ease with which the adsorbent can be regenerated.

The major components of natural gas and/or the product stream of the adsorptive coupling of methane are methane, ethane, ethylene, carbon dioxide and lesser amounts of C_2 hydrocarbons. There is a large amount of data available in literature on the adsorption of methane, ethane, ethylene and carbon dioxide on zeolites (Tables 3.1-3.5). From the literature given in the tables it can be seen that adsorption data are available only for a few selected zeolites and moreover from the available data, it is not possible to make direct comparison of the zeolites for their sorption properties for the various sorbates. It is therefore very essential to collect sorption data for all the sorbates under consideration on the potential zeolite adsorbents under similar experimental conditions for the purpose of comparison. Hence the present study was undertaken with the following objectives:

(i) To perform a systematic and quick screening of a large number of medium and large pore zeolites (viz. ZSM-5, H-Na-ZSM-5, ZSM-8, Na-H-ZSM-8, HY, NaY, CeNaY, KL, HKL, HM, NaM, NaX, Silicalite, and $AlPO_4$-5) for their suitability as adsorbents for the adsorptive separation of methane, ethane, ethylene and carbon dioxide from their mixture using the gc pulse technique.

(ii) To collect the adsorption isotherm data of the above sorbates on potential zeolite adsorbents for comparing their sorption properties.

3.1.2 Gas Chromatographic Techniques in the Study of Adsorption

Gas chromatographic methods have been successfully employed during the past couple of decades for the study of

Table 3.1

Literature on the adsorption of CH_4 and C_2H_6 on NaX zeolite

Zeolite	Adsorbate	Method	Pressure (Pascals)	Temperature (K)	Heat of sorption ($kCal.mol^{-1}$)	Adsorption equil. const.	Remarks	Ref.
NaX	CH_4	-	$0.1\text{-}2.0\times10^7$	120-600	-	-	Langmuir Isotherm, discontinuity in critical region	1
	CH_4	volumetric	$0\text{-}6.7\times10^4$	273,300	4 - 4.5	-	-	2
	CH_4	GC	-	298-353	4.5	-	-	3
	CH_4	GC	$0\text{-}1.34\times10^5$	298-673	4.2	-	only heat of sorption data	4
	CH_4	volumetric	$0\text{-}10^7$	196-243	-	-	generalized correlation curve given	5a
	CH_4	GC	$0\text{-}7\times10^6$	288-388	-	-	adsorption isotherm given	5b
	CH_4	volumetric	$0\text{-}1.5\times10^6$	275-350	-	-	adsorption equilibrium data given	5c
	C_2H_6	volumetric	$0\text{-}1.38\times10^5$	273-373	heat of sorption for 3 models given	-	-	6
	C_2H_6	volumetric	$0\text{-}1.07\times10^5$	273-423	6.1	4.92	Virial equation	7
	C_2H_6	volumetric	$0\text{-}6.67\times10^4$	273-307	6-7.5	-	-	2
	C_2H_6	GC	-	333-433	6.2	-	-	3
	C_2H_6	-	-	-	6.2	-	-	8
	C_2H_6	GC tracer pulse	$0\text{-}2\times10^5$	298	-	-	method development	9
	C_2H_6	volumetric	$0\text{-}1.38\times10^5$	298-323	-	-	-	10
	C_2H_6	GC	$0\text{-}1.33\times10^5$	298-673	6.0	-	adsorption isotherm given	4

Table 3.2

Literature on the adsorption of C_2H_4 and CO_2 on NaX zeolite

Zeolite	Adsorbate	Method	Pressure (Pascals)	Temperature (K)	Heat of sorption ($kCal.mol^{-1}$)	Adsorption equil. const.	Remarks	Ref.
	C_2H_4	thermal desorption spectroscopy	-	120-250	8.9	-	-	11
	C_2H_4	--"--	-	114	8.7	-	-	12
	C_2H_4	volumetric	$0-1.38x10^5$	273-373	-	-	diffusion models	6
	C_2H_4	volumetric	$0-1.07x10^5$	273-423	8.9	2.09	Virial equation	7
	C_2H_4	GC	-	353-453	9.0	-	-	3
	C_2H_4	GC tracer pulse	$0-2.4x10^5$	298	-	-	method development	9
	C_2H_4	volumetric	$0-1.38x10^5$	298-323	-	-	-	10
	C_2H_4	GC	$0-1.33x10^5$	298-673	8.4	-	adsorption isotherm	4
	C_2H_4	-	$0-1.07x10^5$	323-363	9.2	-	-	8
NaX								
	CO_2	volumetric	$0-1.38x10^5$	273-373	table of heat of sorption data available	-	-	6
	CO_2	volumetric	$0-6.6x10^4$	303	-	-	-	13
	CO_2	volumetric	$0-8.53x10^4$	303-423	11.0	53.7(303K) 1710.0(373K)	virial equation	14

Table 3.3

Literature on the adsorption of CH_4, C_2H_4 and CO_2 on NaY zeolite

Zeolite	Adsorbate	Method	Pressure (Pascals)	Temperature (K)	Heat of sorption ($KCal.mol^{-1}$)	Adsorption equil. const.	Remarks	Ref.
NaY	CH_4	gravimetric	$0-2.66x10^3$	294	4.05-4.30	-	-	15
	C_2H_4	thermal desorption spectroscopy	-	-	10.4	-	-	16
	CO_2	volumetric	$0-1.47x10^4$	273-313	7.6	-	-	17
	CO_2	volumetric	$0-8.5x10^4$	303-423	-	1660 (303&373K)	virial equation	14

Table 3.4

Literature on the adsorption of CO_2 and light hydrocarbons on mordenite

Zeolite	Adsorbate	Method	Pressure (Pascals)	Temperature (K)	Heat of sorption ($KCal.mol^{-1}$)	Adsorption equil. const.	Remarks	Ref.
NaM	CO_2	volumetric, calorimetric thermogravimetric	$1-5.06\times10^6$	196-433	-	-	-	18
HM	CO_2	gravimetric	$0-9.3\times10^4$	273	-	-	spring balance	19
.	CO_2	volumetric	$0-8.5\times10^4$	303-323	11.1	-	-	14
.	CO_2	volumetric	$0-6.6\times10^4$	303-463	10.8	-	-	20
.	CO_2	volumetric	$0-3.0\times10^5$	282-323	-	-	adsorption isotherm	21a
H-Zeolon	CH_4	volumetric	$0-10^7$	196-303	-	-	-	5
HM	CH_4	GC	-	303-623	6.1+0.5	-	GC values compared with that from adsorption potential calculations	21b
HM	C_2H_6	GC	-	--"--	8.0+0.3	-	--"--	21b

Table 3.5

Literature on the adsorption of CO_2 and light hydrocarbons on Silicalite and $AlPO_4$-5

Zeolite	Adsorbate	Method	Pressure (Pascals)	Temperature (K)	Heat of sorption ($KCal.mol^{-1}$)	Adsorption equil. const.	Remarks	Ref.
Silicalite	CH_4	theoretical	-	273-423	4.3	-	Monte-Carlo simulation	22
.	CH_4	calorimetric	-	296	5(exptal.) 9.4(theoritical)	-	initial heat of sorption	23
.	CH_4	GC	-	293-403	4.76	40	moment analysis	24
.	CH_4	theoretical	-	-	5	-	initial heat of sorption, molecular statistical calc.	25a
.	CH_4	volumetric	$1.2x10^4$-$1.6x10^6$	275-350	-	-	Toth equation	25b
Silicalite	C_2H_6	theoretical	-	-	7.14	-	molecular statistical calc.	25a
.	C_2H_6	volumetric	$2.3x10^2$-$3.3x10^5$	275-350	-	-	Toth equation	25b
Silicalite	CO_2	theoretical	-	-	6.67	-	molecular statistical calc.	25a
$AlPO_4$-5	CH_4	theoretical	-	-	4.4	-	initial heat of sorption	26
$AlPO_4$-5	C_2H_6	experimental & theoretical	-	301	5.71(exptal.) 6.86(theoretical)	-	initial heat of sorption	26

adsorption, diffusion and mass transfer in solid materials. The application of gaschromatographic techniques for the determination of physico-chemical properties of adsorbents and in catalysis has been reviewed by Choudhary and Doraiswamy [27].

The heat of adsorption can be obtained from the chromatographic retention time data using the relationship derived by Eberly, Jr. and Spencer [28].

$$\beta = t_m U_e / L = V_R / V_P \qquad (3.1)$$

where the constant β can be treated as the thermodynamic equilibrium constant [29], t_m is the corrected retention time, U_e the superficial gas velocity, L the length of the column, and V_P and V_R are the volume of the adsorbent packing and the corrected retention volume respectively. V_R is calculated using the equation

$$V_R = (t_r - t_d) F (T_c / T_F) \qquad (3.2)$$

where t_r and t_d are the retention times for the adsorbate and the non-adsorbate, T_c the column temperature and T_F, the temperature at which the flow rate F is measured. By making appropriate substitution in Equation (3.1), the following equation can be obtained.

$$\log V_R = a - \Delta H / (2.303 R T_c) \qquad (3.3)$$

where 'a' is a constant, ΔH the heat of adsorption, R the gas constant and T_c the column temperature.

Recently, Carrott and Sing [30] have utilized the gc heat of adsorption data to elucidate structural information and characterize microporous carbons. Nikitin et al. [31] have used a similar technique to study the contribution of specific interactions to the total energy of adsorption of some aromatic molecules on silica. In this chapter we are using the heat of sorption and equilibrium constant, measured by the gc pulse method, as the basis for the quick initial screening of a number of zeolites (medium and large pore) for their suitability in the adsorptive separation of light hydrocarbons.

3.1.3 Sorption in Zeolites and Zeolite-like Materials

During the adsorption process, the micropores in the zeolites are filled and emptied reversibly. For this reason, adsorption in zeolites is considered to be a matter of pore filling, and the usual concepts of surface area as they are applied to other adsorbents are not applicable here. Again, in these solids the equilibrium adsorption corresponds to the sorbate concentration around the crystals and not the intracrystalline concentration. Thus, the usual concepts of adsorption at the equilibrium sorbate concentration above the solid surface is not valid. It is therefore more appropriate to refer to the uptake of sorbate in zeolites and zeolite-like materials as sorption than adsorption. This sorption depends on the equilibrium pressure and temperature, and also on the nature of the sorbate and the micropores.

3.1.3.1 Measurement of Adsorption Isotherms

The adsorption methods are generally divided into two groups - dynamic and static methods. Dynamic methods are exemplified by chromatographic determination of isotherms whereas static measurements are normally made by volumetric or gravimetric techniques. For sorption in zeolites, isotherms are commonly collected by the gravimetric method due to its inherent advantages like the simplicity, accuracy etc.

The earliest work on the gravimetric measurement of sorption is the McBain sorption balance [38]. There have been several modifications of this balance, and analytical balances have also been modified for gravimetric measurements [39, 40, 41a]. We have developed a simple apparatus (described later) for the gravimetric measurement of adsorption isotherms.

3.1.3.2 Isosteric Heat of Sorption

The isosteric heat of sorption is derived from sorption isosteres. It can be obtained from a plot of the logarithm of pressure versus the reciprocal of the intracrystalline sorbate concentration in the zeolite by the Clausius-Clapeyron equation [41b].

$$Q_a = -R\,(\partial(\ln P)/\partial(1/T))_q \qquad (3.4)$$

$$\text{or} \quad \log P = E - Q_a/(2.303RT) \qquad (3.5)$$

$$\text{or} \quad Q_a = (2.303RT_1T_2/(T_1-T_2))\log(P_1/P_2) \qquad (3.6)$$

The isosteric heat of sorption Q_a in zeolites generally depends on the intracrystalline sorbate concentration [41b].

3.1.3.3 Sorption Isotherm Equations

Several attempts have been made to derive a standard sorption equation which can satisfy the data on sorption in zeolites under all conditions. Although many of these equations have some degree of broad applicability, no universal adsorption equation has been arrived at. Table 3.6 gives a list of the model isotherm equations attempted in this work to fit the sorption data.

3.2 EXPERIMENTAL

3.2.1 Gases and Materials

Methane : High purity (>99.9%), obtained from Matheson, U.S.A.

Ethylene : High purity (>99.5%), obtained from AIRCO Industrial gases, U.S.A.

Ethane : High purity (>99.95%), obtained from Air-Liquid, France.

Nitrogen : IOLAR Grade II, obtained from Indian Oxygen Ltd., Bombay.

CO_2, Helium : Obtained from Indian Oxygen Ltd., Bombay.

Zeolites

The chemical composition (viz. Si/Al ratio, degree of cation exchange and unit cell composition) of the zeolites is given in Table 3.7.

H-ZSM-5

This was obtained by deammoniating NH_4-ZSM-5 (Si/Al = 31.1, Na/Al = 0.01, prepared by Nayak [42]) at 773 K in a flow

Table 3.6

Model isotherms for single component adsorption

1. Langmuir isotherm [32]

$$\theta = q/q_m = kP/(1+kP)$$

2. Freundlich isotherm [33]

$$q = kP^c$$

3. Sips isotherm [34]

$$\theta = q/q_m = (kP/(1+kP))^c$$

4. Toth isotherm [35]

$$\theta = q/q_m = P/(k+P^c)^{1/c}$$

5. Dubinin - Polanyi isotherm [36]

$$\log q = C - D(\log(P_s/P))^2$$

6. Dubinin - Astakhov isotherm [37]

$$\ln q = A - B(\ln(P_s/P))^C$$

Table 3.7

Chemical composition of the zeolites

Zeolite	Si/Al	Degree of NH_4^+-, H^+- or Ce^{+3}- exchange	Unit cell composition
H-ZSM-5	31.1	0.99	$H_{2.98}Na_{0.01}(AlO_2)_{2.99}(SiO_2)_{93.01}.nH_2O$
Na-H-ZSM-5	31.1	0.45	$H_{1.34}Na_{1.65}(AlO_2)_{2.99}(SiO_2)_{93.01}.nH_2O$
H-Na-ZSM-8	29.6	0.96	$H_{3.01}Na_{0.13}(AlO_2)_{3.14}(SiO_2)_{92.86}.nH_2O$
H-Na-ZSM-8	29.6	0.08	$H_{0.25}Na_{2.89}(AlO_2)_{3.14}(SiO_2)_{92.86}.nH_2O$
HM	6.5	0.97	$H_{7.8}Na_{0.2}(AlO_2)_{8.0}(SiO_2)_{51.6}.26.3H_2O$
NaM	5.5	0.07	$H_{0.6}Na_{7.4}(AlO_2)_{8.0}(SiO_2)_{44.3}.23.0H_2O$
NH_4Y	2.4	0.92	$(NH_4)_{51.5}Na_{4.5}(AlO_2)_{56.0}(SiO_2)_{136.0}.nH_2O$
NaY	2.4	-	$Na_{56}(AlO_2)_{56}(SiO_2)_{136}.nH_2O$
CeNaY	2.4	0.46	$Ce_{8.6}Na_{30.2}(AlO_2)_{56}(SiO_2)_{136}.nH_2O$
CeNaY	2.4	0.72	$Ce_{13.5}Na_{15.5}(AlO_2)_{56}(SiO_2)_{136}.nH_2O$
KL	2.8	0.07	$K_{8.761}H_{0.624}(AlO_2)_{9.385}(SiO_2)_{26.6}.nH_2O$
NaX	1.3	-	$Na_{83.12}(AlO_2)_{83.12}(SiO_2)_{108.88}.nH_2O$

of nitrogen (10 $cm^3.min^{-1}$) passing through the zeolite bed for 4 h. The preparation and characterization of NH_4-ZSM-5 have been described elsewhere [42,43].

H-Na-ZSM-5

H-Na-ZSM-5 (degree of H^+ exchange = 0.45) was prepared by exchanging the H-ZSM-5 with 1 M $NaNO_3$ solution at 353 K eight times. The first five exchanges were for 2 h each and next three exchanges were for 4 h each. After the exchange, the zeolite was washed with deionized water, dried at 393 K for 4 h and calcined in air at 773 K for 12 h.

Na-H-ZSM-8

Na-H-ZSM-8 (H^+ exchange 0.96 and 0.08) were obtained by repeatedly exchanging the calcined Na-H-ZSM-8 zeolite (prepared by Akolekar [44]) with 0.1 M HCl at 353 K. After the H^+ exchange, the zeolite was washed with deionized water, dried in air at 393 K for 12 h, pressed binder-free, crushed to particles of 0.2-0.3 mm size and finally calcined in air at 813 K for 12 h. The preparation and characterization of Na-H-ZSM-8 have been described elsewhere [44].

Mordenites

Commercial grade synthetic HM (Zeolon 900 H) and NaM (Zeolon 900 Na) of particle size 20-50 mesh were obtained from Norton Co., U.S.A.

Silicalite-I

It was prepared without adding aluminium chloride in the synthesis mixture (prepared by Akolekar [44]). The crystals

were filtered, washed thoroughly with distilled - deionized water, finally dried in an air oven at 393 K for 24 h and calcined at 813 K for 12 h in a flow of nitrogen. It was further treated with 0.5 M HCl, washed and dried at 813 K for 12 h before use. The synthesis and characterization of the silicalite (S-8) are given by Akolekar [44].

$AlPO_4$-5

$AlPO_4$-5 was obtained by removing the organic template from Pr_3N-$AlPO_4$-5 (prepared by Akolekar [44]) by heating it in air at 813 K for 12 h. The synthesis of Pr_3N-$AlPO_4$-5 and the detailed characterization of $AlPO_4$-5 are given elsewhere [44, 45].

NaY

NaY zeolite was procured from Union Carbide (Linde Division), U.S.A. The Si/Al ratio and the unit cell composition of the zeolite are given in Table 3.7. The zeolite was pelletized binder-free, and crushed to particles of 0.2-0.3 mm size.

NH_4Y

This was prepared by Choudhary and Pataskar [46] by repeatedly exchanging NaY (obtained from Union Carbide, U.S.A.) with 0.5 M ammonium nitrate solution at 353 K. The exchanged zeolite was thoroughly washed with deionized water and dried at 393 K in air for 4 h. The crystallinity of the zeolite was not changed significantly after the NH_4 - exchange. This was treated *in situ* at 623 K for 2 h in a flow of helium to get HY zeolite.

CeNaY

Samples of zeolite CeNaY (Ce^{+3} exchange : 46% and 72%) were provided by Prof. J. Weitkamp (University of Oldenburg, W.Germany). These were prepared by repeatedly exchanging the Na-form of the zeolite with cerium nitrate solution at 353 K, washing the exchanged zeolites with deionized water and drying in air at 383 K. These zeolites have been thoroughly characterized earlier by Choudhary and coworkers [47, 48].

KL, HKL

Zeolite KL (Laposil 200 series obtained from Laporte, U.K.) has been pelletized binder-free, crushed and particles of 0.2-0.3 mm were taken. HKL was prepared by exchanging KL with 0.1 M HCl, washing the exchanged zeolite repeatedly with deionized water and drying in air at 383 K.

NaX

NaX (RD 1097/88. fine powder, Si/Al = 1.3) was obtained from Laporte, U.K. It was pelletized binder-free, crushed to particles of 0.2-0.3 mm size.

SAPO-5

SAPO-5 (provided by Dr. K.R.Kamble, Inorganic Chemistry Division, NCL) was prepared by adding 1.5 moles of Et_3N to a homogeneous gel containing 1 mole of o-phosphoric acid, 40-60 moles of water, 1 mole of pseudobhomite and 1 mole of microfine silica. The pH of the gel was about 3-4. The gel was transferred to a ss autoclave and was kept in the oven at

473 K for 48 h. to get the crystallized product which was characterized by XRD.

3.2.2 Measurement of Adsorption Equilibrium Constant and Heat of Sorption at Near Zero Coverage by GC Pulse Technique

The gc pulse data have been collected using CHEMITO (Toshiniwal-Dani) gas chromatograph with thermal conductivity detector (TCD). The experimental setup used for the gc pulse technique is shown schematically in Fig. 3.1a.

The adsorbent was packed in a ss column 15 cm long and 2 mm i.d. The outlet of the column was connected to the TCD and the inlet to the injection port using a 1.6 mm o.d. ss connecting tube. Helium of flow rate 10 $cm^3.min^{-1}$ was used as the carrier gas for all the experiments. The pressure drop across the zeolite column was negligibly small. The sample gases were diluted with the carrier gas to a concentration of 2-3 % with the help of flow control valves. The flow rate of the gas through the gas sampling valve was 20 $cm^3.min^{-1}$.

Adsorbents of particle size 0.2-0.3 mm were used for the experiments. The zeolite in the column was pretreated *in situ* at 623 K for 2 h in a flow of helium before the start of each experiment and cooled down to 313 K. The column was heated from 313 to 573 K in increments of 10 K and at each temperature, a gas sample pulse of 0.3 ml was injected into the column. The chromatograms were recorded using a Spectra-Physics integrator. At each temperature, a pulse of nitrogen (non-adsorbate) was injected into the column in the same manner as that of the adsorbate and its chromatogram was also recorded.

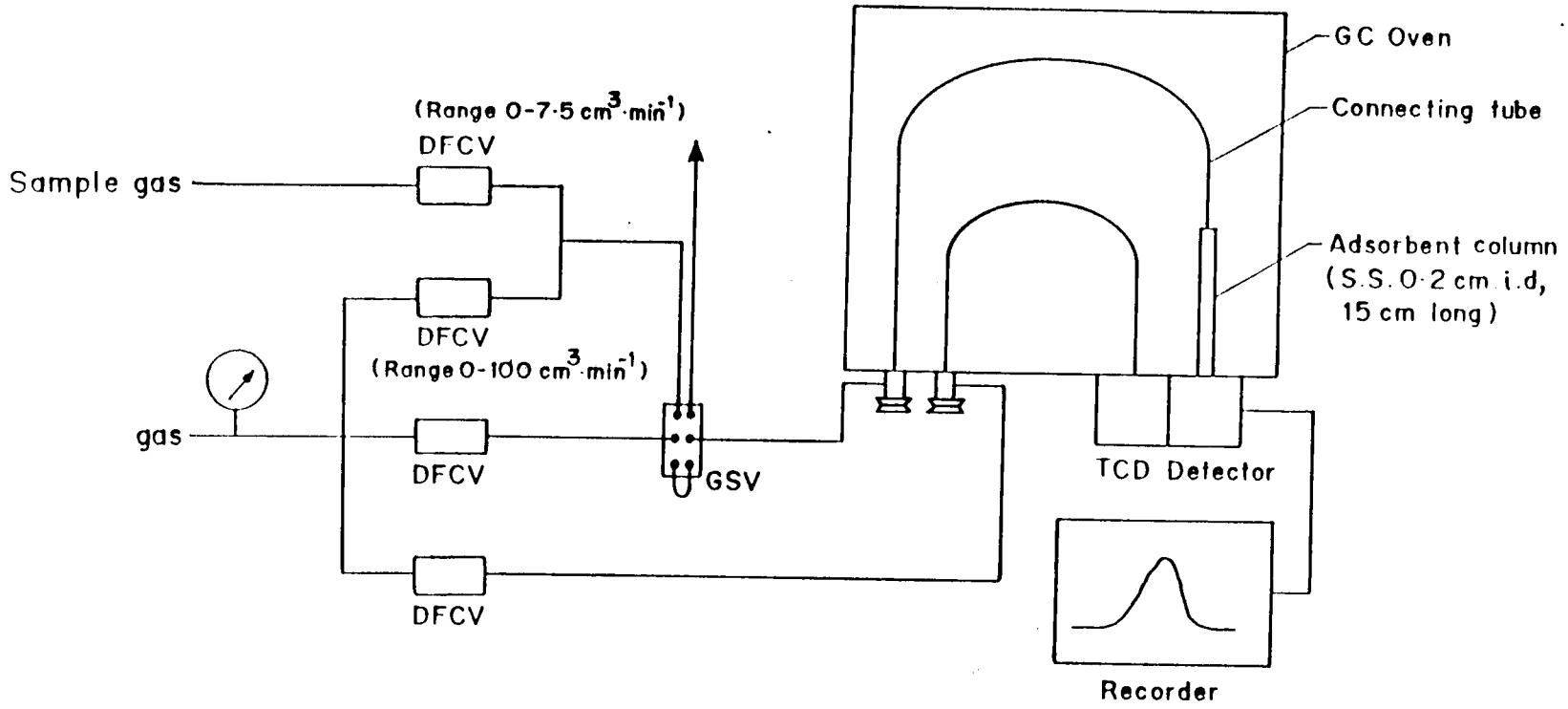

FIG. 3·1a : SCHEMATIC DIAGRAM OF THE EXPERIMENTAL SETUP FOR THE GC PULSE TECHNIQUE.
[DFCV - DIGITAL FLOW CONTROL VALVE, GSV - GAS SAMPLING VALVE]

For collecting gc retention data for water, 0.1 ul of water was injected into the column through the sample injection port. The dead time correction in this case was done by injecting 0.1 ml of pure nitrogen using a gas tight syringe and noting its retention time.

The adsorption equilibrium constant was calculated using Equations (3.1) and (3.2). The heat of sorption at near zero coverage was estimated from the slope of the linear plots of $\log V_R$ versus $1/T_C$ according to Equation (3.3).

3.2.3 Gravimetric Measurement of Adsorption Isotherms

A new simple apparatus has been developed for the measurement of adsorption isotherms of gases and vapors by gravimetric method. The schematic representation of the experimental setup is given in Fig. 3.1b.

The key part of the setup is a set of four ball valves BV1, BV2, BV3 and BV4 connected together by a stainless steel cross. BV1 is connected to a vacuum pump through a fine metering valve FMV1 to regulate the vacuum that is applied. This is required to avoid the carry over of the zeolite particles during evacuation. BV2 is connected to a vacuum gauge which has been calibrated in mmHg vacuum and indicates the adsorption pressure. BV3 is the gas inlet. About 2 g of the zeolite is accurately weighed and taken in a glass bulb, the stem of which is connected to BV4 using ss ultra-torr (1/4") to Swagelok (1/8") reducing union and Swagelok single end shut-off quick connect. The connection through quick connect permits the easy attachment/detachment of the zeolite sample cell to the unit and

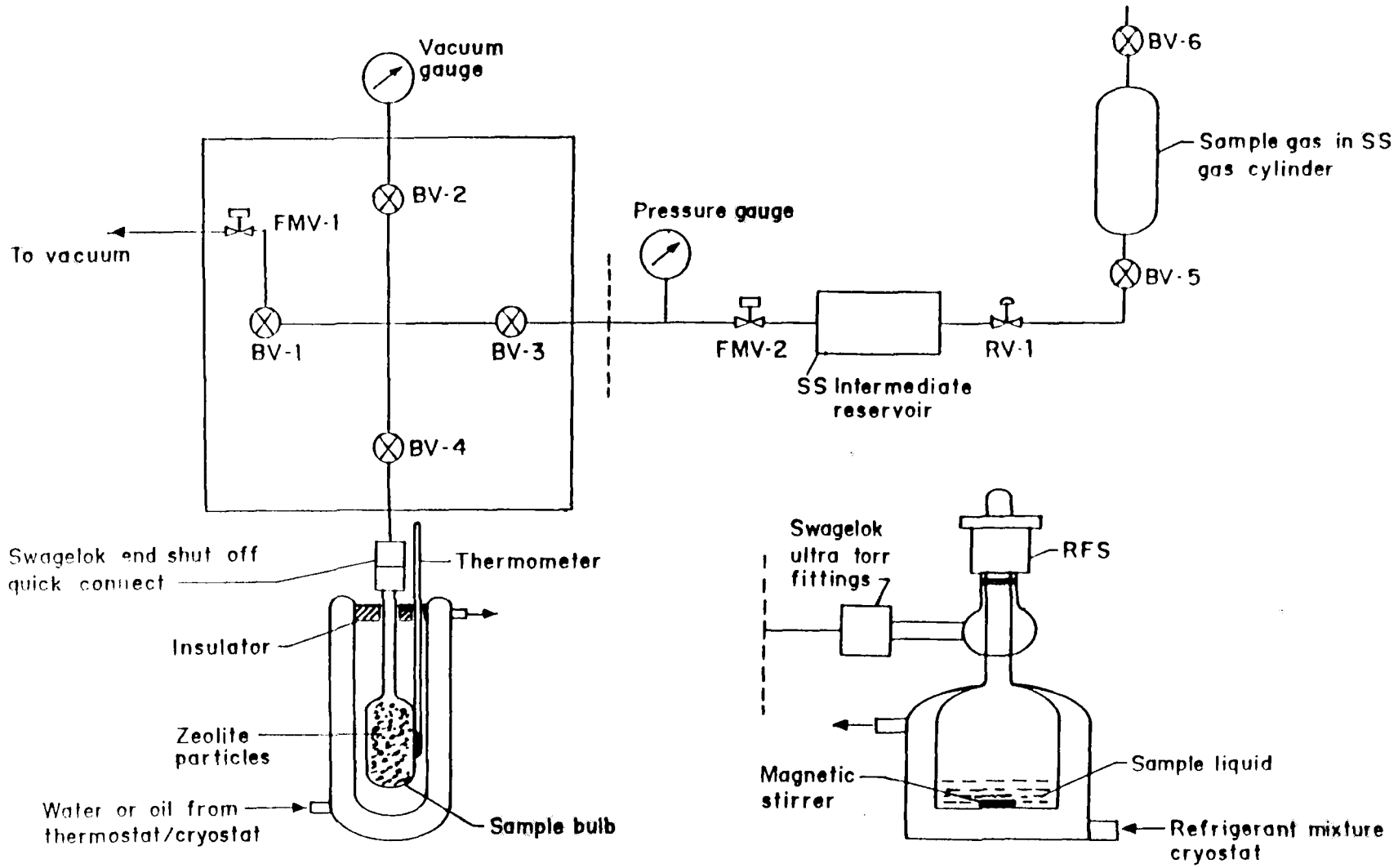

FIG. 3·1b: EXPERIMENTAL SET UP FOR THE MEASUREMENT OF ADSORPTION ISOTHERMS OF GASES AND VAPOURS
(BV - BALL VALVE, FMV - FINE METERING VALVE, RV - REGULATING VALVE AND RFS - ROTAFLOW STOP COCK)

the cell gets automatically sealed off when detached from the unit. BV1, BV2, BV3, BV4 and FMV1 are fixed on an aluminium panel and enclosed in a metallic casing which is heated to avoid condensation of vapors in the lines.

During adsorption, the temperature in the cell is maintained using a removable jacketed glass vessel through the jacket of which water/oil of the required temperature is circulated using a thermostat/cryostat. The temperature of the cell is measured using a thermometer (0-100 and 0-250 C range) which is inserted through the lid of the glass vessel as shown in Fig. 3.1b.

At the beginning of each experiment, the sample in the cell is heated <u>in situ</u> under vacuum at 623 K for 2 h using a removable glass furnace in place of the jacketed vessel. The temperature of the furnace is measured using a thermocouple (K-type) and controlled using a Foronix temperature indicator/controller. BV4 is then closed, the cell assembly cooled, detached from the unit and weighed using a Sartorius electronic balance. The difference between this weight and the weight of the empty cell assembly is taken as the weight of the dry sample.

3.2.3.1 Adsorption Isotherms of Gases

The sample gas in a stainless steel cylinder (capacity : 500 cm^3) is connected to BV3 through a ss intermediate reservoir as shown in Fig. 3.1b. A pressure gauge (range -1 to 1 $kg.cm^{-2}$) is connected to the line between FMV2 and BV3 so that data upto 2 $kg.cm^{-2}$ (absolute) can be collected using the setup.

BV2 is kept closed while collecting adsorption data above 1 $kg.cm^{-2}$ (absolute).

During the pretreatment of the zeolite, the entire unit upto BV5 is evacuated to 0.005 torr. When the pretreatment is completed, BV1, BV3, BV4 and FMV1 are closed, the zeolite cell is cooled and its weight taken. The cell assembly is then reconnected to the system and the adsorption unit upto BV3 is evacuated before taking the adsorption data. The above step is repeated each time the zeolite cell assembly is detached from the unit.

For the measurement of adsorption isotherm data, at each point, the gas sample of the required pressure is initially taken in the intermediate reservoir by opening BV5 and controlling the gas flow through RV1. BV3 is kept closed and FMV2 open so that the pressure can be read on the gauge. When the required pressure is reached, BV5, RV1, FMV2 and FMV1 are closed and BV3 opened. FMV2 is then slowly opened and the zeolite in the cell is exposed to the gas in the intermediate reservoir for 90 min. to ensure complete equilibration. BV3 and BV4 are then closed, the cell is allowed to cool and is detached from the unit for direct weighing. The experiment is then repeated for collecting isotherm data at different pressures.

3.2.3.2 Adsorption Isotherms of Vapors

For the measurement of adsorption isotherms of vapors, the sample liquid is taken in a jacketed glass bottle with a teflon rotaflow stop-cock as shown in Fig. 3.1b. The outlet of the stop-cock is connected to BV3 using ss ultra-torr (1/4") to

Swagelok (1/8") reducing union. The connecting line was heated using a heating tape to avoid the condensation of the vapors. The sample liquid is stirred using a magnetic stirrer to increase the mass transfer (evaporation) rate. The sorption measurement at different sorbate pressures could be made by changing the vapor pressure of the liquid by changing the temperature of the circulating refrigerant mixture (water-ethylene glycol, 40% E.G) through the outer jacket of the vessel.

The liquid sorbate is introduced into the liquid reservoir through the top, after removing the teflon plunger of the rotaflow stop-cock. The sorbate is then cooled to a low temperature (263 K) by circulating the refrigerant mixture through the outer jacket of the container. Valve BV4 is closed, BV3 and stop-cock are opened and the space above the liquid is evacuated for a sufficiently long period (3 h) to ensure the complete removal of the air in the reservoir. It is then sealed using the stop-cock and the connecting line is evacuated before the pretreatment of the zeolite.

The procedure for the pretreatment of the zeolite and the collection of isotherm data for vapors are the same as that for the gases. The isotherm data at different pressures were obtained by changing the vapor pressure of the liquid sorbate through adjusting the temperature of the circulating fluid.

3.3 RESULTS AND DISCUSSION

3.3.1 Heat of Sorption and Thermodynamic Sorption Equilibrium Constant by GC Pulse Technique

The heat of sorption and the adsorption equilibrium constant were calculated for the adsorption of methane, ethane, ethylene, carbon dioxide and water on a number of zeolites (viz. ZSM-5, H-Na-ZSM-5, ZSM-8, Na-H-ZSM-8, HY, NaY, CeNaY, KL, HKL, HM, NaM, and NaX) and zeolite-like materials (Silicalite and $AlPO_4$-5) by the gc pulse technique. For the determination of heat of sorption and/or thermodynamic adsorption equilibrium constant by gc pulse method, it is essential that the data should correspond to the linear region of the adsorption isotherm. This was achieved in the present case by using a sample pulse of very low concentration (2-3%) and small volume (0.3 cm^3). This requirement was further confirmed by changing the carrier gas flow rate from 10 to 30 $cm.^3min^{-1}$ at the lowest temperature of study for each sorbate. There was no significant change in the retention volume of the sorbates when the carrier gas flow rate was increased from 10 to 30 $cm.^3min^{-1}$. This clearly shows that the data correspond to the linear region of the sorption isotherm of the sorbates.

The retention time data of the gases and water vapor on the adsorbents are given in Appendix 3.1. Figs. 3.2-3.16 give the plots of log(corrected retention volume) versus reciprocal column temperature for methane, ethane, ethylene, carbon dioxide and water on the different zeolites in the temperature range 317-473 K. The heat of sorption of the gases/vapor has been

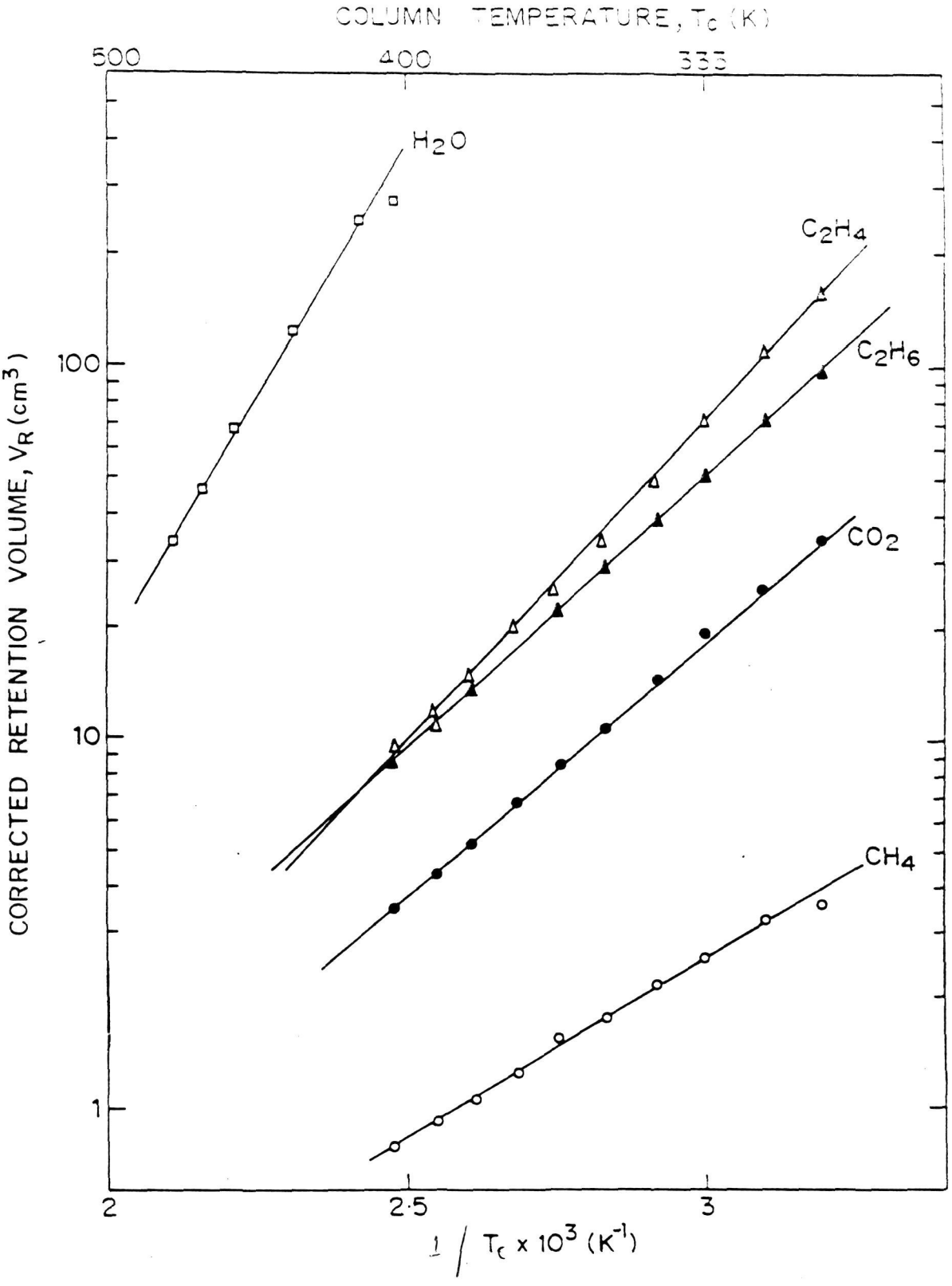

FIG.3·2: PLOT OF CORRECTED RETENTION VOLUME vs RECIPROCAL COLUMN TEMPERATURE FOR THE ADSORPTION OF METHANE, ETHANE, ETHYLENE, CARBONDIOXIDE AND WATER ON H-ZSM-5 ZEOLITE

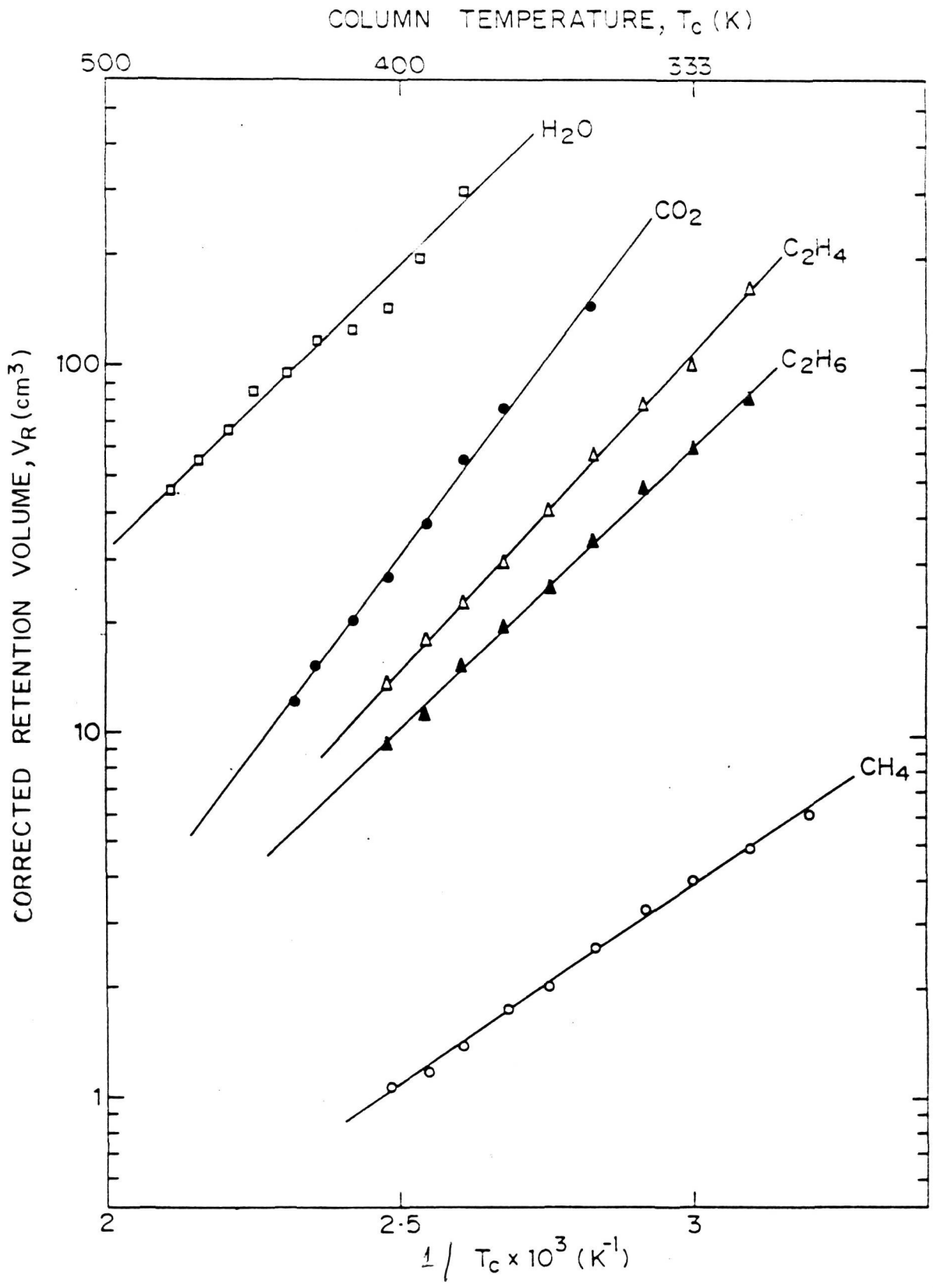

FIG. 3·3: PLOT OF CORRECTED RETENTION VOLUME vs RECIPROCAL COLUMN TEMPERATURE FOR THE ADSORPTION OF METHANE, ETHANE, ETHYLENE, CARBONDIOXIDE AND WATER ON Na-ZSM-5 ZEOLITE

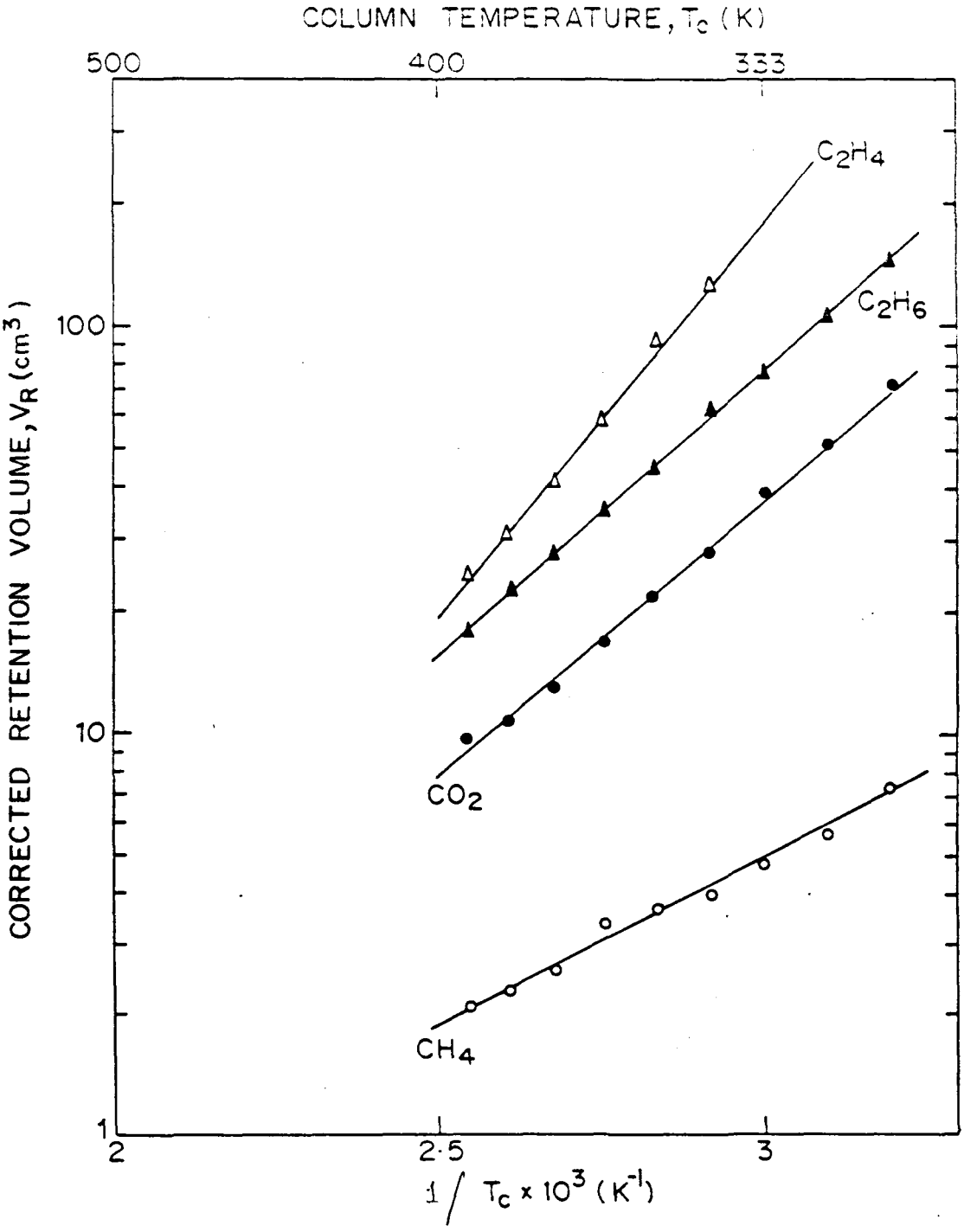

FIG. 3·4: PLOT OF CORRECTED RETENTION VOLUME vs RECIPROCAL COLUMN TEMPERATURE FOR THE ADSORPTION OF METHANE, ETHANE, ETHYLENE AND CARBONDIOXIDE ON H-ZSM-8 ZEOLITE

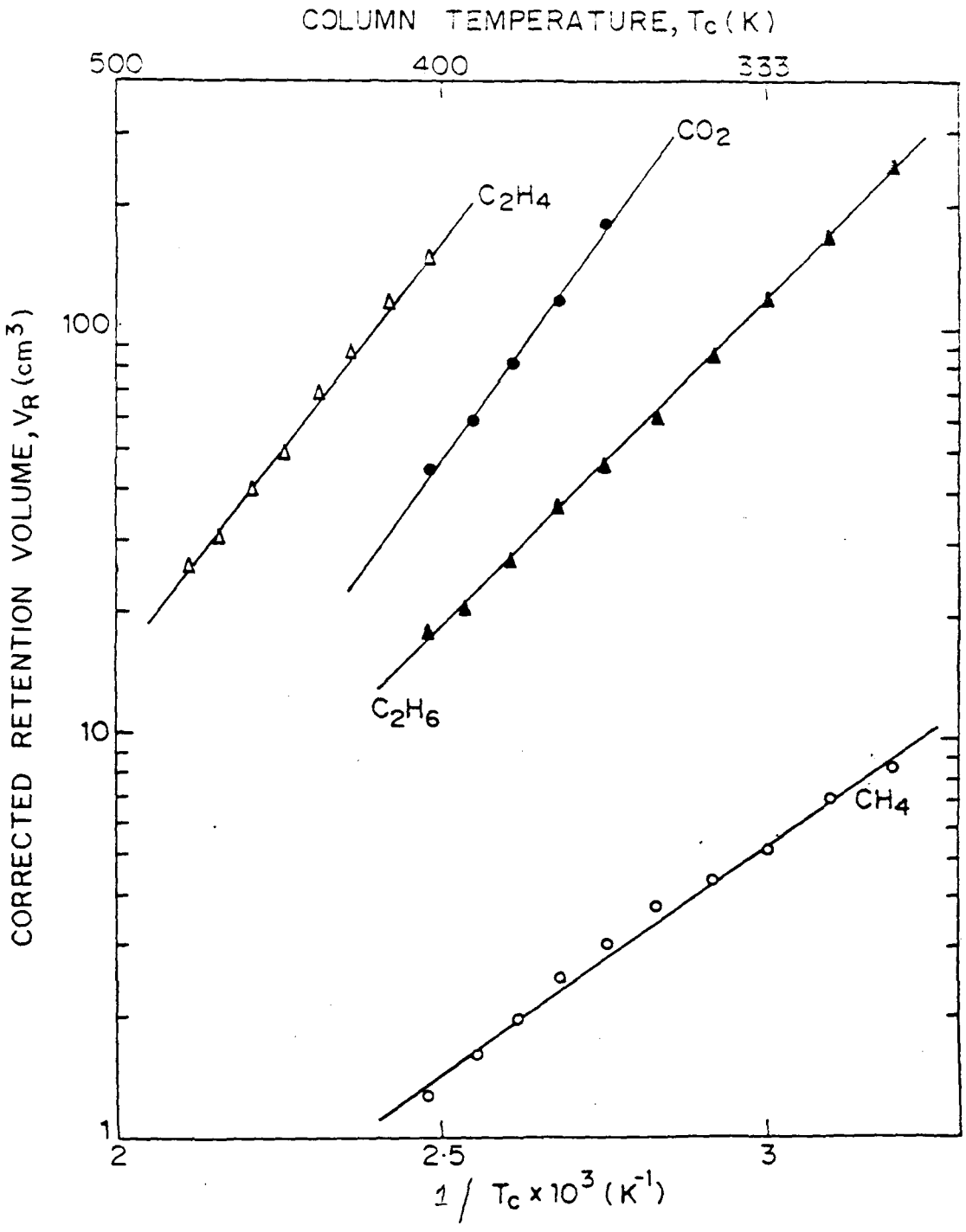

FIG.3·5: PLOT OF CORRECTED RETENTION VOLUME vs RECIPROCAL COLUMN TEMPERATURE FOR THE ADSORPTION OF METHANE, ETHANE, ETHYLENE AND CARBONDIOXID ON Na-ZSM-8 ZEOLITE

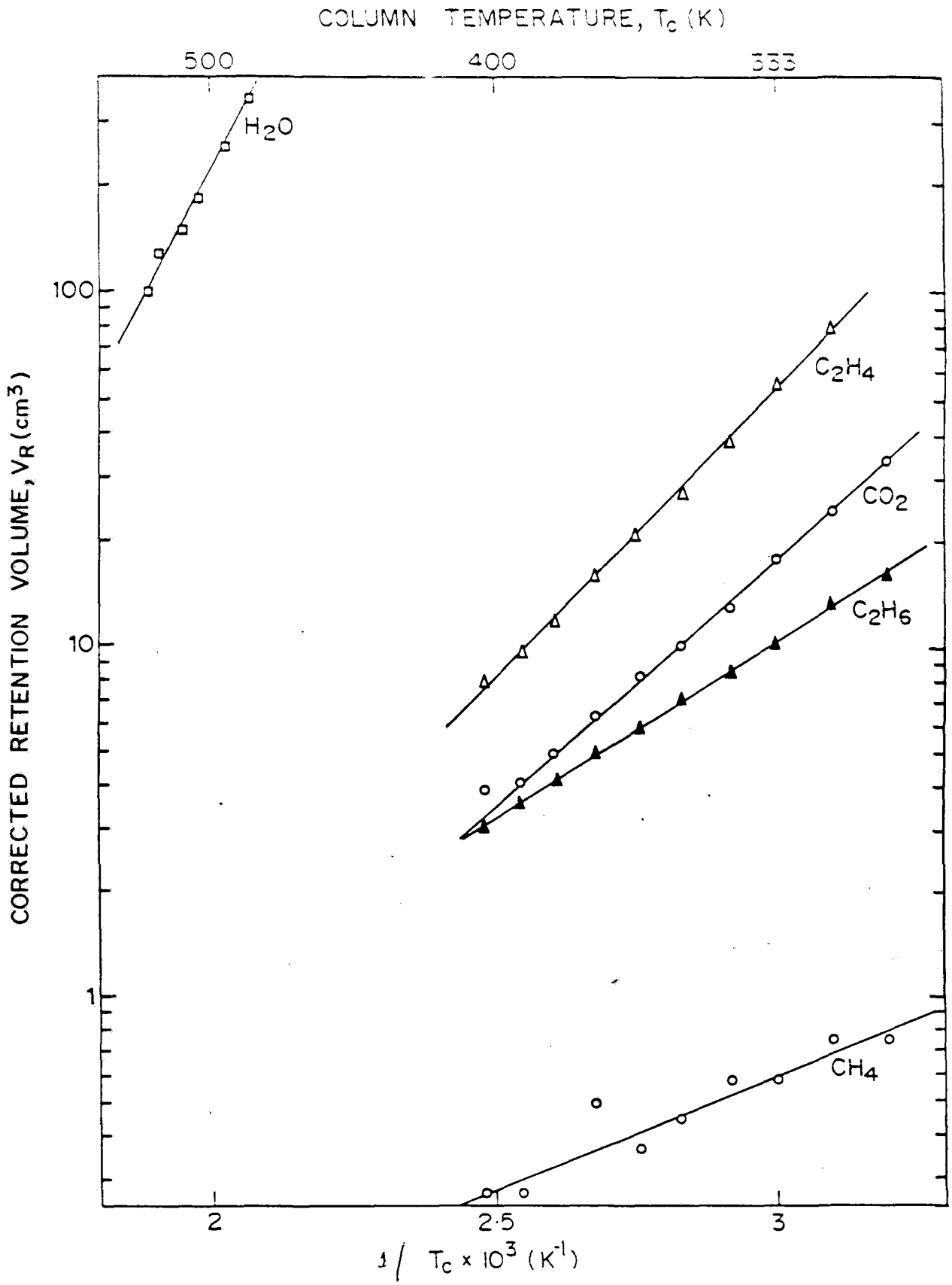

FIG.3·6 : PLOT OF CORRECTED RETENTION VOLUME vs RECIPROCAL COLUMN TEMPERATURE FOR THE ADSORPTION OF METHANE, ETHANE, ETHYLENE, CARBONDIOXIDE AND WATER ON HY ZEOLITE

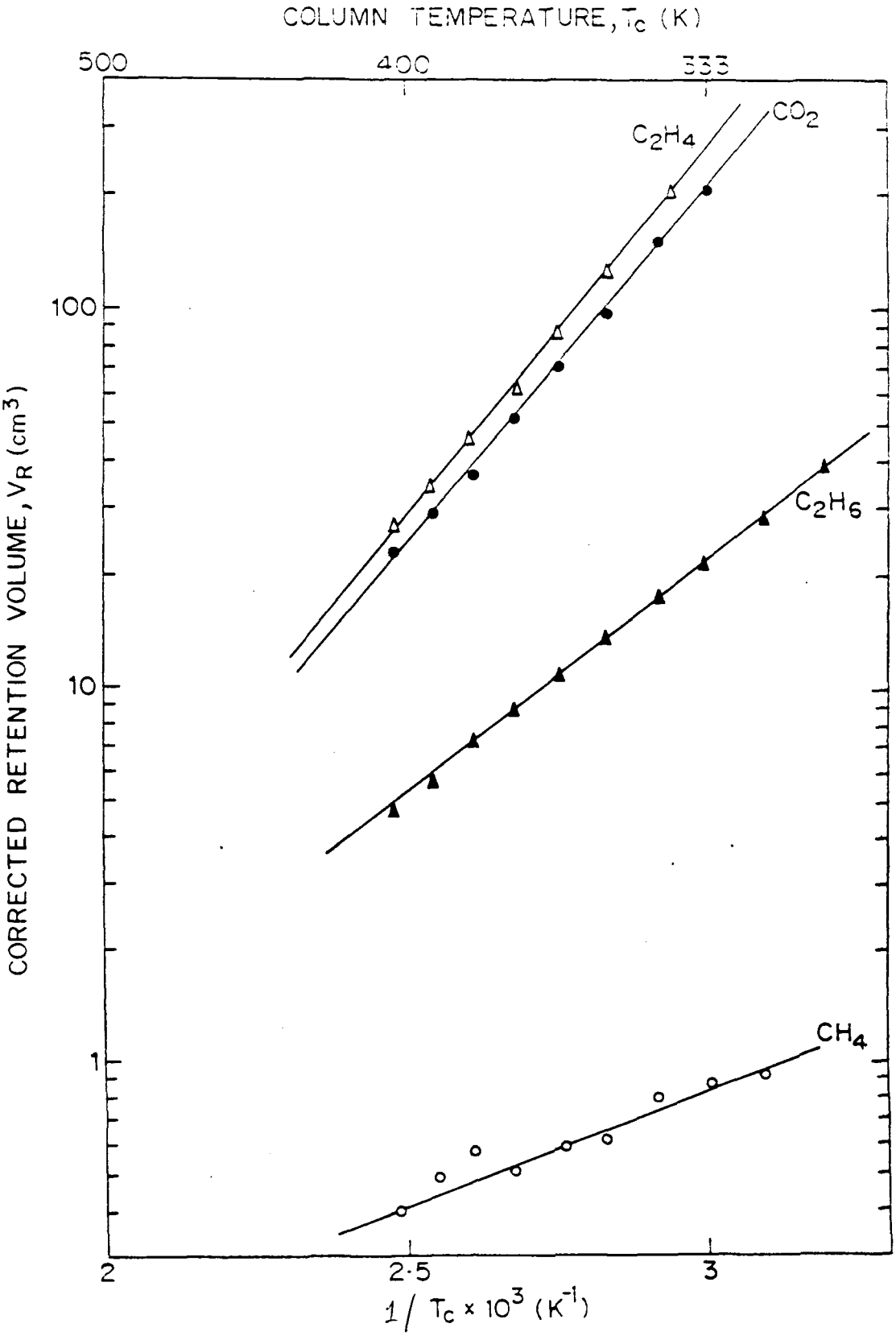

FIG.3·7: PLOT OF CORRECTED RETENTION VOLUME vs RECIPROCAL COLUMN TEMPERATURE FOR THE ADSORPTION OF METHANE, ETHANE, ETHYLENE AND CARBONDIOXIDE ON NaY ZEOLITE

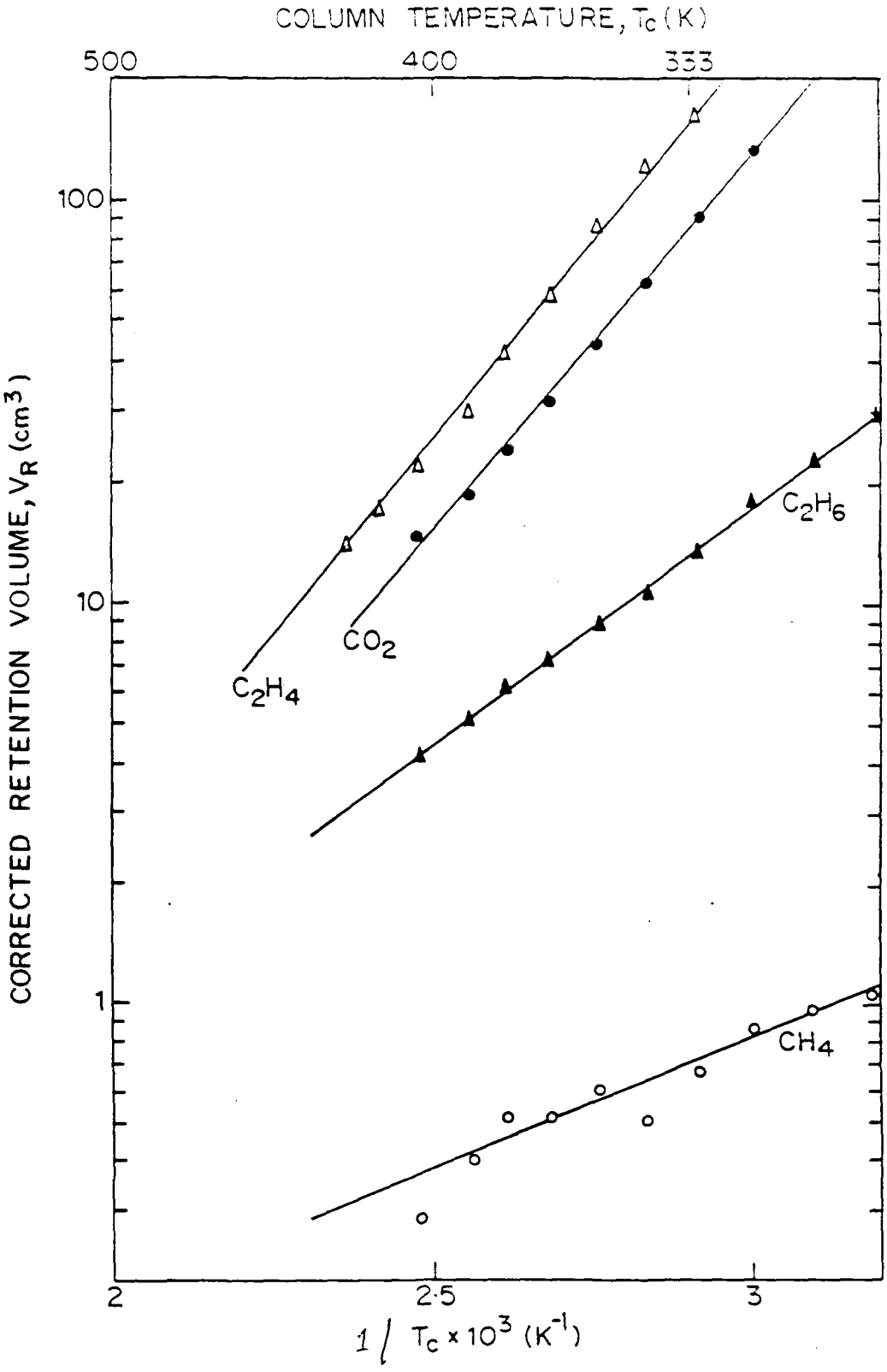

FIG.3·8: PLOT OF CORRECTED RETENTION VOLUME vs RECIPROCAL COLUMN TEMPERATURE FOR THE ADSORPTION OF METHANE, ETHANE, ETHYLENE AND CARBONDIOXIDE ON ZEOLITE CeNaY (46%)

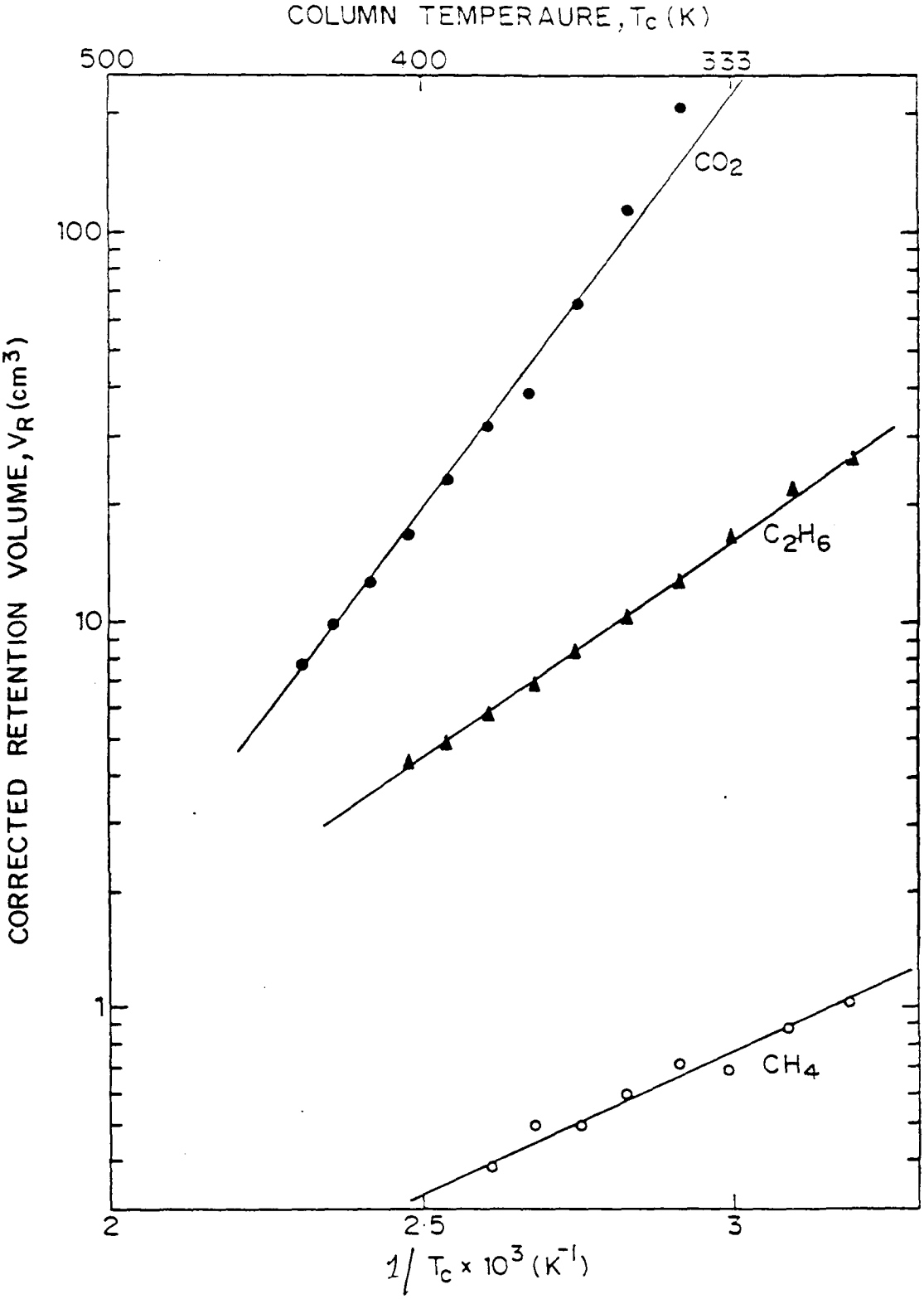

FIG.3·9: PLOT OF CORRECTED RETENTION VOLUME vs RECIPROCAL COLUMN TEMPERATURE FOR THE ADSORPTION OF METHANE, ETHANE AND CARBONDIOXIDE ON ZEOLITE CeNaY (72 %)

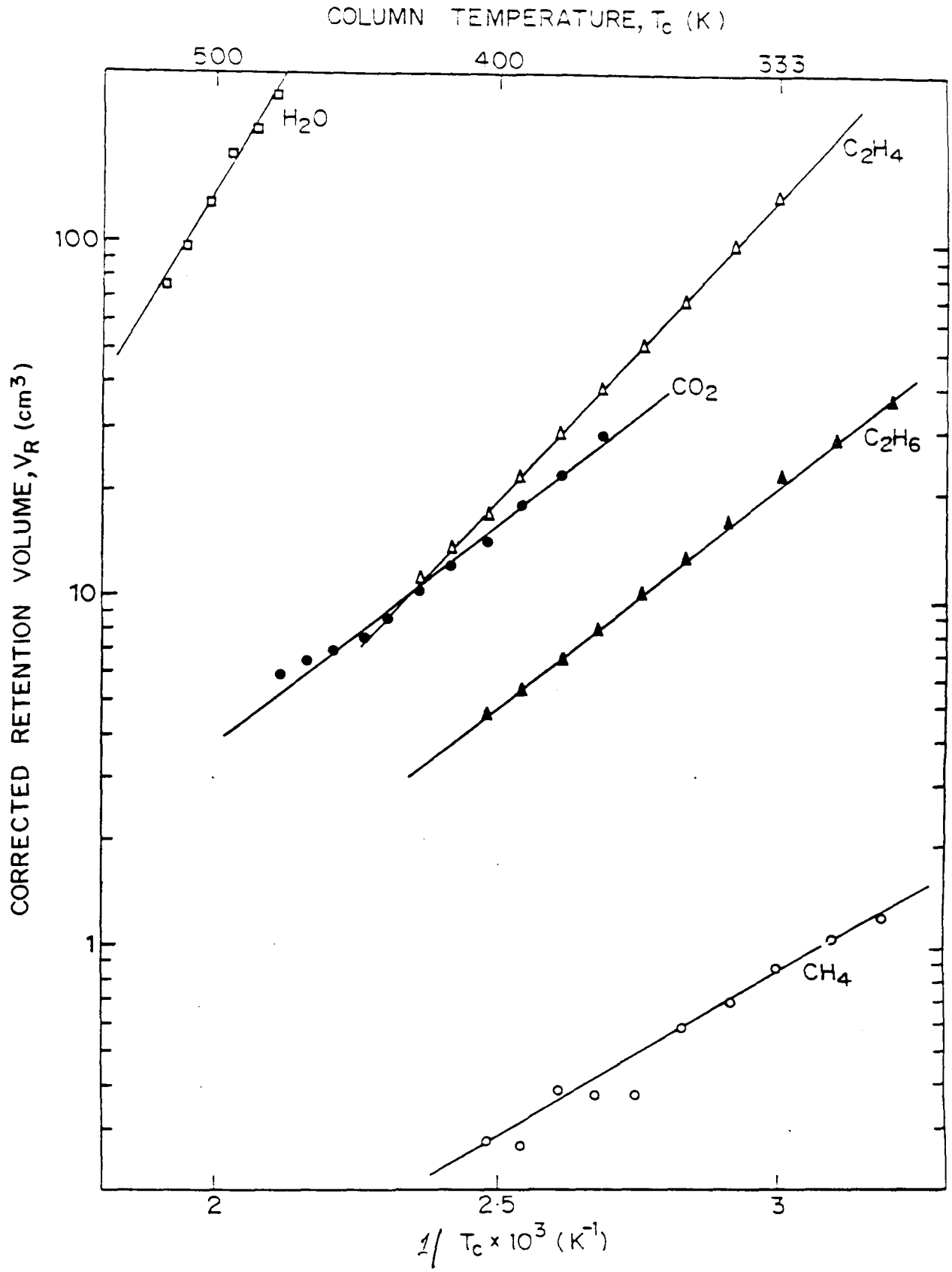

FIG. 3·10: PLOT OF CORRECTED RETENTION VOLUME vs RECIPROCAL COLUMN TEMPERATURE FOR THE ADSORPTION OF METHANE, ETHANE, ETHYLENE, CARBONDIOXIDE AND WATER ON ZEOLITE KL

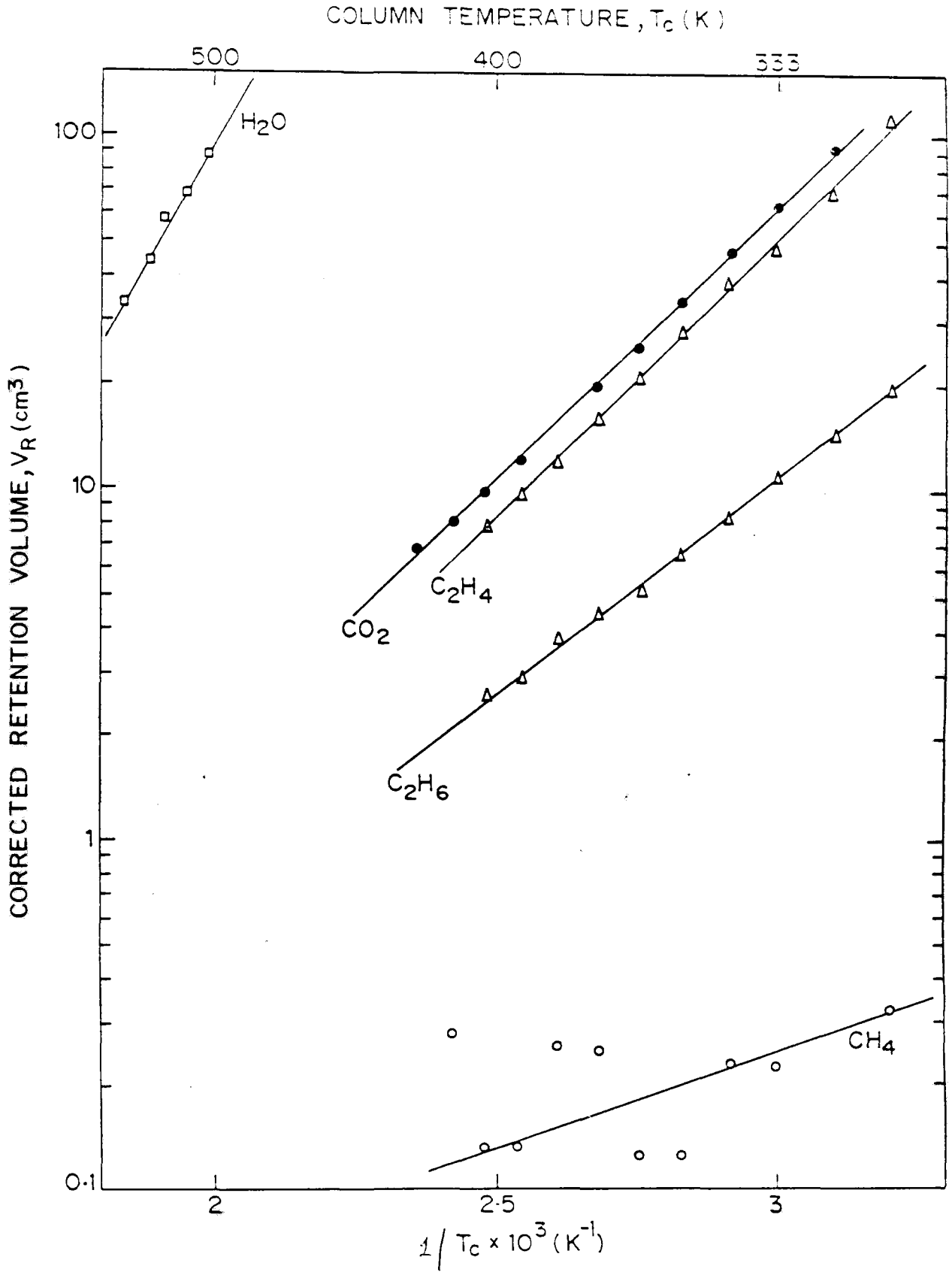

FIG.3·11: PLOT OF CORRECTED RETENTION VOLUME vs RECIPROCAL COLUMN TEMPERATURE FOR THE ADSORPTION OF METHANE, ETHANE, ETHYLENE, CARBONDIOXIDE AND WATER ON ZEOLITE HKL

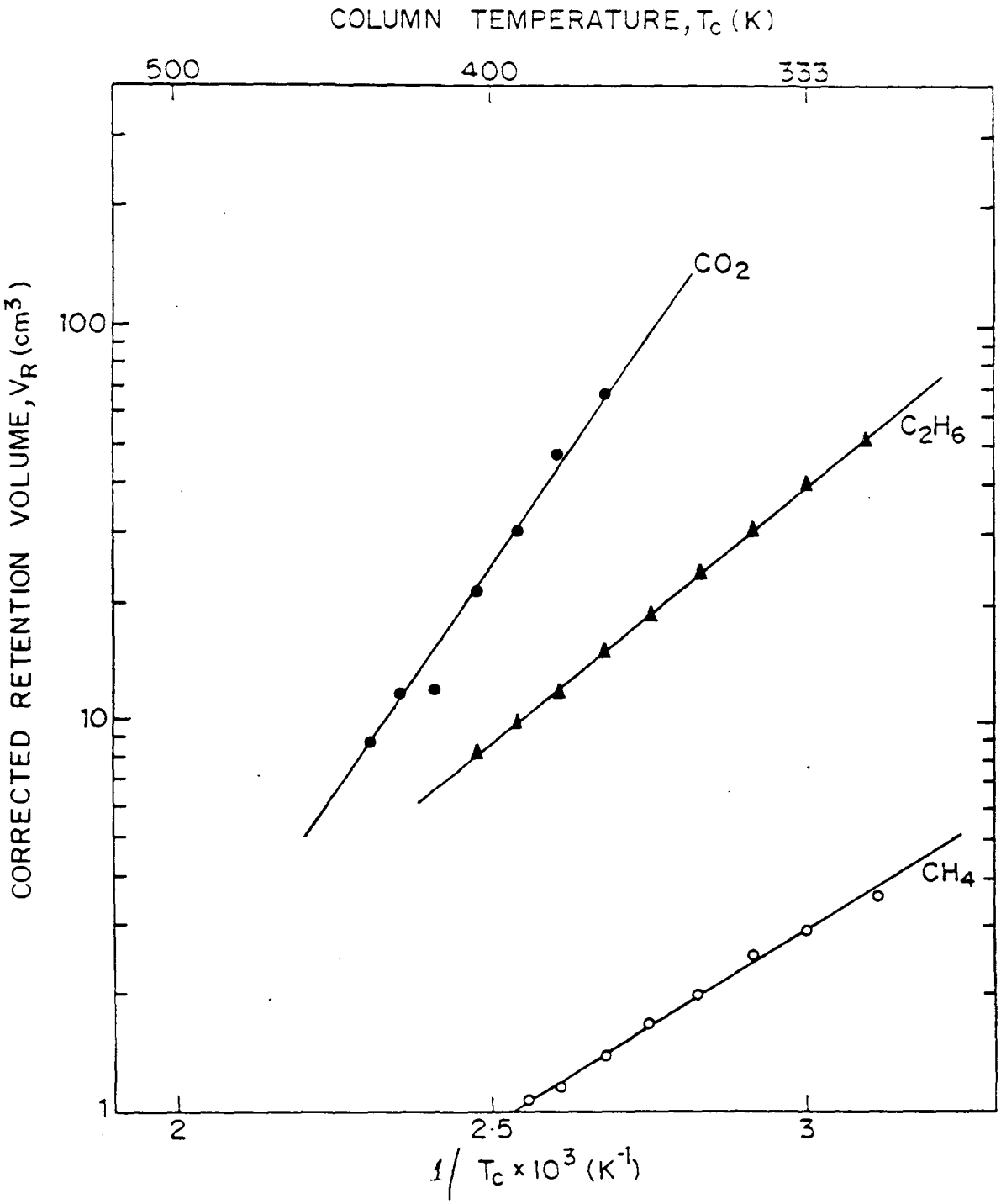

FIG.3·12: PLOT OF CORRECTED RETENTION VOLUME vs RECIPROCAL COLUMN TEMPERATURE FOR THE ADSORPTION OF METHANE, ETHANE AND CARBONDIOXIDE ON ZEOLITE HM

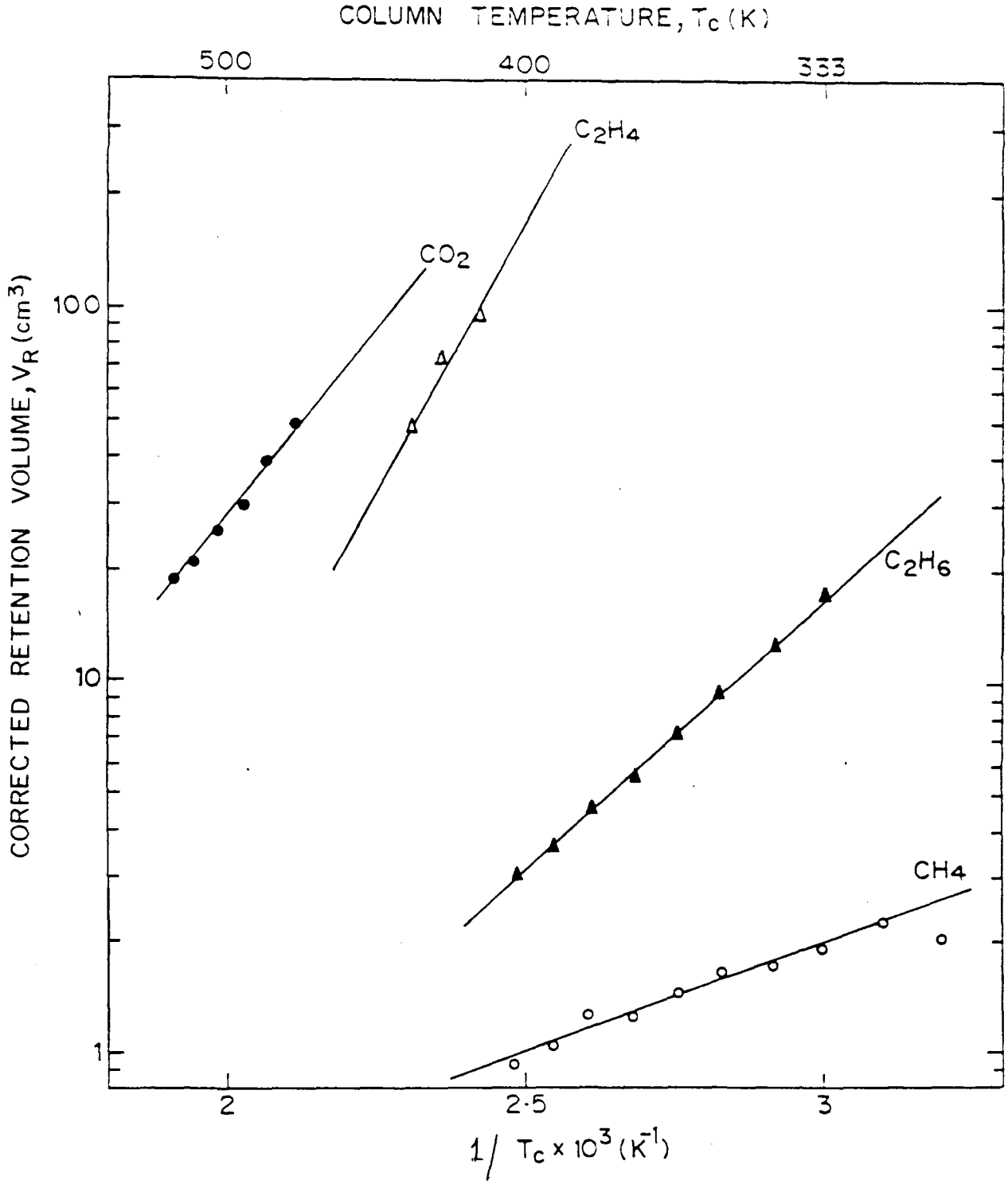

FIG.3·13: PLOT OF CORRECTED RETENTION VOLUME vs RECIPROCAL COLUMN TEMPERATURE FOR THE ADSORPTION OF METHANE, ETHANE, ETHYLENE AND CARBONDIOXIDE ON NaM ZEOLITE

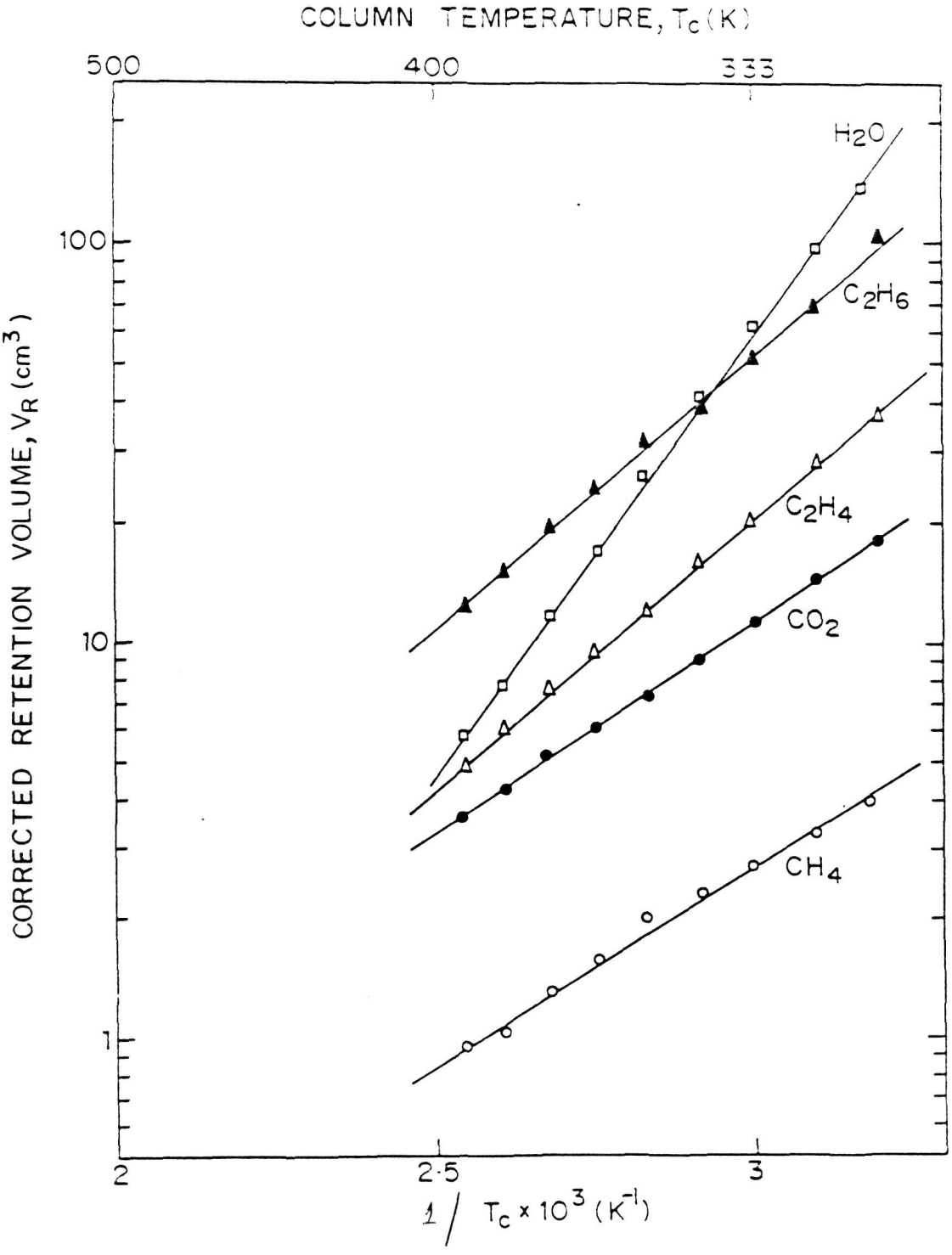

FIG.3·14: PLOT OF CORRECTED RETENTION VOLUME vs RECIPROCAL COLUMN TEMPERATURE FOR THE ADSORPTION OF METHANE, ETHANE, ETHYLENE, CARBONDIOXIDE AND WATER ON SILICALITE I

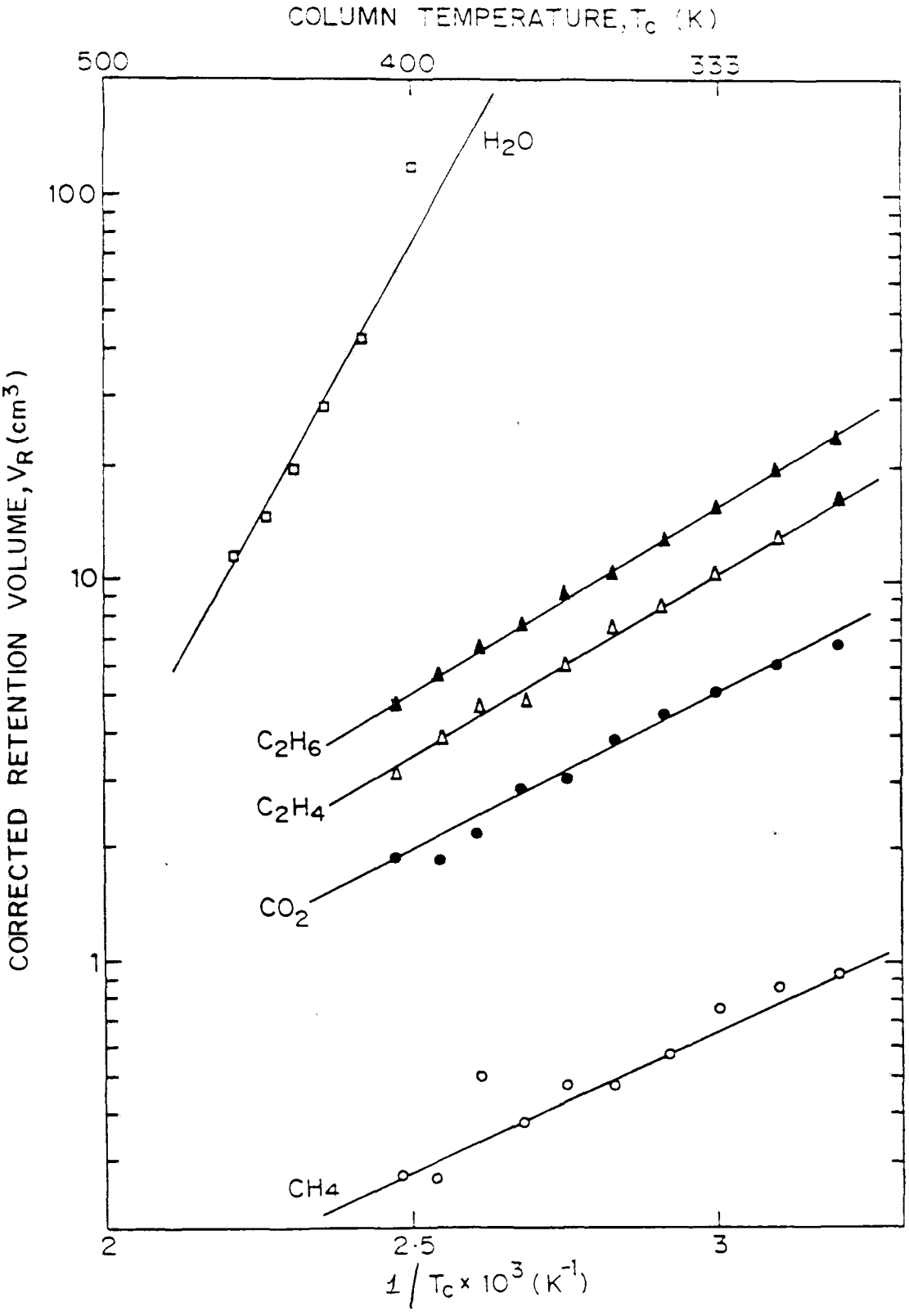

FIG.3·15: PLOT OF CORRECTED RETENTION VOLUME vs RECIPROCAL COLUMN TEMPERATURE FOR THE ADSORPTION OF METHANE, ETHANE, ETHYLENE, CARBONDIOXIDE AND WATER ON $AlPO_4$-5

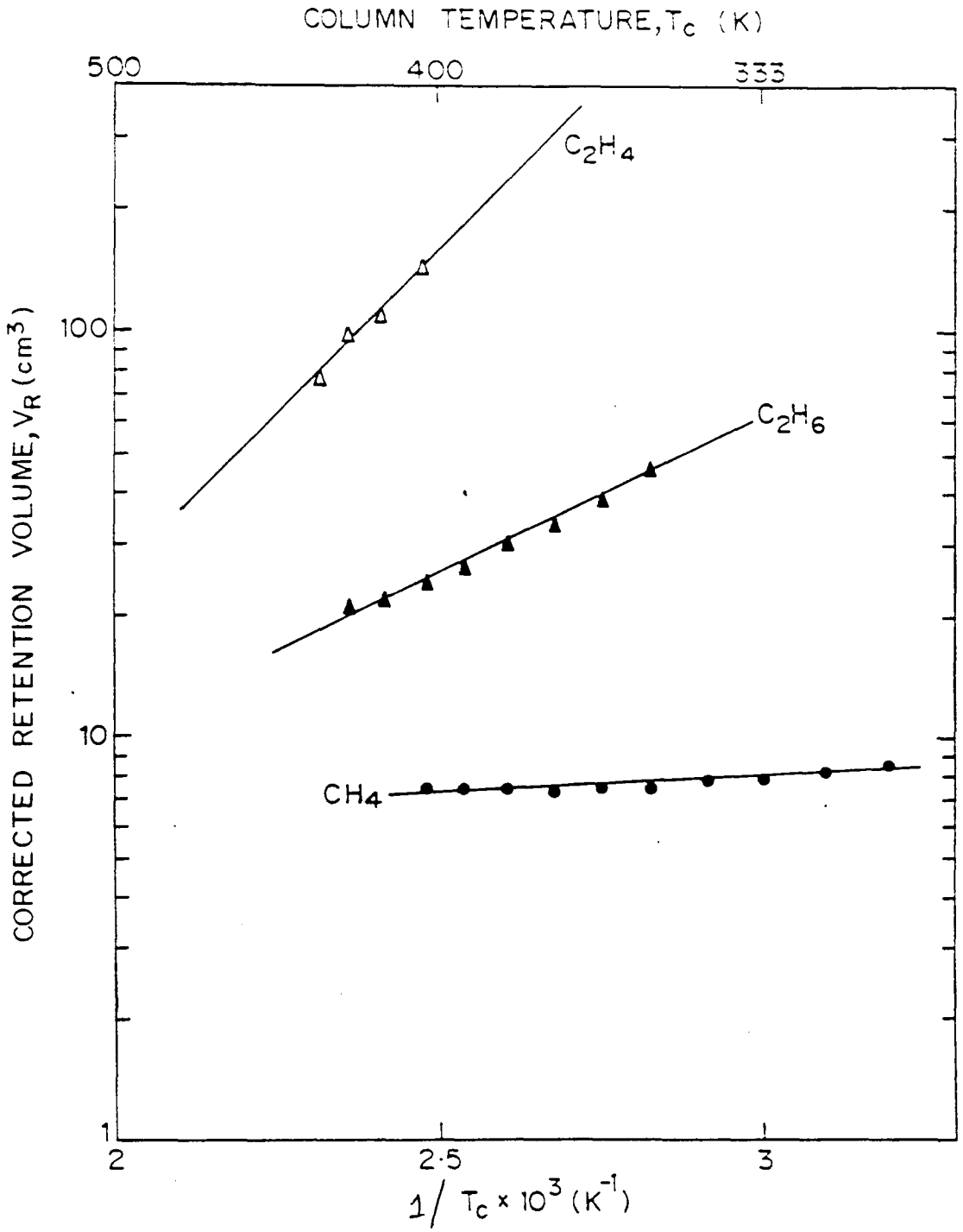

FIG.3·16: PLOT OF CORRECTED RETENTION VOLUME vs RECIPROCAL COLUMN TEMPERATURE FOR THE ADSORPTION OF METHANE, ETHANE AND ETHYLENE ON NaX ZEOLITE

estimated from the slopes of these plots using Equation (3.3). The heat of sorption data for the different gases and water vapor on the different adsorbents are presented in Table 3.8. The temperature dependence of the adsorption equilibrium constant for the adsorption of the hydrocarbons and water on the various adsorbents, estimated using Equation (3.1), are shown in Figs. 3.17-3.31. For the purpose of comparison, four base temperatures 303, 373, 423 and 473 K were chosen and the values of adsorption equilibrium constants at these temperatures are given in Table 3.9.

The values of heat of sorption, obtained by the gc pulse method, for the different sorbates on NaX, NaY, HM, KL, silicalite and $AlPO_4$-5 are compared with those reported earlier in Table 3.10. The values of heat of sorption of ethylene in NaX, ethylene and carbon dioxide in NaY, carbon dioxide in HM, and methane and ethane in silicalite and KL are quite comparable with those reported earlier whereas the other heat of sorption values obtained by gc pulse technique are somewhat lower.

3.3.2. Sorption Isotherms by Gravimetric Technique

As a test for the validity of the data collected using the new apparatus, the intracrystalline sorption capacity for n-hexane on silicalite-I at 305 K and P/P_0=0.4 was measured. It was found to be 0.2 $cm.^3g^{-1}$ and is in good agreement with the reported results [49].

Adsorption isotherm data were collected for the sorption of n-hexane on silicalite-I, and n-hexane and water on NaM using the apparatus. The adsorption data for vapors are

Table 3.8

Data on heat of sorption (ΔH kJ) of methane, ethane, ethylene and carbon dioxide in different zeolites and zeolite-like adsorbents by gc pulse technique (Temperature range: 300-400 K)

Gas \ Adsorbent	HM	NaM	KL	HKL	$AlPO_4$-5	HY	NaY	CeNaY (46%)	CeNaY (72%)	NaX	Silica-lite	HZSM8	NaHZSM8	HZSM5	HNaZSM5
CH_4	19.3	11.2	18.1	10.6	14.3	14.7	12.1	12.7	14.3	very small	18.4	14.5	19.4	19.0	21.2
C_2H_6	24.9	28.2	24.7	24.1	18.7	20.3	24.3	23.2	21.6	15.0	28.3	26.5	26.6	28.0	30.0
C_2H_4	-	55.6	33.2	30.3	22.6	32.6	37.8	38.1	-	31.5 (403-433K)	26.5	34.6	35.8 (400-473K)	33.7	34.0
CO_2	44.5	38.2 (373-473K)	24.3	30.1	16.0	27.0	36.5	35.7	40.8	-	21.7	27.0	35.9	26.1 (350-440K)	42.0

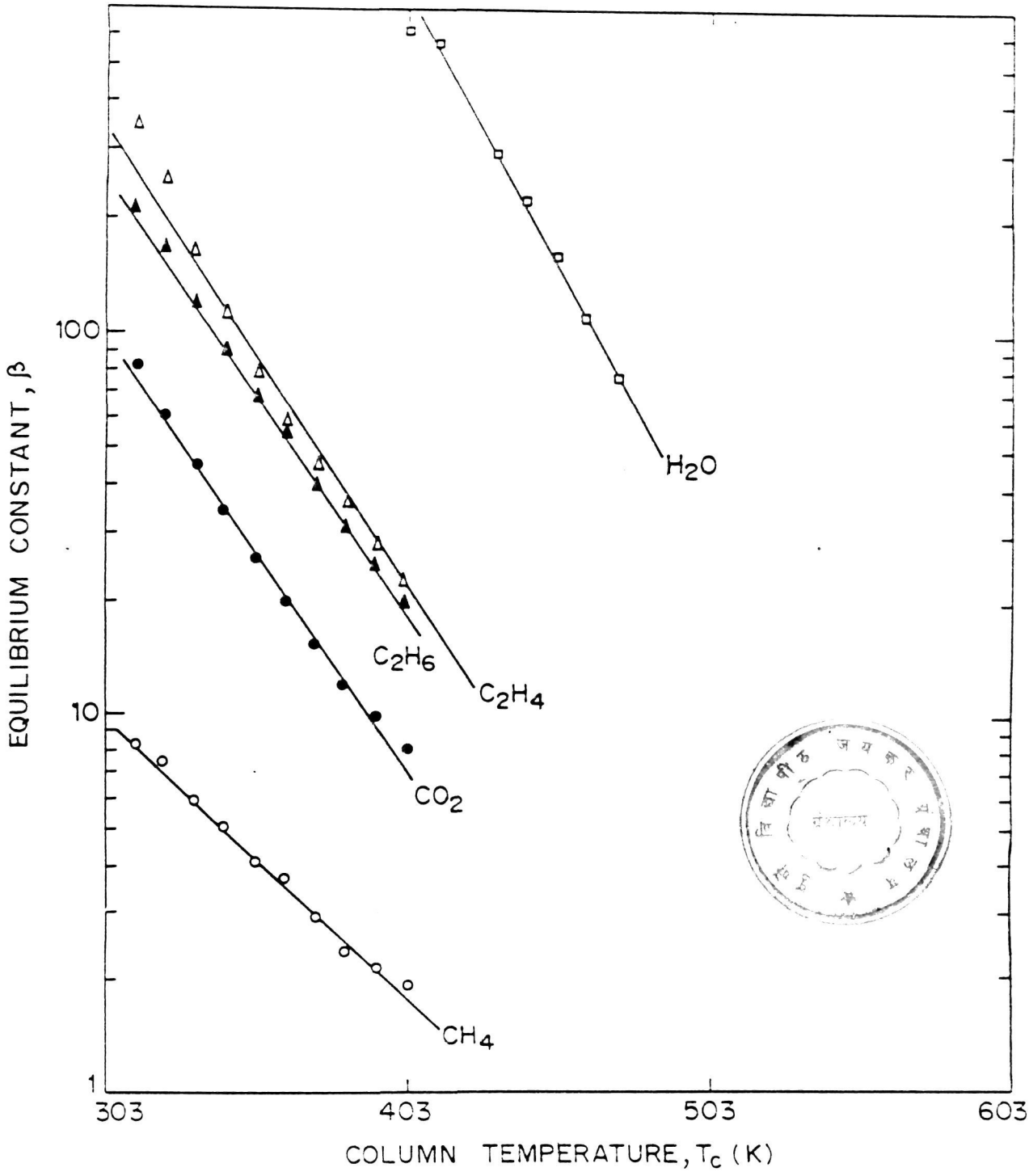

FIG. 3·17: TEMPERATURE DEPENDENCE OF ADSORPTION EQUILIBRIUM CONSTANT FOR THE ADSORPTION OF METHANE, ETHANE, ETHYLENE, CARBONDIOXIDE AND WATER ON H-ZSM-5 ZEOLITE

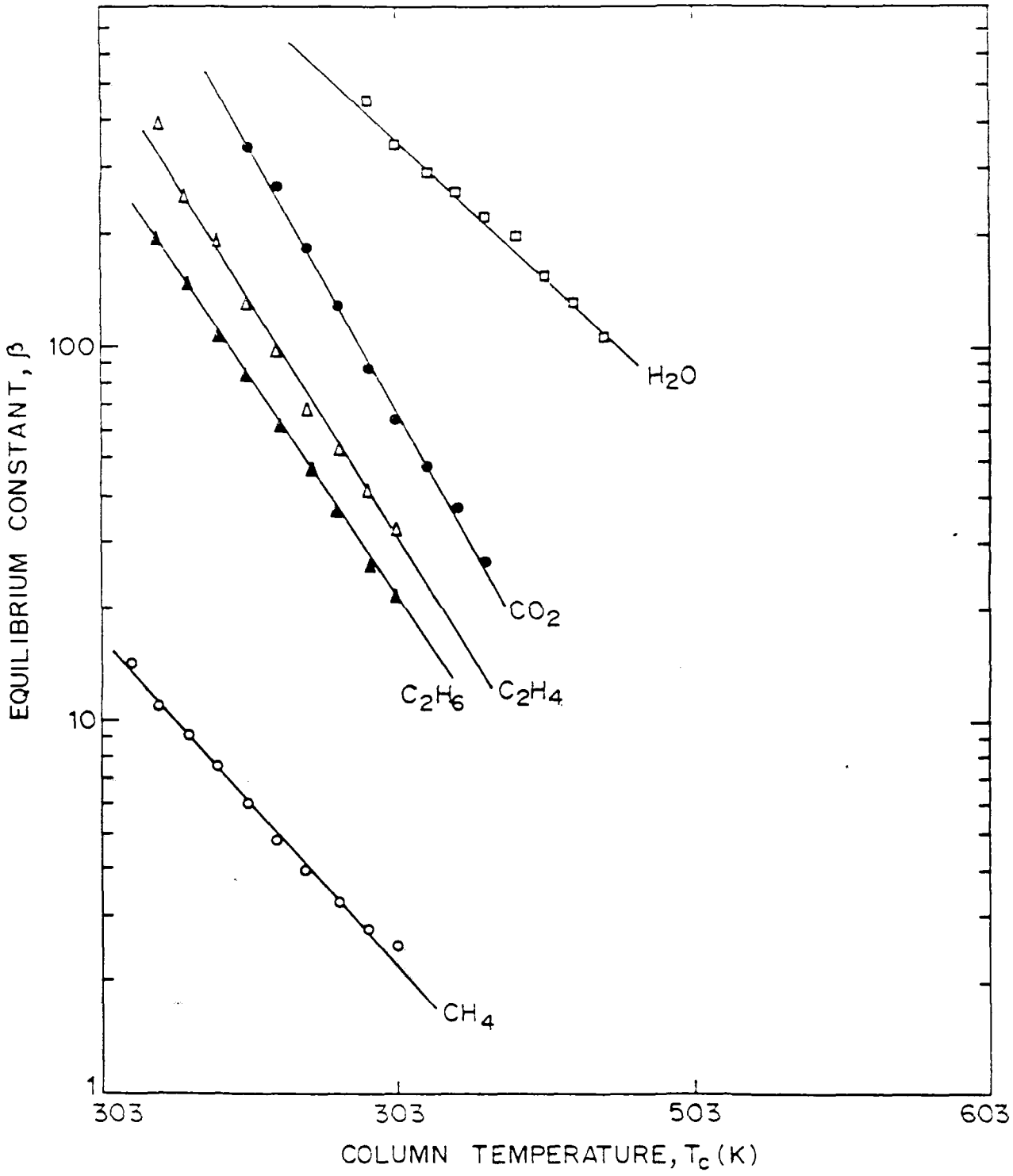

FIG.3·18: TEMPERATURE DEPENDENCE OF ADSORPTION EQUILIBRIUM CONSTANT FOR THE ADSORPTION OF METHANE, ETHANE, ETHYLENE, CARBONDIOXIDE AND WATER ON Na-ZSM-5 ZEOLITE

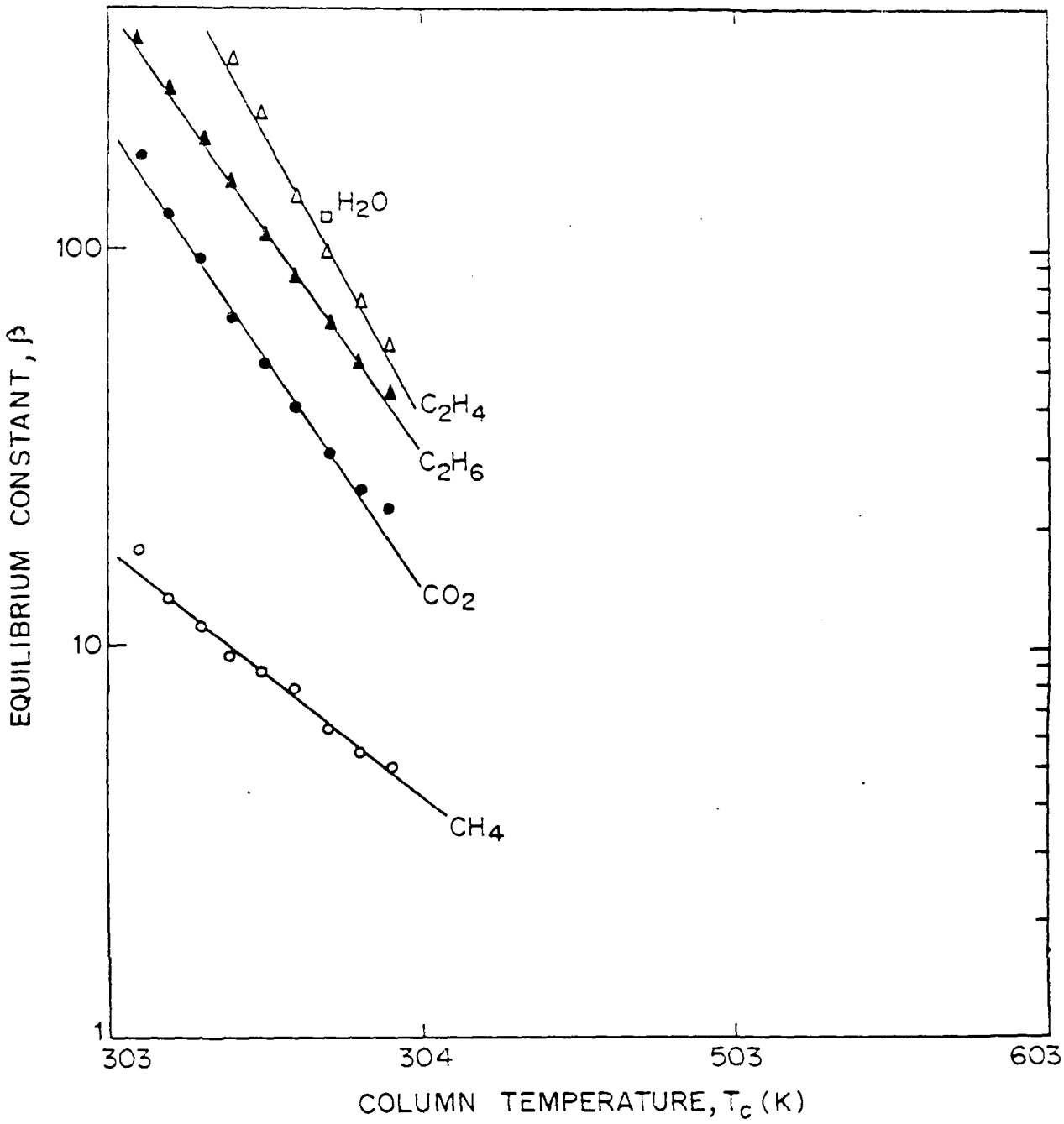

FIG.3·19: TEMPERATURE DEPENDENCE OF ADSORPTION EQUILIBRIUM CONSTANT FOR THE ADSORPTION OF METHANE, ETHANE, ETHYLENE AND CARBONDIOXIDE ON H-ZSM-8 ZEOLITE

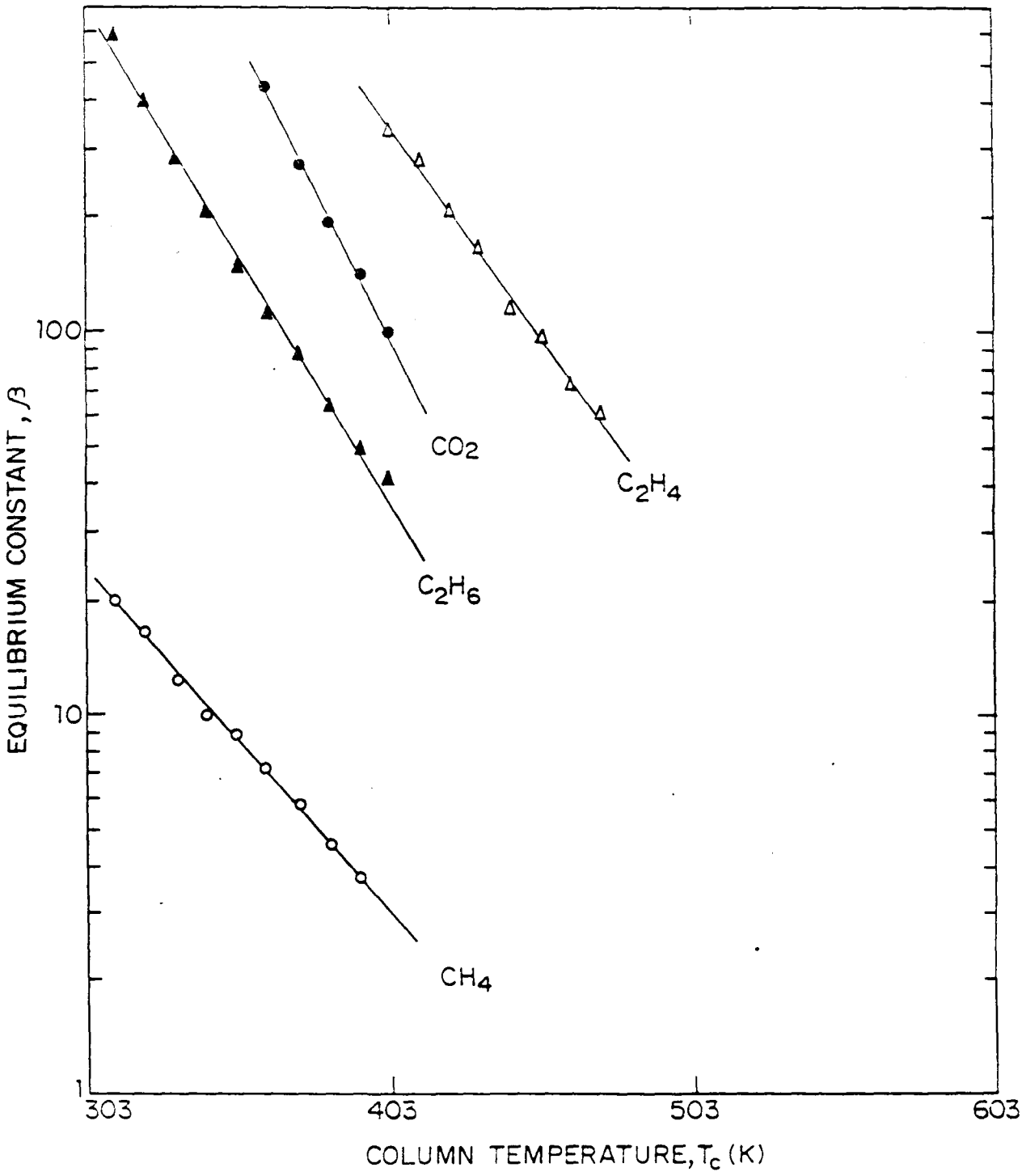

FIG. 3·20: TEMPERATURE DEPENDENCE OF ADSORPTION EQUILIBRIUM CONSTANT FOR THE ADSORPTION OF METHANE, ETHANE, ETHYLENE AND CARBONDIOXIDE ON NaZSM-8 ZEOLITE

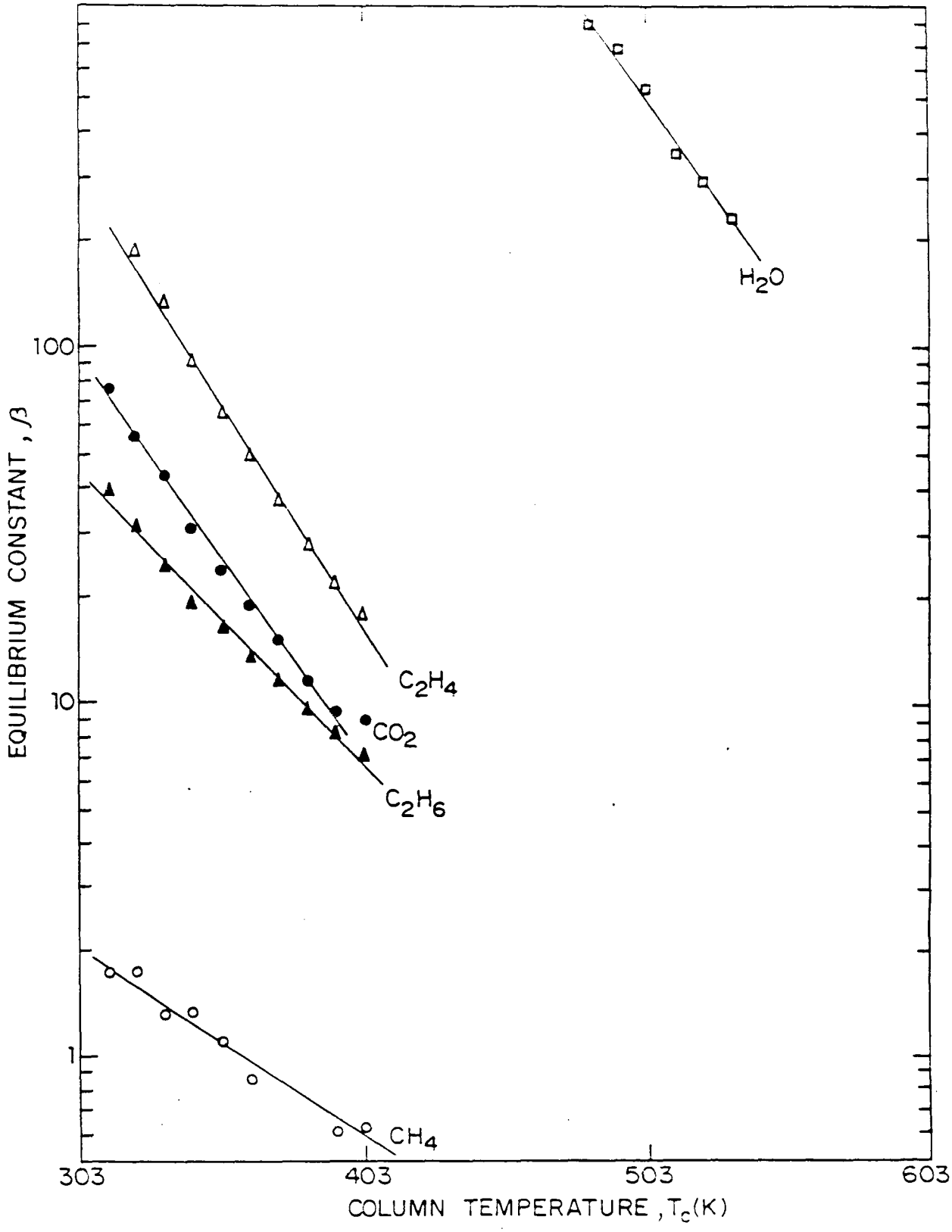

FIG. 3·21 : TEMPERATURE DEPENDENCE OF ADSORPTION EQUILIBRIUM CONSTANT FOR THE ADSORPTION OF METHANE, ETHANE, ETHYLENE, CARBONDIOXIDE AND WATER ON HY ZEOLITE

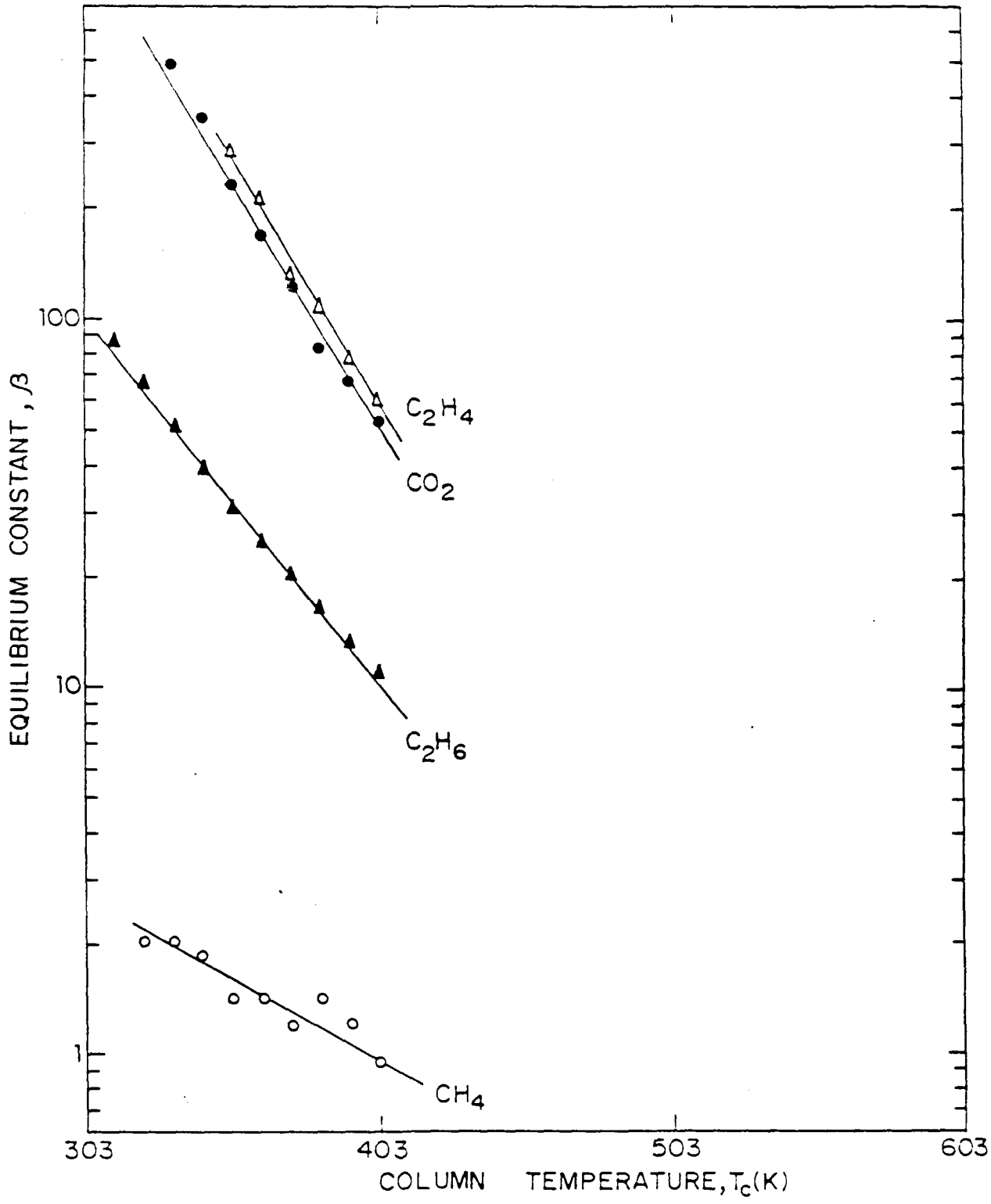

FIG. 3-22: TEMPERATURE DEPENDENCE OF ADSORPTION EQUILIBRIUM CONSTANT FOR THE ADSORPTION OF METHANE, ETHANE, ETHYLENE AND CARBONDIOXIDE ON NaY ZEOLITE

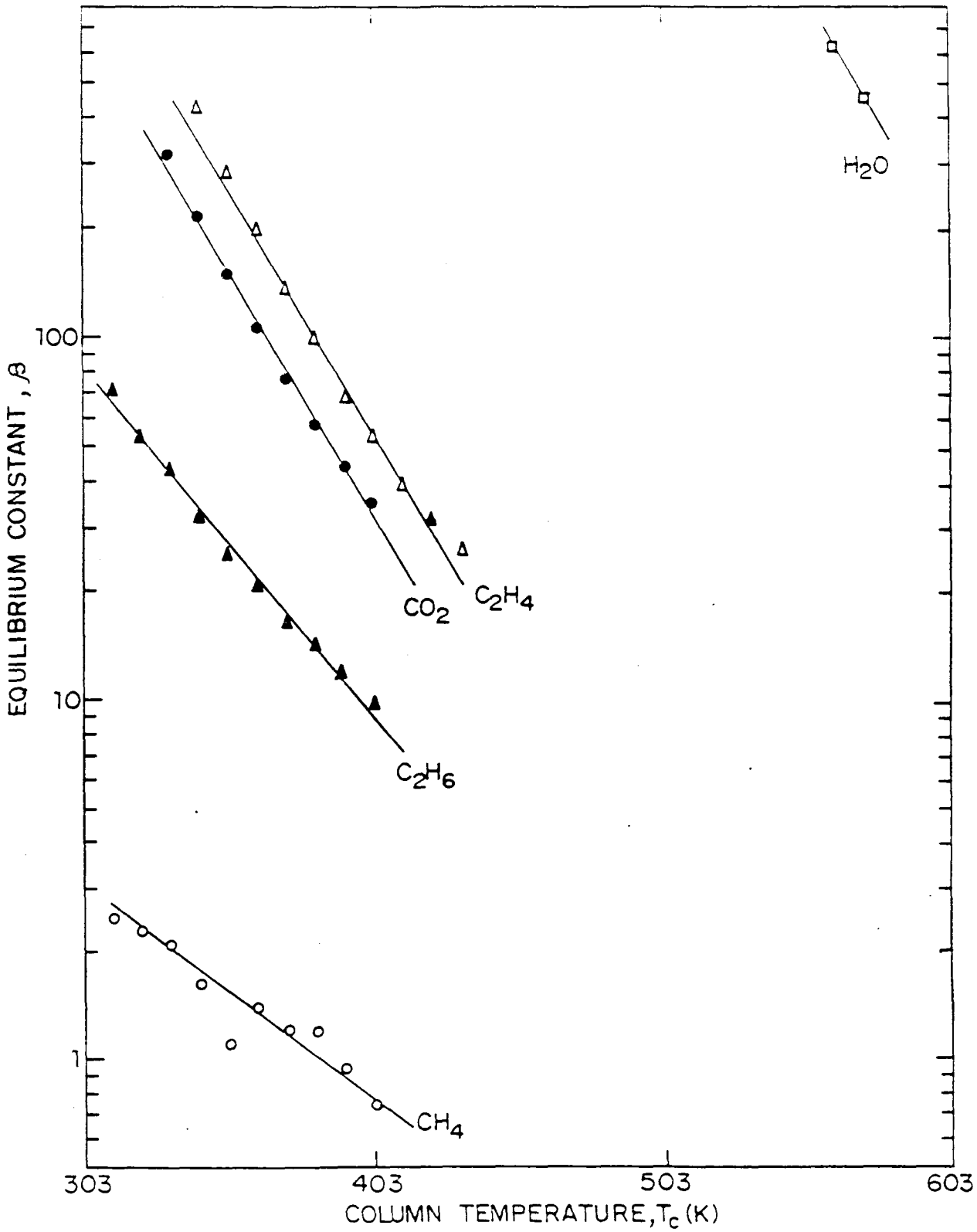

FIG. 3·23 : TEMPERATURE DEPENDENCE OF ADSORPTION EQUILIBRIUM CONSTANT FOR THE ADSORPTION OF METHANE, ETHANE, ETHYLENE, CARBON DIOXIDE AND WATER ON ZEOLITE Ce Na Y (Ce^{+3} 46 %)

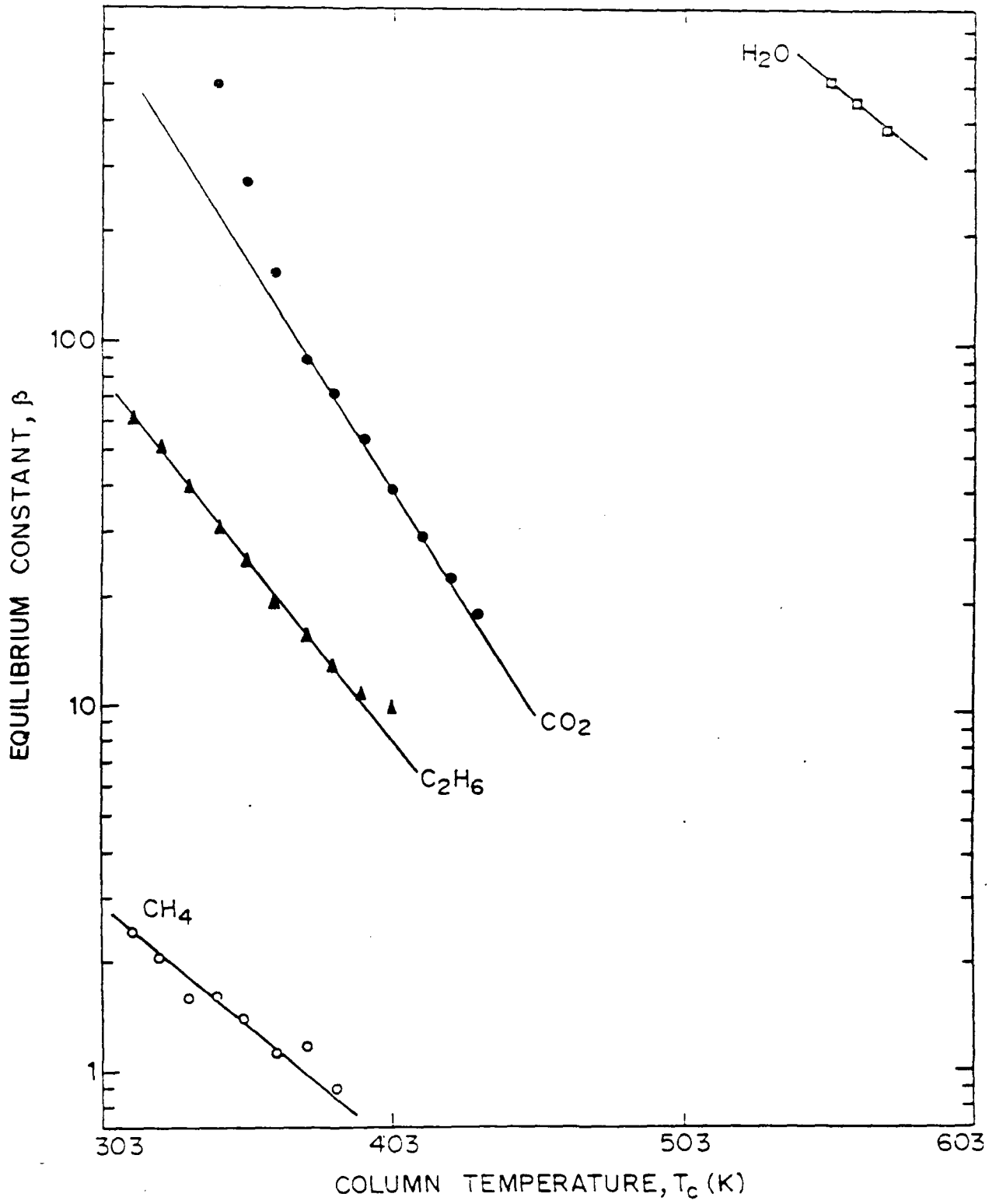

FIG. 3-24: TEMPERATURE DEPENDENCE OF ADSORPTION EQUILIBRIUM CONSTANT FOR THE ADSORPTION OF METHANE, ETHANE, CARBONDIOXIDE AND WATER ON ZEOLITE CeNaY (Ce^{+3} 72%)

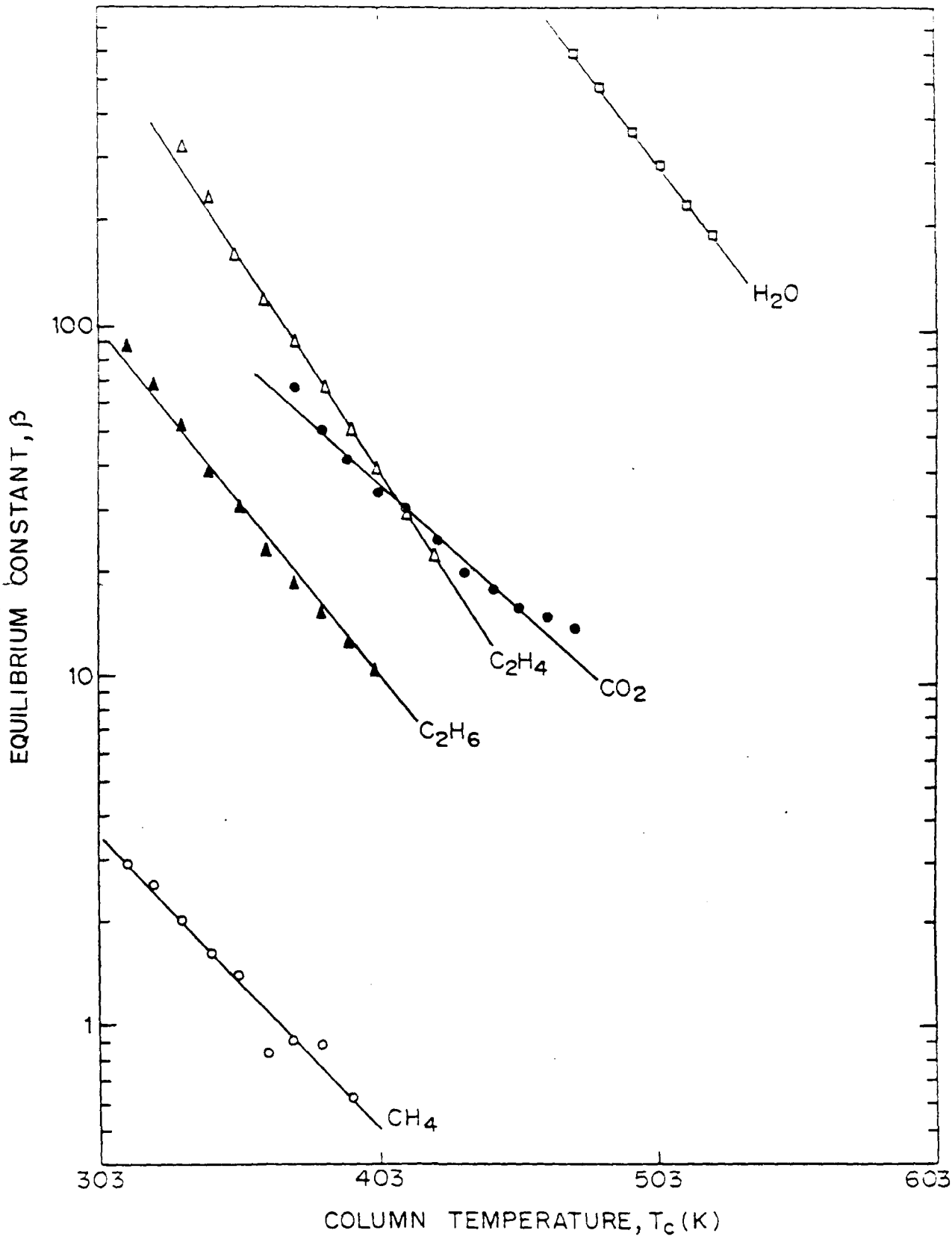

FIG. 3·25: TEMPERATURE DEPENDENCE OF ADSORPTION EQUILIBRIUM CONSTANT FOR THE ADSORPTION OF METHANE, ETHANE, ETHYLENE, CARBONDIOXIDE AND WATER ON KL ZEOLITE

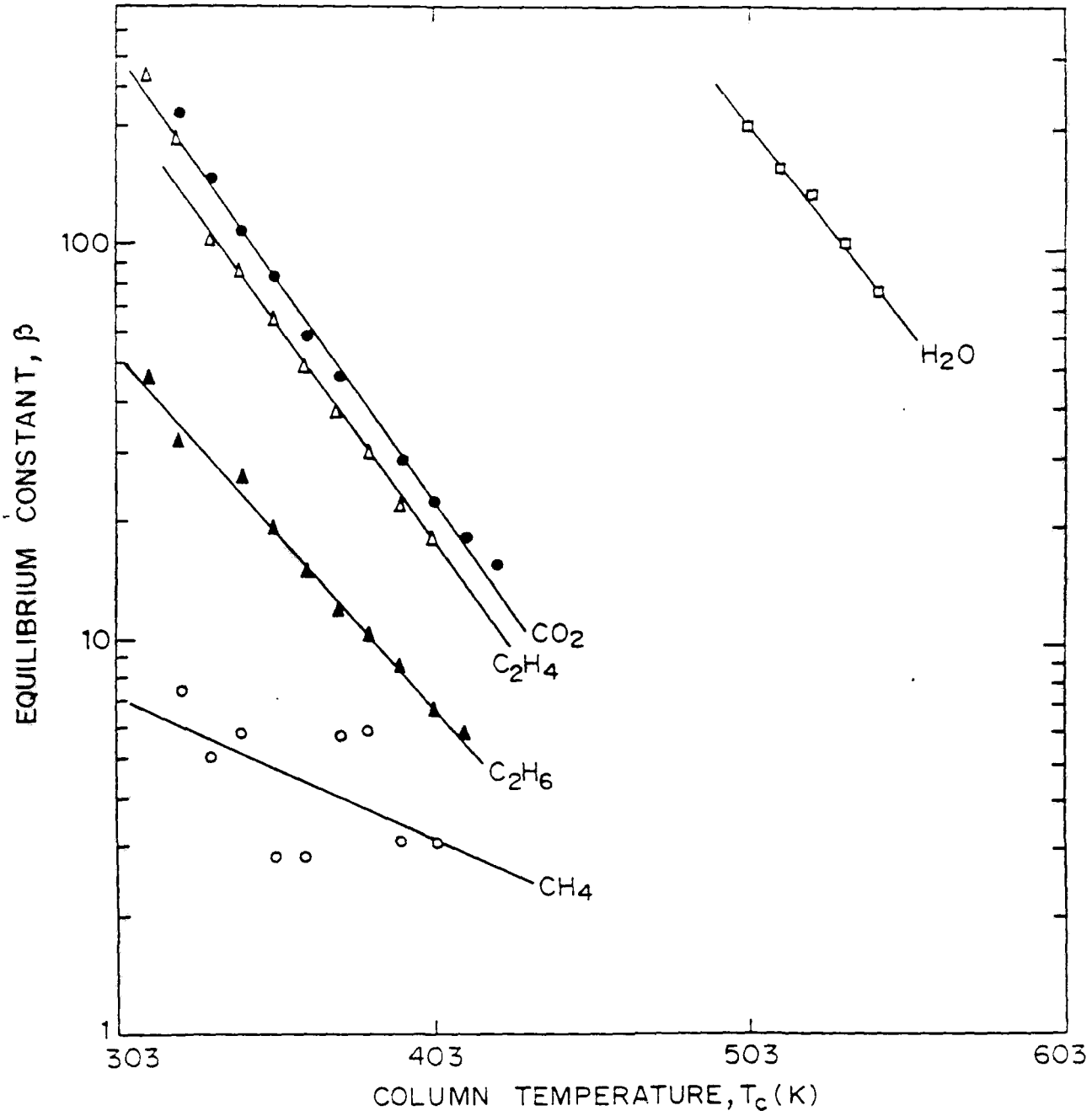

FIG.3·26: TEMPERATURE DEPENDENCE OF ADSORPTION EQUILIBRIUM CONSTANT FOR THE ADSORPTION OF METHANE, ETHANE, ETHYLENE, CARBONDIOXIDE AND WATER ON HKL ZEOLITE

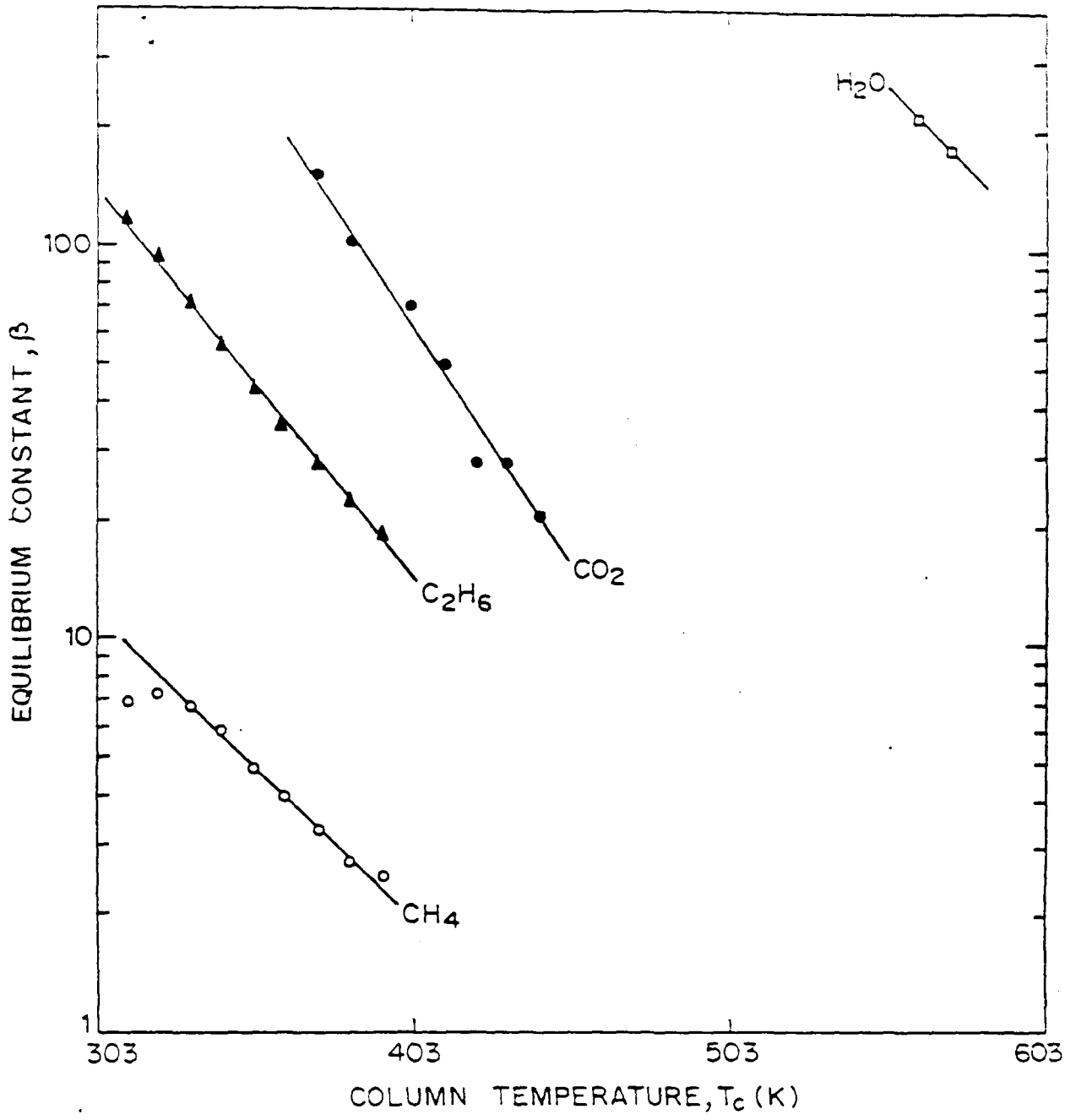

FIG. 3·27: TEMPERATURE DEPENDENCE OF ADSORPTION EQUILIBRIUM CONSTANT FOR THE ADSORPTION OF METHANE, ETHANE, WATER AND CARBONDIOXIDE ON HM ZEOLITE

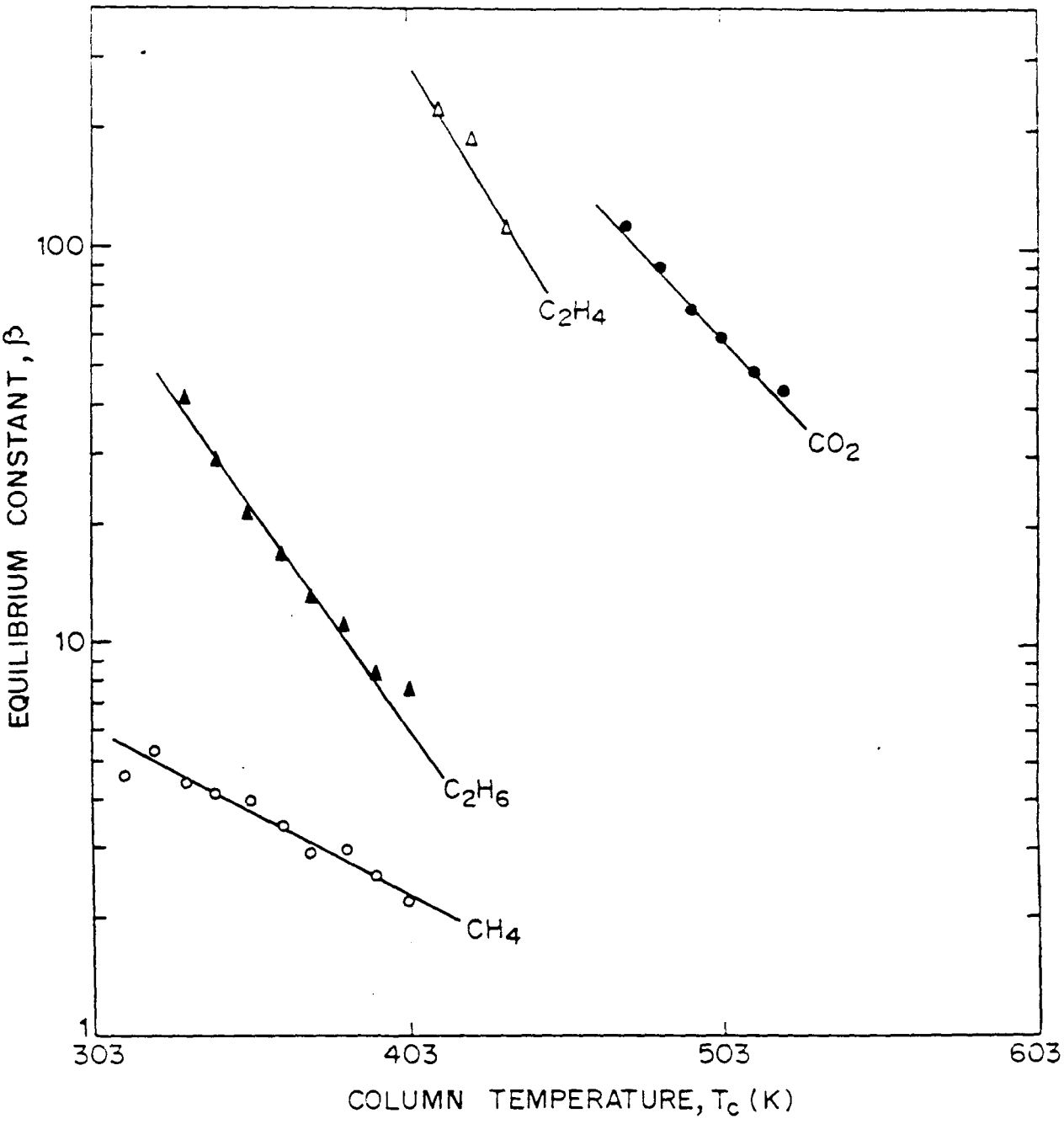

FIG.3·28: TEMPERATURE DEPENDENCE OF ADSORPTION EQUILIBRIUM CONSTANT FOR THE ADSORPTION OF METHANE, ETHANE, ETHYLENE AND CARBONDIOXIDE ON NaM ZEOLITE

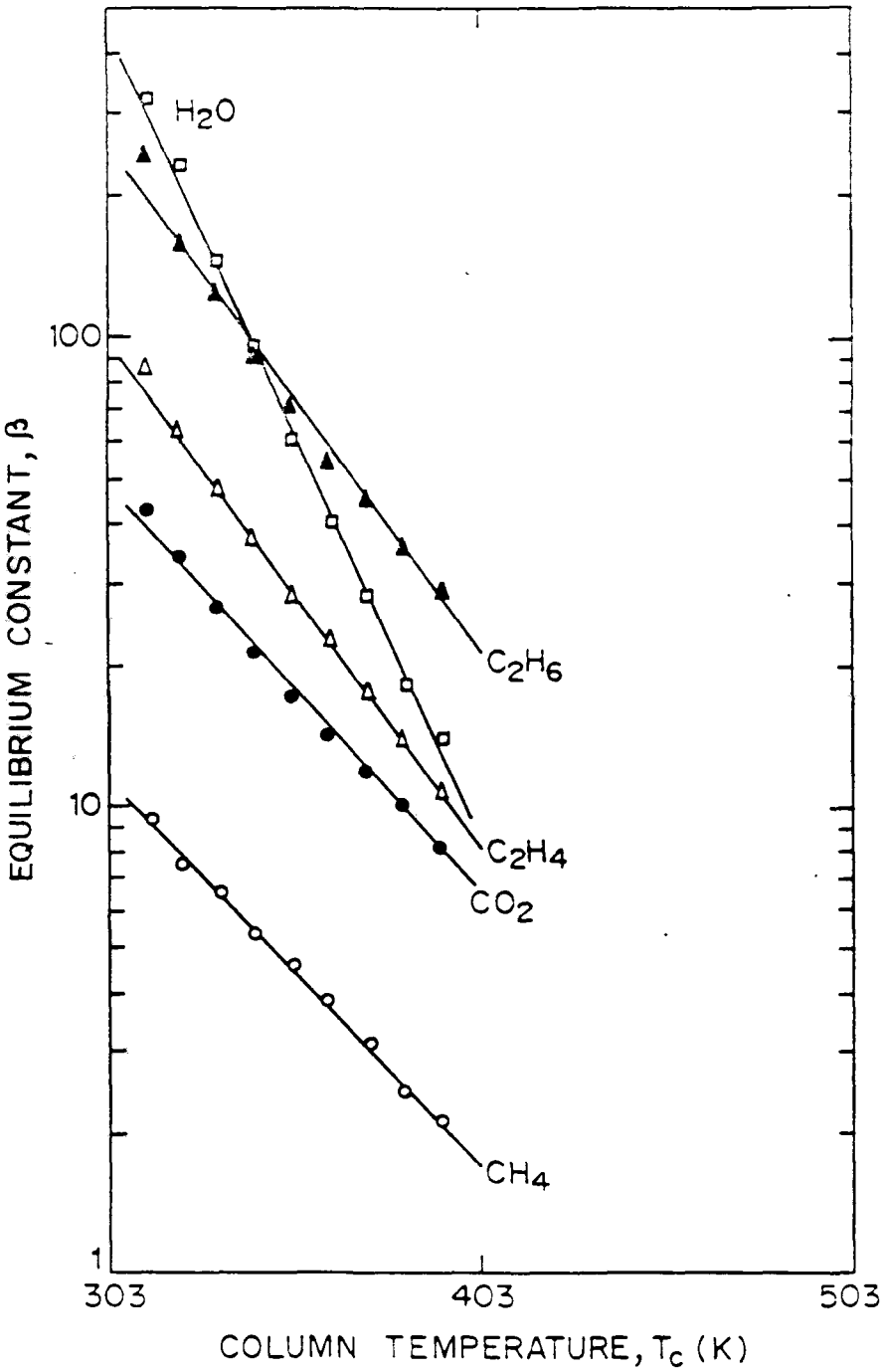

FIG.3·29: TEMPERATURE DEPENDENCE OF ADSORPTION EQUILIBRIUM CONSTANT FOR THE ADSORPTION OF METHANE, ETHANE, ETHYLENE, CARBONDIOXIDE AND WATER ON SLICALITE-I

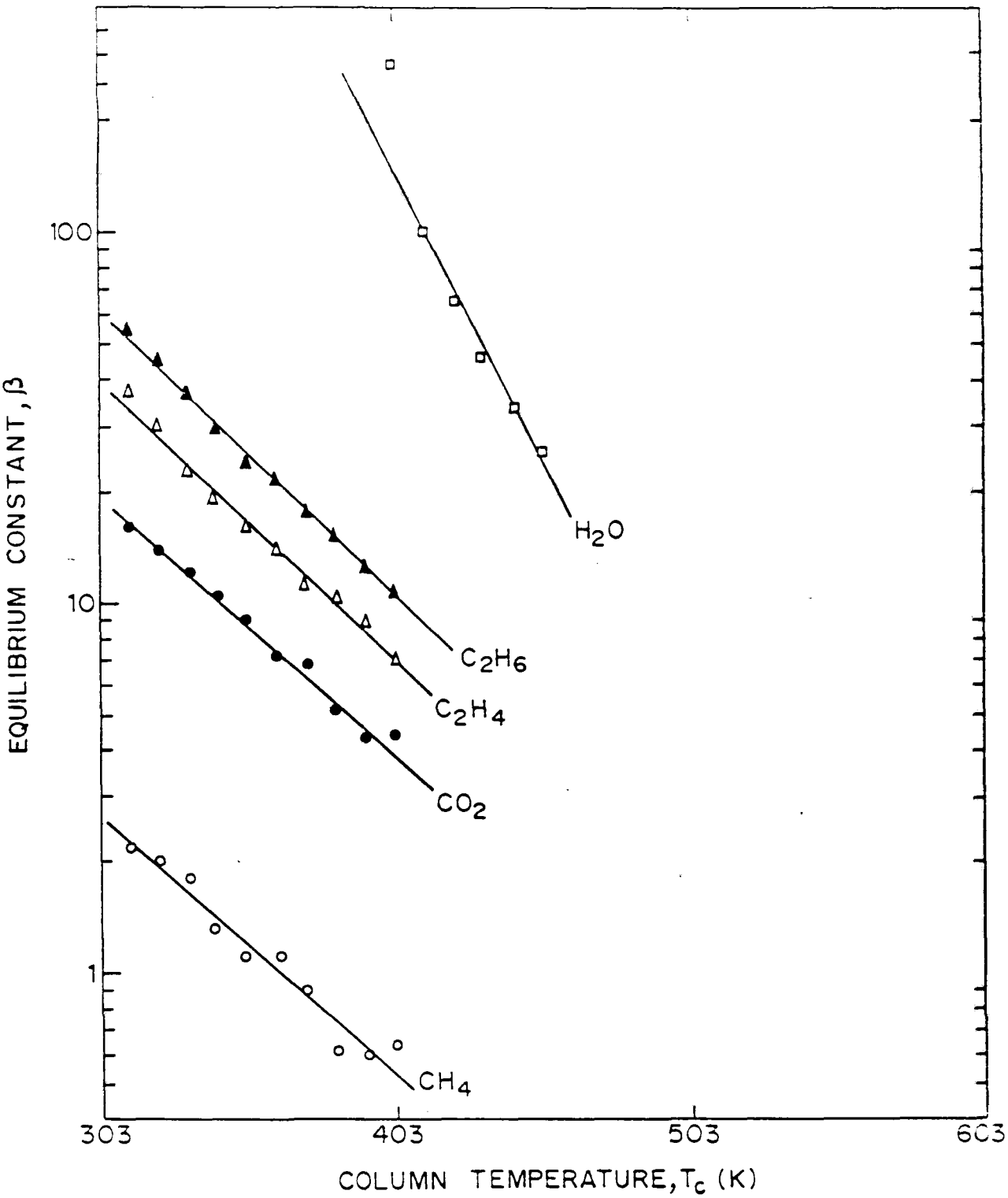

FIG. 3·30: TEMPERATURE DEPENDENCE OF ADSORPTION EQUILIBRIUM CONSTANT FOR THE ADSORPTION OF METHANE, ETHANE, ETHYLENE, CARBONDIOXIDE AND WATER ON $AlPO_4$-5

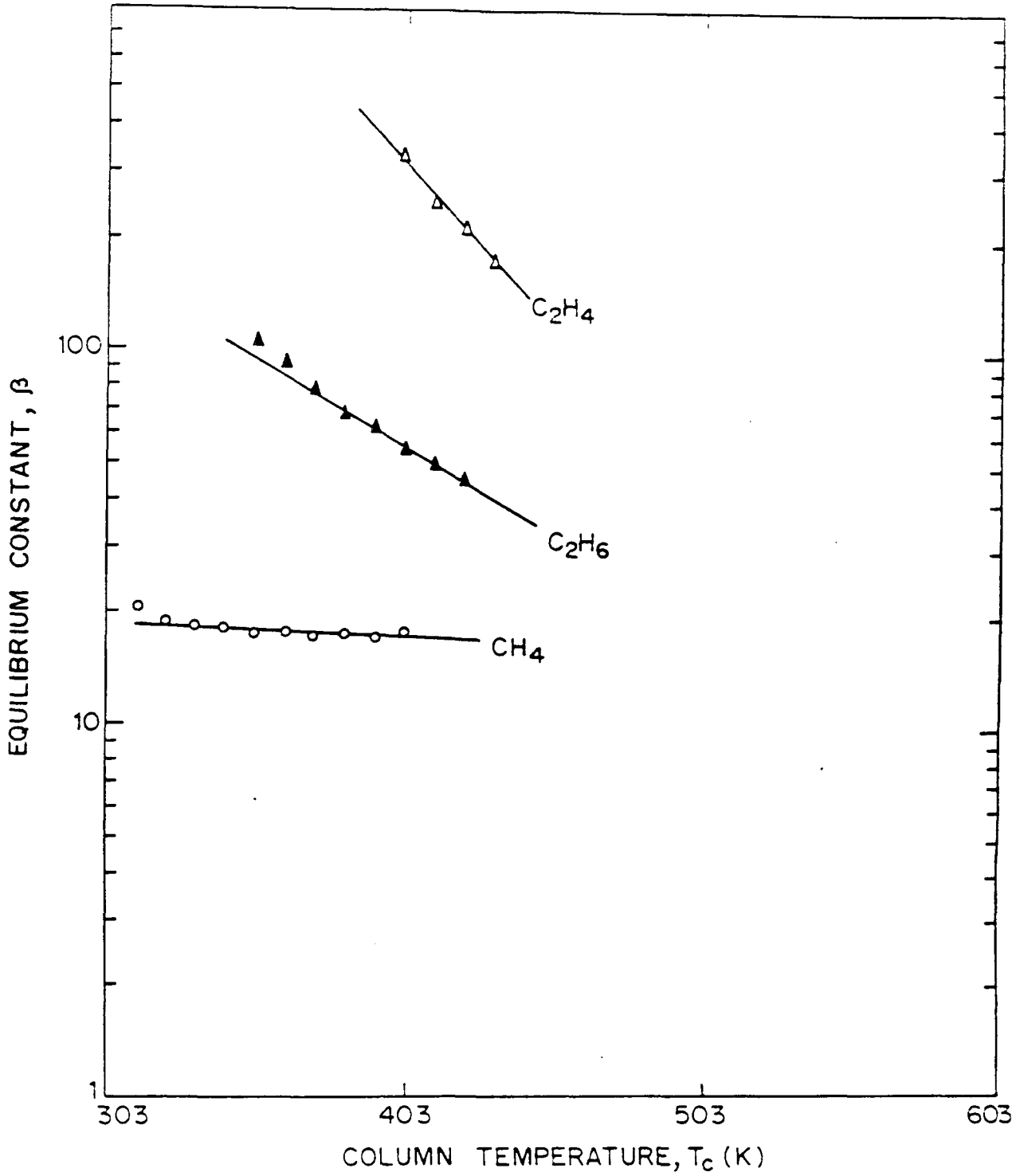

FIG.3·31: TEMPERATURE DEPENDENCE OF ADSORPTION EQUILIBRIUM CONSTANT FOR THE ADSORPTION OF METHANE, ETHANE AND ETHYLENE ON NaX ZEOLITE

Table 3.9

Comparison of adsorption equilibrium constants for the adsorption of methane, ethane, ethylene, carbon dioxide and water on different adsorbents

Zeolite: H-ZSM-5

Temperature (K)	Ads. equil. const. for CH_4	Relative equilibrium constant**			
		C_2H_6/CH_4	C_2H_4/CH_4	CO_2/CH_4	H_2O/CH_4
303	10.0*	25.0*	34.5*	10.0*	>1000*
373	2.9	13.9	15.5	5.4	793*
423	1.3*	10.8*	9.6*	3.4*	308*
473	0.54*	5.4*	5.9*	2.2*	146

Zeolite: H-Na-ZSM-5

Temperature (K)	Ads. equil. const. for CH_4	Relative equilibrium constant**			
		C_2H_6/CH_4	C_2H_4/CH_4	CO_2/CH_4	H_2O/CH_4
303	16.5*	19.4*	34.5*	115*	118*
373	4.1	11.3	16.7	44.2	141*
423	1.5*	6.3*	11.3*	24.4	178
473	0.55*	5.6*	6.9*	12.0*	195

* Data extrapolated from graph

** Sorption equilibrium constant of sorbate relative to that of methane

Table 3.9 (Contd.)

Zeolite: H-ZSM-8

Temperature (K)	Ads. equil. const. for CH_4	Relative equilibrium constant**			
		C_2H_6/CH_4	C_2H_4/CH_4	CO_2/CH_4	H_2O/CH_4
303	17.0*	23.5*	58.8*	12.3*	-
373	6.1	10.7	16.3	5.0	19.7
423	3.1*	6.1*	6.5*	2.7*	-
473	-	-	-	-	-

Zeolite: Na-H-ZSM-8

Temperature (K)	Ads. equil. const. for CH_4	Relative equilibrium constant**			
		C_2H_6/CH_4	C_2H_4/CH_4	CO_2/CH_4	H_2O/CH_4
303	24.0*	29.2*	196*	154*	-
373	5.8	14.9	124*	46.9	-
423	2.0*	10.0*	103	23.0*	-
473	0.7*	6.3*	84.8	10.7*	-

* Data extrapolated from graph

** Sorption equilibrium constant of sorbate relative to that of methane

Table 3.9 (Contd.)

Zeolite: HY

Temperature (K)	Ads. equil. const. for CH_4	Relative equilibrium constant**			
		C_2H_6/CH_4	C_2H_4/CH_4	CO_2/CH_4	H_2O/CH_4
303	2.0*	21.5*	140*	45.0*	very large
373	1.2	10.2	31.2	12.3	>8300*
423	0.45*	9.7*	18.9*	9.3*	8889*
473	0.24*	7.5*	8.3*	4.6*	4167*

Zeolite: NaY

Temperature (K)	Ads. equil. const. for CH_4	Relative equilibrium constant**			
		C_2H_6/CH_4	C_2H_4/CH_4	CO_2/CH_4	H_2O/CH_4
303	2.7*	37.0*	463*	389*	-
373	1.2	17.0	116	101	-
423	0.8*	8.5*	42.0*	35.5*	-
473	0.5*	4.6*	15.2*	13.0*	-

* Data extrapolated from graph

** Sorption equilibrium constant of sorbate relative to that of methane

Table 3.9 (Contd.)

Zeolite: CeNaY(Ce^{+3} exchange 46%)

Temperature (K)	Ads. equil. const. for CH_4	Relative equilibrium constant**			
		C_2H_6/CH_4	C_2H_4/CH_4	CO_2/CH_4	H_2O/CH_4
303	3.0*	26.7*	367*	233*	very large
373	1.2	14.1	113	64.6	--"--
423	0.6*	9.6*	55.2	29.3*	113800*
473	0.3*	6.3*	20.7*	11.7*	42000*

Zeolite: CeNaY(Ce^{+3} exchange 72%)

Temperature (K)	Ads. equil. const. for CH_4	Relative equilibrium constant**			
		C_2H_6/CH_4	C_2H_4/CH_4	CO_2/CH_4	H_2O/CH_4
303	2.9*	27.2*	-	248*	-
373	1.2	13.3	-	74.2	-
423	0.5*	11.1*	-	50.2	5652*
473	0.2*	7.6*	-	24.3*	7619*

* Data extrapolated from graph

** Sorption equilibrium constant of sorbate relative to that of methane

Table 3.9 (Contd.)

Zeolite: KL

Temperature (K)	Ads. equil. const. for CH_4	Relative equilibrium constant** C_2H_6/CH_4	C_2H_4/CH_4	CO_2/CH_4	H_2O/CH_4
303	3.5*	28.6*	183*	51.4*	-
373	0.9	21.8	102	79.0	7126*
423	0.3*	18.8*	75.6	70.9	5588*
473	0.13*	16.1*	43.1*	108	4569

Zeolite: HKL

Temperature (K)	Ads. equil. const. for CH_4	Relative equilibrium constant** C_2H_6/CH_4	C_2H_4/CH_4	CO_2/CH_4	H_2O/CH_4
303	6.1*	8.5*	36.1*	50.0*	-
373	5.8	1.8	6.5	8.0	793*
423	2.6*	1.7*	4.2*	6.2	519*
473	1.7*	0.9*	1.8*	2.1*	241*

* Data extrapolated from graph

** Sorption equilibrium constant of sorbate relative to that of methane

Table 3.9 (Contd.)

Zeolite: HM

Temperature (K)	Ads. equil. const. for CH_4	Relative equilibrium constant **			
		C_2H_6/CH_4	C_2H_4/CH_4	CO_2/CH_4	H_2O/CH_4
303	12.0*	11.2*	-	87.5*	-
373	3.2	10.8	-	47.5	-
423	1.3*	6.9*	-	21.3	2385*
473	0.5*	5.6*	-	17.3*	2308*

Zeolite: NaM

Temperature (K)	Ads. equil. const. for CH_4	Relative equilibrium constant **			
		C_2H_6/CH_4	C_2H_4/CH_4	CO_2/CH_4	H_2O/CH_4
303	6.0*	13.8*	2833*	483*	-
373	2.9	5.7	241*	255*	-
423	1.9*	1.8*	93.9	147*	-
473	1.1*	0.9*	30.4*	98.9	-

* Data extrapolated from graph

** Sorption equilibrium constant of sorbate relative to that of methane

Table 3.9 (Contd.)

Zeolite: Silicalite

Temperature (K)	Ads. equil. const. for CH_4	Relative equilibrium constant**			
		C_2H_6/CH_4	C_2H_4/CH_4	CO_2/CH_4	H_2O/CH_4
303	11.8*	21.2*	8.5*	4.2*	40.7*
373	3.1	14.5	5.6	3.8	8.9
423	1.2*	11.2*	4.3*	3.8*	3.3*
473	-	-	-	-	-

Zeolite: $AlPO_4$-5

Temperature (K)	Ads. equil. const. for CH_4	Relative equilibrium constant**			
		C_2H_6/CH_4	C_2H_4/CH_4	CO_2/CH_4	H_2O/CH_4
303	2.6*	23.5*	15.4*	7.5*	2308*
373	0.9	20.1	12.6	8.0	506*
423	0.4*	19.2*	13.1*	7.4*	173
473	0.2*	17.6*	11.8*	7.0*	70.6*

* Data extrapolated from graph

** Sorption equilibrium constant of sorbate relative to that of methane

Table 3.9 (Contd.)

Zeolite: NaX

Temperature (K)	Ads. equil. const. for CH_4	Relative equilibrium constant**			
		C_2H_6/CH_4	C_2H_4/CH_4	CO_2/CH_4	H_2O/CH_4
303	18.5*	8.6*	162*	-	-
373	17.2	4.6	33.4*	-	-
423	16.5*	2.9	13.5	-	-
473	16.0*	1.6*	4.9*	-	-

* Data extrapolated from graph

** Sorption equilibrium constant of sorbate relative to that of methane

Table 3.10

Comparison of the present and reported heat of sorption values for various sorbates on different zeolites

Zeolite	Sorbate	Heat of sorption ($kJ.mol^{-1}$)	
		Present (by gc pulse method)	Reported data [Ref]
NaX	C_2H_6	15.0	25-26 [3,4,7,8]
	C_2H_4	31.5	36-38.5 [3,4,7,8, 10,11,12]
NaY	CH_4	12.1	16.9-18 [15]
	C_2H_4	37.8	31.8 [17]
	CO_2	36.5	31-33.5 [13,17]
HM	CH_4	19.3	25.5 [21b]
	C_2H_6	24.9	33.3 [21b]
	CO_2	44.5	46.4 [14]
KL	CH_4	18.1	18.4 [55]
	C_2H_6	24.7	29.3 [55]
Silicalite	CH_4	18.4	18.0*, 19.9 [22,24]
	C_2H_6	28.3	29.8** [25a]
	CO_2	21.7	27.9 [25a]
$AlPO_4$-5	CH_4	14.3	18.4 [26]
	C_2H_6	18.7	23.9 [26]

* Theoretical value estimated by Monte-Carlo simulation

** Theoretical value estimated by molecular statistical calculations

given in Appendix 3.2. Fig. 3.32 shows the adsorption isotherms of n-hexane on silicalite at two temperatures (302 and 423 K). The adsorption isotherms of n-hexane and water on NaM are given in Fig. 3.33. The amount of water vapor sorbed on NaM at 9.3 kPa and 350 K (0.14 $cm.^3g^{-1}$) is well within the limiting volume of mordenite for water (0.16 $cm.^3g^{-1}$) reported in the literature [41b].

The isotherms of sorption of methane, ethane, ethylene and carbon dioxide in NaX, NaY, NaM, Silicalite, $AlPO_4$-5 and SAPO-5 at different temperatures are presented in Figs. 3.34-3.39. The isotherm data are given in Appendix 3.3-3.8.

3.3.2.1 Fitting of Isotherms to Standard Isotherm Models

Several theories and correlations of adsorption equilibria for microporous adsorbents are available in literature. To represent the equilibrium relation for single component adsorption, a number of model isotherms reported in literature have been tested. A list of the model isotherms evaluated in this work is given in Table 3.6. The isotherm data were fitted initially to simpler models like the Langmuir, Freundlich and Dubinin-Polanyi equations. For these models, the data were fitted by linear regression using a scientific pocket calculator. The discrimination of the model was mainly based on the regression coefficient and the percentage deviation of the value of q estimated using the model parameters from that measured experimentally. In the case of Langmuir model, an additional logical discrimination was made based on the values of q_m at the two temperatures studied.

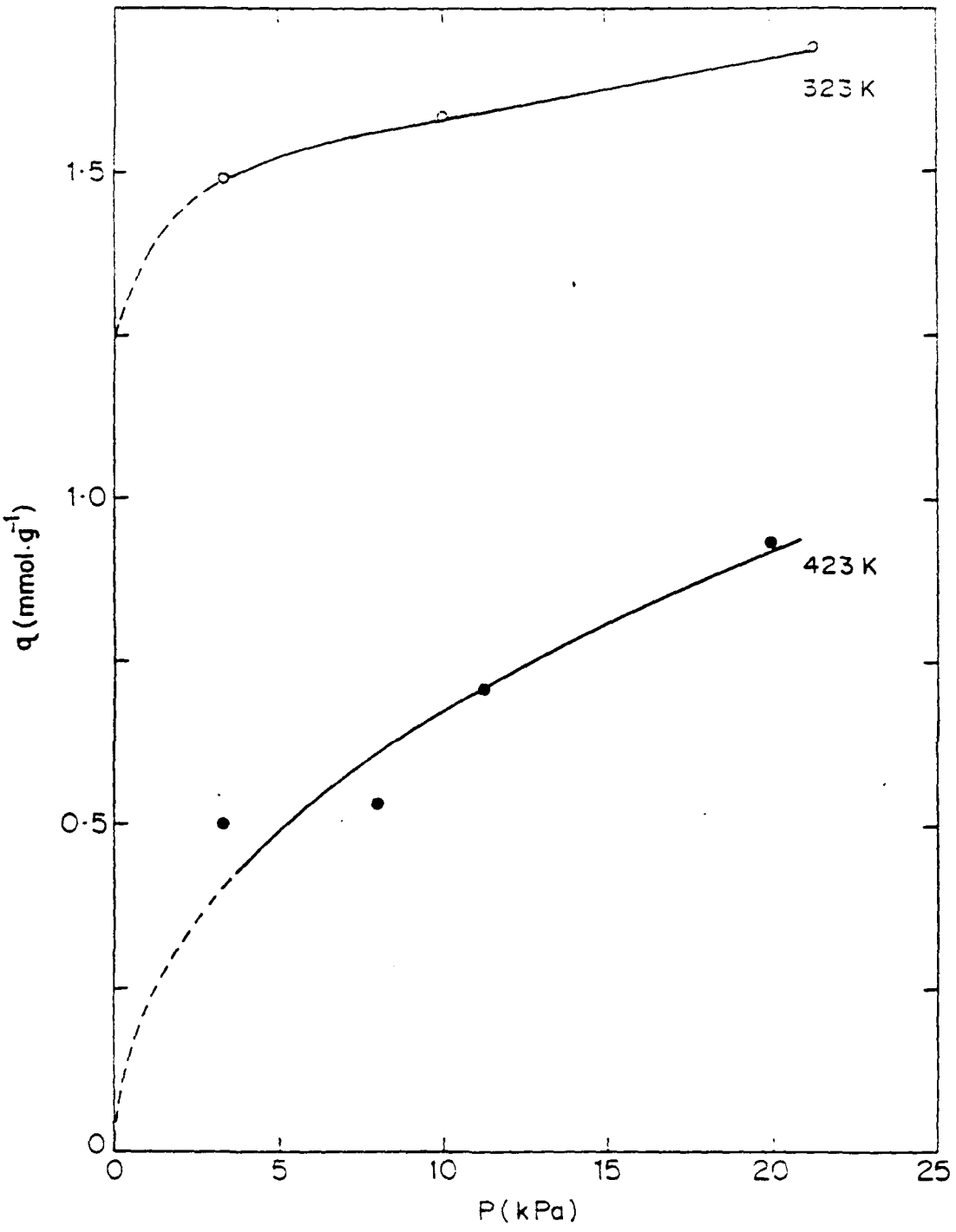

FIG. 3·32: ADSORPTION ISOTHERMS OF n-HEXANE ON SILICALITE-I

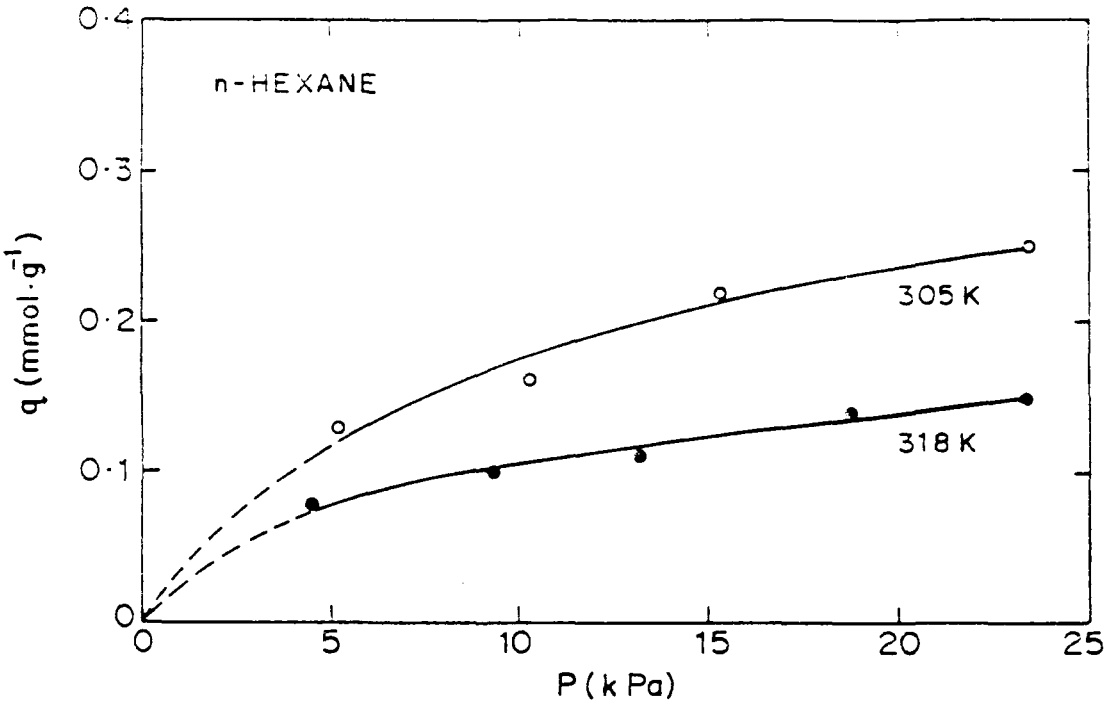

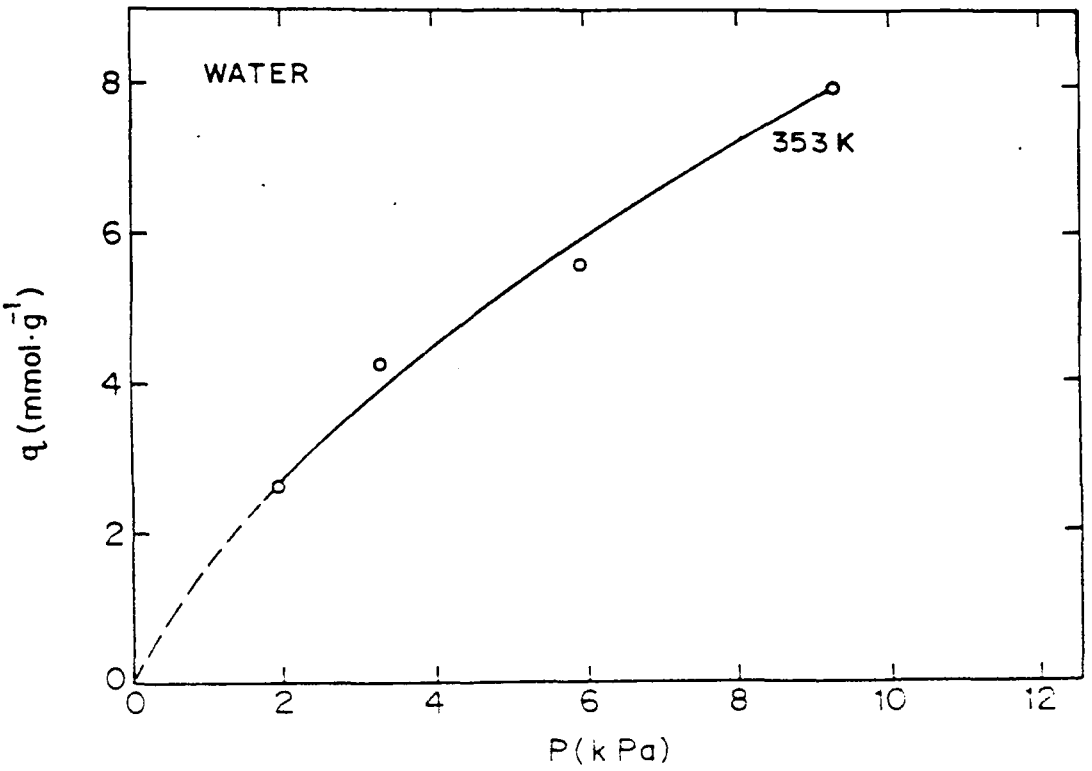

FIG.3·33: ADSORPTION ISOTHERMS OF n-HEXANE AND WATER ON NaM

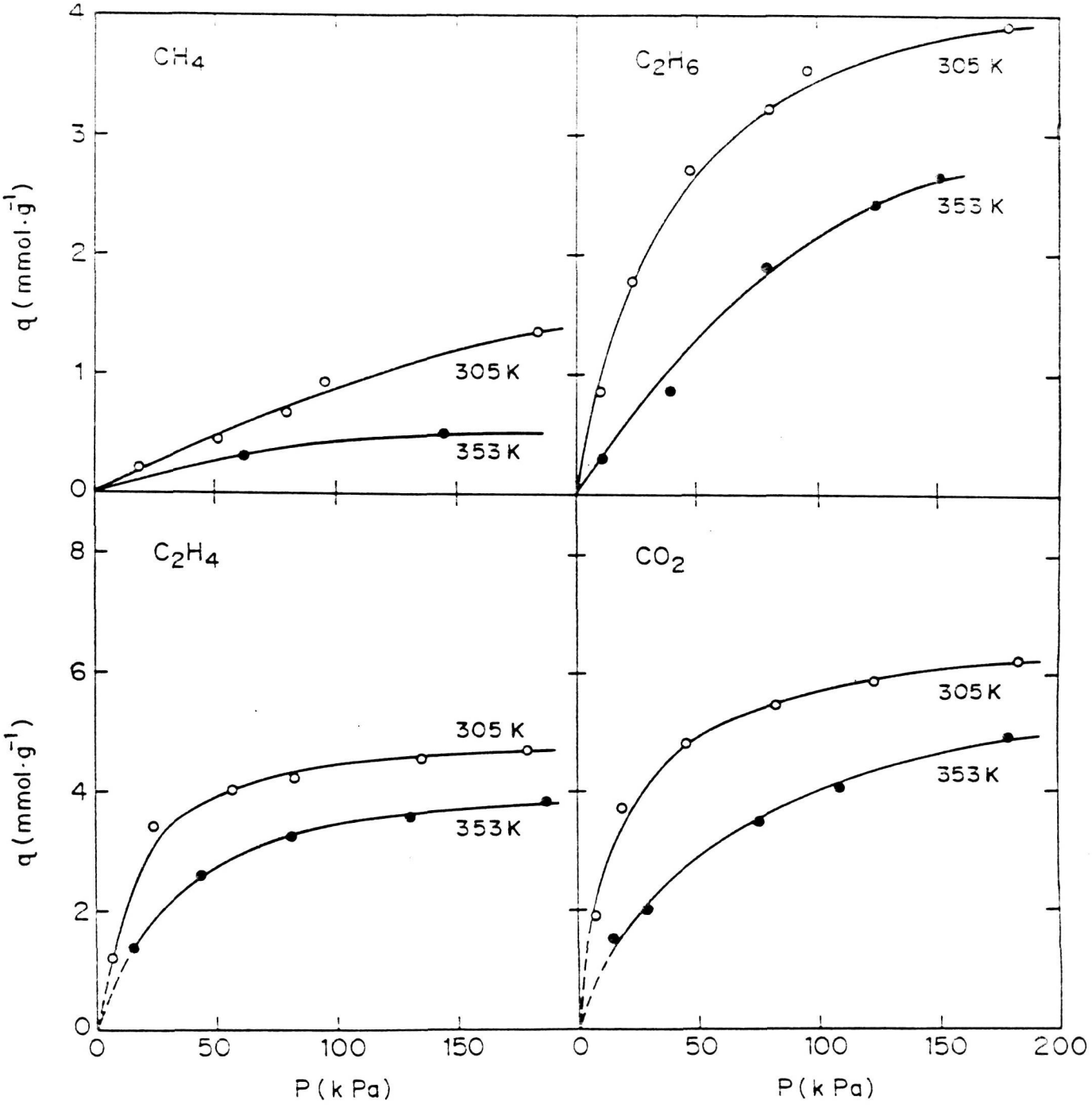

FIG.3·34: ADSORPTION ISOTHERMS OF METHANE, ETHANE, ETHYLENE AND CARBONDIOXIDE ON NaX ZEOLITE BY GRAVIMETRIC METHOD

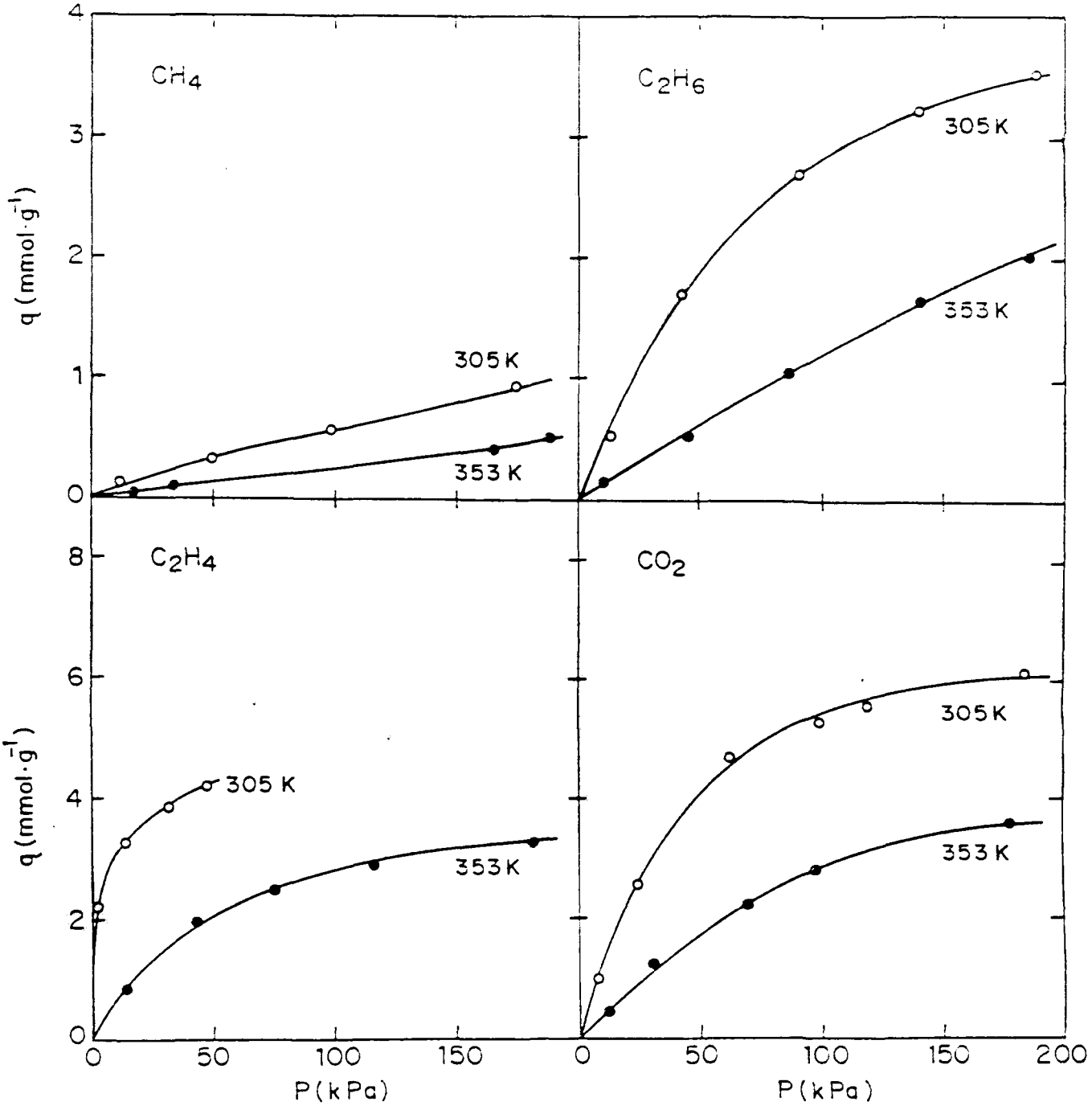

FIG. 3·35 : ADSORPTION ISOTHERMS OF METHANE, ETHANE, ETHYLENE AND CARBONDIOXIDE ON NaY ZEOLITE BY GRAVIMETRIC METHOD

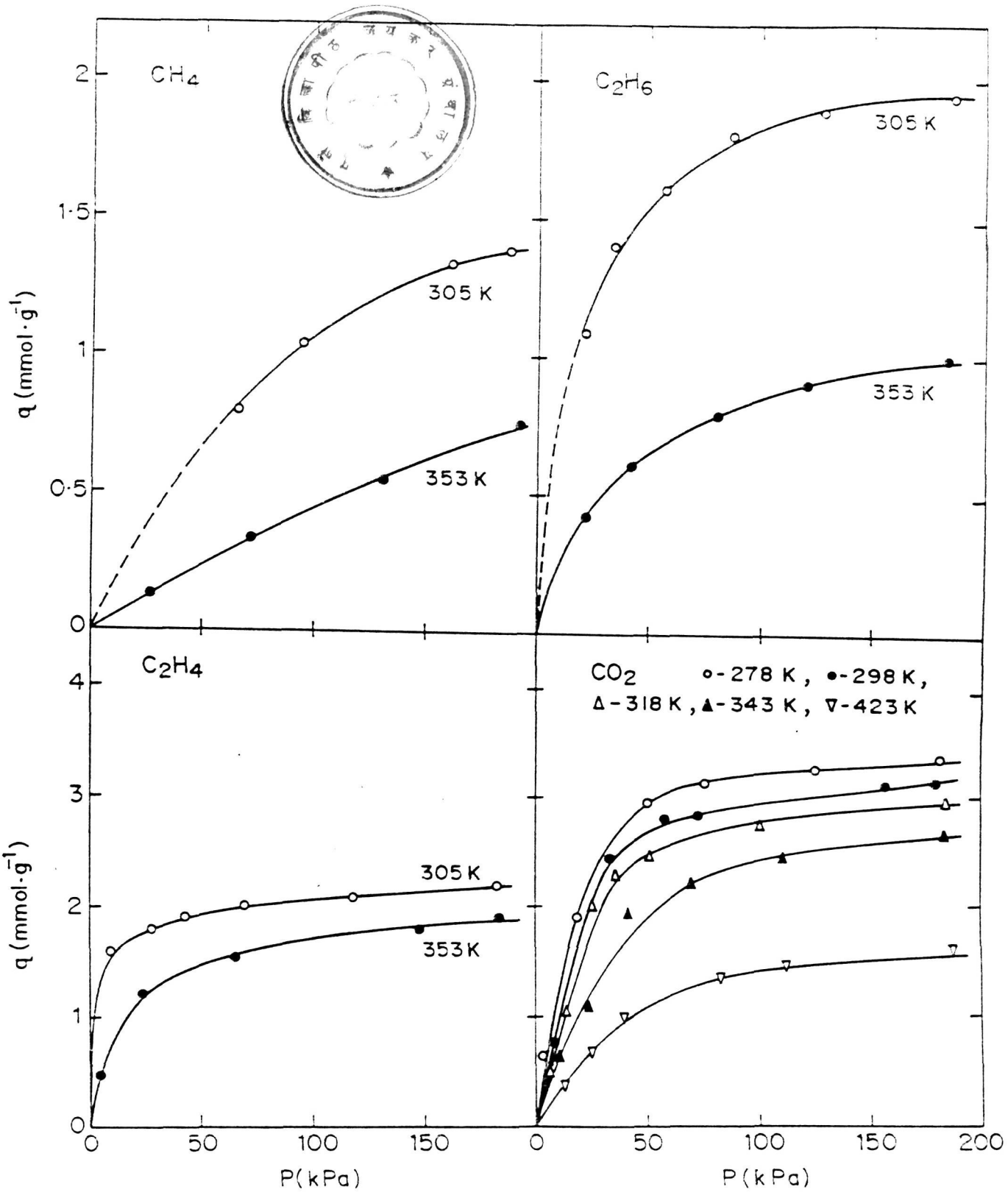

FIG.3·36: ADSORPTION ISOTHERMS OF METHANE, ETHANE, ETHYLENE AND CARBONDIOXIDE ON SODIUM MORDENITE BY GRAVIMETRIC METHOD

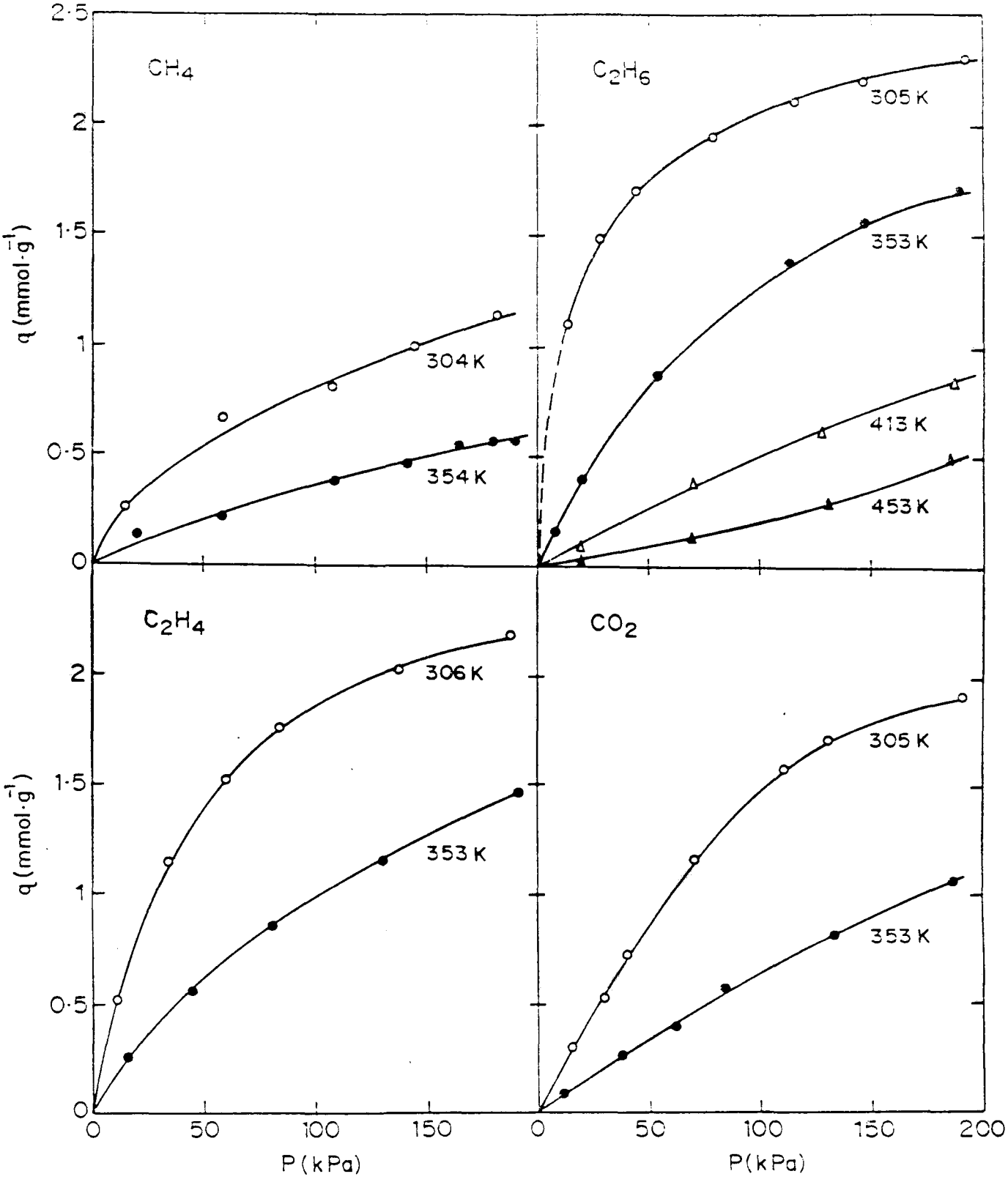

FIG.3·37: ADSORPTION ISOTHERMS OF METHANE, ETHANE, ETHYLENE AND CARBONDIOXIDE ON SILICALITE BY GRAVIMETRIC METHOD

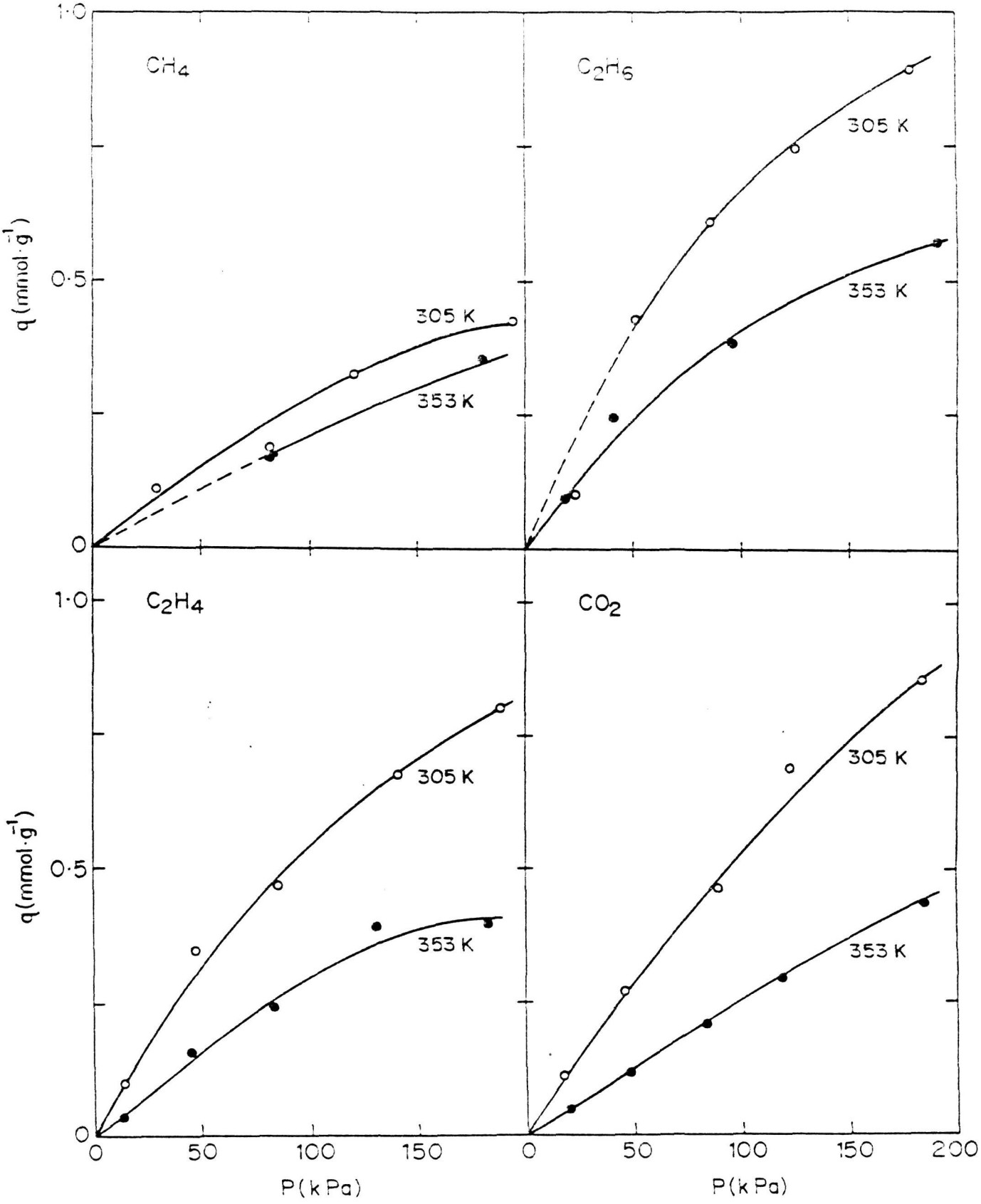

FIG.3·38: ADSORPTION ISOTHERMS OF METHANE, ETHANE, ETHYLENE AND CARBONDIOXIDE ON $AlPO_4$-5 BY GRAVIMETRIC METHOD

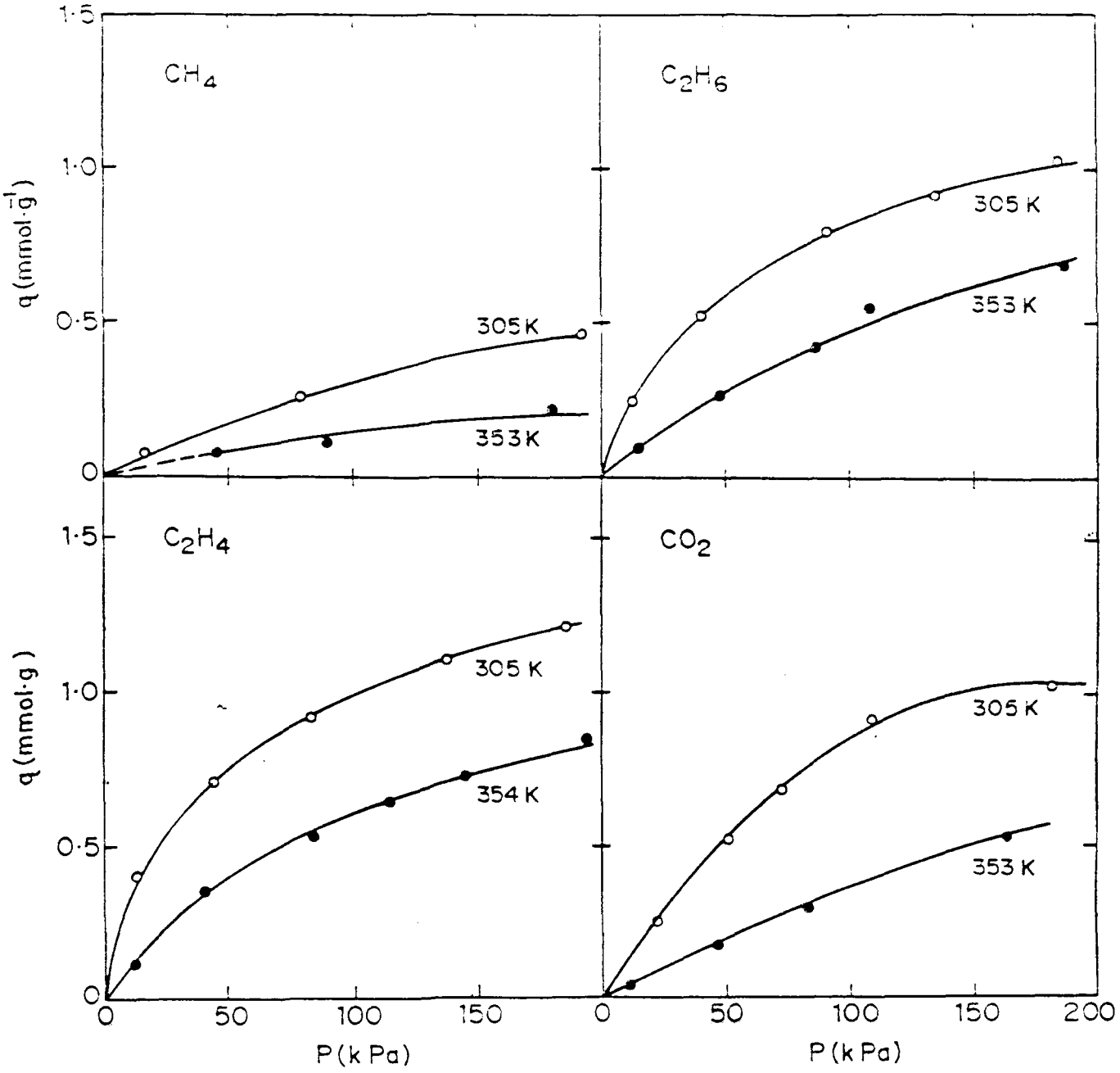

FIG.3·39: ADSORPTION ISOTHERMS OF METHANE, ETHANE, ETHYLENE AND CARBONDIOXIDE ON $SAPO_4$-5 BY GRAVIMETRIC METHOD

For those cases where the two parameter models were found to give poor fits, more complex three parameter models like the Sips', Toth and Dubinin-Astakhov isotherms were tried for fitting the sorption data. The value of P_s in the Dubinin-Polanyi and Dubinin-Astakhov models were estimated using the generalized form of the Clapeyron equation [53]. The model parameters were estimated by non-linear regression analysis using Marquardt's algorithm [51,52]. All the computations were done in Fortran 77 using an IBM-XT PC. Here the model discrimination was made based on the percentage deviation between the estimated and experimentally measured value of q.

Tables 3.11 and 3.12 give the statistical analysis of the curve fitting data for the sorption of methane, ethane, ethylene and carbon dioxide in the different adsorbents. The values of model parameters for the equilibrium sorption of the gases in the various adsorbents studied are given in Tables 3.13-3.16.

In general, it is observed that the Dubinin-Polanyi model gives a good fit for the sorption of methane, ethane and ethylene in most of the adsorbents studied. This is to be expected as the theory for this model is based on pore volume filling, which is the mechanism of sorption in zeolites and is considered to represent well the equilibrium adsorption of non-polar molecules on many adsorbents. Langmuir model fits the equilibrium sorption data of CO_2 on the adsorbents except $AlPO_4$-5 and SAPO-5. Langmuir model also gives a good fit for the sorption isotherms of C_2H_4 on NaY, NaM, Silicalite and that of C_2H_6 on NaM. Freundlich model gives a reasonably good fit for

Table 3.11

Statistical analysis of curve fitting data for the adsorption of methane and ethane on different adsorbents (0-200 kPa, 305-353K)

METHANE

Adsorbent	Best fitting equation	Percentage deviation of q	Regression coefficient*
NaX	Dubinin - Polanyi	-0.5 to 3	-
NaY	Freundlich	-3 to 2	0.999, 1.0
	Dubinin - Polanyi	-3 to 4	0.998, 1.0
NaM	Dubinin - Polanyi	-4 to 5	0.998, 0.9999
Silicalite	Freundlich	-2 to 5	0.9997, 0.9997
	Dubinin - Polanyi	-5 to 5	0.998, 0.9993
$AlPO_4$-5	Dubinin - Polanyi	-6 to 6	0.9997, 0.9989
SAPO-5	Dubinin - Polanyi	-5 to 5	0.9993, 0.999

ETHANE

NaX	Dubinin - Polanyi	-3 to 6	-
NaM	Langmuir	-2 to 3	0.9997, 0.9993
Silicalite (305-413 K)	Dubinin - Polanyi	-4 to 4	0.999[illegible], 0.9994
Silicalite (453 K)	Freundlich	-6 to 2	0.9997, 0.9993
$AlPO_4$-5	Dubinin - Polanyi	-5 to 6	0.9993, 0.9989
SAPO-5	Dubinin - Polanyi	-2 to 3	0.9996, 0.9997
NaY	Dubinin - Astakhov	-6 to 3	-

* The values indicate regression coefficients for isotherm models at different temperatures.

Table 3.12

Statistical analysis of curve fitting data for the adsorption of ethylene and carbondioxide on different adsorbents (0-200 kPa, 305-353K)

ETHYLENE

Adsorbent	Best fitting equation	Percentage deviation of q	Regression coefficient*
NaY	Langmuir	-3 to 2	0.998, 0.9999
	Dubinin - Polanyi	-3 to 5	0.9988, 0.994
NaM	Langmuir	-4 to 3	0.9997, 0.9998
Silicalite	Langmuir	-4 to 3	0.9896, 0.993
$AlPO_4$-5	Dubinin - Polanyi	-5 to 5	0.9996, 0.9987
SAPO-5	Dubinin - Polanyi	-7 to 5	0.9994, 0.9977
NaX	Dubinin - Astakhov	-5 to 5	-

CARBONDIOXIDE

NaX	Langmuir	-5 to 4	-
NaY	Langmuir	-4 to 4	0.998, 0.982
NaM (305-423 K)	Langmuir	-7 to 8	0.964, 0.959, 0.998, 0.998, 0.997
Silicalite	Freundlich (353 K)	-4 to 2	0.9997
	Langmuir (305 K)	-4 to 5	0.9985
$AlPO_4$-5	Freundlich	-6 to 5	0.9999, 0.9995
SAPO-5	Dubinin - Polanyi	-6 to 9	0.9977, 0.9996

* The values indicate regression coefficients for isotherm models at different temperatures.

Table 3.13

Constants of the best fitting isotherm models for the adsorption of METHANE on different adsorbents (pressure range 0-200 kPa)

Adsorbent	Temperature (K)	Dubinin - Polanyi constants C	-D	Maximum deviation in q (%)
NaX	305	2.193	0.0683	-0.5 to 3
	353	1.081	0.0502	0 to 0.3
NaY	305	1.6393	0.0637	-3 to 4
	353	2.4762	0.097	0 to 0.02
NaM	305	1.8305	0.0526	-4 to 5
	353	1.8654	0.0671	-1 to 2
Silicalite	304	1.3118	0.0446	-5 to 5
	354	1.3493	0.0590	-4 to 3
$AlPO_4$ -5	305	1.1257	0.0709	-3 to 4
	353	1.2153	0.0705	-6 to 6
SAPO-5	305	1.1346	0.0685	-5 to 4
	353	0.4860	0.0621	-6 to 4

Adsorbent	Temperature (K)	Freundlich constants k	c	Maximum deviation in q (%)
NaY	305	0.0148	0.7945	-1 to 2
	353	0.0011	1.1682	-3 to 0
Silicalite	304	0.0530	0.5892	-2 to 2
	353	0.0077	0.8350	-2 to 5

Table 3.14

Constants of the best fitting isotherm models for the adsorption of ETHANE on different adsorbents (pressure range 0-200 kPa)

Adsorbent	Temperature (K)	Dubinin - Polanyi constants C	-D	Maximum deviation in q (%)
NaX	305	2.1411	0.0571	-3 to 6
	353	2.3670	0.0737	0 to 4
Silicalite	305	1.1746	0.0303	-2 to 3
	353	1.6258	0.0638	-3 to 4
	413	1.6691	0.0801	-4 to 3
$AlPO_4$ -5	305	0.8502	0.0848	-6 to 6
	353	0.7745	0.0774	-5 to 6
SAPO-5	305	0.6480	0.0574	-2 to 2
	353	0.9022	0.0752	-2 to 3

Adsorbent	Temperature (K)	Langmuir constants q_m	k	Maximum deviation in q (%)
NaM	305	2.2133	0.0456	-2 to 1
	353	1.1975	0.0256	0 to 3

Adsorbent	Temperature (K)	Freundlich constants k	c	Maximum deviation in q (%)
Silicalite	453	0.0010	1.1648	-6 to 2

Adsorbent	Temperature (K)	Dubinin - Astakhov constants A	B	C	Maximum deviation in q (%)
NaY	305	1.554	0.005	3.430	-5 to 2
	353	3.184	0.350	1.395	-6 to 3

Table 3.15

Constants of the best fitting isotherm models for the adsorption of ETHYLENE on different adsorbents (pressure range 0-200 kPa)

Adsorbent	Temperature (K)	Dubinin - Polanyi constants C	-D	Maximum deviation in q (%)
NaY	305	1.9018	0.0178	-1 to 1
	353	2.0892	0.0419	-4 to 5
$AlPO_4$ -5	305	0.8290	0.0764	-3 to 3
	353	0.8903	0.0834	-5 to 5
SAPO-5	305	0.7664	0.0412	-3 to 3
	353	1.0530	0.0610	-7 to 5

Adsorbent	Temperature (K)	Langmuir constants q_m	k	Maximum deviation in q (%)
NaY	305	4.8152	0.1451	-4 to 2
	353	4.3260	0.0181	-1 to 1
NaM	305	2.2182	0.1451	-1 to 3
	353	2.0465	0.0520	-4 to 2
Silicalite	305	2.6148	0.0222	-4 to 1
	353	2.5882	0.0064	-3 to 3

Adsorbent	Temperature (K)	Dubinin - Astakhov constants A	B	C	Maximum deviation in q (%)
NaX	305	1.553	1.0×10^{-5}	6.024	-5 to 5
	353	1.555	5.9×10^{-4}	3.932	-1 to 1

Table 3.16

Constants of the best fitting isotherm models for the adsorption of CARBON DIOXIDE on different adsorbents (pressure 0-200 kPa)

Adsorbent	Temperature (K)	Langmuir constants q_m	Langmuir constants k	Maximum deviation in q (%)
NaX	305	6.723	0.0579	-1 to 3
	353	6.262	0.0180	-5 to 3
NaY	305	7.6863	0.0218	-3 to 2
	353	6.9816	0.0064	-3 to 4
NaM	278	3.6245	0.0697	-4 to 1
	298	3.5131	0.0520	-5 to 1
	318	3.3334	0.0444	-7 to 2
	343	3.2663	0.0255	-6 to 8
	423	1.9706	0.0222	-6 to 2
Silicalite	305	3.8117	0.0059	-4 to 5

Adsorbent	Temperature (K)	Freundlich constants k	Freundlich constants c	Maximum deviation in q (%)
Silicalite	353	0.0101	0.8924	-4 to 2
$AlPO_4$-5	305	0.0085	0.8919	-1 to 3
	353	0.0020	1.0426	-6 to 4

Adsorbent	Temperature (K)	Dubinin - Polanyi constants C	Dubinin - Polanyi constants -D	Maximum deviation in q (%)
SAPO-5	305	0.9572	0.0913	-6 to 5
	353	0.7332	0.1027	-3 to 5

the sorption of all the gases on silicalite except ethylene for which Langmuir is the best fitting model. Only Dubinin-Astakhov model represent well the adsorption of ethane on NaY and ethylene on NaX.

3.3.2.2 Heat of Sorption as a Function of Surface Coverage

According to the ideal Langmuir model, the heat of adsorption should be independent of surface coverage. This requirement is rarely fulfilled in real systems because the effects of surface heterogeneity and sorbate-sorbate interaction are generally significant. Information regarding the magnitude of the heat of sorption and its variation with coverage can provide useful information concerning the nature of the surface and the adsorbed phase.

The isosteric heat of sorption can be obtained from the adsorption isotherms using the Clausius-Clapeyron equation (Equations (3.4)-(3.6)). For a set of isotherms it can be obtained from the slope of the logP versus 1/T plots at constant surface coverage (Equation (3.5)). The isosteric heat of sorption at various surface coverages for the adsorption of CO_2 on NaM and C_2H_4 on silicalite have been estimated in this manner. Figs. 3.40 and 3.41 give the plots of logP versus 1/T for the sorption of CO_2 on NaM and of C_2H_4 on silicalite, respectively.

The isosteric heat of sorption at different surface coverages can be calculated from a pair of isotherms using Equation (3.6). The heat of sorption at different coverages, estimated using Equation (3.6), for the adsorption of methane,

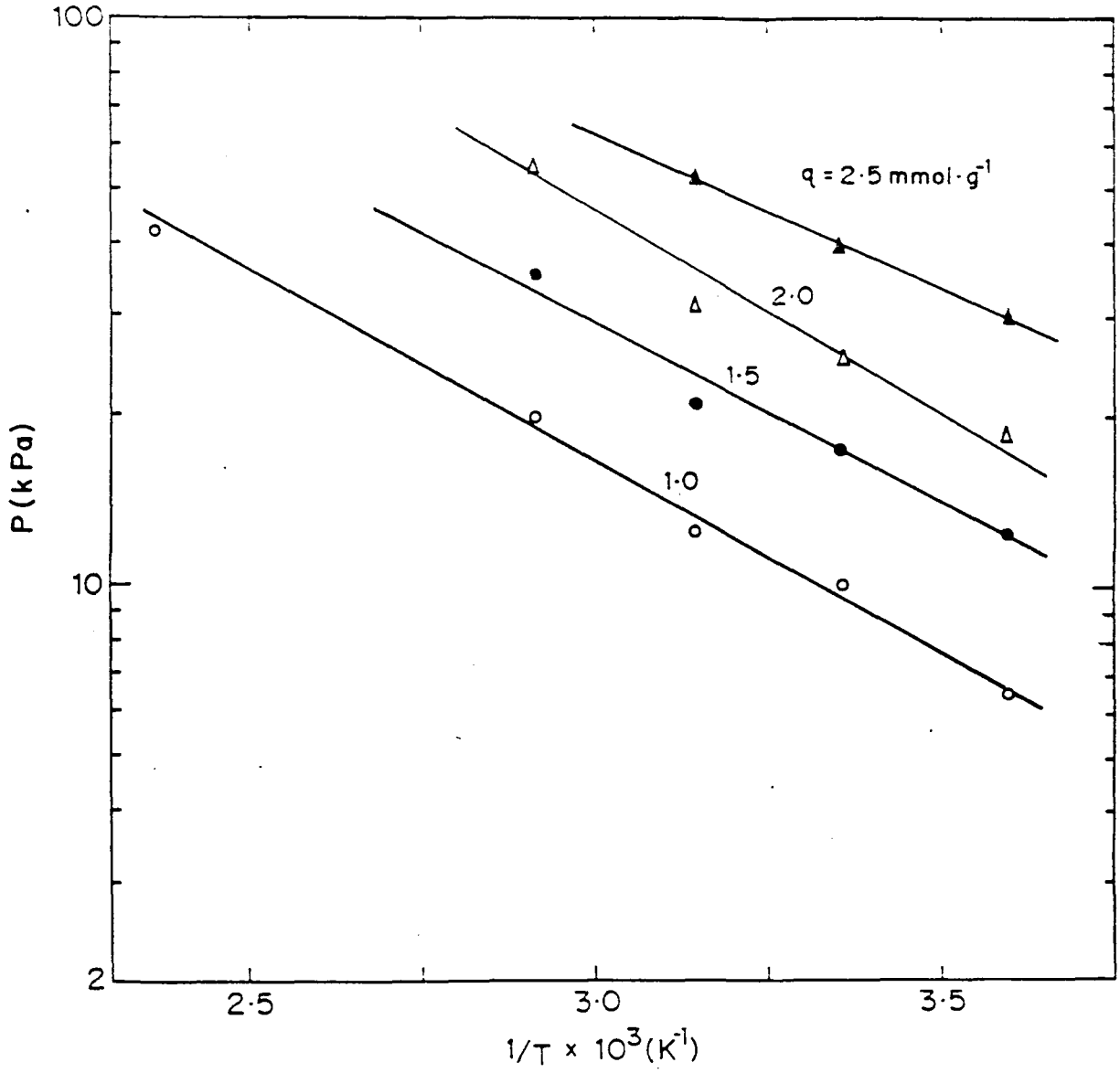

FIG.3·40: CALCULATION OF ISOSTERIC HEAT OF SORPTION OF CARBONDIOXIDE ON SODIUM MORDERITE FOR DIFFERENT COVERAGES

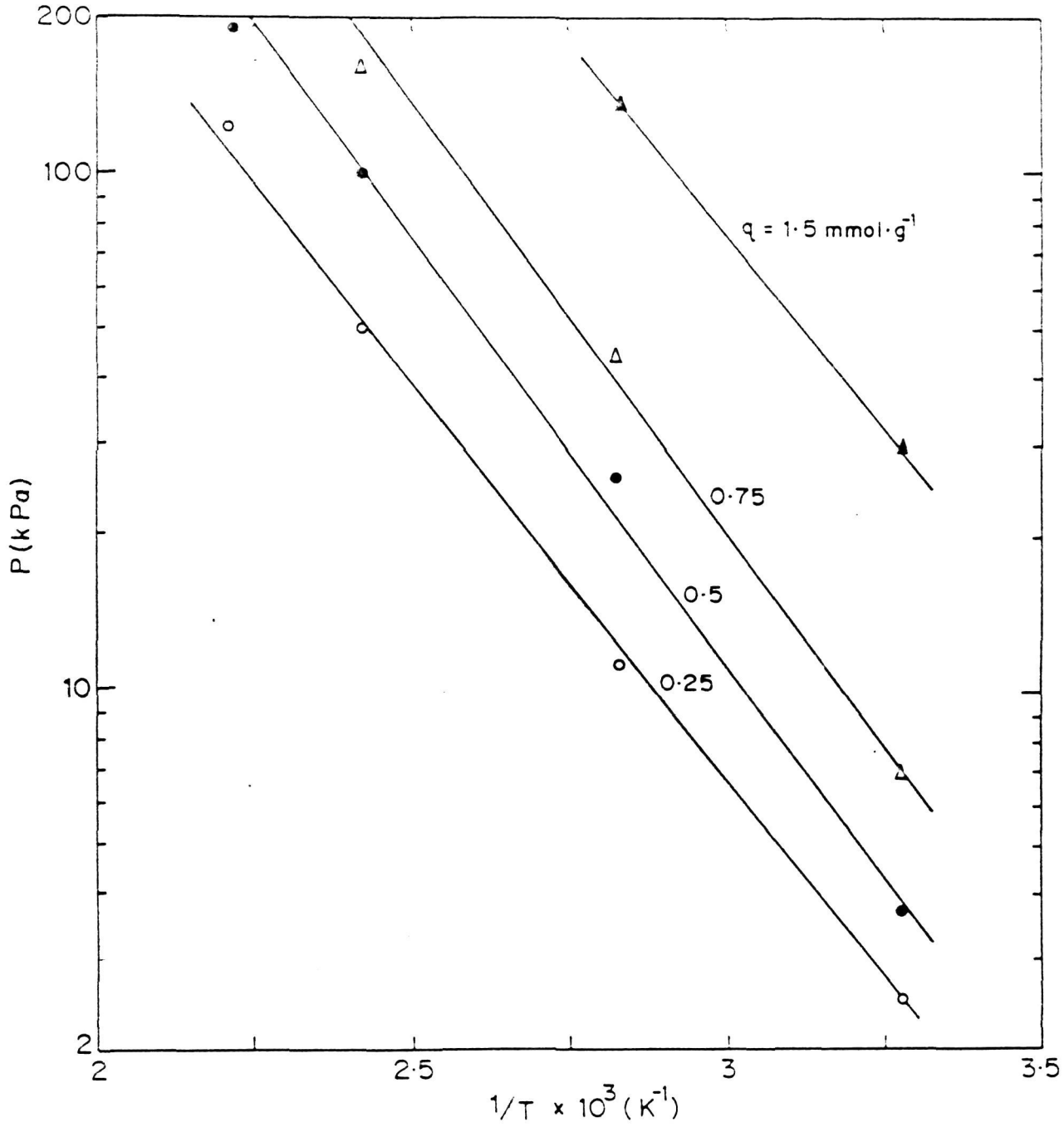

FIG.3·41: CALCULATION OF THE ISOSTERIC HEAT OF SORPTION OF ETHYLENE ON SILICALITE FOR DIFFERENT SURFACE COVERAGES

ethane, ethylene and carbon dioxide in the different adsorbents are given in Appendices 3.9-3.14.

The plots of isosteric heat of sorption (Q_a) versus surface coverage (i.e. amount sorbed, q) for the sorption of methane, ethane, ethylene and carbon dioxide in NaX, NaY, NaM, silicalite, $AlPO_4$-5 and SAPO-5 are presented in Figs. 3.42-3.47, respectively. The results (Fig. 3.42-3.47) show that the variation of heat of sorption with the amount sorbed depends strongly on the sorbate-zeolite system and the observed trend changes from system to system. In general, an initial sharp decrease of heat of sorption with increasing the sorbate in the zeolite reveals site heterogeneity whereas a small increase or decrease in the heat of sorption with increasing sorbate loading indicates attractive or repulsive sorbate-sorbate interaction among the sorbed species. A sharp increase in the heat of sorption with increasing sorbate loading may be due to an induced surface heterogeneity, probably due to increase in the energy of adsorption sites. Sometimes sorbate-sorbate interactions manifest themselves giving rise to a very complex trend for the dependence of heat of sorption on the sorbate loading.

3.3.3 Comparison of Zeolites for their Sorption Properties

3.3.3.1 Heat of Sorption

Heat of sorption of a sorbate on an adsorbent is a measure of the ease with which the adsorbent can be regenerated. Generally, a sorbent with a low heat of sorption is preferred as

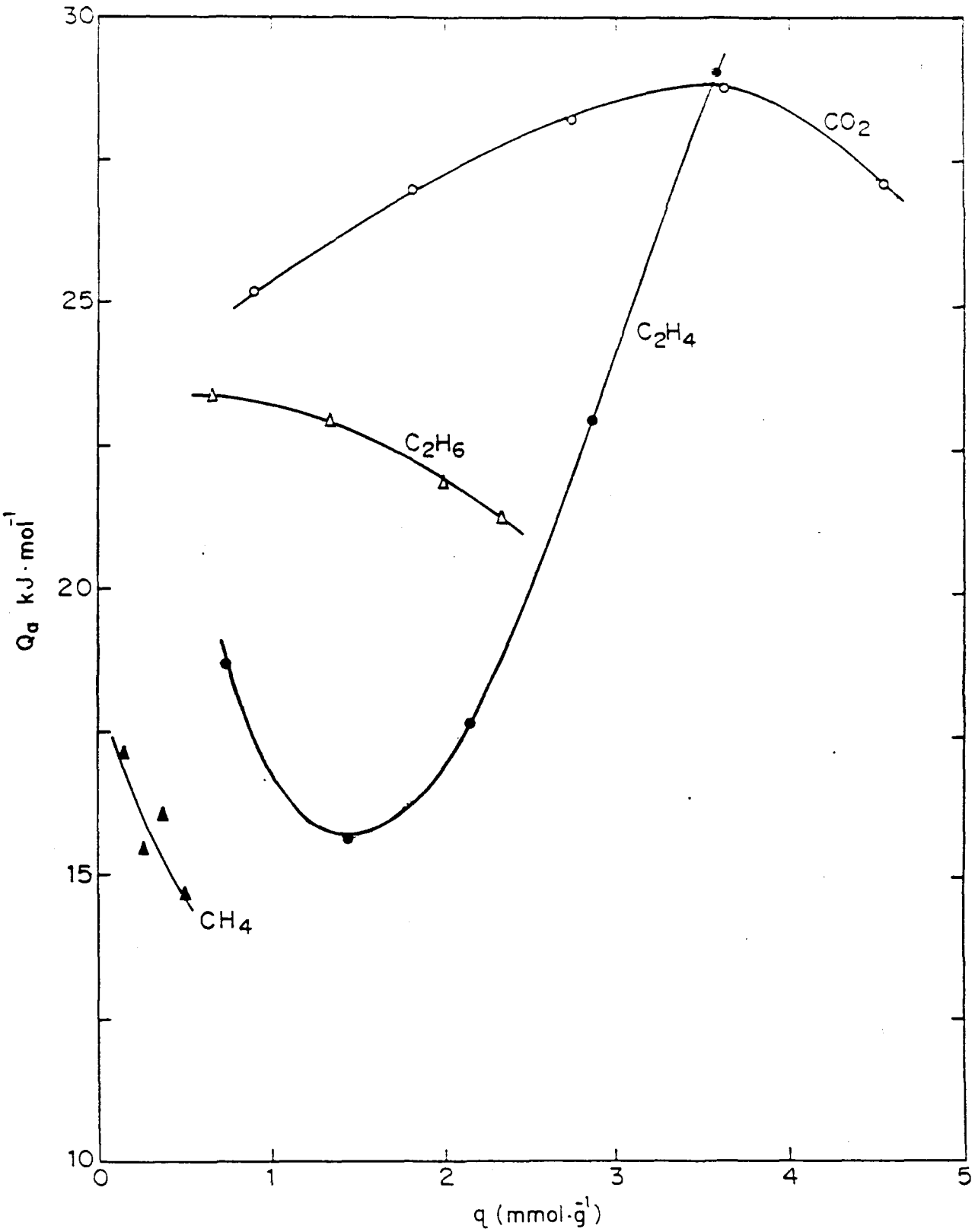

FIG.3·42: VARIATION OF ISOSTERIC HEAT OF SORPTION WITH SURFACE COVERAGE FOR THE ADSORPTION OF METHANE, ETHANE, ETHYLENE AND CARBONDIOXIDE ON NaX ZEOLITE

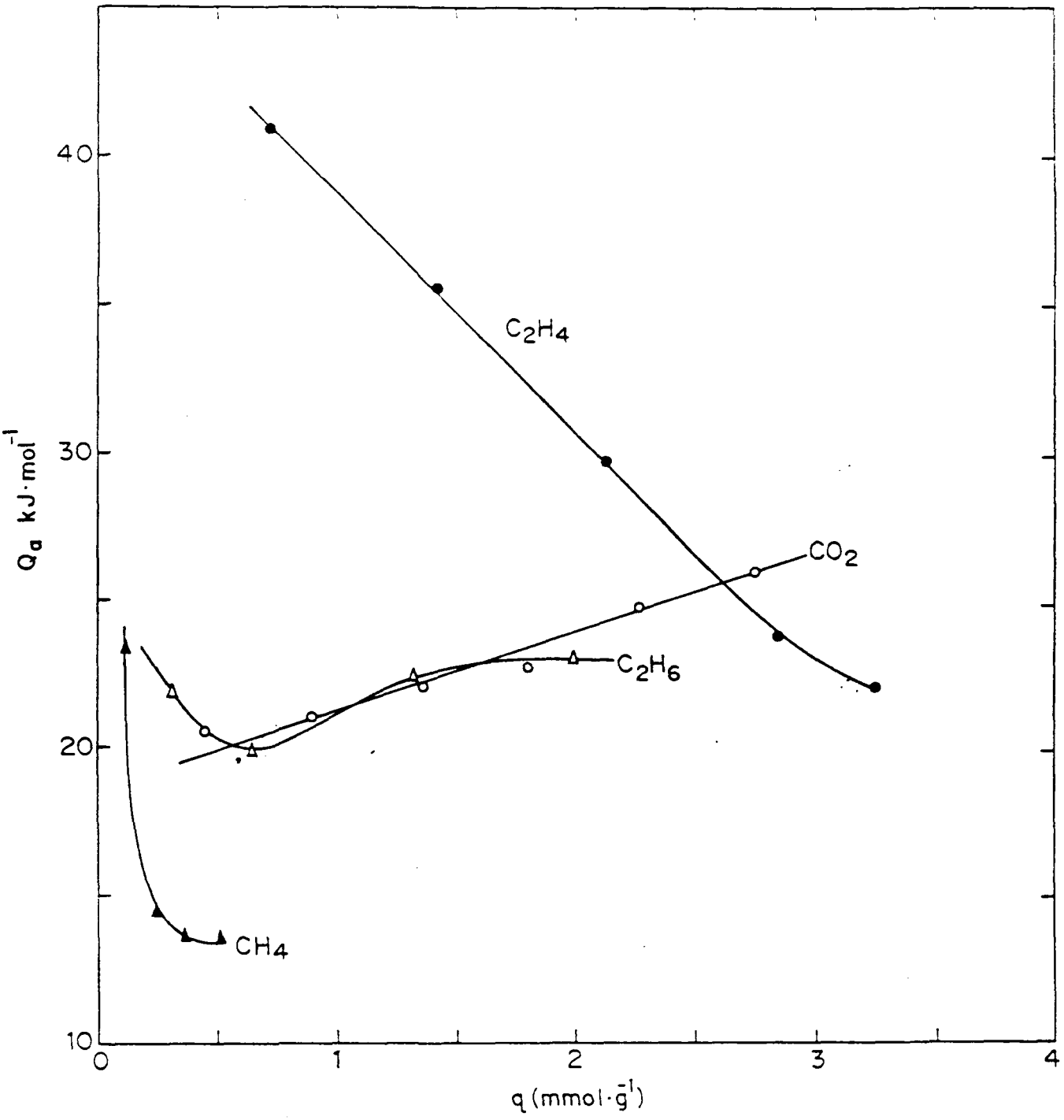

FIG.3·43: VARIATION OF ISOSTERIC HEAT OF SORPTION WITH SURFACE COVERAGE FOR THE ADSORPTION OF METHANE, ETHANE, ETHYLENE AND CARBONDIOXIDE ON Na-Y ZEOLITE

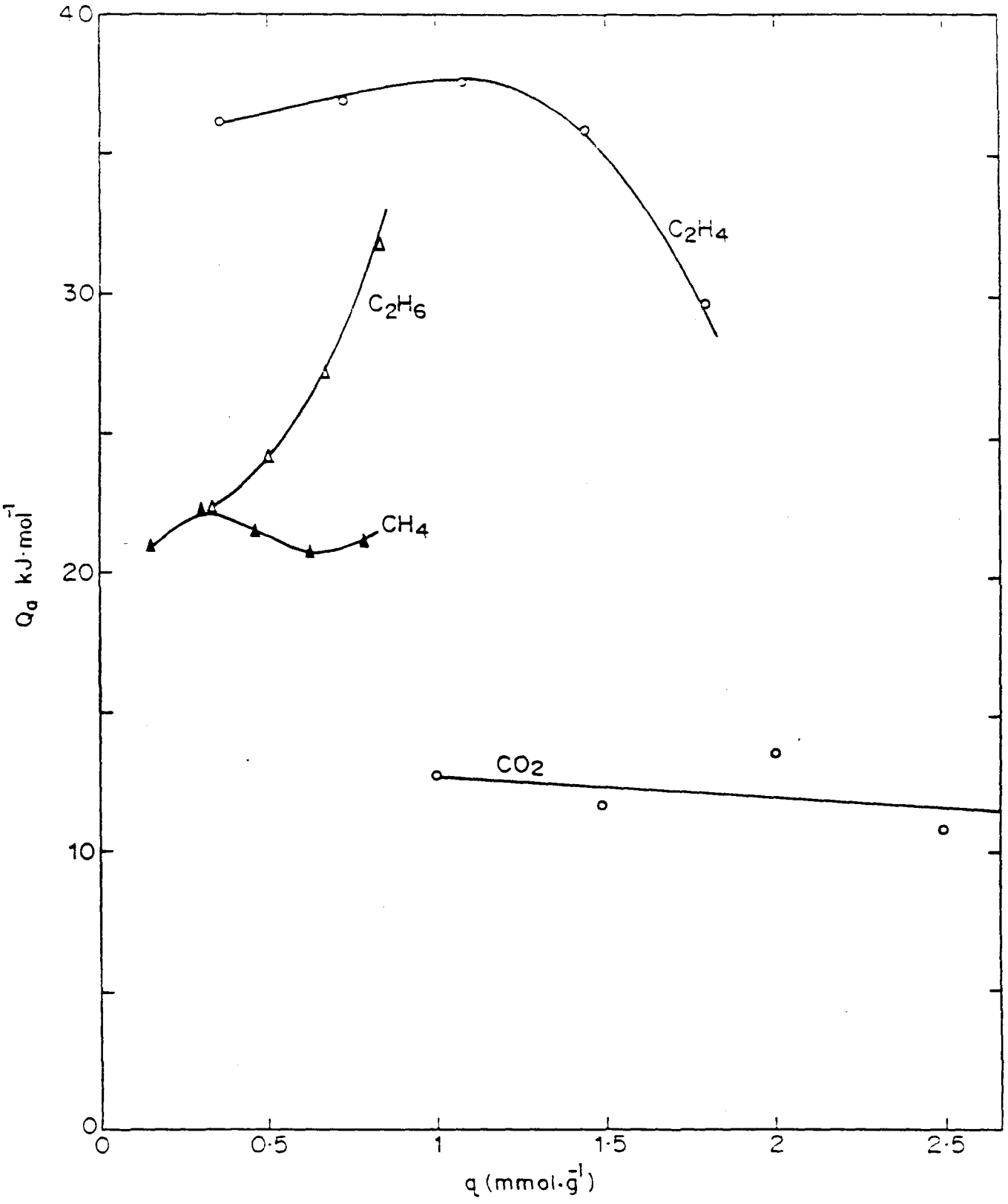

FIG.3·44: VARIATION OF ISOSTERIC HEAT OF SORPTION WITH SURFACE COVERAGE FOR THE ADSORPTION OF METHANE, ETHANE, ETHYLENE AND CARBONDIOXIDE ON SODIUM MORDENITE

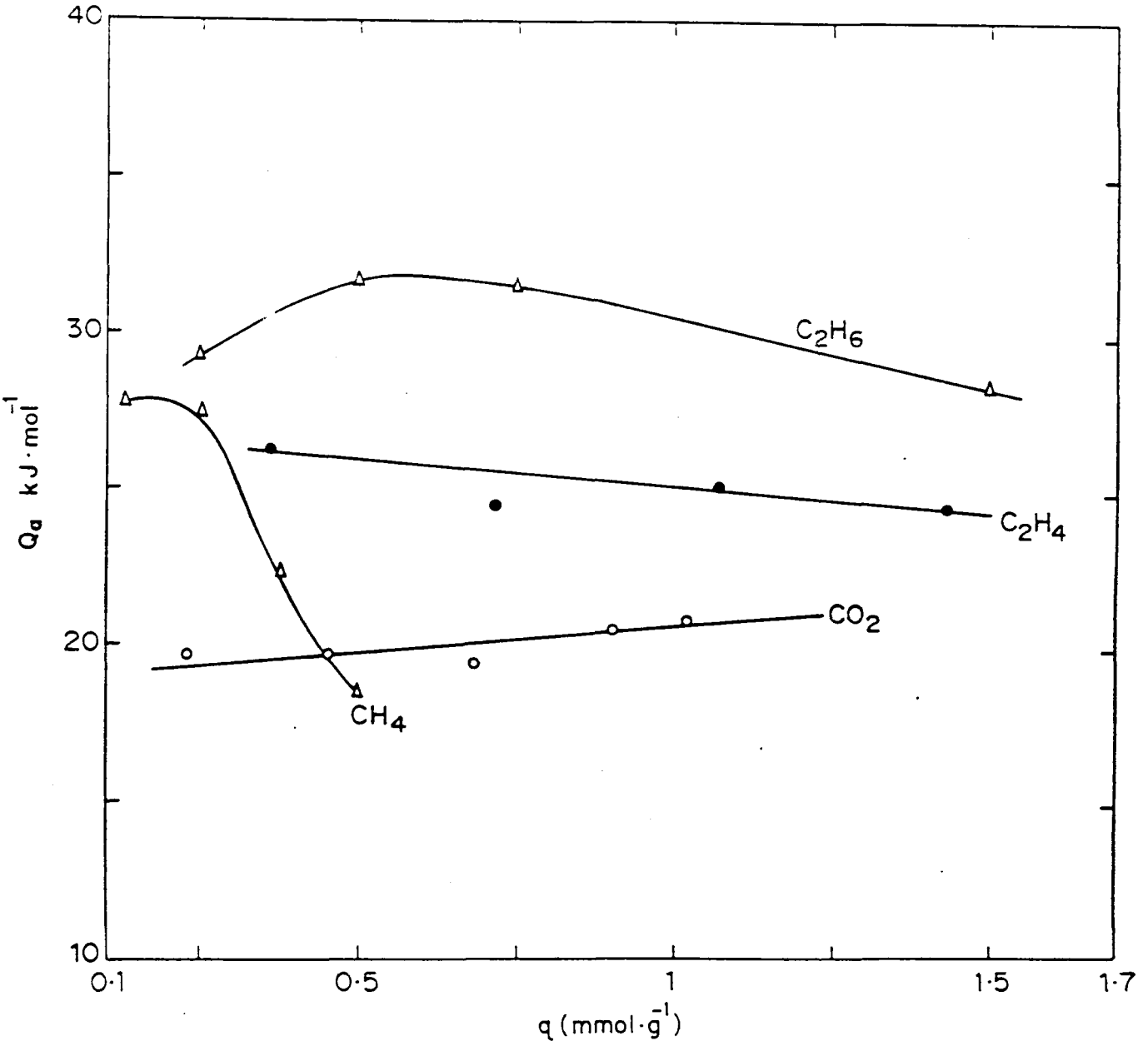

FIG.3·45 : VARIATION OF ISOSTERIC HEAT OF SORPTION WITH SURFACE COVERAGE FOR THE ADSORPTION OF METHANE, ETHANE ETHYLENE AND CARBONDIOXIDE ON SILICALITE-I

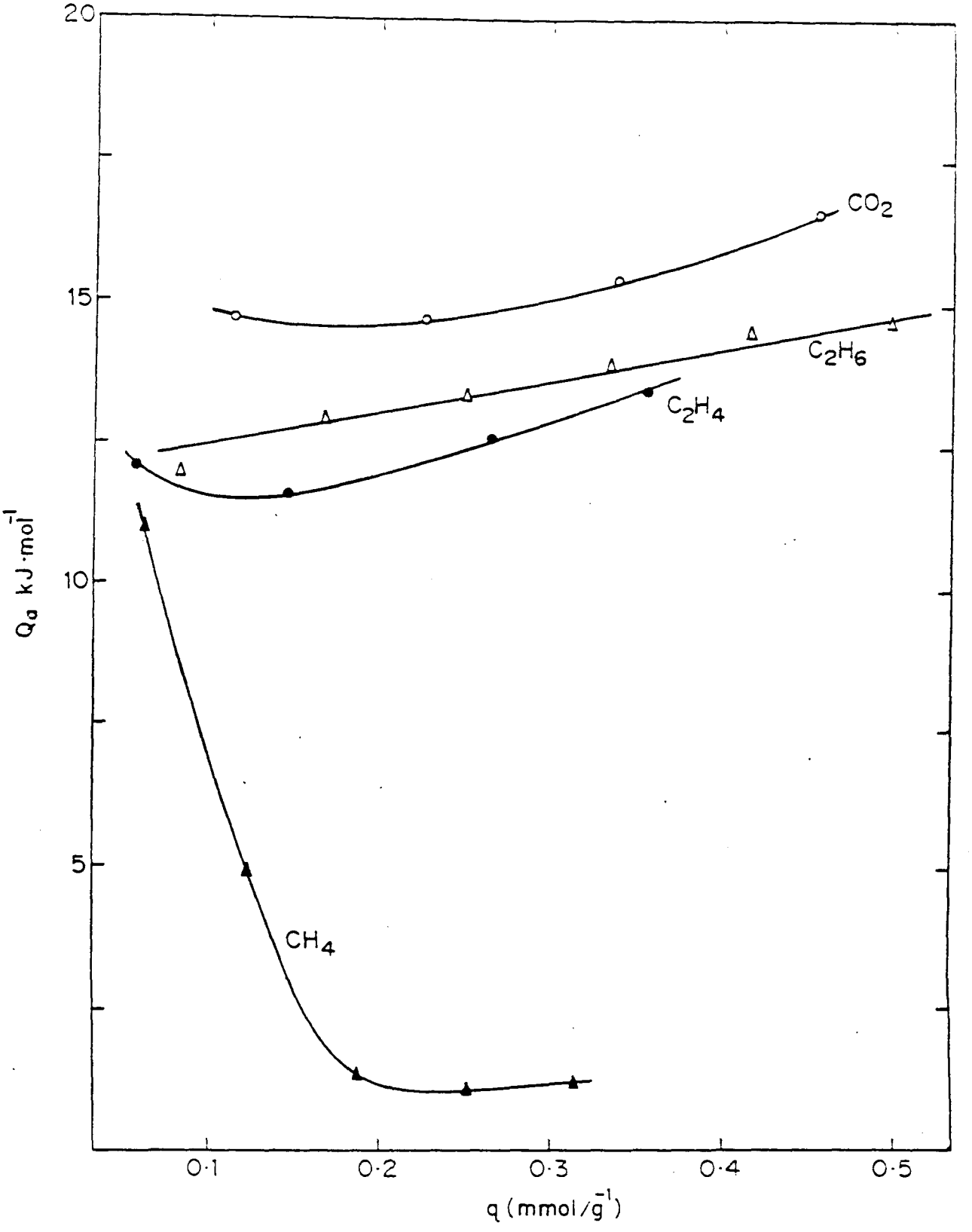

FIG.3·46: VARIATION OF ISOSTERIC HEAT OF SORPTION WITH SURFACE COVERAGE FOR THE ADSORPTION OF METHANE, ETHANE, ETHYLENE AND CARBONDIOXIDE ON $AlPO_4$-5

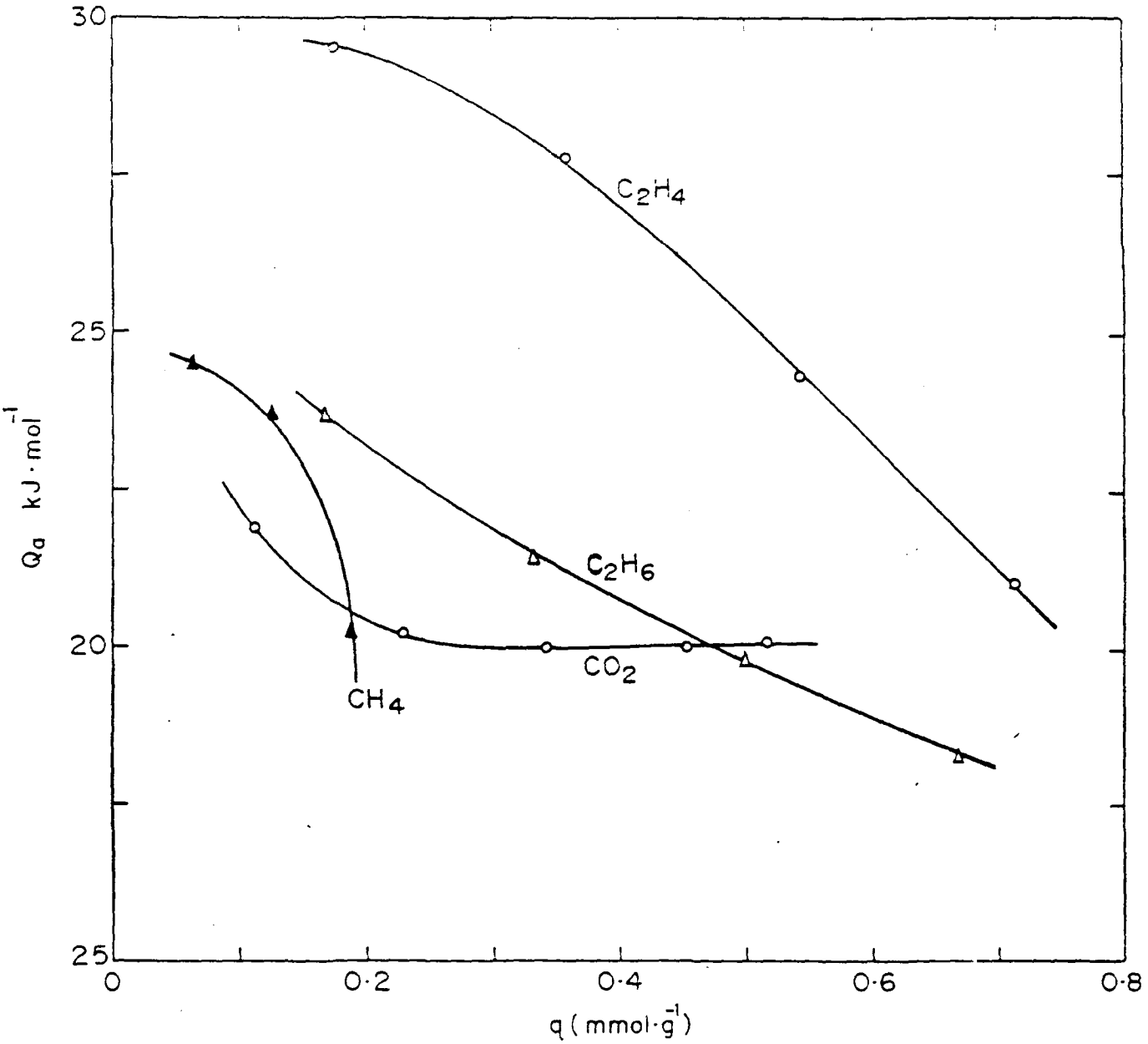

FIG.3·47 : VARIATION OF ISOSTRIC HEAT OF SORPTION WITH SURFACE COVERAGE FOR THE ADSORPTION OF METHANE, ETHANE, ETHYLENE AND CARBONDIOXIDE ON $SAPO_4$-5

it implies a greater ease of its regeneration. High value of heat of sorption is attributed to strong sorbate-sorbent interactions and hence desorption of the sorbate from the sorbent is difficult. In such cases, regeneration of the sorbent is effected by increasing the temperature (thermal swing) to a high value and/or by the application of vacuum, which increases the energy cost of the process. Further, heating the adsorbent repeatedly can affect the adsorbent life as it can cause structural degradation or fouling of the adsorbent and/or reaction of the sorbate on the adsorbent.

The heats of sorption (at near zero coverage) of methane, ethane, ethylene and carbon dioxide on the different adsorbents are compared in Table 3.8. Among the sorbates, the heat of sorption of methane in all the sorbents is the lowest. For NaM, HM, KL, HKL, $AlPO_4$-5, HY, NaY, CeNaY(Ce^{+3} exchange : 46%) and CeNaY(Ce^{+3} exchange : 72%), the heat of sorption of the different sorbates have the following order:

$$CH_4 < C_2H_6 < CO_2 < C_2H_4$$

whereas, for the remaining adsorbents the sorbates have the following orders of heat of sorption.

For H-Na-ZSM-5

$$CH_4 < C_2H_6 < C_2H_4 < CO_2$$

For Na-H-ZSM-8

$$CH_4 < C_2H_6 < C_2H_4 < CO_2$$

For silicalite

$$CH_4 < CO_2 < C_2H_4 < C_2H_6$$

For H-ZSM-5

$$CH_4 < CO_2 < C_2H_6 < C_2H_4$$

For H-ZSM-8

$$CH_4 < C_2H_6 < CO_2 < C_2H_4$$

It is also interesting to compare the sorbents for the heat of sorption of the different sorbates. The sorbents show the following orders for the heat of sorption of the different sorbates.

For the heat of sorption of methane

H-Na-ZSM-5 > Na-H-ZSM-8 > HM > H-ZSM-5 > silicalite > KL > HY > CeNaY (Ce^{+3} exchange 72%) = $AlPO_4$-5 > CeNaY (Ce^{+3} exchange 46%) > NaY > NaM

For the heat of sorption of ethane

H-Na-ZSM-5 > silicalite > NaM > H-ZSM-5 > Na-H-ZSM-8 > H-ZSM-8 > HM > KL > NaY > HKL > CeNaY (Ce^{+3} exchange 72%) > HY > $AlPO_4$-5 > NaX

For the heat of sorption of ethylene

NaM > CeNaY (Ce^{+3} exchange 46%) > NaY > Na-H-ZSM-8 > H-ZSM-8 > H-Na-ZSM-5 > H-ZSM-5 > KL > HY > NaX > HKL > silicalite

For the heat of sorption of carbon dioxide

HM > H-Na-ZSM-5 > CeNaY (Ce^{+3} exchange 72%) > NaM > NaY > Na-H-ZSM-8 > CeNaY (Ce^{+3} exchange 46%) > HKL > H-ZSM-8 > HY > H-ZSM-5 > KL > silicalite > $AlPO_4$-5

The above comparisons reveal that the sorbate-sorbent interactions for a particular sorbate varies from sorbent to

sorbent and also the order for the heat of sorption of the sorbates depends on the adsorbent.

3.3.3.2 Thermodynamic Adsorption Equilibrium Constant

The thermodynamic equilibrium constant (β) obtained from the gc pulse technique using Equation (3.1), which is equivalent to sorbate retention volume per unit volume of sorbent for the various sorbates and sorbents at different temperatures (viz. 303, 373, 423 and 473 K) is compared in Table 3.9. In the table, the second column gives the actual value of the equilibrium constant for methane and the other columns give the equilibrium constant of the sorbate relative to that of methane (i.e. relative equilibrium constant).

Following observations have been made on the temperature dependence of the relative equilibrium constant for the different sorbates.

1. For all the adsorbents, the relative equilibrium constants for ethane and ethylene are decreased with increasing temperature.

2. For all the adsorbents except $AlPO_4$-5, KL and silicalite, the relative equilibrium constant for CO_2 is decreased with increasing temperature. For $AlPO_4$-5, it passes through a maximum, for KL it passes through a maximum and then a minimum, whereas for silicalite, it decreases slightly and then remains constant with increasing temperature.

3. The relative equilibrium constant for water is decreased for H-ZSM-5, CeNaY (Ce^{+3} exchange 46%), KL, HKL, HM

and silicalite, but is increased for H-Na-ZSM-5 and CeNaY (Ce^{+3} exchange 72%) with increasing temperature.

The adsorbents could be arranged in the decreasing order of the equilibrium constant for the various sorbates (viz. CH_4, C_2H_6, C_2H_4 and CO_2) at two different temperatures (303 and 473 K), as follows:

For CH_4 (at 303 K)

Na-H-ZSM-8 > NaX > H-ZSM-8 > H-Na-ZSM-5 > H-ZSM-5 > silicalite > HM > NaM > HKL > KL > CeNaY (Ce^{+3} exchange 46%) > CeNaY (Ce^{+3} exchange 72%) > NaY > $AlPO_4$-5 > HY

For CH_4 (at 473 K)

NaX >> HKL > NaM > H-ZSM-5 > H-Na-ZSM-5 > Na-H-ZSM-8 > NaY > HM > CeNaY (Ce^{+3} exchange 46%) > HY > CeNaY (Ce^{+3} exchange 72%) > $AlPO_4$-5 > KL

For C_2H_4 (at 303 K)

NaM > Na-H-ZSM-8 > NaX > CeNaY (Ce^{+3} exchange 46%) > H-ZSM-8 > H-Na-ZSM-5 > KL > H-ZSM-5 > HKL > silicalite > $AlPO_4$-5

For C_2H_4 (at 473 K)

NaX > Na-H-ZSM-8 > NaM > NaY > CeNaY (Ce^{+3} exchange 46%) > KL > silicalite > H-Na-ZSM-5 > H-ZSM-5 > HKL > $AlPO_4$-5 = HY

For C_2H_6 (at 303 k)

Na-H-ZSM-8 > H-ZSM-8 > H-Na-ZSM-5 > silicalite > NaX > HM > NaY = HKL > NaM > CeNaY (Ce^{+3} exchange 46%) > CeNaY (Ce^{+3} exchange 72%) > $AlPO_4$-5 > HKL > HY

For C_2H_6 (at 473 K)

NaX > Na-H-ZSM-8 > H-Na-ZSM-5 > $AlPO_4$-5 > H-ZSM-5 = HM > KL = NaY > CeNaY (Ce^{+3} exchange 46%) > HY > CeNaY (Ce^{+3} exchange 72%) = HKL > NaM

For CO_2 (at 303 K)

Na-H-ZSM-8 > NaM > H-Na-ZSM-5 > HM = NaY > H-ZSM-8 > CeNaY (Ce^{+3} exchange 72%) > CeNaY (Ce^{+3} exchange 46%) > HKL > KL > H-ZSM-5 > HY > silicalite > $AlPO_4$-5

For CO_2 (at 473 K)

NaM > NaX > KL > HM > Na-H-ZSM-8 > H-Na-ZSM-5 > NaY > CeNaY (Ce^{+3} exchange 72%) > HKL > CeNaY (Ce^{+3} exchange 46%) > H-ZSM-5 = $AlPO_4$-5 > HY

The above comparison shows a strong influence of temperature on the order of the sorbents for the equilibrium constant of the different sorbates.

At the two temperatures, the data on the relative equilibrium constant for C_2H_6, C_2H_4 and CO_2 on the different sorbates are summarized below.

Zeolites	Temperature (K)	Order of the relative equilibrium constant for sorbates
NaY, Na-H-ZSM-8, CeNaY (Ce^{+3} exchange 46%)	303 & 473	$C_2H_4 > CO_2 > C_2H_6$
Silicalite, $AlPO_4$-5	303 & 473	$C_2H_6 > C_2H_4 > CO_2$
H-ZSM-5	303 & 473	$C_2H_4 > C_2H_6 > CO_2$
H-Na-ZSM-5, HKL	303 & 473	$CO_2 > C_2H_4 > C_2H_6$

NaM, HY, KL	303	$C_2H_4 > CO_2 > C_2H_6$
KL, NaM	473	$CO_2 > C_2H_4 > C_2H_6$
HY	473	$C_2H_4 > C_2H_6 > CO_2$

The above observations reveal that the order of the relative equilibrium constant for the sorbates is influenced by temperature for some of the adsorbents (e.g. HY, KL, NaM)

3.3.3.3. Sorption at Different Temperatures and Pressures

For the purpose of comparison, the sorption of various sorbates relative to that of methane at different temperatures (305 and 353 K) and sorbate pressures (25, 100 and 150 kPa) in the different adsorbents (viz. NaX, NaY, NaM, silicalite, $AlPO_4$-5 and SAPO-5) has been presented in Table 3.17. The following observations could be made from the results (Table 3.17).

1. For all the adsorbents, the sorption of ethane relative to that of methane at 305 K decreases with increasing pressure. However, at 353 K, the relative sorption of ethane decreases with increasing pressure for NaY, NaM, silicalite and $AlPO_4$-5; increases with increasing pressure for NaX and decreases slightly to a constant value for SAPO-5.

2. For all the sorbents, the relative sorption of ethylene at 305 K also decreases with increasing pressure. At 353 K, it decreases with increasing pressure for all the sorbents except SAPO-5, for which it passes through a maximum.

3. The sorption of CO_2 relative to that of methane decreases with increasing pressure at 305 K for NaY, NaM and NaX. In $AlPO_4$-5, there is a small increase of the relative

Table 3.17

The amount of gases adsorbed (relative to methane) at different pressure and temperature

Adsorbent	Temp. (K)	Pressure (kPa)	CH_4 adsorption, q_{CH_4} (mmol.g^{-1})	Relative sorption $q_{C_2H_6}/q_{CH_4}$	$q_{C_2H_4}/q_{CH_4}$	q_{CO_2}/q_{CH_4}
NaX	305	25	0.25	6.2	12.8	15.8
		100	0.85	4.1	5.2	6.7
		150	1.20	3.2	3.8	5.1
	353	25	0.15	4.7	12.7	13.3
		100	0.42	5.0	8.1	9.4
		150	0.50	5.2	7.4	9.3
NaY	305	25	0.20	5.5	18.5	12.7
		100	0.55	5.1	-	9.8
		150	0.80	4.1	-	7.3
	353	25	0.05	6.5	27.0	51.0
		100	0.25	4.8	11.2	11.4
		150	0.375	4.7	8.5	9.1
NaM	305	25	0.39	3.0	4.5	5.1*
		100	1.06	1.7	1.9	2.8*
		150	1.30	1.4	1.6	2.4
	353	25	0.12	3.8	10.0	9.8**
		100	0.45	1.9	3.8	5.3**
		150	0.62	1.5	2.9	4.1

Table 3.17 (contd.)

Adsorbent	Temp. (K)	Pressure (kPa)	CH_4 adsorption, q_{CH_4} (mmol.g^{-1})	Relative sorption $q_{C_2H_6}/q_{CH_4}$	$q_{C_2H_4}/q_{CH_4}$	q_{CO_2}/q_{CH_4}
		25	0.35	4.1	2.8	1.3
	305	100	0.81	2.5	2.3	1.8
		150	1.01	2.2	2.0	1.8
Silicalite						
		25	0.11	4.2	3.1	1.5
	353	100	0.35	3.6	2.9	1.8
		150	0.50	3.1	2.5	1.8
		25	0.08	2.7	2.2	1.9
	305	100	0.27	2.4	2.0	1.9
		150	0.37	2.2	1.9	2.0
$AlPO_4$-5						
		25	0.05	2.5	10.0	1.2
	353	100	0.20	2.0	1.4	1.2
		150	0.30	1.7	1.3	1.2
		25	0.09	4.2	6.0	2.9
	305	100	0.30	2.7	3.3	2.9
		150	0.40	2.4	2.8	2.5
SAPO-5						
		25	0.04	3.7	3.0	2.5
	353	100	0.14	3.4	4.3	2.6
		150	0.18	3.4	4.0	2.8

* q collected at 298 K

** q collected at 343 K

sorption with increasing pressure, whereas in SAPO-5, there is a small decrease. In silicalite, the relative sorption of CO_2 at the higher temperature decreases with the increase in pressure for NaY and NaM, decreases to a constant value for NaX, increases to a constant value for $AlPO_4$-5 and increases gradually for SAPO-5.

The order of the sorption of the various sorbates relative to that of methane at two different temperatures (305 and 353 K) and pressures (25 and 150 kPa) is presented in Table 3.18 for the purpose of comparison. The results reveal the following:

1. For NaX and silicalite, the order of the relative sorption is not affected due to the change in temperature or pressure. However, for NaM, $AlPO_4$-5 and SAPO-5, the order is changed due to the increase in the temperature at 25 kPa pressure and also due to the increase in pressure at 353 K whereas for NaY, the order is changed due to the increase in temperature.

2. The order of the relative sorption of sorbates depends strongly on the adsorbent (Table 3.18). For NaX, NaY and NaM, the relative sorption of ethane is the least, whereas that of CO_2 is the highest. However almost reverse trend is observed for the other adsorbents (silicalite, $AlPO_4$-5 and SAPO-5).

3.3.3.4 Selection of the Adsorbent

The important factors that are to be considered in the selection of a suitable adsorbent for a particular adsorption separation process are the efficiency of separation (i.e. high

Table 3.18

Order of the relative sorption of sorbates in the adsorbents at different temperature and pressure

Adsorbent	Temperature (K)	Pressure (kPa)	Order of relative sorption of sorbates
NaX	305	25	$CO_2 > C_2H_4 > C_2H_6$
		150	$CO_2 > C_2H_4 > C_2H_6$
	353	25	$CO_2 > C_2H_4 > C_2H_6$
		150	$CO_2 > C_2H_4 > C_2H_6$
NaY	305	25	$C_2H_4 > CO_2 > C_2H_6$
	353	25	$CO_2 > C_2H_4 > C_2H_6$
		150	$CO_2 > C_2H_4 > C_2H_6$
NaM	305	25	$CO_2 > C_2H_4 > C_2H_6$
		150	$CO_2 > C_2H_4 > C_2H_6$
	353	25	$C_2H_4 > CO_2 > C_2H_6$
		150	$CO_2 > C_2H_4 > C_2H_6$
Silicalite	305	25	$C_2H_6 > C_2H_4 > CO_2$
		150	$C_2H_6 > C_2H_4 > CO_2$
	353	25	$C_2H_6 > C_2H_4 > CO_2$
		150	$C_2H_6 > C_2H_4 > CO_2$
$AlPO_4$-5	305	25	$C_2H_6 > C_2H_4 > CO_2$
		150	$C_2H_6 > C_2H_4 > CO_2$
	353	25	$C_2H_6 > C_2H_4 > CO_2$
		150	$C_2H_6 > C_2H_4 > CO_2$
SAPO-5	305	25	$C_2H_4 > C_2H_6 > CO_2$
		150	$C_2H_4 > C_2H_6 > CO_2$
	353	25	$C_2H_6 > C_2H_4 > CO_2$
		150	$C_2H_6 > C_2H_4 > CO_2$

separation factor which depends on the concentration or pressure and temperature), the sorption capacity, the ease of regeneration of the sorbent, the reactivity of the sorbates in the sorbent, the structural stability and also the cost of the adsorbent. The ideal adsorbent should possess a high separation factor, high sorption capacity for one or more of the sorbates, should regenerate easily (i.e. should have low heat of sorption), should be inactive to all the sorbates both at the conditions of adsorption and regeneration, should possess high structural stability and also should be cheap. However, all these requirements are rarely met in any single adsorbent and the selection of a suitable adsorbent is usually a compromise between the favorable and unfavorable characteristics depending upon its capability of achieving the required separation effectively.

Though detailed investigation is required for understanding the exact behavior of the adsorbents towards the adsorptive separation of methane, ethane, ethylene and carbon dioxide from their mixtures, some important clues can be obtained from the preliminary screening by the gc pulse technique. This method may be used for the initial selection of a few promising adsorbents which have a greater potential for achieving a particular separation, thus resulting in a considerable saving in time and efforts.

The heat of sorption at zero coverage is a measure of the sorbate-sorbent interaction and can be taken as indicative of the ease of regeneration in terms of the energy input required. Very high values of heat of sorption indicate stronger

interactions and hence the difficulty in the regeneration. The comparison of the zeolites for the heat of sorption of the various sorbates, determined by the gc pulse technique (Table 3.8) reveals that $AlPO_4$-5 and silicalite have the lowest heat of sorption for almost all the sorbates. So, from the point of view of the cost of regeneration, $AlPO_4$-5 and silicalite can be considered as the most preferred adsorbents. The other possible choices with respect to lower heat of sorption are NaY, NaX and KL.

The relative thermodynamic equilibrium constants (relative to methane) obtained from the gc pulse data may be taken as a rough measure of the separation factor (with respect to methane). A high value of the relative equilibrium constant is indicative of a high separation factor. At 303 K, all the sorbents are having a relative equilibrium value >> 1 which implies that a good separation of methane from the other sorbates is possible.

Among the adsorbents, NaM, NaY, NaX, Na-H-ZSM-8, CeNaY and KL are having the relative values of equilibrium constant (at 303 K) very much greater than unity. However, acidic zeolites like HM, HKL, HY, CeNaY, H-ZSM-8, Na-H-ZSM-8, H-ZSM-5, H-Na-ZSM-5 are not suitable for use as adsorbents due to their reactivity towards ethylene and ethane and may be eliminated.

The data from the gc pulse method gives the values of heat of sorption and sorption equilibrium constant at near zero coverage and hence can be taken only as indicative of the sorption behavior. The separation factor is dependent on

temperature, pressure and also may be affected by the presence of other sorbates. For determining the true performance of these selected sorbents (viz. $AlPO_4$-5, SAPO-5, NaY, NaX, KL and NaM) detailed experimentation under actual conditions of operation are therefore required.

NOMENCLATURE

A,B	Constants of Dubinin - Astakhov equation
a	Constant in Equation (3.3)
C,D	Constants of Dubinin - Polanyi equation
c	Constant in model isotherms
E	Constant in Equation (3.5)
F	Flow rate, $cm.^3s^{-1}$
H	Heat of adsorption, $kJ.mol^{-1}$
k	Constant in model isotherms
L	Length of the packing, cm
P	Equilibrium pressure, atm
P_s	Vapor pressure of pure sorbate, atm
Q_a	Isosteric heat of sorption, $kJ.mol^{-1}$
q	Sorbed phase concentration, $mol.g^{-1}$
q_m	Maximum concentration in the sorbed phase, $mol.g^{-1}$
R	Gas constant
T	Temperature, K
T_c	Column temperature, K
T_F	Temperature at which F is measured, K
t_m	Corrected retention time, s
t_d	Retention time of non-adsorbate, s
t_r	Retention time of adsorbate, s
U_e	Superficial gas velocity, $cm.s^{-1}$
V_R	Retention volume, cm^3
V_P	Volume of packing, cm^3

Greek Letters

β	Adsorption equilibrium constant
θ	Fractional saturation, q/q_m

REFERENCES

1. CA 103: 27823c Chkhaidze, E.V., Fomkin, A.A., Serpinski, V.V. and Tstisishvili, G.V., Izv. Akad. Nauk. SSR, Ser. Khim., 5, 974 (1985)
2. Barrer, R.M. and Sutherland, J.W., Proc. Roy. Soc. Ser. A., **237**, 439 (1956)
3. Tsitsishvili, G.V. and Andronikashvili, T.G., J. Chromatogr., **58**, 39 (1971)
4. Habgood, H.W., Can. J. Chem., **42**, 10, 2340 (1964)

5a. Ding Tong-Fu, Ozawa, S., Yamazaki, T., Watanuki, I. and Ogino, Y., Langmuir, **4**, 392 (1988)

5b. Rolniak, P.D. and Kobayashi, R., AIChE J., **26**, 4, 616 (1980)

5c. Loughlin, K.F., Hasanain, M.A. and Abdul-Rehman, H.B., Ind. Eng. Chem. Res., **29**, 1535 (1990)

6. Hyun, S.H., Danner, R.P., J. Chem. Eng. Data, **27**, 196 (1982)
7. Bezus, A.G., Kiselev, A.V., Sedlacek, Z. and Pham Quang Du, Trans. Faraday Soc. I., **67**, 468 (1971)
8. Kiselev, A.V. and Lopatkin, A. A. in 'Molecular sieves', Soc. Chem. Ind., London. (1968) p.252
9. Danner, R.P., Nicoletti, M.P. and Al-Ameeri, R.S., Chem. Eng. Sci., **35**, 2129 (1980)
10. Danner, R.P., Choi, E.C.F., Ind. Eng. Chem. Fundam., **17**, 248 (1978)
11. Kiskinova, M., Griffin, G.L. and Yates, J.T.Jr., J. Catal., **71**, 278 (1981)

12. Basu, P. and Yates, J.T.Jr., Surf. Sci., **177**, 2, 291 (1986)

13. Barrer, R.M. and Gibbons, R.M., Trans. Faraday Soc., **61**, 948 (1965)

14. Barrer, R.M. and Coughlan, B. in 'Molecular Sieves', Soc. Chem. Ind., London (1968) p.241

15. Patzelova, V., J. Chromatogr., **191**, 175 (1980)

16. Miertus, S. and Miertusova, J., J. Chromatogr., **286**, 31 (1984)

17. Peeters, G., Vasant, E.F. and De Bievre, P., ACS Symp. Ser. **40**, ACS, Washington DC (1977) p. 343

18. Cartrand, P., Cointot, A. and Chauvean, B., ACS Symp. Ser., **40**, ACS, Washington DC (1977) p. 367

19. Roux, A., Huang, A.A., Ma, Y.H. and Zwiebel, I., AIChE Symp. Ser., **69**, 134, 46 (1973)

20. Barrer, R.M. and Murphy, E.V.T., J. Chem. Soc. A., 2506 (1970)

21a. Talu, O. and Ziebel, I., AIChE J., **32**, 8, 1263 (1986)

21b. Mayorga, G.D. and Peterson, D.L., J. Phys. Chem., **76**, 11, 1647 (1972)

22. June, R.L., Bell, A.T., Theodorou, D.N., J. Phys. Chem., **94**, 4, 1508 (1990)

23. Vigne-Maeder, F. and Auroux, A., J. Phys. Chem. **94**, 1, 316 (1990)

24. Chiang, A.S., Dixon, A.G. and Ma, Y.H., Chem. Eng. Sci., **39**, 10, 1461 (1984)

25a. Kiselev, A.V., Lopatkin, A.A. and Shugla, A.A., Zeolites, **5**, 261 (1985)

25b. Abdul-Rehman, H.B., Hasanain, M.A. and Loughlin, K.F., Ind. Eng. Chem. Res., **29**, 1525 (1990)

26. Stach, H., Thamm, H., Fiedler, K., Granert, B., Weiker, W., Jahn, E., Oehlmann, G. in 'New Developments in Zeolite Science and Technology', Stud. Surf. Sci. Catal., **28**, 5

(1986)

27. Choudhary, V.R. and Doraiswamy, L.K., Ind. Eng. Chem. Prod. Res. Develop. **10**, 218 (1971)

28. Eberly, P.E.Jr. and Spencer, E.M., Trans. Faraday Soc., **56**, 289 (1961)

29. Greens, S.A. and Pust, H., J. Phys. Chem., **62**, 55 (1958)

30. Carrott, P.J.M. and Sing, K.S.W., J. Chromatogr., **406**, 139 (1987)

31. Nikitin, Yu.S., Ron Tak Ro and Shonia, N.K., J. Chromatogr., **446**, 56 (1988)

32. Langmuir, L., J. Am. Chem. Soc., **40**, 1361 (1918)

33. Sips, R., J. Chem. Phys., **16**, 490 (1948)

34. Sips, R., J. Chem. Phys., **18**, 1024 (1950)

35. Toth, J., Acta. Chim. Acad. Sci. Hung., **69**, 311 (1971)

36. Bering, B.P., Dubinin, M.M. and Serpinsky, V.V., J. Colloid. Interface Sci., **21**, 378 (1966)

37. Hacskaylo, J.J. and Le Van, M.D., Langmuir, **1**, 97 (1985)

38. McBain, J.W. and Britton, G.T., J. Am. Chem. Soc., **52**, 2198 (1930)

39. Boehlen, B. and Guyer, A., Helv. Chim. Acta., **47**, 1815 (1964)

40. Zuech, J.L., Hines, A.L. and Sloan, E.D., Ind. Eng. Chem. Process Des. Dev., **22**, 1, 172 (1983)

41a. Hayhurst, D.T. and Lee, J.C., AIChE Symp. Ser., **79**, 230 (1983)

41b. Breck, D.W., 'Zeolite Molecular Sieves', John Wiley & Sons, N.Y. (1974)

42. Nayak, V.S., 'Studies in Synthetic Zeolites', PhD Thesis, Univ. Poona, Pune (1982)

43. Nayak, V.S. and Choudhary, V.R., Appl. Catal. **4**, 333 (1982)

44. Akolekar, D.B., 'Sorption, Diffusion and Catalytic Reactions on Zeolites and Zeolite-like Materials', PhD Thesis, Univ. Poona, Pune (1987)

45. Choudhary, V.R., Akolekar, D.B. and Sansare, S.D., Material. Phys. Chem., **18**, 245 (1987)

46. Choudhary, V.R. and Pataskar, S.G., Zeolites, **6**, 307 (1986)

47. Choudhary, V.R., Zeolites, **7**, 272 (1987)

48. Choudhary, V.R., Srinivasan, K.R. and Akolekar, D.B., Zeolites, **9**, 115 (1989)

49. Choudhary, V.R. and Singh, A.P., Zeolites, **6**, 206 (1986)

50. Marquardt, D.W., 'Least Square Estimation of Non-linear Parameters', IBM SHARE Library Program No. 3094 Exhibit B

51. Witzheimer, W.W., PhD Thesis, Univ. Pennsylvania (1969)

52. Reid, R.C., Prautnitz, J.M. and Sherwood, T.K., 'The Properties of Gases and Liquids', 3rd Ed., McGraw-Hill Book Company, N.Y. (1977)

53. Stach, H., Thamn, H., Janchen, J., Fielder, K. and Schirmer, W., Proceedings of the 6th international Zeolite Conference. Ed. Olson, D.H. and Attillo Bisio (1983) p.225

54. BOlow, M. and Schlodder, H. 'New Developments in Zeolite Science and Technology', Stud. Surf. Sci. Catal., **28**, 579 (1986)

55. Barrer, R.M., 'Zeolites and Clay Minerals as Sorbents and Molecular sieves', Academic Press, London (1978)

Appendix 3.1

Retention time data for the calculation of heat of sorption of different adsorbents by gc pulse technique

Zeolite : H-ZSM-5

Column temperature T_c (K)	RT for N_2 (GSV inj) t_d (min)	RT for adsorbate (GSV inj.) t_r (min) CH_4	C_2H_6	C_2H_4	CO_2	RT for N_2 (syringe inj) t_d (min)	RT for H_2O (syringe inj) t_r (min)
313	0.45	0.79	9.90	15.37	3.79		
323	0.42	0.72	7.14	10.81	2.83		
333	0.40	0.63	5.07	6.81	2.14		
343	0.37	0.56	3.77	4.58	1.65		
353	0.36	0.51	2.82	3.21	1.29		
363	0.34	0.47	2.22	2.41	1.05		
373	0.33	0.43	1.72	1.88	0.87		
383	0.32	0.40	1.40	1.49	0.73		
393	0.31	0.38	1.16	1.21	0.64		
403	0.30	0.36	0.98	1.01	0.56	0.15	19.76
413						0.14	17.58
423						-	-
433						0.13	8.58
443						0.13	6.47
453						0.12	4.45
463						0.12	3.08
473						0.11	2.14

Zeolite : H-Na-ZSM-5

Column temperature T_c (K)	RT for N_2 (GSV inj) t_d (min)	RT for adsorbate (GSV inj.) t_r (min) CH_4	C_2H_6	C_2H_4	CO_2	RT for N_2 (syringe inj) t_d (min)	RT for H_2O (syringe inj) t_r (min)
313	0.44	1.03	-	-			
323	0.41	0.86	8.21	16.16			
333	0.38	0.74	5.94	9.89			
343	0.35	0.64	4.43	7.41			
353	0.33	0.55	3.33	5.14	12.72		
363	0.33	0.50	2.46	3.77	9.83		
373	0.32	0.46	1.91	2.67	6.55		
383	0.31	0.42	1.53	2.09	4.56	0.14	25.00
393	0.30	0.39	1.15	1.67	3.21	0.14	15.01
403	0.29	0.37	0.99	1.33	2.34	0.13	11.11

Appendix 3.1 (contd.)

Zeolite : Na-ZSM-5

Column temperature T_c (K)	RT for N_2 (GSV inj) t_d (min)	RT for adsorbate (GSV inj.) t_r (min) CH_4	C_2H_6	C_2H_4	CO_2	RT for N_2 (syringe inj) t_d (min)	RT for (syringe t_r (mi
413	0.29				1.78	0.13	9.25
423	0.28				1.39	0.13	8.29
433	0.27				1.10	0.12	6.92
443						0.12	5.99
453						0.12	4.49
463						0.11	3.80
473						0.10	3.01

Zeolite : H-ZSM-8

Column temperature T_c (K)	RT for N_2 (GSV inj) t_d (min)	RT for adsorbate (GSV inj.) t_r (min) CH_4	C_2H_6	C_2H_4	CO_2	RT for N_2 (syringe inj) t_d (min)	RT for H (syringe t_r (mir
313	0.51	1.22	14.46	-	7.53		
323	0.48	1.01	10.43	-	5.40		
333	0.46	0.89	7.59	-	4.12		
343	0.44	0.79	5.96	11.59	2.91		
353	0.42	0.73	4.36	8.36	2.30		
363	0.41	0.69	3.33	5.91	1.84		
373	0.40	0.61	2.65	3.81	1.45	0.26	4.39
383	0.39	0.57	2.15	2.89	1.23		(very sl
393	0.38	0.54	1.78	2.27	1.13		desorpti

Zeolite : Na-H-ZSM-8

Column temperature T_c (K)	RT for N_2 (GSV inj) t_d (min)	RT for adsorbate (GSV inj.) t_r (min) CH_4	C_2H_6	C_2H_4	CO_2	RT for N_2 (syringe inj) t_d (min)	RT for H_2 (syringe i t_r (min)
313	0.73	1.53	24.90				
323	0.66	1.31	16.29				
333	0.60	1.07	11.38	-	-	-	-
343	0.55	0.92	8.09				
353	0.52	0.84	5.82				

Appendix 3.1 (contd.)

Zeolite : Na-H-ZSM-8

Column temperature T_c (K)	RT for N_2 (GSV inj) t_d (min)	RT for adsorbate (GSV inj.) t_r (min) CH_4	C_2H_6	C_2H_4	CO_2	RT for N_2 (syringe inj) t_d (min)	RT fo (syrir t_r (
363	0.49	0.74	4.36		15.56		
373	0.47	0.67	3.45		9.82		
383	0.45	0.60	2.58	-	6.91	-	
393	0.43	0.55	2.03		4.96		
403	0.42	0.51	1.75	11.33	3.59		
413	0.38			8.90			
423	0.37			6.63			
433	0.37			5.19		-	
443	0.36			3.68			
453	0.35			3.06			
463	0.35			2.36			
473	0.35			1.96			

Zeolite : HY

Column temperature T_c (K)	RT for N_2 (GSV inj) t_d (min)	RT for adsorbate (GSV inj.) t_r (min) CH_4	C_2H_6	C_2H_4	CO_2	RT for N_2 (syringe inj) t_d (min)	RT for (syringe t_r (mi
313	0.37	0.44	1.96	-	3.50		
323	0.35	0.42	1.61	7.81	2.60		
333	0.35	0.40	1.29	5.49	2.00		
343	0.33	0.38	1.07	3.69	1.49		
353	0.33	0.37	0.93	2.68	1.19		
363	0.32	0.35	0.80	2.07	0.99		
373	0.31	0.35	0.71	1.60	0.82		
383	0.30	0.34	0.63	1.24	0.69		
393	0.30	0.32	0.57	1.03	0.61		
403	0.29	0.31	0.52	0.87	0.58		
483						0.10	21.73
493						0.10	15.59
503						0.10	11.12
513						0.10	8.61
523						0.10	7.30
533						0.09	5.58

Appendix 3.1 (contd.)

Zeolite : NaY

Column temperature T_c (K)	RT for N_2 (GSV inj) t_d (min)	RT for adsorbate (GSV inj.) t_r (min) CH_4	C_2H_6	C_2H_4	CO_2	RT for N_2 (syringe inj) t_d (min)	RT for H_2 (syringe t_r (min
313	0.46	-	4.13	-	-		
323	0.42	0.50	3.10	-	-		
333	0.40	0.48	2.37	-	19.11	-	-
343	0.37	0.44	1.85	-	13.51		Not deso
353	0.36	0.41	1.51	10.83	8.71		at 513 K 30 min.
363	0.34	0.39	1.23	7.77	6.14		
373	0.33	0.37	1.03	5.13	4.49		
383	0.31	0.36	0.87	3.83	3.14	-	-
393	0.31	0.35	0.75	2.87	2.55		
403	0.30	0.33	0.66	2.25	1.99		

Zeolite : CeNaY(Ce^{+3} exchange = 46%)

Column temperature T_c (K)	RT for N_2 (GSV inj) t_d (min)	RT for adsorbate (GSV inj.) t_r (min) CH_4	C_2H_6	C_2H_4	CO_2	RT for N_2 (syringe inj) t_d (min)	RT for H_2 (syringe t_r (min)
313	0.42	0.52	3.37	-	-		
323	0.39	0.48	2.55	-	-		
333	0.37	0.45	2.03	-	12.49		
343	0.36	0.42	1.55	15.81	8.34		
353	0.35	0.39	1.27	10.65	5.64		
363	0.33	0.38	1.07	7.41	4.09		
373	0.32	0.36	0.90	4.99	2.98		
383	0.31	0.35	0.78	3.58	2.25		
393	0.30	0.33	0.69	2.58	1.73		
403	0.30	0.32	0.61	1.99	1.40		
413	0.29			1.53			
423	0.28			1.25			
433	0.27			1.05			
563						0.09	12.29
573						0.08	10.28

Appendix 3.1 (contd.)

Zeolite : CeNaY(Ce^{+3} exchange = 72%)

Column temperature T_c (K)	RT for N_2 (GSV inj) t_d (min)	RT for adsorbate (GSV inj.) t_r (min) CH_4	C_2H_6	C_2H_4	CO_2	RT for N_2 (syringe inj) t_d (min)	RT for H (syringe t_r (min
313	0.42	0.52	2.92	Not eluted	-		
323	0.38	0.48	2.43	at 423 K	-		
333	0.36	0.42	1.89	in 30 min.	-		
343	0.34	0.40	1.47		19.04		
353	0.33	0.38	1.21		10.18		
363	0.31	0.35	0.99		5.77		
373	0.30	0.34	0.85		3.36		
383	0.29	0.32	0.74		2.77		
393	0.28		0.65		2.08		
403	0.26		0.58		1.51		
413	0.26				1.19		
423	0.25				0.96		
433	0.24				0.80		
553						0.09	12.29
563						0.09	10.63
573						0.07	8.85

Zeolite : KL

Column temperature T_c (K)	RT for N_2 (GSV inj) t_d (min)	RT for adsorbate (GSV inj.) t_r (min) CH_4	C_2H_6	C_2H_4	CO_2	RT for N_2 (syringe inj) t_d (min)	RT for H_2 (syringe i t_r (min)
313	0.40	0.52	3.91				
323	0.39	0.49	3.05				
333	0.37	0.45	2.34	12.98			
343	0.36	0.42	1.81	9.09			
353	0.35	0.40	1.46	6.20			
363	0.34	0.37	1.21	4.49			
373	0.33	0.36	1.01	3.38	2.69		
383	0.32	0.35	0.85	2.57	2.07		
393	0.32	0.34	0.75	1.98	1.75		
403	0.31	0.33	0.66	1.55	1.40		
413	0.31			1.29	1.23		
423	0.30			1.08	1.03		
433	0.30				0.90		
443	0.30				0.81		
453	0.29				0.76		

Appendix 3.1 (contd.)

Zeolite : KL

Column temperature T_c (K)	RT for N_2 (GSV inj) t_d (min)	RT for adsorbate (GSV inj.) t_r (min) CH_4	C_2H_6	C_2H_4	CO_2	RT for N_2 (syringe inj) t_d (min)	RT for H (syringe t_r (min
463	0.29				0.71		
473	0.29				0.67	0.11	16.20
483						0.10	12.90
493						0.10	9.70
503						0.10	7.67
513						0.10	5.70
523						0.09	4.49

Zeolite : HKL

Column temperature T_c (K)	RT for N_2 (GSV inj) t_d (min)	RT for adsorbate (GSV inj.) t_r (min) CH_4	C_2H_6	C_2H_4	CO_2	RT for N_2 (syringe inj) t_d (min)	RT for H (syringe t_r (min
313	0.43	-	2.28	11.53	-		
323	0.41	0.44	1.77	7.81	9.11		
333	0.40	0.42	1.41	4.69	6.15		
343	0.39	0.41	1.11	3.70	4.45		
353	0.38	0.39	0.93	2.75	3.31		
363	0.37	0.38	0.80	2.09	2.42		
373	0.35	0.37	0.71	1.64	1.94		
383	0.35	0.37	0.64	1.32	-		
393	0.35	0.36	0.57	1.08	1.27		
403	0.34	0.35	0.53	0.91	1.08		
413	0.33	0.35			0.91		
423	0.33				0.82		
503						0.12	5.33
513						0.12	4.07
523						0.12	3.46
533						0.11	2.54
543						0.11	1.95

Appendix 3.1 (contd.)

Zeolite : HM

Column temperature T_c (K)	RT for N_2 (GSV inj) t_d (min)	RT for adsorbate (GSV inj.) t_r (min) CH_4	C_2H_6	C_2H_4	CO_2	RT for N_2 (syringe inj) t_d (min)	RT for H_2 (syringe t_r (min)
313	0.44	0.72	5.16				
323	0.41	0.70	3.95	Not eluted			
333	0.38	0.64	3.01	at 423 K			
343	0.35	0.57	2.36	in 60 min			
353	0.34	0.51	1.85				
363	0.32	0.46	1.50				
373	0.31	0.42	1.24		5.53		
383	0.30	0.39	1.03		3.78		
393	0.29	0.37	0.89		2.61		
403	0.28				1.91		
413	0.27				1.14		
423	0.27				1.11		
433	0.26				0.87		
563						0.10	4.97
573						0.10	4.07

Zeolite : NaM

Column temperature T_c (K)	RT for N_2 (GSV inj) t_d (min)	RT for adsorbate (GSV inj.) t_r (min) CH_4	C_2H_6	C_2H_4	CO_2	RT for N_2 (syringe inj) t_d (min)	RT for H_2 (syringe i t_r (min)
313	0.46	0.65					
323	0.42	0.63					
333	0.40	0.57	1.99				
343	0.37	0.52	1.44				
353	0.36	0.50	1.14				
363	0.34	0.46	0.93				
373	0.33	0.43	0.78				
383	0.31	0.41	0.67				
393	0.31	0.39	0.58				
403	0.30	0.37	0.52				
413	0.29			6.94			
423	0.29			5.70			
433	0.28			3.56			

Appendix 3.1 (contd.)

Zeolite : NaM

Column temperature T_c (K)	RT for N_2 (GSV inj) t_d (min)	RT for adsorbate (GSV inj.) t_r (min) CH_4	C_2H_6	C_2H_4	CO_2	RT for N_2 (syringe inj) t_d (min)	RT for H_2O (syringe inj t_r (min)
473	0.09				3.17		
483	0.09				2.49		
493	0.09				1.90		
503	0.09				1.61		
513	0.09				1.31		
523	0.09				1.17		
623						0.10	12.68

Zeolite : NaX

Column temperature T_c (K)	RT for N_2 (GSV inj) t_d (min)	RT for adsorbate (GSV inj.) t_r (min) CH_4	C_2H_6	C_2H_4	CO_2	RT for N_2 (syringe inj) t_d (min)	RT for H_2O (syringe inj t_r (min)
313	0.46	1.28					
323	0.42	1.19			CO_2 and H_2O are not eluted at 573 K in		
333	0.40	1.11			30 min.		
343	0.37	1.05					
353	0.36	0.99	4.26				
363	0.34	0.96	3.56				
373	0.33	0.92	3.03				
383	0.31	0.89	2.63				
393	0.31	0.87	2.33				
403	0.30	0.85	2.08	10.93			
413	0.29		1.86	7.99			
423	0.29		1.73	7.06			
433	0.28			5.57			

Appendix 3.1(contd.)

SILICALITE-I

Column temperature T_c (K)	RT for N_2 (GSV inj) t_d (min)	RT for adsorbate (GSV inj.) t_r (min) CH_4	C_2H_6	C_2H_4	CO_2	RT for N_2 (syringe inj) t_d (min)	RT for H_2 (syringe i t_r (min)
313	0.51	0.89	10.63	4.03	2.30	0.24(315K)	13.06(31
323	0.48	0.79	6.83	3.00	1.83	0.22	9.15
333	0.46	0.71	5.21	2.33	1.48	0.20	5.47
343	0.44	0.64	3.89	1.83	1.23	0.19	3.39
353	0.42	0.59	3.11	1.46	1.05	0.18	2.19
363	0.41	0.54	2.35	1.21	0.91	0.17	1.40
373	0.40	0.50	1.94	1.00	0.81	0.16	0.95
383	0.39	0.47	1.59	0.85	0.73	0.15	0.61
393	0.38	0.45	1.33	0.74	0.65	0.15	0.45

$AlPO_4$-5

Column temperature T_c (K)	RT for N_2 (GSV inj) t_d (min)	RT for adsorbate (GSV inj.) t_r (min) CH_4	C_2H_6	C_2H_4	CO_2	RT for N_2 (syringe inj) t_d (min)	RT for H_2 (syringe i t_r (min)
313	0.53	0.62	2.79	2.06	1.19		
323	0.53	0.61	2.31	1.71	1.09		
333	0.52	0.59	1.91	1.42	0.99		
343	0.51	0.56	1.63	1.23	0.91		
353	0.51	0.55	1.40	1.09	0.84		
363	0.50	0.54	1.21	0.99	0.75		
373	0.50	0.53	1.10	0.88	0.74		
383	0.49	0.53	1.01	0.85	0.66		
393	0.49	0.51	0.91	0.78	0.63		
403	0.49	0.51	0.84	0.72	0.63	0.18	9.00
413						0.17	3.33
423						0.16	2.15
433						0.16	1.49
443						0.16	1.13
453						0.16	0.92

Appendix 3.2

Adsorption isotherm data of n-hexane on silicalite-I and n-hexane and water on NaM at different temperatures

P (kPa)	q (mmol.g^{-1})	P (kPa)	q (mmol.g^{-1})
n-Hexane-Silicalite-I (323 K)		n-Hexane-NaM (318 K)	
3.3	1.49	4.5	0.08
10.0	1.59	9.3	0.10
21.3	1.69	13.2	0.11
		18.7	0.14
		23.3	0.15
n-Hexane-Silicalite-I (423 K)			
3.3	0.50	Water-NaM (353 K)	
8.0	0.53		
11.3	0.71	2.0	2.63
20.0	0.94	3.3	4.30
		6.0	5.61
		9.3	8.00
n-Hexane-NaM (305 K)			
5.3	0.13		
10.3	0.16		
15.3	0.22		
23.3	0.25		

Appendix 3.3

Adsorption isotherm data of methane, ethane, ethylene and carbon dioxide on NaX zeolite at different temperatures

P (kPa)	q (mmol.g^{-1})	P (kPa)	q (mmol.g^{-1})	P (kPa)	q (mmol.g^{-1})
CH_4 (305 K)		C_2H_6 (353 K)		CO_2 (305 K)	
20.0	0.22	11.3	0.30	6.7	1.90
52.6	0.44	39.3	0.84	18.7	3.69
80.0	0.67	79.3	1.88	44.7	4.80
121.0	0.94	124.0	2.40	83.3	5.45
183.9	1.36	150.0	2.60	123.0	5.82
				183.9	6.26
CH_4 (353 K)		C_2H_4 (305 K)		CO_2 (353 K)	
63.3	0.27	6.7	1.22	14.0	1.51
145.2	0.49	24.7	3.41	30.7	2.00
		58.0	3.99	75.3	3.49
		84.6	4.21	109.0	4.04
		135.0	4.53	179.9	4.95
		179.9	4.68		
C_2H_6 (305 K)					
		C_2H_4 (353 K)			
10.0	0.85				
22.7	1.79	15.3	1.40		
48.0	2.72	46.0	2.59		
79.3	3.20	83.3	3.16		
121.0	3.55	131.0	3.53		
179.9	3.91	187.9	3.85		

Appendix 3.4

Adsorption isotherm data of methane, ethane, ethylene and carbon dioxide on NaY zeolite at different temperatures

P (kPa)	q (mmol.g^{-1})	P (kPa)	q (mmol.g^{-1})	P (kPa)	q (mmol.g^{-1})
CH_4 (305 K)		C_2H_6 (353 K)		CO_2 (305 K)	
12.0	0.14	11.3	0.14	7.3	0.94
50.0	0.32	46.0	0.54	26.0	3.06
96.6	0.56	88.0	1.06	62.6	4.68
75.0	0.93	139.6	1.64	100.0	5.25
		185.5	1.99	118.5	5.55
				183.9	6.11
CH_4 (353 K)		C_2H_4 (305 K)			
18.0	0.03	3.0	2.19	CO_2 (353 K)	
60.6	0.11	14.3	3.27		
166.5	0.44	31.6	3.82	12.7	0.39
189.0	0.50	47.6	4.20	33.3	1.22
				70.6	2.20
				98.0	2.80
C_2H_6 (305 K)		C_2H_4 (353 K)		177.9	3.54
14.0	0.53	14.7	0.85		
44.0	1.71	44.0	1.91		
91.3	2.74	76.0	2.44		
140.5	3.21	118.0	2.82		
188.5	3.54	181.0	3.23		

Appendix 3.5

Adsorption isotherm data of methane, ethane, ethylene carbon-dioxide and n-hexane on NaM zeolite at different temperatures

P (kPa)	q (mmol.g^{-1})	P (kPa)	q (mmol.g^{-1})	P (kPa)	q (mmol.g^{-1})
CH_4 (305 K)		C_2H_4 (353 K)		CO_2 (343 K)	
66.0	0.80	6.0	0.49	10.7	0.64
94.0	1.04	24.0	1.23	25.3	1.57
162.0	1.33	66.0	1.55	40.7	1.98
185.9	1.38	122.0	1.76	70.6	2.18
		183.9	1.89	110.0	2.38
				182.0	2.62
CH_4 (353 K)		CO_2 (278 K)			
27.3	0.13			CO_2 (423 K)	
72.0	0.33	6.0	0.64		
131.0	0.55	21.3	1.88	13.3	0.40
191.0	0.75	50.6	2.96	25.3	0.67
		75.3	3.11	40.0	1.02
		125.0	3.25	54.6	1.02
C_2H_6 (305 K)		181.4	3.36	112.5	1.40
				187.0	1.65
22.7	1.09			84.0	1.37*
36.0	1.41	CO_2 (298 K)			
58.6	1.61				
88.0	1.80	10.7	0.74	$n\text{-}C_6H_{14}$ (305 K)	
128.0	1.88	33.2	2.43		
186.0	1.94	57.3	2.76	5.3	0.13
		72.0	2.82	10.0	0.16
		157.0	3.11	15.3	0.22
C_2H_6 (353 K)		179.0	3.11	23.3	0.25
22.0	0.42				
42.0	0.61	CO_2 (318 K)		$n\text{-}C_6H_{14}$ (318 K)	
80.0	0.79				
119.0	0.90	7.3	0.49	4.7	0.08
182.0	1.02	14.0	1.31	9.3	0.10
		24.0	2.03	13.3	0.11
C_2H_4 (305 K)		36.0	2.29	18.7	0.14
		50.6	2.42	23.3	0.15
10.0	1.60	100.0	2.68		
28.7	1.77	183.9	2.91		
42.0	1.90				
69.3	2.01				
119.0	2.09				
183.0	2.22				

* value from desorption

Appendix 3.6

Adsorption isotherm data of methane, ethane, ethylene carbon dioxide and n-hexane on Silicalite-I at different temperatures

P (kPa)	q (mmol.g^{-1})
CH_4 (305 K)	
14.0	0.27
82.6	0.68
108.0	0.81
144.0	1.00
182.9	1.14
C_2H_4 (354 K)	
19.3	0.13
59.3	0.20
108.0	0.38
140.0	0.44
164.0	0.56
179.9	0.56
186.3	0.56
C_2H_6 (305 K)	
14.0	1.11
28.0	1.48
44.6	1.69
76.6	1.95
114.9	2.10
146.0	2.19
188.9	2.31
C_2H_6 (353 K)	
6.7	0.15
20.0	0.40
54.0	0.87
112.0	1.37
146.9	1.55
189.9	1.70
C_2H_6 (413 K)	
20.0	0.08
69.3	0.37
128.9	0.61
187.9	0.84
C_2H_6 (453 K)	
68.6	0.13
134.0	0.28
185.0	0.48
C_2H_4 (306 K)	
12.0	0.54
33.3	1.16
59.3	1.52
84.6	1.74
136.5	2.02
187.9	2.18
C_2H_4 (353 K)	
18.0	0.25
46.0	0.55
80.0	0.86
129.3	1.15
193.0	1.45
CO_2 (306 K)	
14.7	0.29
26.7	0.52
39.3	0.73
70.6	1.15
109.0	1.57
130.0	1.70
190.0	1.90
CO_2 (353 K)	
11.3	0.10
38.7	0.27
59.3	0.40
82.6	0.56
132.0	0.81
187.0	1.06
n-C_6H_{14} (323 K)	
1.71	0.07
3.33	1.49
10.00	1.59
n-C_6H_{14} (421 K)	
3.33	0.50
8.00	0.52
11.33	0.70
19.99	0.94

Appendix 3.7

Adsorption isotherm data of methane, ethane, ethylene and carbon-dioxide on $AlPO_4$-5 at different temperatures

P (kPa)	q (mmol.g^{-1})	P (kPa)	q (mmol.g^{-1})	P (kPa)	q (mmol.g^{-1})
CH_4 (305 K)		C_2H_6 (353 K)		CO_2 (305 K)	
28.7	0.11	19.3	0.09	18.0	0.11
82.2	0.18	66.0	0.24	46.6	0.26
121.0	0.32	98.8	0.38	88.6	0.46
195.9	0.42	191.0	0.57	121.5	0.85
				185.0	0.85
CH_4 (353 K)		C_2H_4 (305 K)			
				CO_2 (353 K)	
83.3	0.18	16.0	0.09		
178.6	0.35	46.6	0.32	19.3	0.04
		86.0	0.46	47.3	0.12
		142.5	0.68	83.3	0.21
C_2H_6 (305 K)		189.9	0.80	118.5	0.29
				185.9	0.43
23.3	0.09	C_2H_4 (353 K)			
50.6	0.43				
86.0	0.61	14.0	0.03		
126.0	0.75	46.0	0.16		
178.6	0.89	82.0	0.24		
		131.0	0.39		
		184.0	0.39		

Appendix 3.3

Adsorption isotherm data of methane, ethane, ethylene and carbon dioxide on SAPO-5 at different temperatures

P (kPa)	q ($mmol.g^{-1}$)	P (kPa)	q ($mmol.g^{-1}$)	P (kPa)	q ($mmol.g^{-1}$)
CH_4 (305 K)		C_2H_6 (353 K)		CO_2 (305 K)	
16.6	0.08	15.3	0.09	22.0	0.26
82.0	0.24	47.3	0.26	52.6	0.52
194.0	0.45	86.0	0.42	73.3	0.68
		134.0	0.56	107.4	0.91
		187.9	0.69	181.9	1.25
CH_4 (353 K)					
		C_2H_4 (305 K)			
46.0	0.08			CO_2 (353 K)	
90.0	0.10	13.3	0.40		
179.9	0.22	45.4	0.71	12.7	0.03
		82.6	0.91	47.3	0.17
		139.0	1.11	82.0	0.29
C_2H_6 (305 K)		185.0	1.22	163.6	0.53
12.0	0.24	C_2H_4 (354 K)			
40.7	0.52				
90.6	0.79	14.0	0.13		
134.0	0.90	50.0	0.35		
183.9	1.02	84.6	0.52		
		114.0	0.63		
		197.0	0.83		

Appendix 3.9

Estimation of heat of sorption at different surface coverages for the sorption of methane, ethane, ethylene and carbon dioxide in different zeolites T_1 = 305 K, T_2 = 353 K

Adosrbent	Sorbate	q ($mmol.g^{-1}$)	P_1 (mm Hg)	P_2 (mm Hg)	Q_a ($kJ.mol^{-1}$)
NaX	CH_4	0.125	100	250	17.09
		0.250	240	550	15.46
		0.375	360	850	16.01
		0.500	500	1100	14.70
	C_2H_6	0.667	60	210	23.36
		1.333	124	425	22.97
		2.000	208	673	21.90
		2.333	270	845	21.28
	C_2H_4	0.714	22	60	18.71
		1.429	52	120	15.60
		2.143	90	232	17.66
		2.857	134	460	23.00
		3.571	218	1030	28.96
	CO_2	0.909	15	58	25.22
		1.818	40	170	26.98
		2.727	77	350	28.24
		3.636	132	618	28.79
		4.545	318	1360	27.10
NaY	CH_4	0.125	100	350	23.36
		0.250	300	650	14.42
		0.375	480	1000	13.69
		0.500	650	1350	13.63
	C_2H_6	0.333	60	195	21.98
		0.668	130	380	20.00
		1.333	255	850	22.45
		2.000	400	1380	23.09

Appendix 3.9 (contd.)

Adosrbent	Sorbate	q ($mmol.g^{-1}$)	P_1 (mm^{Hg})	P_2 (mm^{Hg})	Q_a ($kJ.mol^{-1}$)
NaY	C_2H_4	0.714	10	90	40.98
		1.429	32	220	35.66
		2.143	85	420	29.79
		2.857	260	930	23.77
		3.214	420	1390	22.32
	CO_2	0.454	30	90	20.49
		0.909	60	185	21.00
		1.364	90	295	22.14
		1.818	120	410	22.91
		2.273	145	550	24.86
		2.727	178	713	25.89
NaM	CH_4	0.156	75	230	20.90
		0.312	155	510	22.21
		0.469	246	780	21.52
		0.625	348	1060	20.77
		0.781	470	1450	21.01
	C_2H_6	0.333	38	125	22.21
		0.500	60	220	24.23
		0.667	90	385	27.10
		0.833	123	680	31.89
	C_2H_4	0.357	5	35	36.29
		0.714	9	65	36.87
		1.071	18	136	37.71
		1.428	50	342	35.86
		1.786	215	1060	29.75
Silicalite	CH_4	0.125	35	155	27.75
		0.250	110	480	27.47
		0.375	245	810	22.30
		0.500	405	1150	19.40

Appendix 3.9 (contd.)

Adosrbent	Sorbate	q ($mmol.g^{-1}$)	P_1 (mm Hg)	P_2 (mm Hg)	Q_a ($kJ.mol^{-1}$)
Silicalite	C_2H_4	0.357	50	205	26.31
		0.714	125	465	24.50
		1.071	220	850	25.20
		1.429	385	1430	24.47
	CO_2	0.227	80	230	19.69
		0.454	170	490	19.74
		0.682	275	780	19.41
		0.909	380	1145	20.57
		1.023	445	1365	20.90
	CH_4	0.089	120	230	12.13
		0.179	220	410	11.61
		0.268	340	670	12.65
		0.357	450	930	13.54
	C_2H_6	0.083	75	140	11.64
		0.167	145	290	12.93
		0.250	220	450	13.34
		0.333	300	630	13.84
		0.417	390	850	14.53
		0.500	500	1100	14.70
$AlPO_4$-5	C_2H_4	0.089	120	230	12.13
		0.179	220	410	11.61
		0.268	340	670	12.65
		0.357	450	930	13.54
	CO_2	0.114	150	330	14.70
		0.227	305	670	14.68
		0.341	460	1050	15.39
		0.454	615	1495	16.56

Appendix 3.9 (contd.)

Adosrbent	Sorbate	q ($mmol.g^{-1}$)	P_1 ($mm^{}Hg$)	P_2 ($mm^{}Hg$)	Q_a ($kJ.mol^{-1}$)
SAPO-5	CH_4	0.062	110	410	24.54
		0.125	210	750	23.74
		0.187	390	1150	20.17
	C_2H_6	0.167	56	200	23.74
		0.333	152	480	21.44
		0.500	286	828	19.82
		0.667	500	1335	18.31
	C_2H_4*	0.179	30	150	29.50
		0.357	80	365	27.80
		0.536	180	680	24.30
		0.714	345	1090	21.10
		0.804	455	1370	20.20
	CO_2**	0.114	68	230	21.94
		0.227	150	460	20.17
		0.341	230	700	20.04
		0.454	320	975	20.06
		0.514	370	1130	20.10

* T_2 = 354 K

** T_2 = 355 K

CHAPTER - 4

ADSORPTION OF OXYGEN AND NITROGEN ON $AlPO_4$-5 AND SAPO-5 AT MODERATE PRESSURE USING SIMPLE VOLUMETRIC ADSORPTION/DESORPTION APPARATUS

4 ADSORPTION OF OXYGEN AND NITROGEN ON $ALPO_4$-5 AND SAPO-5 AT MODERATE PRESSURE USING SIMPLE VOLUMETRIC ADSORPTION/DESORPTION APPARATUS

4.1 INTRODUCTION

High pressure adsorption is being increasingly used for purification and separation of gases using pressure swing adsorption.

4.1.1 Measurement of Adsorption at High Pressure

The earliest investigation on high pressure adsorption is that of McBain and Britton [1] on the sorption of N_2O, C_2H_4 and N_2 on activated sugar charcoal upto 50 atm. The adsorbent was taken in a quartz spiral, which was mounted in a thick-walled glass tube. The amount adsorbed was determined gravimetrically from the elongation of the calibrated spiral as measured with a precision cathetometer. There have been many refinements of the balance [2-5]. Analytical balances have also been modified for the gravimetric measurement of adsorption at moderate to high pressures [6-8].

Gilmer and Kobayashi [9] used a direct gravimetric method to determine the adsorption isotherms of methane on silica gel upto 140 atm. The method consisted of first equilibrating a chromatographic column packed with adsorbent by a steady flow of methane through it at the desired temperature and pressure, then closing off the column with valves at both ends, removing the assembly from the rest of the system, and weighing it on an analytical balance.

In the volumetric methods employed for the measurement of adsorption at high pressure, in general, a known quantity of

gas is introduced into an evacuated constant volume adsorption chamber [10-15]. From the equilibrium pressure, the amount adsorbed is calculated using material balance. Ozawa et al. [16] have introduced a refinement in the pressure measurement. The inlet and equilibrium pressures are accurately calculated by introducing the same gas in a gas pipette and releasing it to a low pressure system. In another method [17], thermal compression was employed to obtain high pressure. A known amount of gas, measured at 1 atm., was transferred into a calibrated steel U-tube cooled in liquid nitrogen. The coolant was removed and the U-tube was opened to the evacuated adsorption vessel, helium dead space of which was already known. At equilibrium, the U-tube was isolated from the vessel and the gas in it measured after expansion to 1 atm. From these data, the amount of the gas adsorbed was calculated. Details of this method has been reproduced in a monograph [18].

The glass piezometer technique where the volumes of the piezometer bulbs were calibrated with mercury and the pressure measured by Michel's balance is reported to give adsorption data of high accuracy [19]. This technique was used by Michels and Menon [20,21] to obtain adsorption isotherms of N_2 and CO on alumina upto 3000 atm.

Application of gas chromatographic techniques for the measurement of adsorption at high pressure has been reported by many authors [9,22-25]. The isotherms determined by such methods showed a good agreement with those by conventional adsorption measurements [19].

4.1.2 Adsorption of Gases/Vapors on $AlPO_4$-5 and SAPO-5

Wilson et al. [26,27] have introduced a new class of crystalline aluminophosphate molecular sieves, which are similar to zeolites in many properties, and $AlPO_4$-5 belongs to this class. The crystal structure of $AlPO_4$-5 has been well established [28]. It has a novel three-dimensional structure with hexagonal symmetry (cell constants a = 1.373 nm, c = 0.848 nm, and $\gamma = 120^0$; unit cell composition $12AlPO_4 . nH_2O$) and contains one-dimensional channels (pore dia. = 0.8 nm) oriented parallel to the c-axis and bounded by 12-membered rings composed of alternating AlO_4 and PO_4 tetrahedra. The axis in $AlPO_4$-5 is crystallographically polar [28]. The polar nature of its structure is expected to be due to the vertical assignment of P-O-Al bonds in one direction caused by the strict up-down alteration of all the tetrahedra. $AlPO_4$-5 has neutral framework with no extra framework cations. However, it has a polar pore system consisting of unidimensional cylindrical channels of uniform cross section. It contains weak acid sites, both Lewis and protonic [29,30]. It is moderately hydrophilic and has interesting water sorption properties [27]. Water sorption on $AlPO_4$-5 (at 297 K) follows a type V isotherm shape, unusual for microporous solids and zeolites. A knowledge of the sorption properties of $AlPO_4$-5 for various organic compounds is of great interest. However, only a few related studies have been carried out so far. Wilson et al. [27] have measured the sorption isotherms of water (at 297 K) and oxygen (at 90 K) on $AlPO_4$-5. Choudhary and Akolekar [30] have investigated the chemisorption

and temperature-programmed desorption (TPD) of pyridine on $AlPO_4$-5. Choudhary et al. [31] have recently measured the sorption capacity of a number of sorbates, viz. alcohols and hydrocarbons, and the isotherms of sorption of methanol, n-hexane, and benzene in $AlPO_4$-5 by gravimetric technique. The isotherms of sorption of n-hexane, cyclohexane, benzene and pyridine in the $AlPO_4$-5, at higher temperatures (523-673 K) were determined by the GC peak maxima method.

Lok et al.[32] have reported the synthesis of SAPO-5, which is a crystalline microporous (channel or pore diameter 0.8 nm) silicon aluminium phosphate of similar structure to $AlPO_4$-5 and shows interesting, unique properties for potential use in catalytic, adsorptive and ion-exchange applications. Pyke et al. [33] determined the total micropore volume of SAPO-5 from nitrogen adsorption/desorption isotherms. They have also given the data on single point adsorption of water, n-hexane and p-xylene on SAPO-5 at 273 K. The use of Rh and Pd supported on SAPO-5 [34,35] for hydrocarbon synthesis from CO hydrogenation and the CO adsorption on these catalysts are also reported in literature. Thompson et al. [35] have characterized the supported catalyst by argon adsorption.

The potential of $AlPO_4$-5 and SAPO-5 as adsorbents for the sorption of nitrogen and oxygen has not been explored so far. The present study has been undertaken for the measurement of adsorption isotherms of nitrogen and oxygen on $AlPO_4$-5 and SAPO-5 at moderate pressures. Two simple and inexpensive methods have been developed for the measurement of adsorption of nitrogen and oxygen on these materials.

4.2 EXPERIMENTAL

4.2.1 Gases and Materials

Nitrogen, oxygen : IOLAR (Grade II), obtained from Indian Oxygen Ltd., Bombay.

Helium : High purity, obtained from Indian Oxygen Ltd., Bombay.

$AlPO_4$-5, SAPO-5

These samples were provided by Dr. (Ms.) K.R. Kamble, Inorganic Chemistry Division, NCL. The synthesis of these samples has been discussed in Chapter 3.

4.2.2 Measurement of Adsorption Isotherms

The adsorption isotherms of oxygen and nitrogen on $AlPO_4$-5 and SAPO-5 at moderate pressures (upto 40 atm.) were collected by two different methods - one by the desorption of the adsorbed gases to vacuum and the other by the measurement of the volume of the water displaced by the desorbed gases at atmospheric pressure.

A stainless steel tube (0.625 cm. o.d., 20 cm. long) packed with adsorbent (about 2.0 g., particle size : 30-52 mesh) shown in Fig. 4.1 was used as the adsorption column for the experiments. It was connected at the gas inlet side to a Whitey ball valve for on-off service through a Swagelok reducing union and a 0.31 cm. o.d. ss connecting tube. A 0.16 cm. o.d. ss connecting tube with short 0.31 cm. o.d. tubes welded at both ends was used at the outlet of the column to minimize the dead volume. The outlet of the column was connected to a Nupro fine

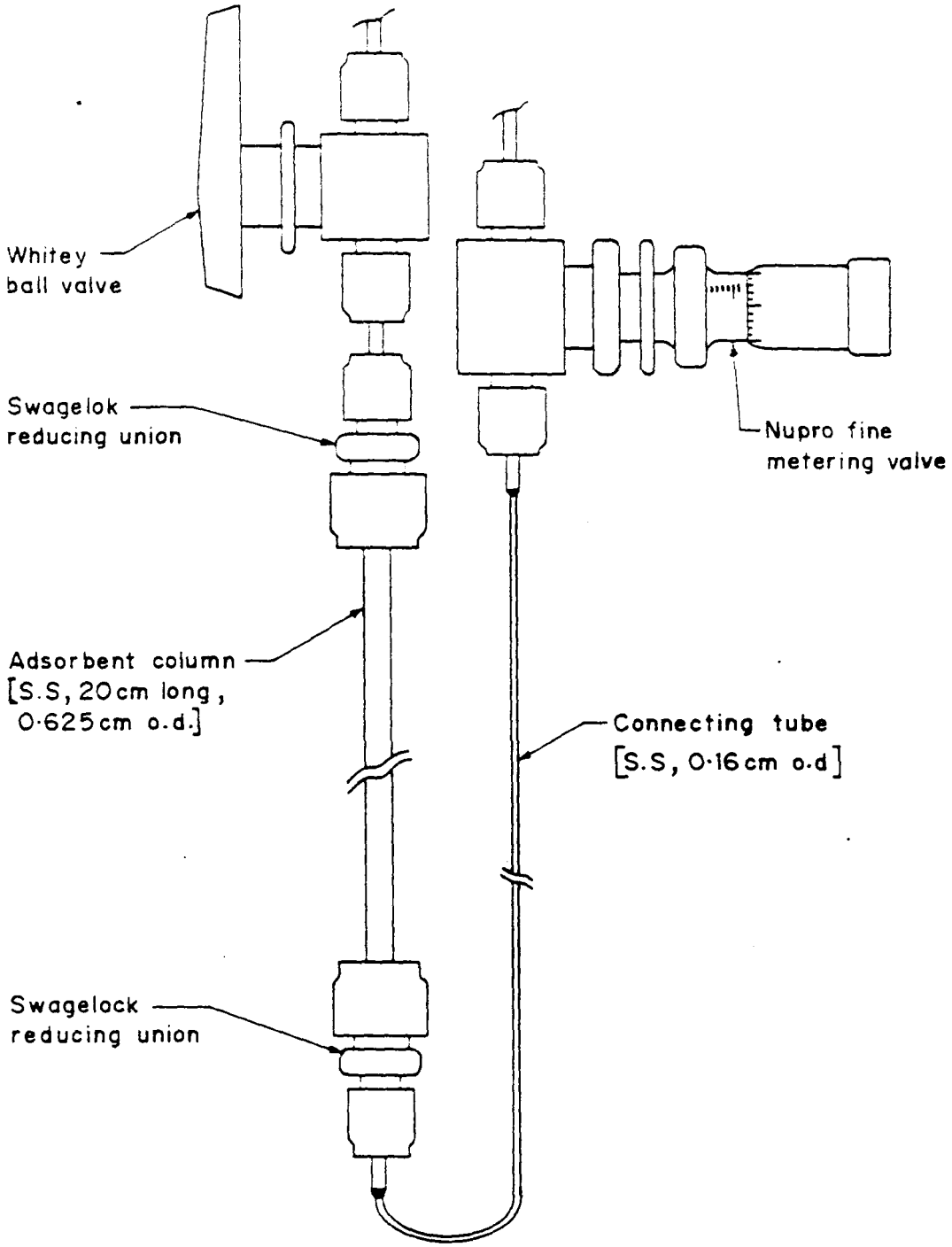

FIG. 4·1 : ADSORBENT COLUMN AND CONNECTIONS

metering valve through a Swagelok reducing union and the connecting tube. The details of the column and the connections are given in Fig. 4.1. At the beginning of each experiment, the adsorbent in the column was heated in a GC oven (Perkin-Elmer Sigma 3B GC with helium flow, 20 $cm^3.min^{-1}$) at 623 K for 2 h to desorb the adsorbed gases , if any.

The schematic diagram of the adsorption unit is shown in Fig. 4.2(a). The adsorbent column was kept inside a jacketed glass vessel through which hot water of the required temperature was circulated. The temperature of adsorption was measured using a thermometer (range 273-373 K) tied to the column. The adsorption pressure was measured using a pressure gauge (range 0-40 $kg.cm^{-2}$) connected between valves 1 and 2. A small amount of gas was continuously let off through valve 3 during adsorption and the column pressure was maintained constant by regulating the gas flow through valves 2 and 3. At each pressure, a period of 1 h was allowed to establish the adsorption equilibrium.

The amount of gas in the adsorption unit (between valves 1 and 3), n_T, is given by the sum of the amount of gas adsorbed on the adsorbent and the amount of gas in the void space (between valves 1 and 3); i.e.

$$\begin{aligned} n_T &= (q_{a(Ta,Pa)}.W) + n_{a(Ta,Pa)} \\ &= (q_{a(Ta,Pa)}.W) + P_a.V_a/(R.T_a) \end{aligned} \qquad (4.1)$$

where n_T is the total number of moles of gas in the adsorption unit, q_a, the moles adsorbed per unit weight of the adsorbent at the adsorption temperature T_a and pressure P_a; W, the weight of

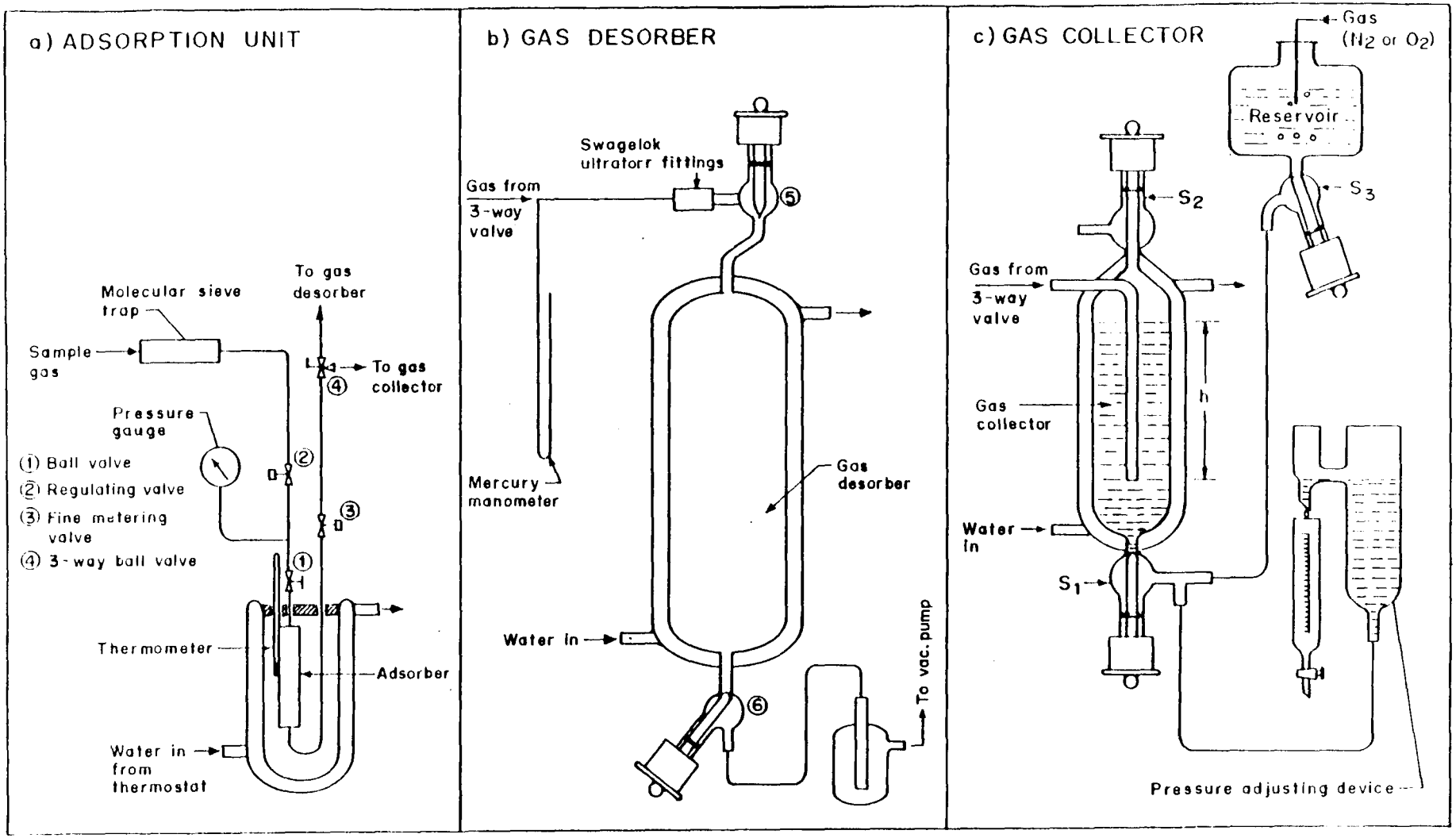

FIG. 4·2 : EXPERIMENTAL SET-UP FOR THE MEASUREMENT OF ADSORPTION ISOTHERMS OF GASES AT MODERATE PRESSURES a) ADSORPTION UNIT b) GAS DESORBER c) GAS COLLECTOR (WATER DISPLACEMENT)

the adsorbent and R, the gas constant. V_a is the free (i.e. voids) volume between valves 1 and 3 and was measured, for each adsorbent, by helium (a non-adsorbate) displacement method. The method is similar to Method-1 which is described in the succeeding part of this section. Helium at different pressures was introduced into the adsorber and expanded to the evacuated desorber unit. The free volume of the adsorber was calculated each time from the desorber volume and the increase in the desorber pressure using material balance and the average value was taken as V_a. The values of compressibility factor for nitrogen and oxygen under the experimental conditions vary from 0.997 to 1 and hence was taken as unity.

Method-1

In Method-1, the amount of gas adsorbed is calculated by desorbing it to a constant volume pre-evacuated desorber (made up of glass). Figure 4.2(b) gives the diagram of the desorption unit. Before starting desorption, the desorber and the connecting line to valve 3 were evacuated by applying vacuum (0.005 torr) through a trap connected to the outlet of the desorber. The rotaflow stop-cock at the bottom of the desorber was then closed and the pressure measured by a U-tube mercury manometer connected to the desorption line. Valve 3 was then opened slowly to let the gases desorb to the desorber. A period of 30 min. was found to be more than sufficient for the desorption process to reach equilibrium, at the end of which, the desorption pressure P_{d1} was noted from the manometer. After closing valve 3, the desorber unit was evacuated again and the

gases in the adsorber were allowed to desorb a second time to a pressure P_{d2}. The increase in the pressure in the desorber due to the desorption steps is given by $P_d = P_{d1} + P_{d2}$. Thermostated water was circulated continuously through the outer jacket of the desorber and its temperature taken as the desorber temperature, T_d.

The total number of moles in the adsorption/desorption unit (i.e. from valve 1 to valve 6) at the end of adsorption is given by

$$\begin{aligned} n_T &= q_{a(Ta,Pd2)} \cdot W + n_{a(Ta,Pd2)} + n_{d(Td,\ Pd)} \\ &= q_{a(Ta,Pd2)} \cdot W + P_{d2}V_a/(RT_a) + P_dV_d/(RT_d) \end{aligned} \qquad (4.2)$$

where V_d is the volume of the desorber and connecting line (initially measured by filling it with water). The quantity $q_{a(Ta,Pd2)}$ (i.e. the amount of gas remaining adsorbed at the end of experiment) is negligibly small and hence can be ignored. By applying the law of conservation of mass to Equations (4.1) and (4.2) and rearranging,

$$q_{a(Ta,Pa)} = ((P_dV_d/T_d + (P_{d2}-P_a) \cdot V_a/T_a)/RW \qquad (4.3)$$

Equation (4.3) was used for calculating the quantity adsorbed at each experimental point.

Method-2

In this method, the desorbed gases displace an equal amount of water from a constant pressure gas collector, the volume of which is measured and used for the calculations. The unit consists of a gas collector, a reservoir and a pressure

adjusting device connected using flexible teflon tubings as shown in Fig. 4.2(c). The gas collector is provided with a water jacket for keeping the temperature constant during the experiment.

Before the start of the desorption step, the gas collector was completely filled with water (saturated with the gas under study, i.e. N_2 or O_2) by raising the pressure adjusting device above the water level in the water reservoir and by opening the teflon stop-cocks S_2 and S_3 until the water in the gas collector reached stop-cock S_2. Stop-cocks S_2 and S_3 were then closed. The pressure adjusting device was then lowered and the water level in it was brought to the same level as at the tip of the gas inlet tube. The gas inlet to the gas collector was then connected to valve 3 of the adsorption unit (Fig. 4.2(a)) by a teflon tubing. The water level in the pressure adjusting device was adjusted very close to the level of the tip of the gas inlet tube by lowering or raising the pressure adjusting device. Gas bubbles, if any, in the gas collector were removed by following the procedure described earlier. Thus the system was made ready for the desorption step. Valve 3 was opened slowly and the volume of the desorbed gas was determined by measuring quantitatively the volume of water displaced from the gas collector into the graduated burette. Sufficient time was allowed for the complete desorption of the gas at 303 K and atmospheric pressure (715 torr).

The gas pressure in the adsorber at the end of the desorption step, P_{a2}, was taken as atmospheric. The pressure of

gas in the gas collector, P_D, is given by

$$P_D = (715-P_w-h/13.6)/760 \qquad (4.4)$$

where h is the height of the water column in the gas collector at the end of desorption, as shown in Fig. 4.2(c). The total amount of gas is given by

$$\begin{aligned} n_T &= q_{a(PD,Ta)}W + n_{a(Pa2,Ta)} + n_{d(PD,Td)} \\ &= q_{a(PD,Ta)}W + P_{a2}V_a/RT_a + P_DV_D/T_d \end{aligned} \qquad (4.5)$$

V_D is the volume of water displaced and P_D is calculated by Equation (4.4). Applying the law of conservation of mass to Equations (4.1) and (4.5) and rearranging,

$$q_{a(Pa,Ta)} = q_{a(PD,Ta)} + ((P_DV_D/T_d) + (P_{a2}-P_{a1})V_a/T_a))/RW \qquad (4.6)$$

The amount adsorbed at each pressure and temperature is calculated using Equation (4.6). The quantity $q_{a(PD,Ta)}$ which is the amount of gas remaining adsorbed on the adsorbent at pressure P_D has been determined by desorbing it to the desorber unit (Fig. 4.2(b)) and noting the increase in pressure as explained in the earlier method.

4.2.3 Fitting of Adsorption Data to Standard Isotherm Models

The isotherms were fitted to standard isotherm models as per the procedure given in Chapter 3.

4.3 RESULTS AND DISCUSSION

4.3.1 Adsorption of N_2 and O_2 on NaM Zeolite

The reliability of the adsorption methods developed and used in the present study has been tested by carrying out adsorption experiments for oxygen and nitrogen on NaM and comparing the data with the published one [7]. Figure 4.3 shows the adsorption isotherms of nitrogen and oxygen on NaM at 309-329 K and 500-3000 kPa. The dark dots in the figure indicate the data taken from literature and it can be seen that they match well with the data obtained in the present study.

Since it has been reported [7] that Dubinin-Astakhov model [36] fits the data, the model has been tried for fitting the adsorption data. The isotherm equation for this model is given by

$$\ln q = A-B(\ln(P_s/P)^C \qquad (4.7)$$

where q is the quantity adsorbed at equilibrium pressure P and A,B,C are constants. The saturation vapor pressure P_s has been estimated from the generalized form of the Clapeyron equation [37].

$$\ln P_{sr} = h_r(1-1/T_r) \qquad (4.8)$$

$$h_r = T_{br} \ln (P_c/(1-T_{br})) \qquad (4.9)$$

where $P_{sr} = P_s/P_c$ is the reduced vapor pressure, $T_r = T/T_c$ is the reduced temperature, $T_{br} = T_{bp}/T_c$ is the reduced boiling point and P_c and T_c are the critical pressure and critical temperature respectively.

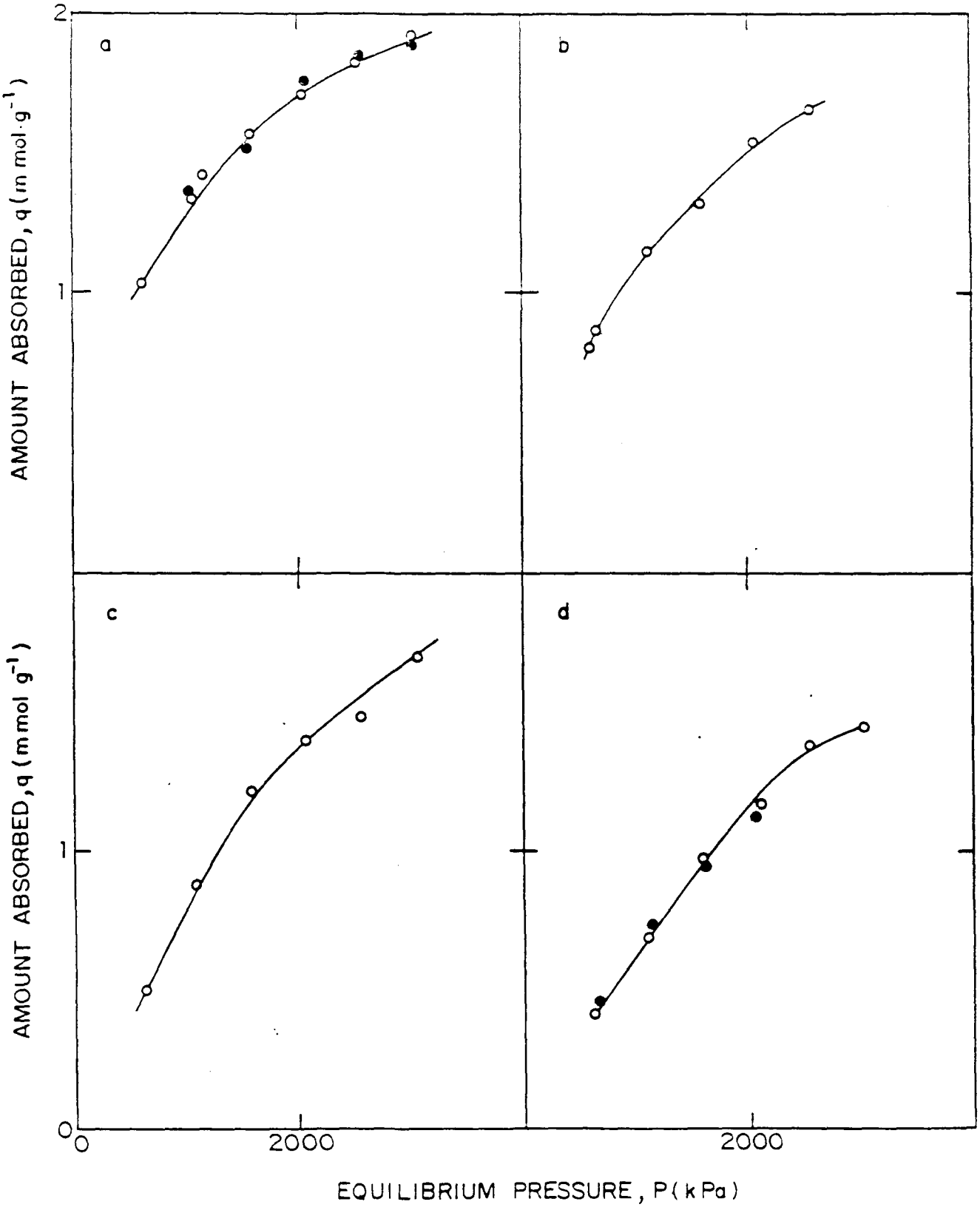

FIG. 4·3 : ADSORPTION OF NITROGEN AND OXYGEN ON NaM AT MODERATE PRESSURES (a) N_2 309 K (b) N_2 329 K (c) O_2 309 K (d) O_2 329 K
(• INDICATES VALUE FROM REFERENCE)

The constants of the Dubinin-Astakhov isotherm are given in Table 4.1. The model gives a good fit of the experimental data (at 309 and 329 K) for both nitrogen and oxygen on the NaM. The isotherm data for the adsorption of N_2 and O_2 on the NaM are given in Appendices 4.1 and 4.2, respectively.

4.3.2 Adsorption of N_2 and O_2 on $AlPO_4$-5 and SAPO-5

The adsorption isotherms of nitrogen and oxygen (at 309 and 329 K and 500-3000 kPa) for $AlPO_4$-5 and SAPO-5 by Method-1 are given in Figs. 4.4 and 4.5 , respectively. Figure 4.4 also shows the isotherm data for nitrogen on $AlPO_4$-5 (for 500-3000 kPa at 309 K) collected by Method-2. It can be seen that both the data compare very well. The adsorption data for nitrogen and oxygen on the two adsorbents are presented in Appendices 4.1 and 4.2, respectively.

Sips' equation [38],

$$q/q_m = ((kP/(1+kP))^c \qquad (4.10)$$

is found to give a good fit for the adsorption isotherm data for nitrogen and oxygen on $AlPO_4$-5 and SAPO-5, covering the whole range of temperature and pressure studied. In Equation (4.10), q is quantity adsorbed at equilibrium pressure P and q_m is the maximum quantity that can be adsorbed. Figures 4.6 and 4.7 show the plots of $q_{experimental}$ versus $q_{theoretical}$ for oxygen and nitrogen on the $AlPO_4$-5 and SAPO-5, respectively. The plots show very little scatter which reveals that the model equation fits the data quite well. The values of the Sips' constants for the

Table 4.1

Constants of the best fitting isotherm models for the adsorption of nitrogen and oxygen on different adsorbents at moderate pressures (500-3000 kPa)

System	Temperature	Dubinin - Astakhov Constants A	B	C	deviation
O_2-NaM	309	1.49	0.1	1.92	-4 to 6
	329	1.005	0.01	3.168	-5 to 4
N_2-NaM	309	1.085	0.023	2.35	-2 to 3
	329	1.107	0.0275	2.349	-2 to 2

System	Temperature (K)	Constants of Sips' isotherm q_m	k	c	Maximum deviation in q (%)
N_2-SAPO-5	309	1.974	0.0006	2.0	-5 to 3
	329	1.523	0.0023	5.22	-5 to 3
O_2-SAPO-5	309	2.488	0.0008	2.75	-6 to 4
	329	1.32	0.0152	27.4	-6 to 4
N_2-$AlPO_4$-5	309	1.16	0.0057	10.75	-2 to 2
	329	1.10	0.0049	10.60	-12 to 6
O_2-$AlPO_4$-5	309	2.90	0.0009	3.66	-5 to 5
	329	1.63	0.0021	5.60	-8 to 4

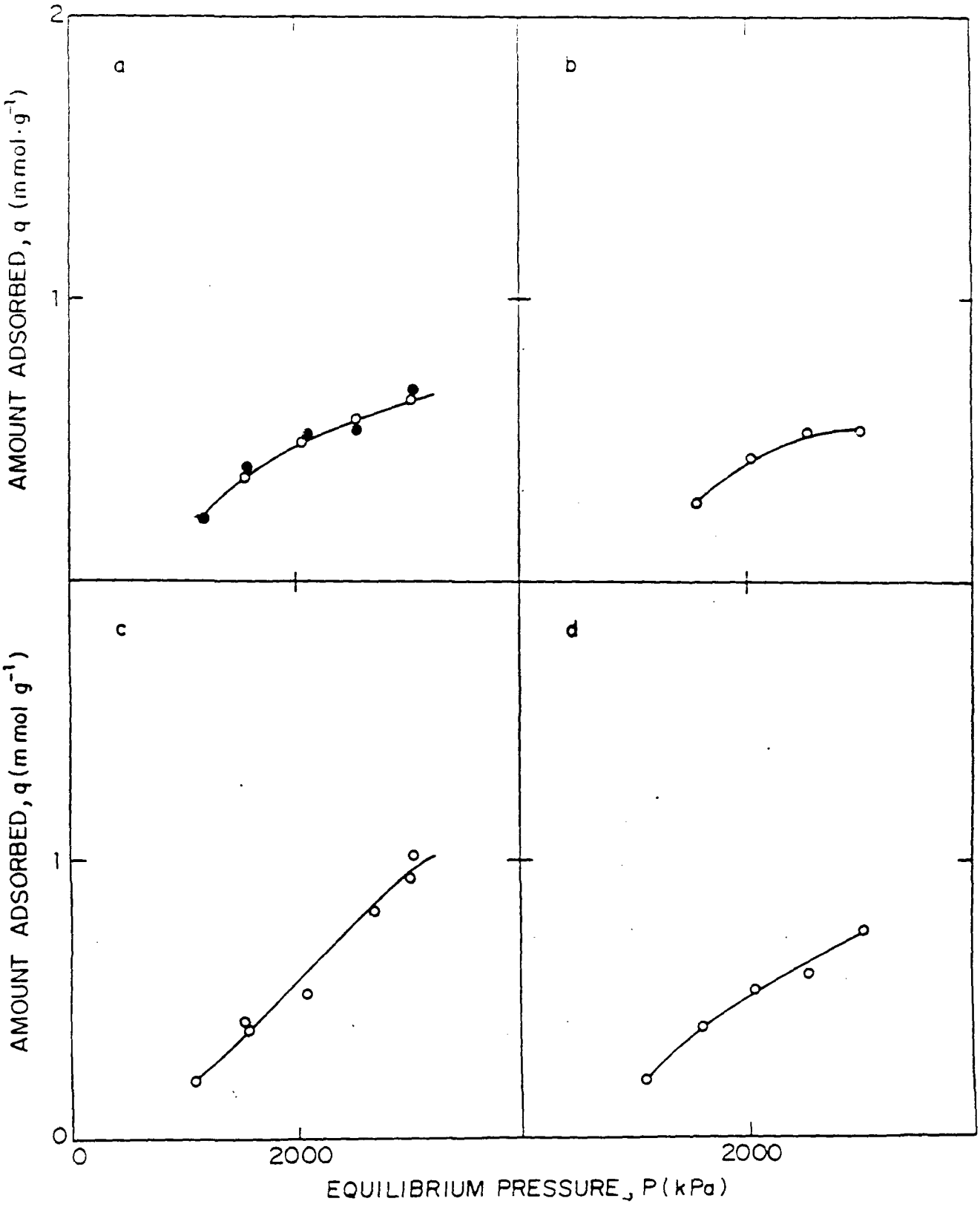

FIG. 4·4: ADSORPTION OF NITROGEN AND OXYGEN ON $AlPO_4$-5 AT MODERATE PRESSURES (a) N_2 309 K (b) N_2 329 K (c) O_2 309 K (d) O_2 329K

(• INDICATES VALUE OBTAINED BY WATER DISPLACEMENT)

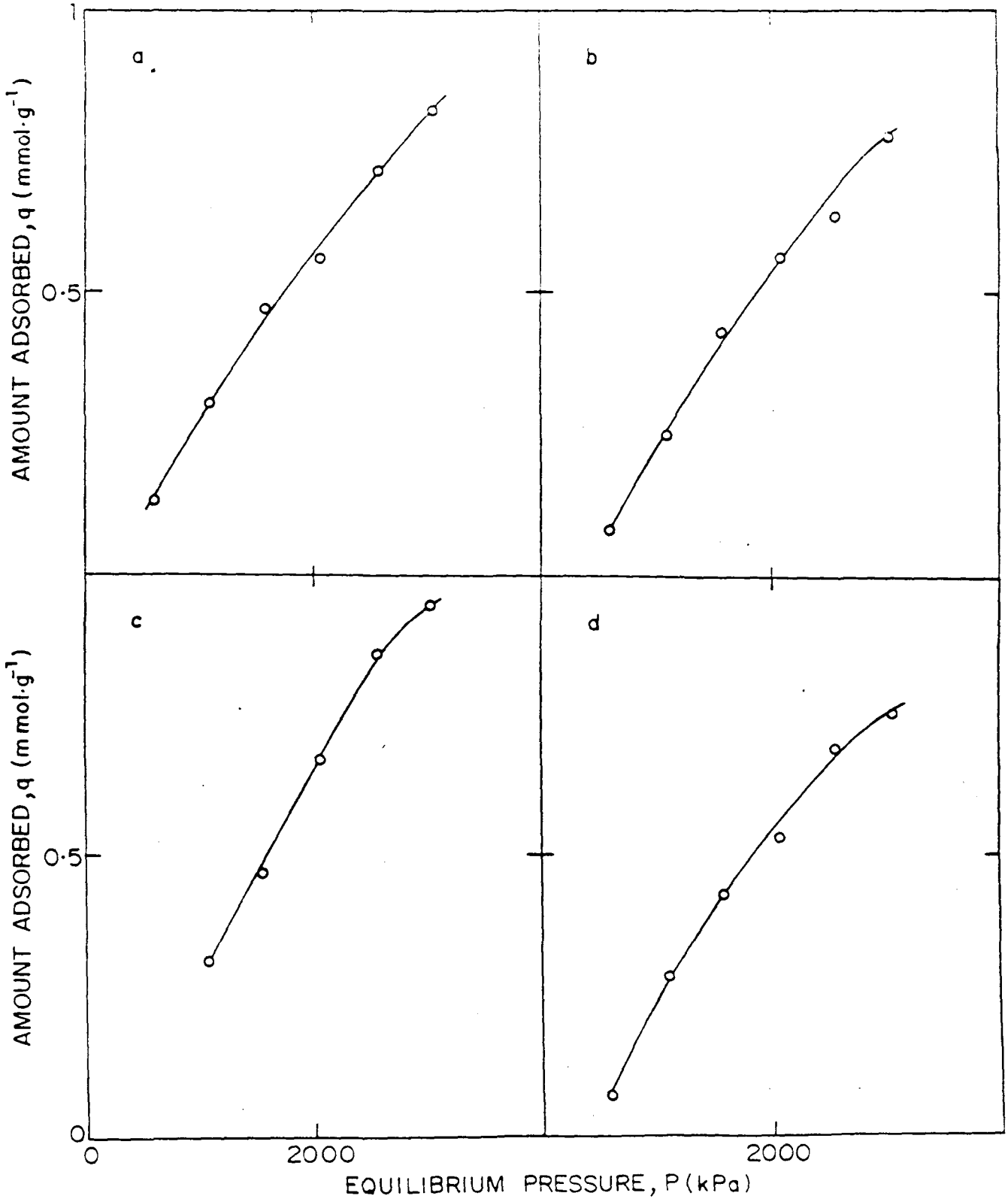

FIG. 4·5 : ADSORPTION OF NITROGEN AND OXYGEN ON SAPO-5 AT MODERATE PRESSURES (a) N_2 309 K (b) N_2 329 K (c) O_2 309 K (d) O_2 329 K

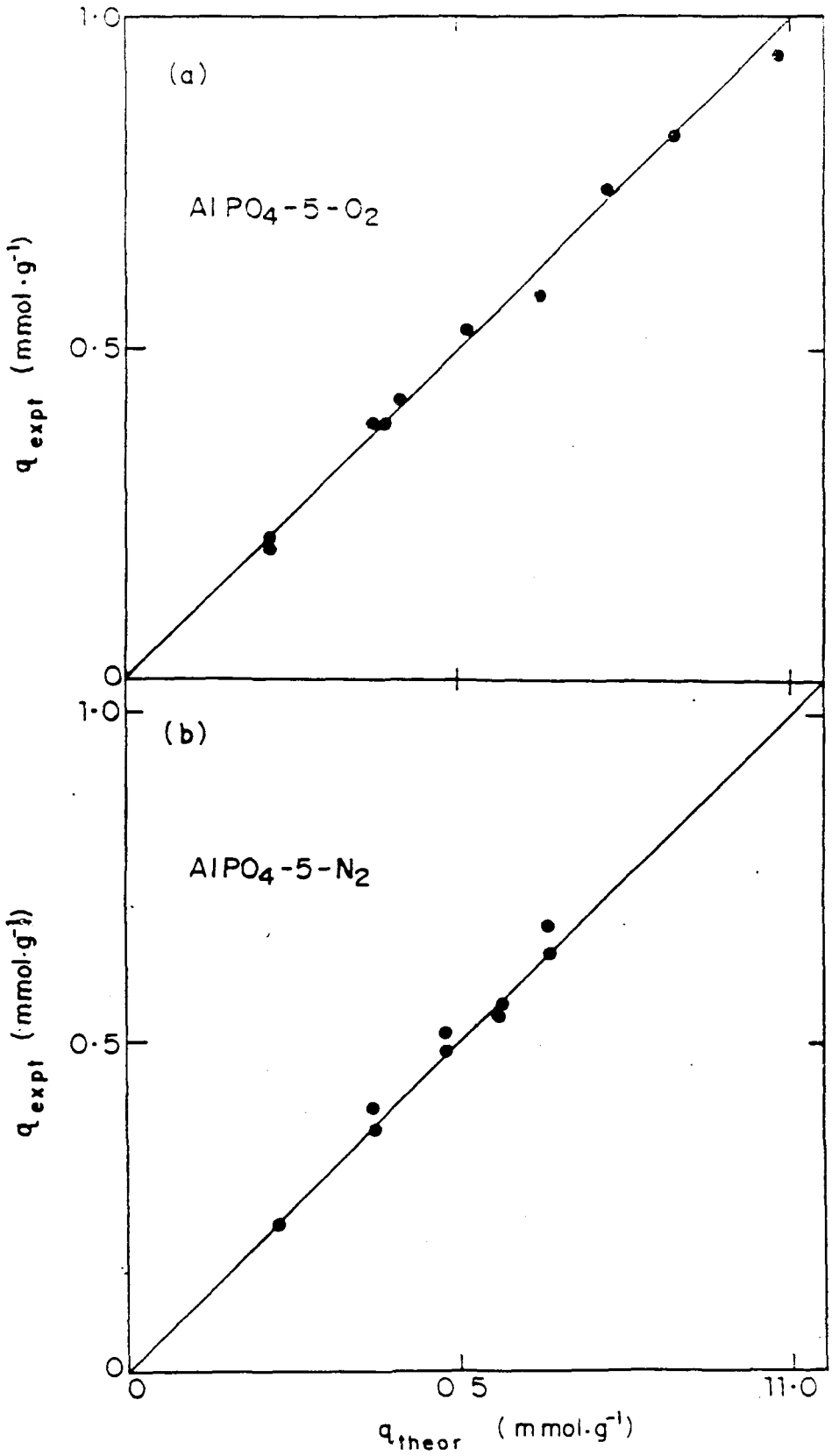

FIG. 4·6 : PLOTS OF q(EXPERIMENTAL) VERSUS q(THEORETICAL) (CALCULATED FROM Sips ISOTHERM MODEL) FOR THE ADSORPTION OF (a) OXYGEN AND (b) NITROGEN ON $AlPO_4$-5 (TEMPERATURE: 309-329 K , PRESSURE: 500–3000 kPa)

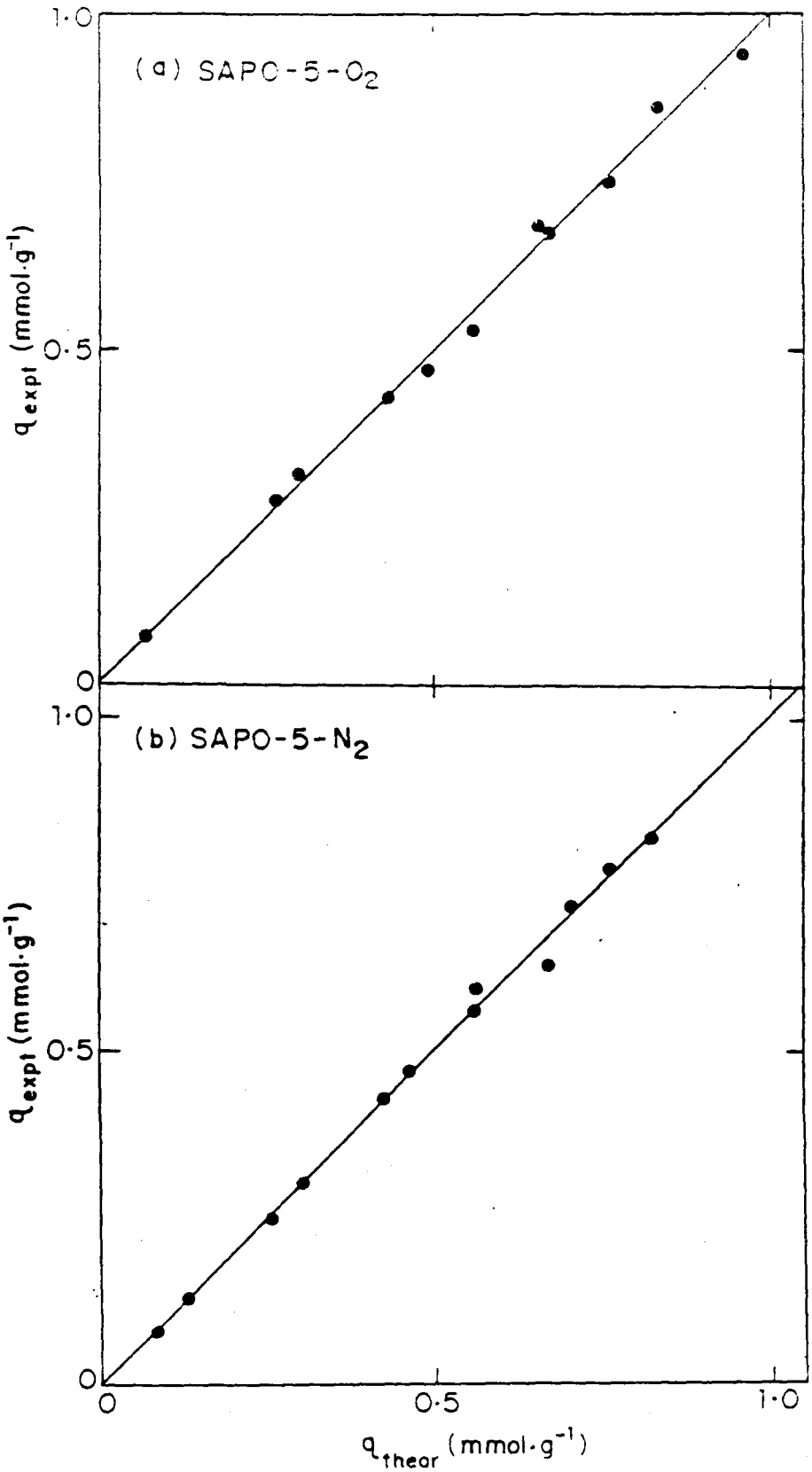

FIG. 4.7: PLOTS OF q (EXPERIMENTAL) VERSUS q (THEORETICAL) (CALCULATED FROM Sips ISOTHERM MODEL) FOR THE ADSORPTION OF (a) OXYGEN AND (b) NITROGEN ON SAPO-5 (TEMPERATURE: 309–329 K, PRESSURE: 500–3000 kPa)

adsorption of nitrogen and oxygen on the SAPO-5 and $AlPO_4$-5 are presented in Table 4.1.

The plots of the ratio of the moles of oxygen adsorbed to the moles of nitrogen adsorbed on SAPO-5 as a function of pressure for the two temperatures are presented in Fig. 4.8(a). At the lower temperature (309 K), more oxygen is adsorbed compared to nitrogen for the entire pressure range of the experiment. There is a small increase in the relative adsorption (q_{O2}/q_{N2}), however, the curve levels off at higher pressures. At the higher temperature (329 K), the relative adsorption shows the reverse trend.

Figure 4.8(b) shows the plots of the ratio of the moles of oxygen adsorbed to that of nitrogen on $AlPO_4$-5 as a function of pressure at 309 and 329 K. At 309 K, there is a continuous increase in the ratio from 1.25 to 1.48 with increasing the pressure from 1500 to 3000 kPa. The trend of the curve shows the potential for further increase in the ratio at higher pressures. This indicates that it may be possible to use $AlPO_4$-5 for the separation of O_2 and N_2 from air at this temperature. At the higher temperature (329 K), the ratio passes through a minimum with increasing the pressure from 1500 to 3000 kPa. The two curves intersect at a pressure of about 2000 kPa.

The comparison of the results in Fig. 4.8(a) with those in Fig. 4.8(b) leads to the conclusion that $AlPO_4$-5 is a better choice for its use in the O_2/N_2 separation from air at higher pressures and lower temperature (309 K).

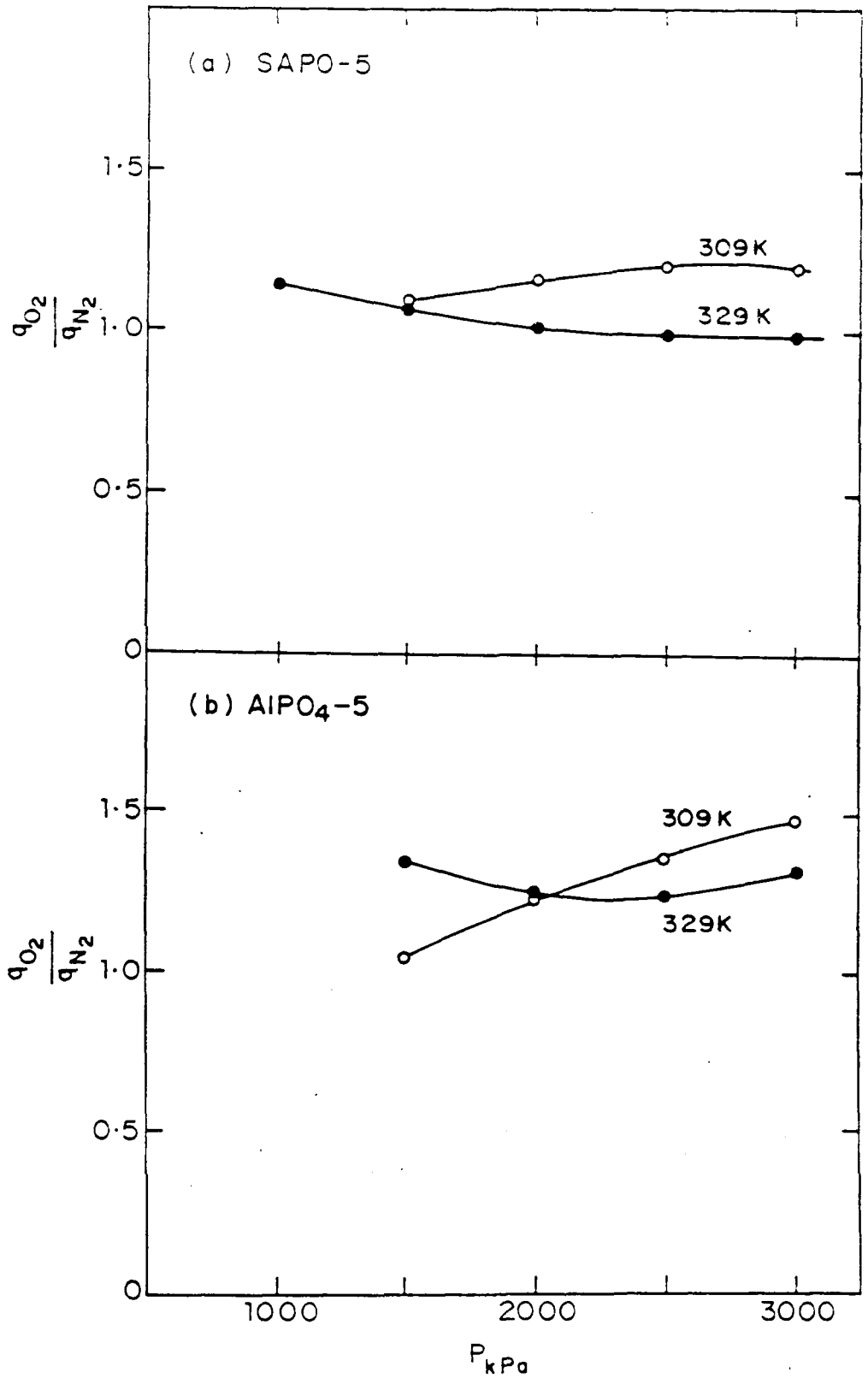

FIG.4·8 : PLOTS OF THE RATIO OF AMOUNT OF OXYGEN ADSORBED TO THE AMOUNT OF NITROGEN ADSORBED VERSUS PRESSURE FOR (a) SAPO-5 AND (b) $AlPO_4$-5

4.4 CONCLUSIONS

Two simple and inexpensive volumetric adsorption/desorption methods have been developed for the collection of adsorption isotherm data for weakly adsorbed gases at moderate pressures. The methods gave results very much comparable to those reported in the literature for the case of adsorption of N_2 and O_2 on NaM zeolite. Adsorption of O_2 and N_2 on $AlPO_4$-5 and SAPO-5 at 309 and 329 K and pressure 500-3000 kPa has been studied using the methods. Sips' equation was found to give a good fit for the adsorption isotherm data for O_2 and N_2 on both the adsorbents. The comparison of the relative adsorption of O_2 and N_2 on the two adsorbents leads to the conclusion that $AlPO_4$-5 is a better choice for its use in the O_2/N_2 separation from air at higher pressures (at 309 K).

NOMENCLATURE

A,B,C	Constants of Dubinin-Astakhov model
h	Height of water column as shown in Fig. 4.1(c)
h_r	Given by Eqn. (4.9)
n_a	Moles of gas in the void space in the adsorber
n_d	Moles of gas in the desorber
n_T	Total number of moles of gas
P_a	Adsorption pressure
P_D	Pressure in the adsorber at the end of desorption in Method-2
P_{d2}	Pressure in the desorber on the completion of desorption in Method-1
P_s	Saturation vapor pressure of the gas
P_{sr}	Reduced vapor pressure
P_w	Vapor pressure of water at the temperature of desorption
$q, q_{a(T,P)}$	Moles of gas adsorbed per unit weight of adsorbent at temperature T and Pressure P
q_m,k,c	Constants of Sips equation
R	Universal gas constant
T_a	Adsorption temperature
T_{bp}	Normal boiling point
T_c, P_c	Critical temperature and pressure
T_d	Temperature of desorber
V_a	Volume of viod space in the adsorber
V_d	Desorber volume measured using water in Method-1
V_D	Volume of water displaced in Method-2
W	Weight of the adsorbent

REFERENCES

1. McBain, J.W. and Britton, G.T., J. Am. Chem. Soc., **52**, 2198 (1930)
2. Morris, H.E. and Maass, O., Can. J. Res., **9**, 240 (1933)
3. Edwards, J.E. and Maass, O., Can. J. Res., **13B**, 133 (1935)
4. Coolidge, A.S. and Forwalt, H.J., J. Am. Chem. Soc., **56**, 561 (1934)
5. Jones, W.M., Isacc, P.J. and Phillips, D., Trans. Faraday Soc., **55**, 1953 (1959)
6. Boehlen, B. and Guyer, A., Helv. Chim. Acta., **47**, 1815 (1964)
7. Hayhurst, D.T. and Lee, J.C., AIChE Symp. Ser., **79**, 230 (1983)
8. Zuech, J.L., Hines, A.L. and Sloan, E.D., Ind. Eng. Chem. Process Des. Dev., **22**, 1, 172 (1983)
9. Gilmer, H.B. and Kobayashi, R., AIChE J., **10**, 797 (1964)
10. Frolich, P.K. and White, A., Ind. Eng. Chem., **22**, 1058 (1930)
11. Ray, G.C. and Box, Jr., E.O., Ind. Eng. Chem., **42**, 7, 1315 (1950)
12. Lewis, W.K., Gilliland, E.R., Chertow, B. and Cadogan, W.P., Ind. Eng. Chem., **42**, 7, 1319 (1950)
13. Lewis, W.K., Gilliland, E.R., Chertow, B. and Cadogan, W.P., Ind. Eng. Chem., **42**, 7, 1326 (1950)
14. Abdul-Rehman, H.B., Hasanain, M.A. and Loughlin, K.F., Ind. Eng. Chem. Res., **29**, 1525 (1990)
15. Loughlin, K.F., Hasanain, M.A. and Abdul-Rehman, H.B., Ind. Eng. Chem. Res., **29**, 1535 (1990)

16. Ozawa, S., Kusumi, S. and Ogino, Y., J. Colloid. Interface Sci., **56**, 1, 83 (1976)

17. Vasilev, B.N., Zh. Fiz. Khim., **31**, 498 (1957)

18. Ross, S. and Olivier, J.P., "On Physical Adsorption", Interscience Publishing Corp., New York, N.Y. (1964)

19. Menon, P.G., Chem. Rev., **68**, 277 (1968)

20. Michels, A., Menon, P.G. and ten Seldam, C.A., Rec. Trav. Chim., **80**, 433 (1961)

21. Menon, P.G., J. Am. Chem. Soc., **87**, 3057 (1965)

22. Stalkup, F.I. and Kobayashi, R., AIChE J., **9**, 121 (1963)

23. Gilmer, H.B. and Kobayashi, R., AIChE J., **11**, 702 (1965)

24. Mason, J.P. and Cooke, Jr., C.E., AIChE J., **12**, 1097 (1966)

25. Eberly, P.E., J. Phys. Chem., **65**, 1261 (1961)

26. Wilson, S.T., Lok, B.M., Messina, C.A., Cannan, T.R. and Flanigen, E.M., J. Am. Chem. Soc., **104**, 1146 (1982)

27. Wilson, S.T., Lok, B.M., Messina, C.A., Cannan, T.R. and Flanigen, E.M., ACS Symp. Ser., **218**, 79 (1983)

28. Bennet, J.M., Cohen, J.P., Flanigen, E.M., Pluth, J.J. and Smith, J.V., ACS Symp. Ser. **218**, 109 (1983)

29. Bond, G.C., Gelstrope, M.R., Sing, K.S.W. and Theocharis, C.R., J. Chem. Soc. Chem. Commun., **15**, 1056 (1985)

30. Choudhary, V.R. and Akolekar, D.B., J. Catal., **103**, 115 (1987)

31. Choudhary, V.R., Akolekar, D.B., Singh, A.P. and Sansare, S.D., J. Catal., **110**, 23 (1988)

32. Lok, B.M., Messina, C.A., Patton, R.L., Gajek, R.T., Cannan, R. and Flanigen, E.M., J. Am. Chem. Soc., **106**, 6092 (1984)

33. Pyke, D.R., Whitney, P. and Houghton, H., Appl. Catal., **18**, 173 (1985)

34. Blackmond, D.G., Swid, K.P., Davis, M.E. and Gallezot, P., J. Catal., **122**, 247 (1990)

35. Thomson, R., Montes, C., Davis, M.E. and Wolf, E.E., J. Catal., **124**, 401 (1990)

36. Hacskaylo, J.J., Le Van, M.D., Langmuir, **1**, 97 (1985)

37. Reid, R.C., Prausnitz, J.M. and Sherwood, T.K., 'The Properties of Gases and Liquids', 3rd Ed., McGraw-Hill Book Company, N.Y. (1977)

38. Sips, R., J. Chem. Phys., **18**, 1024 (1950)

Appendix 4.1

Adsorption isotherm data for nitrogen on NaM, $AlPO_4$-5 and SAPO-5 at moderate pressures

P (kPa)	q (mmol.g^{-1})	P (kPa)	q (mmol.g^{-1})
N_2-NaM (309 K)		N_2-SAPO-5 (309 K)	
585	1.03	585	0.13
1075	1.34	1075	0.30
1124	1.43	1565	0.47
1554	1.57	2054	0.56
1575	1.55	2545	0.71
2052	1.72	3034	0.82
2075	1.77		
2554	1.82		
3054	1.97	N_2-SAPO-5 (329 K)	
N_2-NaM (329 K)		585	0.08
590	0.80	1565	0.43
624	0.86	2054	0.56
1085	1.15	2545	0.63
1556	1.33	3034	0.77
2554	1.66		
N_2-$AlPO_4$-5 (309 K)		N_2-$AlPO_4$-5 (309 K) (water displacement method)	
1565	0.37		
2054	0.49	1075	0.22
2545	0.56	1565	0.40
3034	0.64	2054	0.52
		2545	0.55
N_2-$AlPO_4$-5 (329 K)		3034	0.68
585	0.05		
1565	0.27		
2054	0.43		
2545	0.52		
3034	0.53		

Appendix 4.2

Adsorption isotherm data for oxygen on NaM, $AlPO_4$-5 and SAPO-5 at moderate pressures

P (kPa)	q (mmol.g^{-1})	P (kPa)	q (mmol.g^{-1})
O_2-NaM (309 K)		O_2-$AlPO_4$-5 (329 K)	
600	0.49	1075	0.20
1075	0.88	1565	0.39
1575	1.21	2054	0.53
2055	1.39	2545	0.58
2545	1.48	3034	0.75
3035	1.70		
O_2-NaM (329 K)		O_2-SAPO-5 (309 K)	
605	0.41	1075	0.31
633	0.42	1565	0.47
1075	0.69	2054	0.67
1565	0.97	2545	0.86
2055	1.19	3034	0.94
2545	1.40		
3020	1.46		
		O_2-SAPO-5 (329 K)	
O_2-$AlPO_4$-5 (309 K)		585	0.07
1075	0.21	1100	0.28
1530	0.39	1565	0.43
1565	0.42	2054	0.53
2692	0.82	2545	0.69
3210	0.94	3232	0.75
3232	1.02		

CHAPTER - 5

INTRAPARTICLE MASS TRANSFER OF OXYGEN, CARBON DIOXIDE, METHANE AND ETHYLENE IN MACROPOROUS LOW SURFACE AREA INERT SPHERICAL SUPPORT

5. INTRAPARTICLE MASS TRANSFER OF OXYGEN, CARBON DIOXIDE, METHANE AND ETHYLENE IN MACROPOROUS LOW SURFACE AREA INERT SPHERICAL SUPPORT

5.1 INTRODUCTION

Effective diffusion coefficients are usually used for characterization of diffusional mass transport inside porous catalysts and adsorbents. The knowledge of effective intraparticle diffusivities of reactants and products in porous catalysts is essential for predicting the effects of intraparticle mass transfer on the reaction rate, and also in the design of catalytic reactors. A knowledge of mass transfer rates at ambient conditions is seldom required, and it is desirable to measure the effective diffusivity under actual reaction conditions or atleast at temperatures at which the catalytic process occurs.

Low surface area macroporous inert supports, such as sintered porous alumina and silicon carbide, are commonly used as catalyst supports for a number of hydrocarbon oxidation catalysts. Earlier studies [1-3] have indicated that sintering of porous solids causes a drastic increase in their tortuosity factors. The value of tortuosity factor as high as 79 ± 28 for a support made of refractory oxides [1] and even above 100 for highly sintered nickel oxide pellets [2] have been observed. It is therefore of great interest to determine effective diffusivity and tortuosity factors for different species diffusing in highly sintered macroporous silicon carbide pellets.

During the past twenty five years, gas chromatographic

techniques have been developed into very useful experimental tools for measuring transport properties of solid catalysts and adsorbents [4-6]. Apart from the simplicity and rapidity with which the required data are obtained, the attractive feature of the gc technique is that most of the measurements can be made on a large and representative sample of the porous solid under its operating conditions. The requisite data on pelleted commercial catalysts and/or supports can very well be obtained using the gc techniques, with Single Pellet String Column (SPSC) packed with spherical [7,8] or cylindrical [9] pellets.

The present investigation was undertaken with the objective of measuring the effective diffusivity and tortuosity factors of commercial spherical macroporous silicon carbide pellets for the diffusion of ethylene, oxygen, carbon dioxide and methane at 423-573K. These species are involved in the process of ethylene oxidation to ethylene oxide. The effective diffusivity was determined by the gc pulse technique using SPSC [7,8] and by analyzing the chromatographic peaks by moment analysis [5,6].

5.2 THEORY

5.2.1 Kubin-Kucera Model

The theory, on which the extraction of transport parameters is based, is often referred to as the Kubin-Kucera model after the authors of the original papers [10,11]. In this model the moments of the chromatographic peak leaving the bed are related to the parameters describing the mass transfer processes i.e. the axial dispersion coefficient E_A, external

mass transfer coefficient k_A, intraparticle diffusivity D_e, adsorption rate constant k_{ads} and the adsorption equilibrium constant K_A. The first absolute and the second central moments are given by the following expressions.

$$\mu_1' = L\,(1 + \delta_0)\,/\,v + t_{oA}\,/\,2 \qquad (5.1)$$

$$\mu_2 = (2L\,/\,v)\,[\,\delta_1 + (E_A\,/\alpha)\,(1 + \delta_0)^2\,/\,v^2\,] + t_{oA}^2\,/\,12 \qquad (5.2)$$

where $$\delta_0 = [(1 - \alpha)\,\beta\,/\alpha\,]\,(1 + \rho_p K_A\,/\beta) \qquad (5.3)$$

and $$\delta_1 = \delta_a + \delta_i + \delta_e \qquad (5.4)$$

with $$\delta_a = [(1 - \alpha)\,\beta\,/\alpha]\,\rho_p K_A^2\,/\,k_{ads}\,\beta \qquad (5.5)$$

$$\delta_i = [(1 - \alpha)\,\beta/\alpha]\,[r^2\beta\,/\,\gamma\,(\gamma + 2)]\,(1 + \rho_p K_A\,/\beta)^2 \times 1/\,D_e \qquad (5.6)$$

$$\delta_e = [(1 - \alpha)\,\beta/\alpha]\,[r^2\beta/\,\gamma\,(\gamma + 2)]\,(1 + \rho_p K_A\,/\beta)^2\,(\,5\,/\,k_A r\,) \qquad (5.7)$$

$$v = (F\,/\alpha A\,)(T_c\,/\,T_R) \qquad (5.7a)$$

Initially the model was applied to describe the dispersion of an adsorbable tracer gas pulse in a packed bed of porous adsorbent through which inert gas was flowing. Later it has been shown that the model can also be applied to describe the dispersion of a non-adsorbable tracer gas pulse in a packed bed of porous adsorbent through which inert gas is flowing [12,13].

5.2.2 Diffusion of Non-Adsorbates

For an inert porous solid or a non-adsorbing sample, $K_A = 0$ and hence the equations become

$$\delta_c = (1 - \alpha)\beta / \alpha \qquad (5.3')$$

$$\delta_a = 0 \qquad (5.5')$$

$$\delta_i = [(1 - \alpha)\beta / \alpha][r^2 \beta / \gamma(\gamma + 2)] / D_e \qquad (5.6')$$

$$\delta_e = [(1 - \alpha)\beta / \alpha][r^2 \beta / \gamma(\gamma + 2)](5 / k_A r) \qquad (5.7')$$

At low flow rates reported here, the Nusselt number for external mass transfer (fluid-to-particle) is given by

$$N_{Nu} = 2 = k_A 2r / D_{AB} \qquad (5.8)$$

where D_{AB} is the molecular diffusivity. With this relationship, Equation (5.7') reduces to

$$\delta_e = [(1 - \alpha)\beta / \alpha][r^2 \beta / \gamma(\gamma + 2)](5 / D_{AB}) \qquad (5.9)$$

At higher flow rates, when Equation (5.8) is not valid, the error introduced by replacing Equation (5.7') with Equation (5.9) is usually low, because the contribution of external mass transfer resistance to the overall process is small [14].

The n^{th} absolute (μ'_n) and central (μ_n) moments of the chromatographic curve are defined by the following equations.

$$\mu'_n = m_n / m_0 \qquad (n = 0,1,2,\ldots) \qquad (5.10)$$

$$m_n = \int_0^\infty t^n c(z,t)\, dt \qquad (n = 0,1,2,\ldots) \qquad (5.11)$$

$$\mu_n = (1 / m_0) \int_0^\infty (t - \mu'_1)^n c(z,t)\, dt \qquad (n = 0,1,2,\ldots) \qquad (5.12)$$

$$\bar{\mu}_1 = \mu'_1 - t_{oA} / 2 \qquad (5.13)$$

$$\bar{\mu}_2 = \mu_2 - t_{oA} / 12 \qquad (5.14)$$

From Equation (5.1), it can be seen that a plot of $\bar{\mu}_1$ versus L / v should be linear with slope ($1 + \delta_0$). E_A and δ_1 can be obtained from the slope and intercept, respectively, of the plot of $\bar{\mu}_1 / (2L/v)$ versus $1/v^2$. The effective diffusivity D_e can be obtained from δ_1.

5.2.3 Tortuosity Factor

In diffusion through porous media, the effective diffusivity D_e is smaller than the diffusivity in a straight cylindrical pore. This is the result of two effects; the random orientation of the pores which gives a longer diffusion path and a reduced concentration gradient in the direction of flow, and the variation in the pore diameter. Both these effects are commonly accounted for by the tortuosity factor.

$$D_e = D\beta/\tau \qquad (5.15)$$

where D_e is the effective diffusivity as evaluated from the experimental data and D is the diffusivity under the same conditions in a straight cylindrical pore [15]. D can be either molecular diffusivity D_{AB} or Knudsen diffusivity D_K. When the mean free path of the diffusing molecule is greater than the pore diameter, the pore mass transfer is controlled by Knudsen diffusion. The molecular diffusion predominates when the pore diameter is larger than the mean free path.

5.3 EXPERIMENTAL

5.3.1 Materials and Gases

Silicon carbide	:	SC 5232, spherical pellets (dia: 0.5 cm) obtained from Norton, U.S.A.
Methane	:	High purity (> 99.9 %), obtained from Matheson, U.S.A.
Ethylene	:	High purity (> 99.5 %), obtained from AIRCO Industrial Gases, U.S.A.
Oxygen and Nitrogen	:	IOLAR grade II obtained from Indian Oxygen Ltd., Bombay.
Carbon dioxide and Helium	:	Obtained from Indian Oxygen Ltd., Bombay.
Gas chromatograph	:	AIMIL - NCL dual column GC with TCD detector.

5.3.2 Pore Size Distribution in SiC Pellets

The pore size distribution of the macroporous silicon carbide in the low pressure range has been measured by a low pressure all glass mercury porosimeter developed in our laboratory. The details of the experiment and the setup are described elsewhere [17]. The pore size distribution data in the higher pressure range (34-33,000 psia) has been determined using an Autoscan-33 porosimeter (Quantachrome Corp., U.S.A.) and is given in Appendix 5.1a.

5.3.3 Single Pellet String Column (SPSC)

A single pellet string column (SPSC) was prepared by packing spherical silicon carbide pellets (dia: 0.49 cm) one

after another in a single file in a stainless steel tube (i.d.: 0.53 cm, o.d.: 0.62 cm, length: 100 cm). The tube/pellet diameter ratio of the SPSC was 1.1. Scott et al. [8] have shown that the flow behavior in such columns is very similar to that of a conventional packed bed when the number of pellets is 50 or more. The properties of the SPSC are given in Table 5.1.

5.3.4 Experimental Setup

The schematic diagram of the experimental setup used for the diffusion studies is given in Fig. 5.1. The data were obtained using an AIMIL-NCL dual column gas chromatograph with a thermal conductivity detector. The gc columns were replaced with the SPSC and an empty column. For measuring the diffusion of methane, ethylene and carbon dioxide in the SiC pellets, nitrogen (99.99 % pure) passed over activated molecular sieves was used as the carrier gas. Helium (99.99 % pure) passed over activated molecular sieves was used as the carrier gas for carrying out measurements with oxygen. The gases were injected into the SPSC using a gas sampling valve of volume 0.31 cm^3 at room temperature and atmospheric pressure. The chromatograms were recorded using an Omniscribe single pen chart recorder. All the measurements were carried out at atmospheric pressure. The pressure drop across the column was negligible.

Before carrying out the experiments, the column was conditioned by passing the carrier gas (30 $cm^3.min^{-1}$) at 623 K for 1 h to desorb the adsorbed water, if any. The GC was then cooled down to the desired experimental temperature.

Table 5.1

Pellet and column properties

Pellet properties

Pellet shape	:	Spherical
Pellet diameter (d_p)	:	0.49 cm.
Pellet density	:	1.96 $g.cm^{-3}$.
Pellet pore volume	:	0.25 $cm^3.g^{-1}$.
Pellet porosity (β)	:	0.49

Pellet pore size distribution :

Pore dia. (μm)	Pore volume ($cm^3.g^{-1}$)
0.0072 - 0.012	0.016
12 - 370	0.24
> 370	0.084

Column properties

Length of packed column	:	100 cm.
Column internal diameter	:	0.53 cm.
No. of pellets in the column	:	226
Column void fraction (α)	:	0.36
d_c / d_p	:	1.1

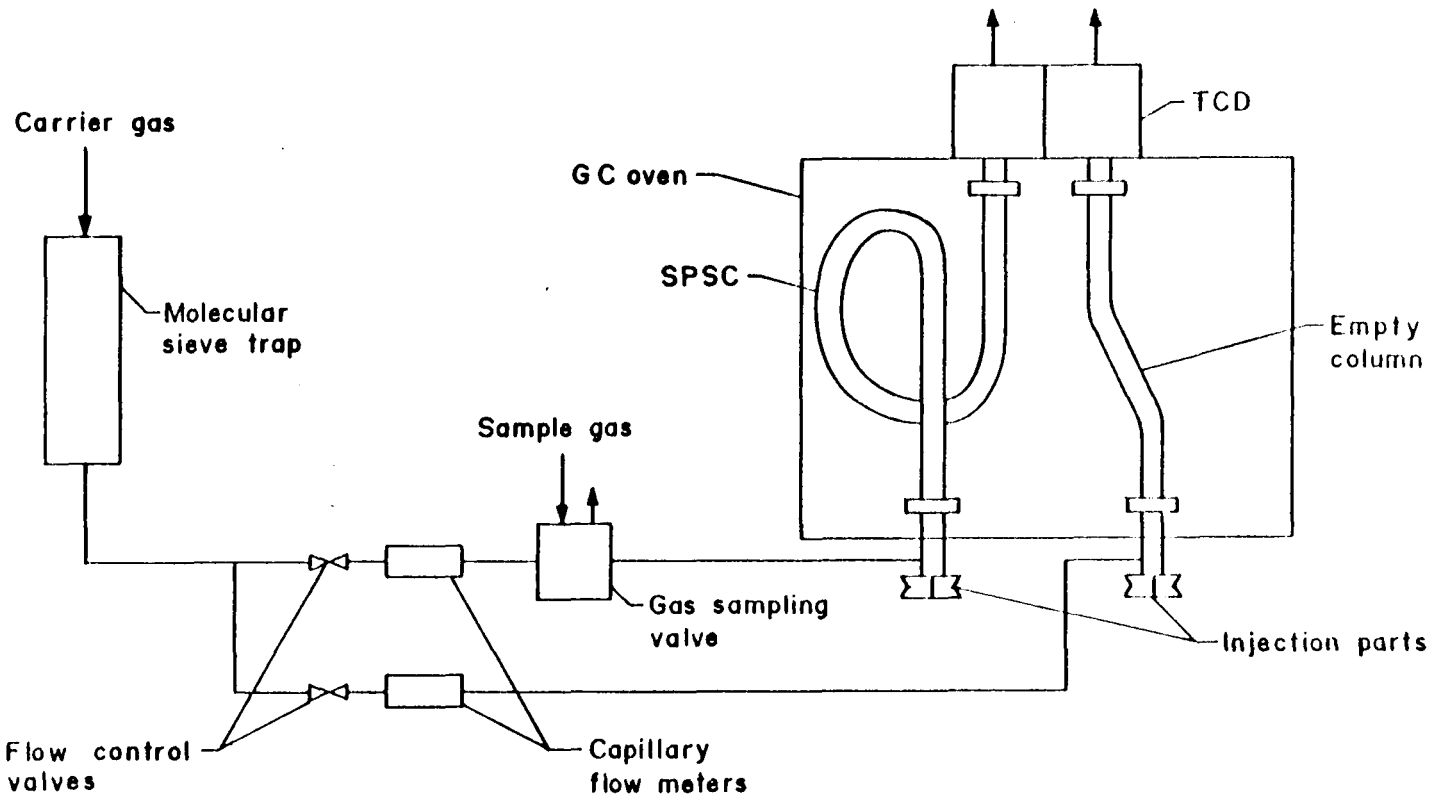

FIG. 5·1: EXPERIMENTAL SET UP FOR MEASURING EFFECTIVE DIFFUSIVITY BY MOMENT ANALYSIS

5.3.5 Determination of the Presence of Reversible and/or Irreversible Adsorption

All the gases were tested for the presence of reversible and irreversible adsorption by gc pulse technique [18].

A known quantity of the sample gas was injected into the SPSC and its retention time for the carrier gas flow rate of 30 $cm^3.min^{-1}$ at 423 and 573 K was noted. The same quantity of an inert gas (helium in case of methane, ethylene and carbon dioxide, and nitrogen in case of oxygen) was injected into the SPSC at exactly similar conditions and its retention time was also noted. The retention time of the gases were found to be identical to that of the respective inert gases. This indicates that the sample gases (viz., C_2H_4, CH_4, CO_2 and O_2) are not adsorbed on the porous solid under study.

The absence of irreversible adsorption of C_2H_4, CH_4, CO_2 and O_2 on the silicon carbide pellets was confirmed by injecting two pulses of each of these gases one after another, into the SPSC packed with fresh silicon carbide pellets (pretreated in the flow of inert carrier gas at 623 K for 1 h) at 423 and 573 K and comparing the area of the two peaks. In all cases, the area of the second peak was exactly the same as that of the first indicating that there is no irreversible adsorption of these gases on the silicon carbide pellet. This was further confirmed by comparing the peak area of sample pulse injected in the column with and without the silicon carbide pellets, under identical experimental conditions.

5.3.6 Measurement of Effective Diffusivity

From Equations (5.1) and (5.2), it can be seen that by making measurements over a range of velocities, it is possible to separate the dispersion and mass transfer effects. The gc pulse data were obtained by injecting 0.31 cm^3 of the gas sample with the help of a gas sampling valve and recording the chromatographic peaks as a function of carrier gas velocity at different temperatures. The carrier gas velocity was varied from 20-40 $cm^3.min^{-1}$ (measured at room temperature) and the temperature from 423-573 K.

The first absolute and the second central moments of the chromatograms were calculated using Equations (5.10) - (5.12). The integrals in the equations were evaluated numerically by the Simpson's rule on a SN-23 computer.

5.3.7 Estimation of Mean Free Path of the Diffusing Molecule

The mean free path of the diffusing molecule has been estimated using the relation [19].

$$\lambda = 1 / (\sqrt{2}\pi\sigma^2 N^*) \qquad (5.16)$$

σ is the collision diameter and

$$N^* = NP/RT \qquad (5.17)$$

where N is the Avagadro's number, 6.023×10^{23} molecules.$mol.^{-1}$; R the universal gas constant, 82.1 $cm.^3atm.mol.^{-1}K^{-1}$; T, temperature and P, pressure in atmospheres. The value of σ has been taken from Bird et al. [20]. The mean free path of all the

diffusing molecules lies between 0.07 and 0.15 μm for the temperature range of the experiments (Appendix 5.1b).

5.3.8 Estimation of Molecular Diffusivity

The molecular diffusivity of the diffusing species has been estimated using the Chapman-Enskog formula [20].

$$D_{AB} = 0.0018583 \sqrt{T^3(1 / M_A + 1 / M_B)} / P\sigma_{AB}^2 \Omega_{D,AB} \quad (5.18)$$

D_{AB} is the molecular diffusivity in $cm.^2 s^{-1}$, the suffix A represents the sample gas and B, the carrier gas. T is the temperature in Kelvin, M_A, M_B are the molecular weights of A and B respectively, P the pressure in atmospheres and $\Omega_{D,AB}$ is a function of $\kappa T / \epsilon_{AB}$.

$$\epsilon_{AB} = \sqrt{\epsilon_A \epsilon_B} \quad (5.19)$$

$$\sigma_{AB} = (\sigma_A + \sigma_B) / 2 \quad (5.20)$$

The values of the Lennard-Jones parameters σ, ϵ and the value of $\Omega_{D,AB}$ have been taken from Appendix B of Bird et al.[19]. The values of D_{AB} for the diffusing species are given in Table 5.2.

5.4 RESULTS AND DISCUSSION

5.4.1 Pore Size Distribution in Silicon Carbide Pellets

The results of the low pressure mercury porosimetry are given in Figs. 5.2 and 5.3. The pore size distribution data are included in Table 5.1. The hysterisis shown by the mercury penetration curve in Fig. 5.2 and the retention of appreciable

Table 5.2

Data on diffusion of methane, ethylene, carbon dioxide and oxygen in silicon carbide pellets

System	Temperature (K)	$E_{A_2} \times 10$ ($cm^2.s^{-1}$)	$D_{AB_2} \times 10$ ($cm^2.s^{-1}$)	$D_e \times 10^2$ ($cm^2.s^{-1}$)	τ
$CH_4(N_2)$*	423	2.3	4.03	1.40	14.1
	473	2.5	4.87	1.40	16.9
	508	3.1	5.49	1.60	17.0
	538	3.4	6.09	1.90	15.7
	573	3.5	6.74	1.95	16.9
					(Av. 16.1)
$C_2H_4(N_2)$	423	2.3	2.94	1.10	13.2
	473	4.0	3.58	1.37	12.8
	508	4.4	4.02	1.40	14.1
	538	3.5	4.48	1.70	12.8
	573	5.5	4.98	1.80	13.8
					(Av. 13.3)
$CO_2(N_2)$	423	0.25	2.85	0.80	16.9
	473	0.21	3.46	0.91	18.7
	508	0.31	3.90	1.03	18.6
	538	0.29	4.35	1.15	18.5
	573	0.45	4.82	1.54	15.3
					(Av. 17.6)
O_2(He)	423	4.5	13.1	1.98	32.5
	473	5.1	15.8	2.38	32.6
	508	7.7	17.7	2.46	35.2
	538	8.5	19.6	2.64	36.3
	573	12.6	21.8	3.30	32.3
					(Av. 33.8)

* The carrier gas used is given in the bracket.

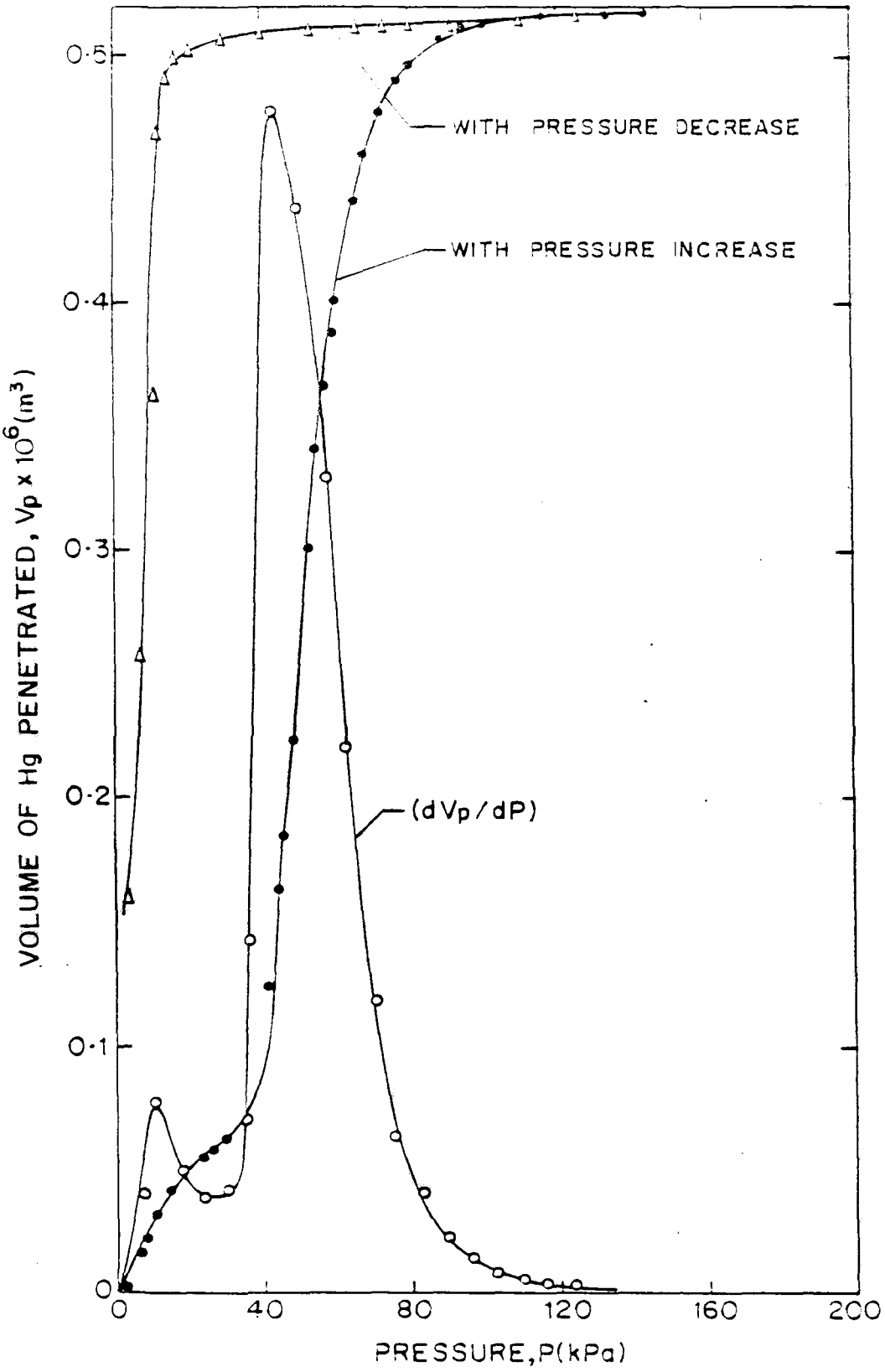

FIG.5·2: PRESSURE DEPENDENCE OF MERCURY PENETRATION IN PORES OF THE SILICON CARBIDE PELLETS (WEIGHT OF PELLETS: $2{\cdot}37 \times 10^{-3}$ kg)

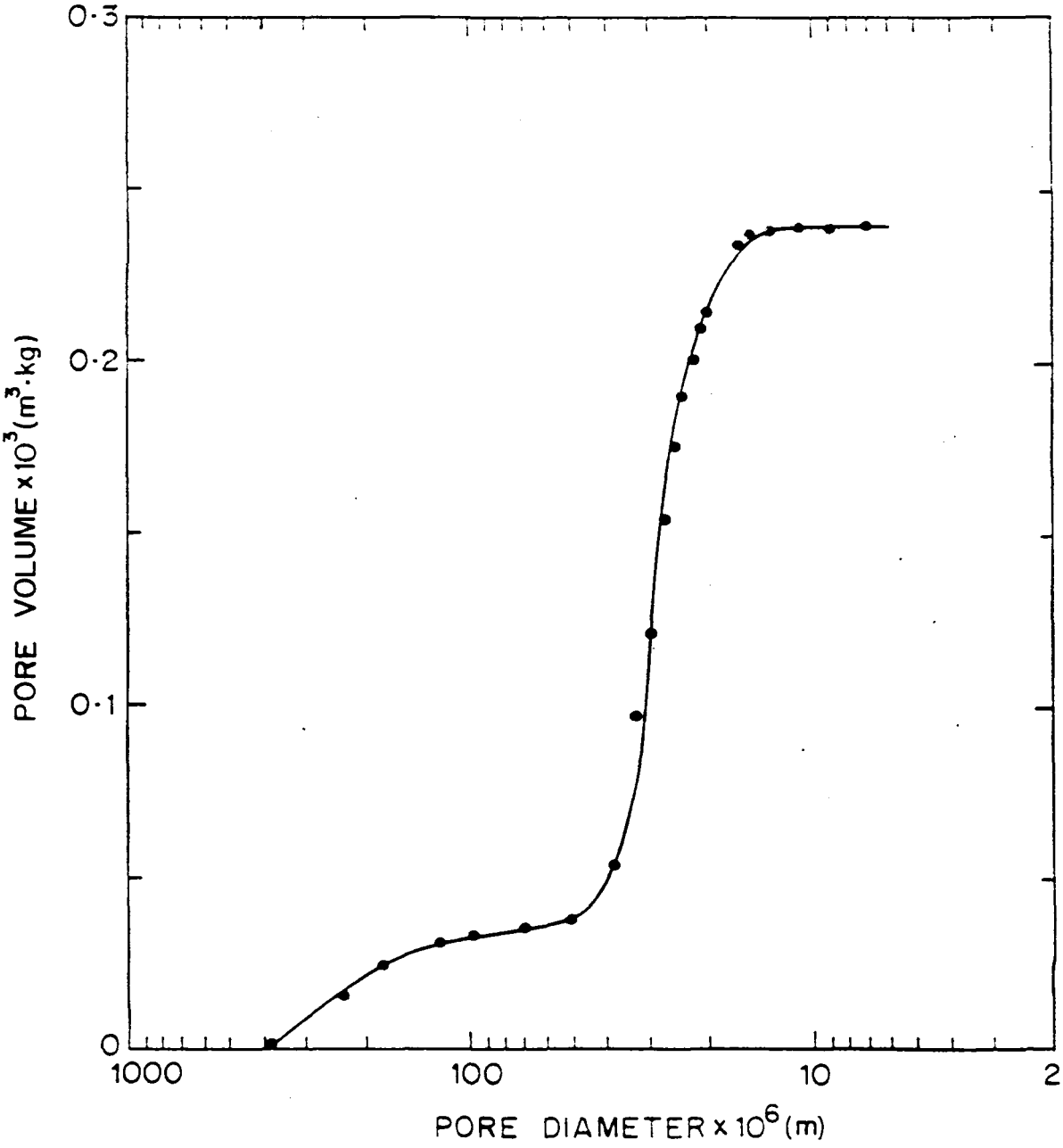

FIG.5·3:PORE SIZE DISTRIBUTION OF THE MACROPOROUS SILICON CARBIDE

amount of mercury in the pores at near zero pressure indicate the presence of dead end pores in the silicon carbide pellets. The results reveal that, in silicon carbide pellets, most of the pore volume has been occupied by the pores of diameter 12-370 μm. The high pressure porosimetry data (Appendix 5.1a) shows the presence of small diameter pores (<0.012 μm) that occupy about 0.016 $cm^3.g^{-1}$ pore volume of the silicon carbide.

5.4.2 Mass Transfer Parameters

The gc pulse data for the diffusion of methane, ethylene, carbon dioxide and oxygen on the silicon carbide pellets are presented in Appendix 5.2.

A representative plot of μ_1' versus L/v for ethylene in the temperature range of the experiment is given in Fig. 5.4. The data for all temperatures fall on a straight line with a slope of 1.9 (δ_0 = 0.9), passing through the origin. The data for methane, carbon dioxide and oxygen in the temperature range of the experiment also fall on the same straight line. This can be possible only when the value of the adsorption equilibrium constant K_A in Equation 5.3 is zero i.e. when none of the diffusing species is adsorbed on the silicon carbide pellets.

The $\bar{\mu}_2/(2L/v)$ versus $1/v^2$ plots for methane, ethylene, carbon dioxide and oxygen on the silicon carbide support at different temperatures are presented in Figs. 5.5-5.8. The axial dispersion coefficient and the effective diffusivity are calculated from the slope and the intercept of these plots. The values of the slope and the intercept for the diffusing species

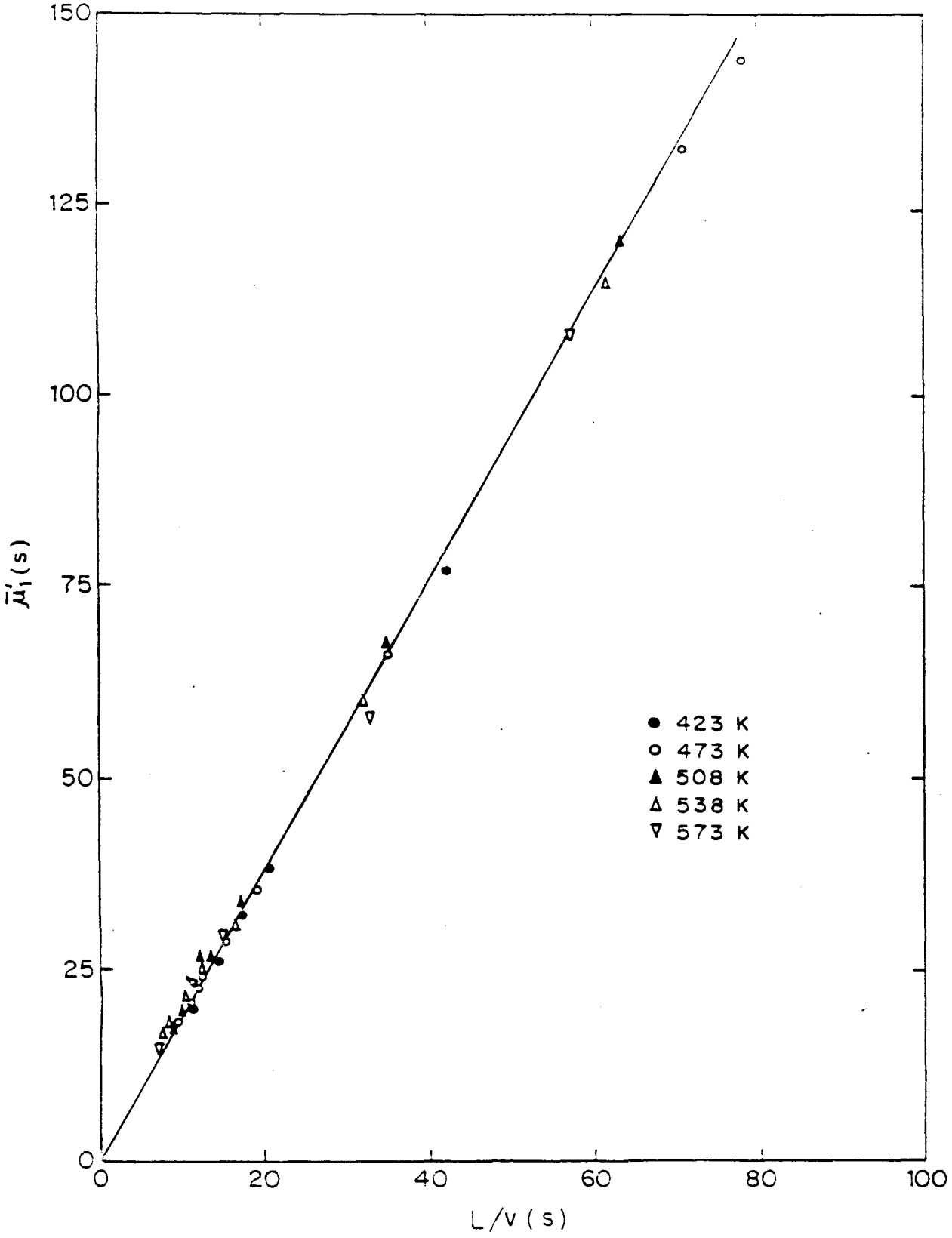

3.5-4: $\overline{\mu_1'}$ vs L/v PLOTS FOR ETHYLENE ON THE MACROPOROUS SILICON CARBIDE AT DIFFERENT TEMPERATURES

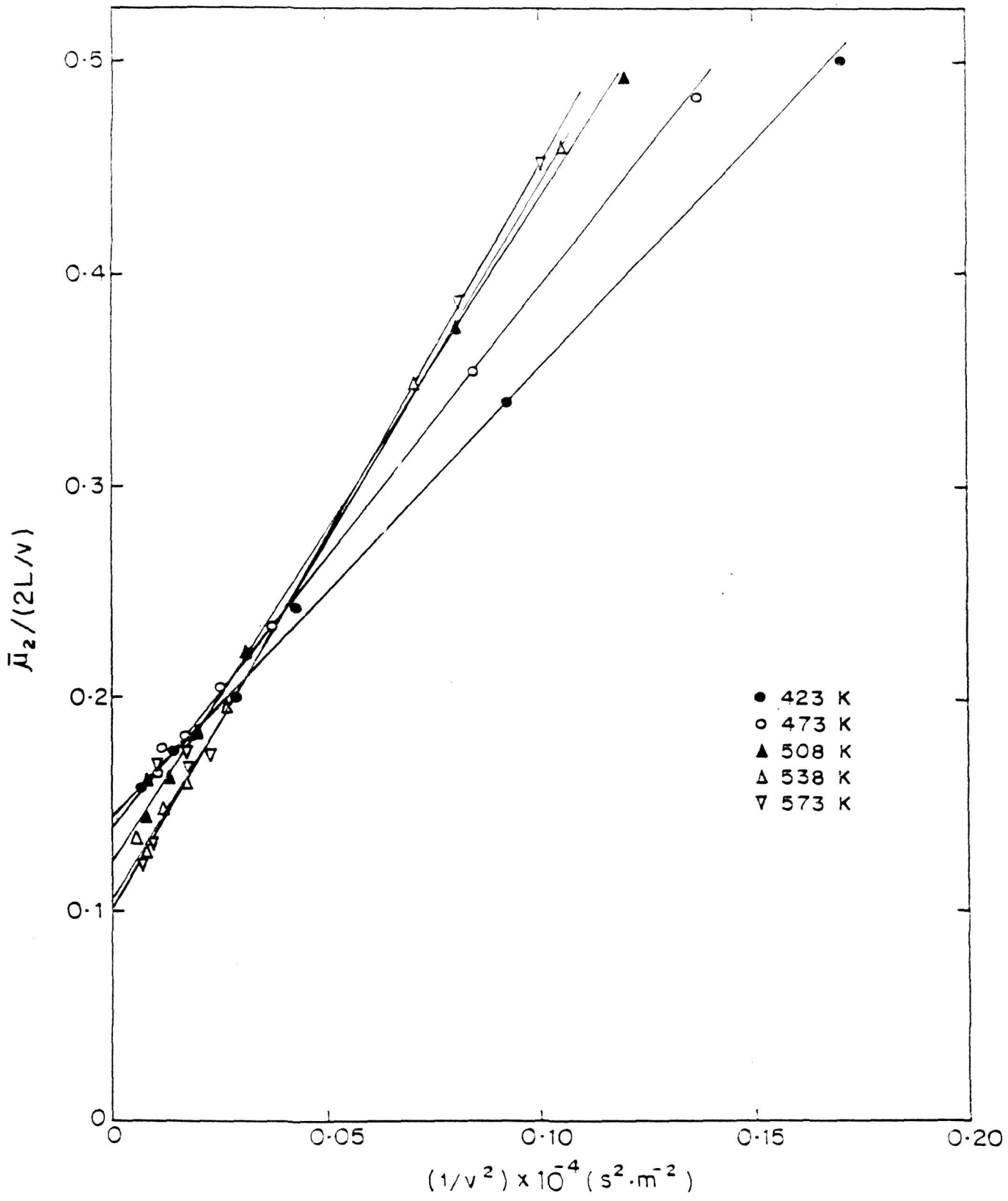

FIG.5·5. $\bar{\mu}_2/(2L/v)$ vs $1/v^2$ PLOTS FOR METHANE ON THE MACROPOROU SILICON CARBIDE AT DIFFERENT TEMPERATURES

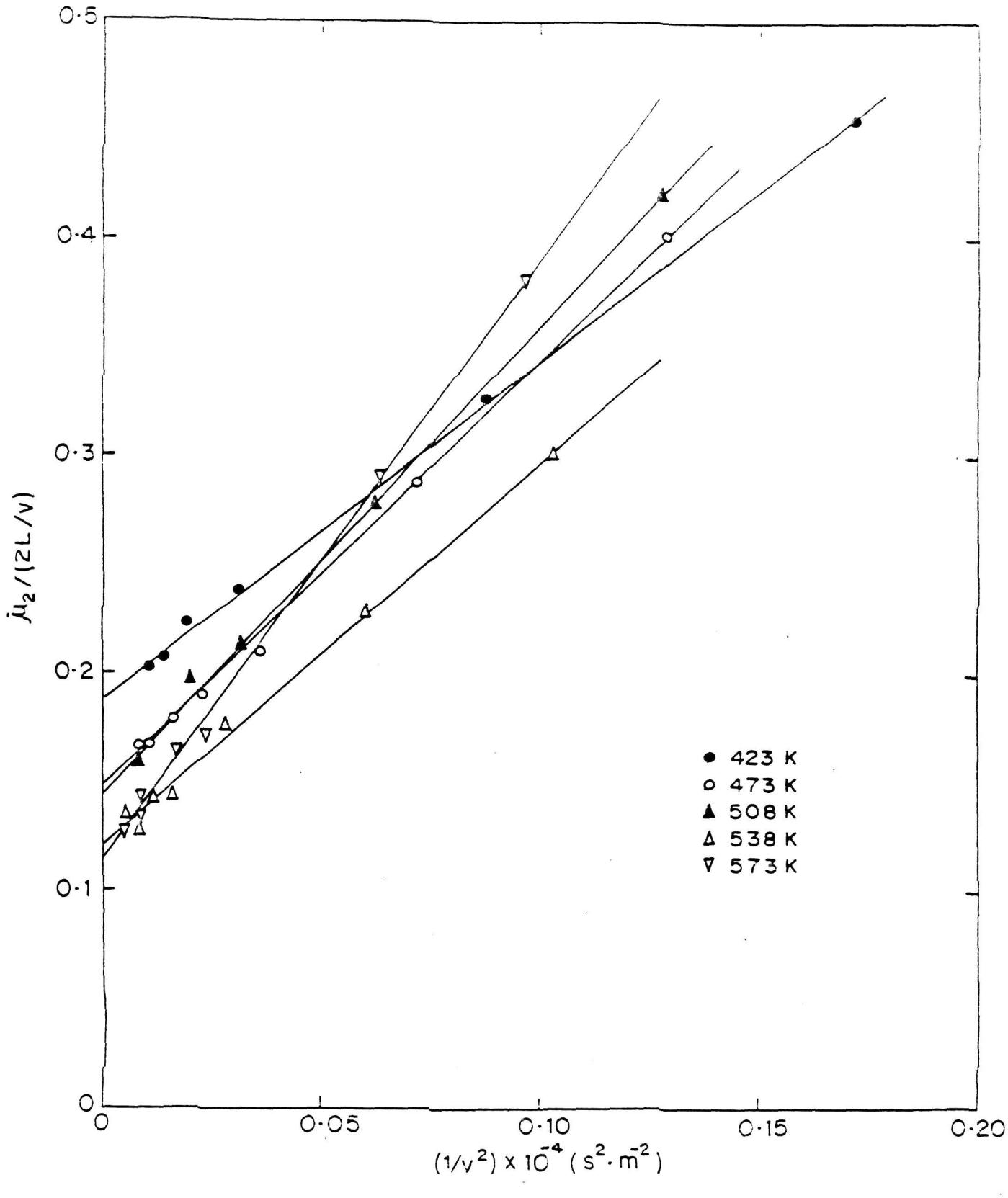

5·6: $\bar{\mu}_2/(2L/v)$ vs $1/v^2$ PLOTS FOR ETHYLENE ON THE MACROPOROUS SILICON CARBIDE AT DIFFERENT TEMPERATURES

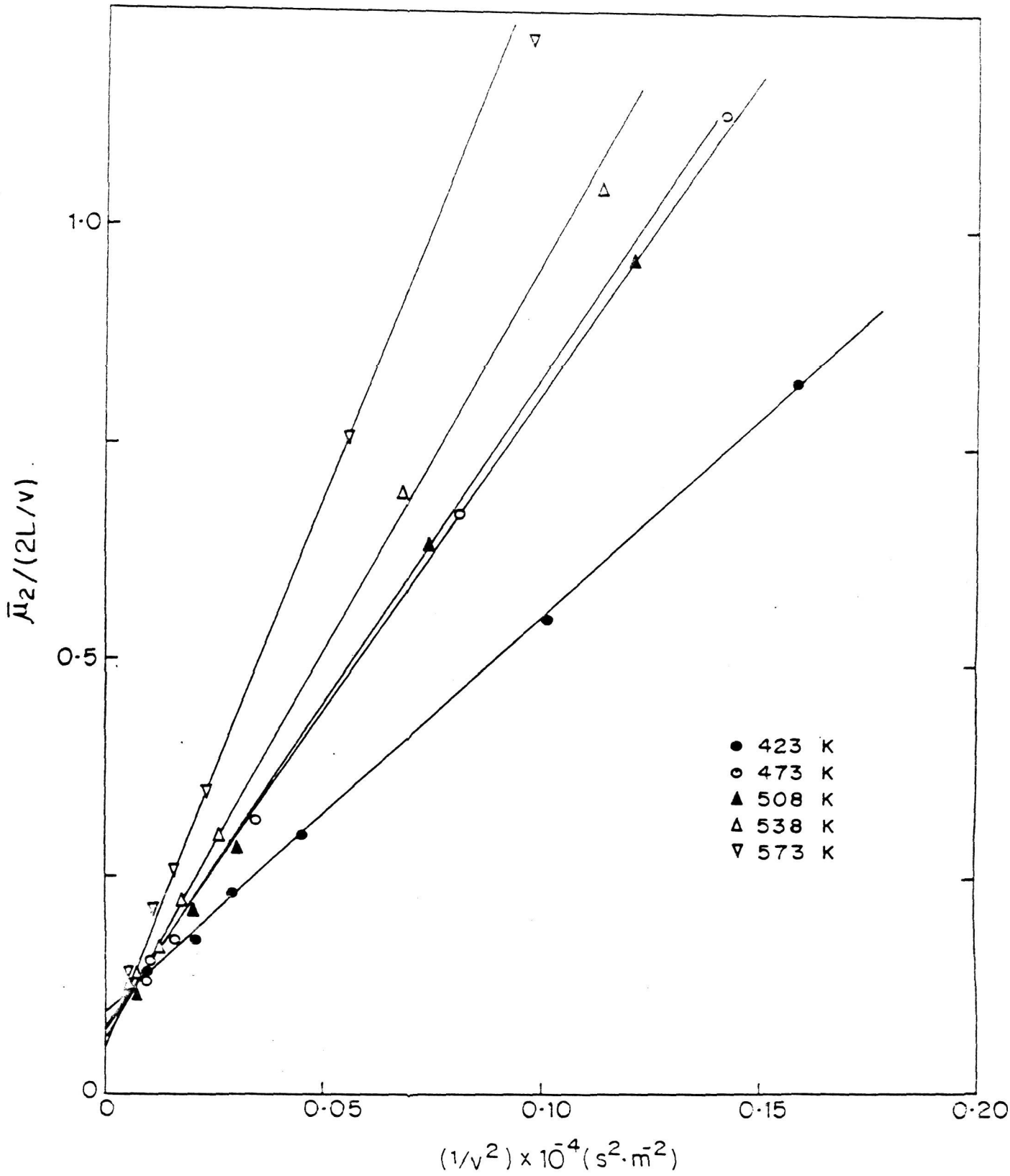

FIG.5·7: $\bar{\mu}_2/(2L/v)$ vs $1/v^2$ PLOTS FOR OXYGEN ON THE MACROPOR(SILICON CARBIDE AT DIFFERENT TEMPERATURES

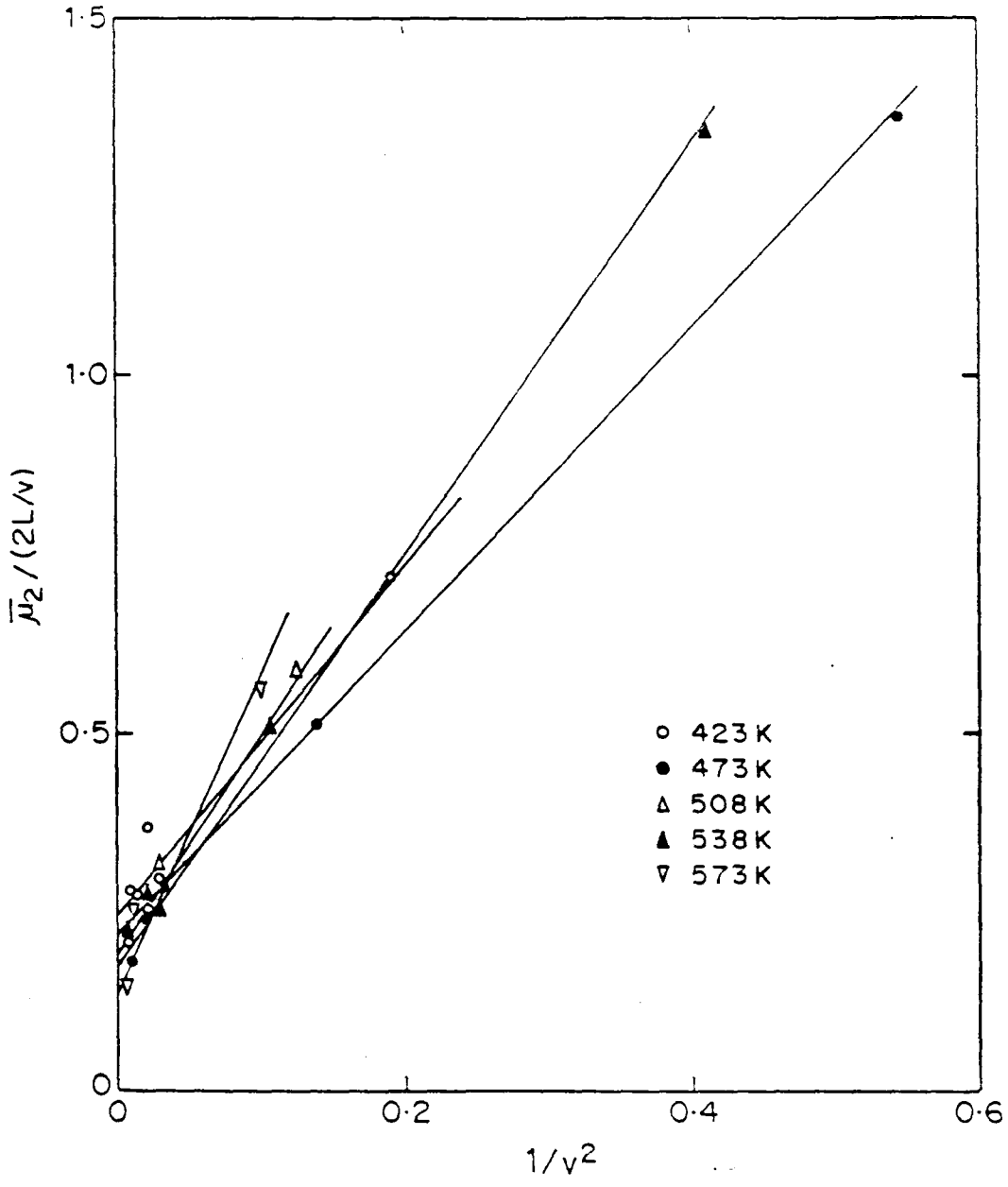

FIG.5·8: $\bar{\mu}_2/(2L/v)$ vs $1/v$ PLOTS FOR CARBONDIOXIDE ON THE MACROPOROUS SILICON CARBIDE AT DIFFERENT TEMPERATURES

at different temperatures are given in Appendix 5.3. The values of axial dispersion coefficient (E_A) and the effective pore diffusivity (D_e) for the diffusing species at different temperatures are included in Table 5.2.

The temperature dependence of mass transfer parameters (E_A and D_e) according to the Arrhenius equation is shown in Fig. 5.9. The activation energy E for the diffusion of various gaseous species has been estimated to be as follows:

Diffusing species	:	$CH_4(N_2)$	$C_2H_4(N_2)$	$CO_2(N_2)$	O_2(He)
E ($kJ.mol^{-1}$)	:	2.36	2.84	3.31	2.76

The values of E, which are more or less similar to that generally observed for the bulk diffusion, indicate a mild temperature dependence of the diffusion in the macroporous silicon carbide pellets.

5.4.3. Tortuosity Factors

The mean free path of all the diffusing species in the temperature range of the experiment lie between 0.07 and 0.15 μm. Mercury porosimeter measurements show that the macropore diameter of the silicon carbide pellets is greater than 12 um and it has some pores below 0.012 μm. Since the macropore diameter is much larger than the mean free path of the diffusing species (pore dia. $/\lambda > 80$) the mass transfer in these pores is expected to be mainly due to bulk diffusion. Therefore the bulk diffusion coefficients D_{AB} for the respective diffusing species-carrier gas system are used in the estimation of tortuosity factor (τ) according to Equation (5.15)

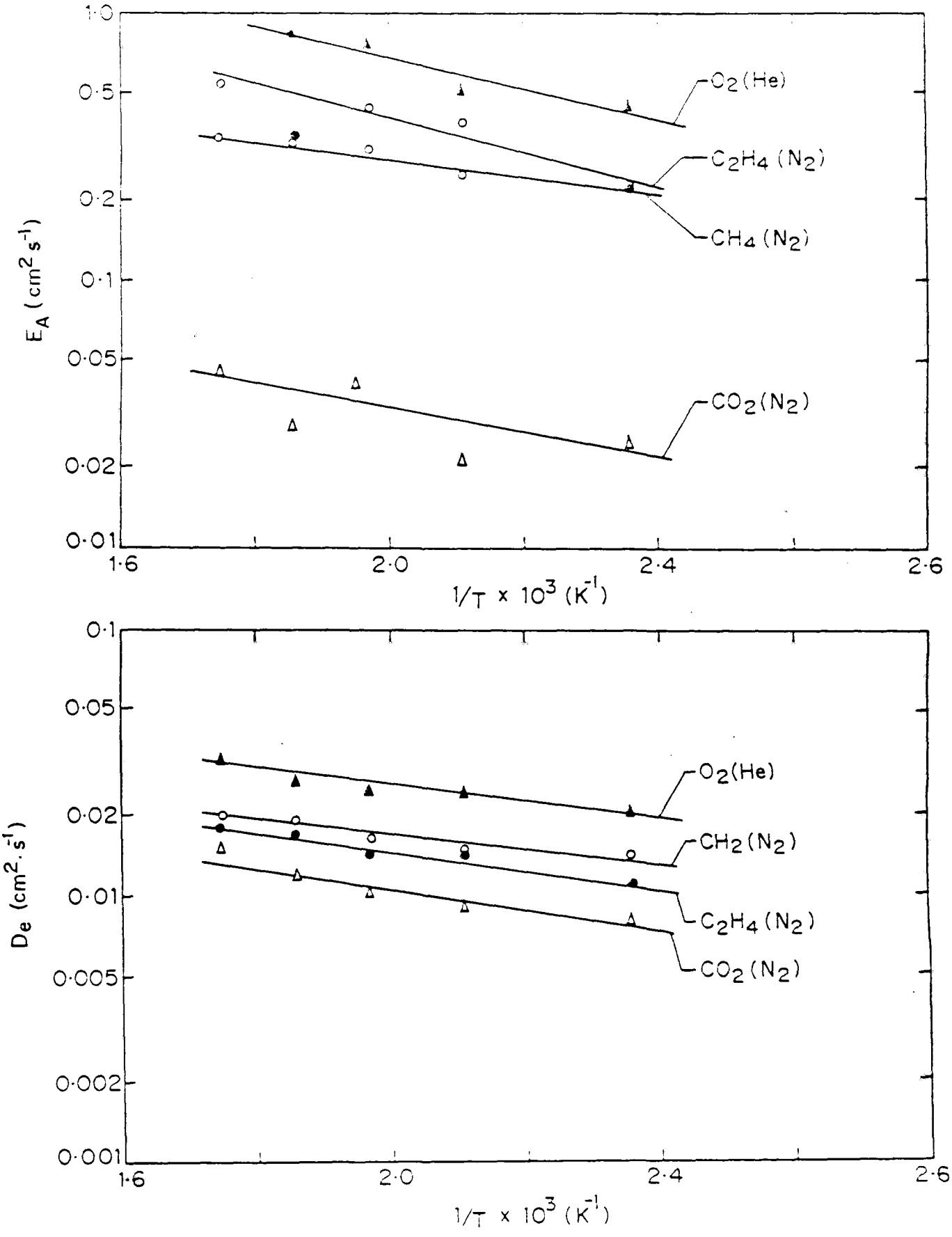

FIG. 5·9: TEMPERATURE DEPENDENCE OF EFFECTIVE DIFFUSIVITY (De) AND AXIAL DISPERSION COEFFICIENT (E_A) FOR THE DIFFERENT DIFFUSION SYSTEMS

Since the pellets contain some pores of diameter less than 0.012 μm, it is expected that there may be some contribution of the Knudsen diffusivity to the observed effective diffusivity. However, as the total volume of these pores (0.016 $cm^3.g^{-1}$) is very small, the contribution of Knudsen diffusion has been ignored for estimating τ in the data in Table 5.2.

The data in Table 5.2 show that the tortuosity factors of the silicon carbide pellets for all the diffusing species are much higher than the most widely accepted theoretical value of $\tau = 3$ [21,22]. For the diffusion of methane, ethylene and carbon dioxide, the tortuosity factor falls in the range of 13-18 with an average value of 15.7. The tortuosity factor for the diffusion of oxygen in the support is very much higher as compared to that of the other three gases. It may be noted that helium is used as the carrier gas for oxygen in the place of nitrogen which has been the carrier gas for methane, ethylene and carbon dioxide pulse experiments. The effective diffusivity of oxygen (Table 5.2) is higher than that of the other species. However, since the binary diffusion coefficient for the O_2-He system is much larger than that of the other diffusing systems, the estimated tortuosity factor for the diffusion of O_2 is higher (almost double). Thus, the difference in the observed value for oxygen is a direct reflection of this difference in the binary diffusivity. Such carrier gas dependent tortuosity factors, measured by pulse chromatographic technique using different carrier gases have been reported by Wolff and Gelbin

[23] for the diffusion of isobutane in bidisperse (macro and micro) pore systems.

Values of tortuosity factors much higher than 3 have been observed earlier. A few recent examples of high tortuosity factors observed for diffusion in porous solids are presented in Table 5.3. High tortuosity factors have been reported for sintered nickel oxide [2], sintered magnetite pellets [8], alumina [24] and HDS catalysts [25]. A few more such examples have also been given by Satterfield [15]. The experimentally estimated higher tortuosity factors ($\tau > 3$, observed generally for coked and sintered porous solids) are commonly attributed to pore constrictions [15].

In the present case, the larger experimental values are expected to be due to the presence of dead end pores and pore constrictions that resulted during the process of sintering of the silicon carbide pellets. The presence of dead end pores has been indicated by the hysterisis curve, observed for the mercury sorption in the pellets (Fig. 5.2). The presence of smaller diameter (< 0.012 μm) pores occupying about 6 % of the total volume, which are likely to be the pore constrictions formed in the sintering of the silicon carbide pellets, may also be responsible for the observed high tortuosity factors and also the observed larger tortuosity factor for oxygen. These smaller diameter pores may contribute to the mass transfer in the pellets by Knudsen diffusion, which has not been accounted for in the calculation of τ by Equation (5.15).

Table 5.3

Examples of high tortuosity factors observed for diffusion in porous solids

Porous solid	Diffusing species	Temperature (K)		Refere
T606 (Special compounded refrac - tory oxide support)	H_2-N_2 (Counter diffu - sion)	293 - 303	79 + 28	1
G 56 (Nickel-based catalyst used for steam reforming of hydrocarbons)	-- " --	-- " --	11.1 + 1.1	1
Sintered, unreduced, pelleted NiO (Calcined in air at 2523 K for different periods)	He-N_2 (Counter diffu - sion)	298	16 - 100	2
Sintered Magnetite pellets	He (N_2)	-	7.8	8
NaMg-A Zeolite (spent)	i - butane (H_2)	-	13.8 - 26.3	2
-- " --	i - butane (Air)	-	9.1 - 15.9	2
NaCa-A Zeolite (Fresh)	i - butane (H_2)	-	8.4	2
Theta - gamma alumina	N_2(He)	333	8.48	2
-- " --	He(N_2)	333	7.22	2
HDS-20A extrudate (unsulfided commercial hydrodesulfurization catalyst)	He (N_2) and H_2 (N_2)	295 - 502	6.1 - 9.6 (based on volume aver- aged diffusivity)	2

5.5 CONCLUSION

Effective diffusivity of methane(N_2), ethylene(N_2), carbon dioxide(N_2) and oxygen(He) in commercial macroporous spherical pellets of silicon carbide at 423-573 K have been determined by gc pulse technique using a single pellet string column and analyzing the chromatographic data using the method of moments. Under the experimental conditions, the pore diffusion mechanism was found to be in the bulk diffusion regime. The effective diffusivity of all the diffusing species showed a mild temperature dependence.

The internal tortuosity factor of the silicon carbide pellets for all the diffusing species was found to be much larger than the theoretical value of $\tau = 3$. The average values of for the diffusion of methane(N_2), ethylene(N_2), carbon dioxide(N_2) and oxygen(He) were found to be 16.1, 13.3, 17.6 and 33.8 respectively. Commercial silicon carbide pellets are highly sintered material. The observed high value of tortuosity factor is due to the presence of dead end pores and pore constrictions in the sintered support material. The wide difference between the τ value of oxygen and that of the other gases has been attributed to the different carrier gases used for the gc pulse experiments.

NOMENCLATURE

A	Area of packing, cm^2
c(z,t)	Concentration as a function of distance and time
D_{AB}	Molecular diffusivity, $cm^2.s^{-1}$
D_e	Effective diffusivity, $cm^2.s^{-1}$
E	Activation energy, $kJ.mol^{-1}$
E_A	Axial dispersion coefficient, $cm^2.s^{-1}$
F	Gas flow rate, $cm^3.s^{-1}$
K_A	Adsorption equilibrium constant
k_A	Mass transfer coefficient, $cm.s^{-1}$
k_{ads}	Adsorption rate constant, s^{-1}
L	Length of SPSC, cm
M_A, M_B	Molecular weights of species A and B
N	Avagadro number
P	Pressure, atm
R	Gas constant
r	Average radius of the particle, cm
T	Temperature, K
T_C	Column temperature, K
t	Time, s
t_{OA}	Sample injection time, s
v	Linear gas velocity in the interparticle space, $cm.s^{-1}$

Greek Letters

α	Column void fraction
β	Pellet porosity
γ	Pellet shape factor (3 for spheres)

λ	Mean free path of the diffusing molecule
μ_1'	First absolute moment
μ_2	Second central moment
γ	Intraparticle tortuosity

REFERENCES

1. Satterfield, C.N. and Cadle, P.J., Ind. Eng. Chem. Proc. Des. Dev., 7, 256, (1968)
2. Kim, K.K. and Smith, J.M., AIChE J., **20**, 670 (1974)
3. Wang, C.T. and Smith, J.M., AIChE J., **29**, 132 (1983)
4. Choudhary, V.R., J. Chromatogr., **98**, 491 (1974)
5. Suzuki, M. and Smith, J.M., Advances in Chromatography., Marcel Dekker Inc., N.Y., **13**, 213 (1975)
6. Furusawa, T., Suzuki, M. and Smith, J.M., Catal. Rev. Sci. Eng., **13**, 43 (1976)
7. Davis, B.R. and Scott, D.S., Measurement of the Effective Diffusivity of Porous Pellets. Paper presented at the 58th annual meeting, AIChE Philadelphia (1965)
8. Scott, D.S., Lee, W. and Papa, J., Chem. Eng.Sci., **29**, 215 (1974)
9. Valus, J. and Schneider, P., Chem. Eng. Sci., **40**, 1457 (1985)
10. Kubin, M., Collection Czechoslov. Chem. commun., **30**, 1104 (1965)
11. Kucera, E., J. Chromatogr., **19**, 237 (1965)
12. Cerro, R.L. and Smith, J.M., AIChE J., **16**, 1034 (1970)
13. Schanel, L., and Schneider, P., Chem. Eng. J., **2**, 274, (1971)
14. Schneider, P. and Smith, J.M., AIChE J., **14**, 762 (1968)
15. Satterfield, C.N., Mass Transfer in Heterogeneous Catalysis., MIT Press, Cambridge (1970)
16. Evans III, R.B., Watson, G.M. and Mason, E.A., J. Chem.

Phys., 35, 2076 (1961)

17. Choudhary, V.R. and Akolekar, D.B., Advances in Catalysis-Science and Technology. (Ed. T.S.R. Prasada Rao), Wiley Eastern Ltd., New Delhi., 425 (1985)

18. Choudhary, V.R. and Doraiswamy, L.K., Ind. Eng. Chem. Prod. Res. Develop., **10**, 218 (1971)

19. Kemp, M.K., Physical Chemistry . A step - by - step approach., Marcel Dekker Inc., N.Y. (1979)

20. Bird, R.B., Stewart, W.E. and Lightfoot, E.N., Transport Phenomena., John Wiley and Sons Inc., N.Y. (1960)

21. Johnson, M.F.L. and Stewart, W.E., J. Catal., **4**, 248 (1965)

22. Feng, C. and Stewart, W.E., Ind. Eng. Chem. Fundam., **12**, 143 (1973)

23. Wolff, H.J. and Gelbin, D., Chem. Tech. (Leipzig), **32**, 7, 362 (1980)

24. McGreavy, C. and Siddiqui, M.A., Chem. Eng. Sci., **35**, 3 (1980)

25. Wang, C.T. and Smith, J.M., AIChE J., **29**, 132 (1983)

Appendix 5.1a

Mercury porosimetry data of silicon carbide pellets using Autoscan-33 porosimeter

SAMPLE ID .5CC
SAMPLE WEIGHT = .3049 GRAMS
WETTING ANGLE = 140.0000 DEGREES
SURFACE TENSION = 480.0000 ERGS/SQ CM
PRINTING EVERY 5 POINTS

PRESSURE PSIA	RADIUS ANGSTROMS	VOLUME C.C.	%V %	DV/DP C.C./PSIA	DV(R) C.C./A	DS(R) SQ M/A	AREA SQ METER
34.91	.3055E+05	0.0000	0.00	.0000E+01	.0000E+01	.0000E+01	.0000E+01
138.52	.7700E+04	0.0000	0.00	.0000E+01	.0000E+01	.0000E+01	.0000E+01
246.54	.4326E+04	0.0000	0.00	.0000E+01	.0000E+01	.0000E+01	.0000E+01
337.19	.3003E+04	0.0000	0.00	.0000E+01	.0000E+01	.0000E+01	.0000E+01
460.69	.2315E+04	0.0000	0.00	.0000E+01	.0000E+01	.0000E+01	.0000E+01
564.92	.1888E+04	0.0000	0.00	.0000E+01	.0000E+01	.0000E+01	.0000E+01
672.94	.1585E+04	0.0000	0.00	.0000E+01	.0000E+01	.0000E+01	.0000E+01
784.13	.1360E+04	0.0000	0.00	.0000E+01	.0000E+01	.0000E+01	.0000E+01
898.47	.1187E+04	0.0000	0.00	.0000E+01	.0000E+01	.0000E+01	.0000E+01
1014.91	.1055E+04	0.0000	0.00	.0000E+01	.0000E+01	.0000E+01	.0000E+01
1123.99	.9490E+03	0.0000	0.00	.0000E+01	.0000E+01	.0000E+01	.0000E+01
1235.17	.8635E+03	0.0000	0.00	.0000E+01	.0000E+01	.0000E+01	.0000E+01
1348.78	.7625E+03	0.0000	0.00	.0000E+01	.0000E+01	.0000E+01	.0000E+01
1460.30	.6835E+03	0.0000	0.00	.0000E+01	.0000E+01	.0000E+01	.0000E+01
1724.11	.6187E+03	0.0000	0.00	.0000E+01	.0000E+01	.0000E+01	.0000E+01
1970.88	.5641E+03	0.0000	0.00	.0000E+01	.0000E+01	.0000E+01	.0000E+01
2087.02	.5185E+03	0.0000	0.00	.0000E+01	.0000E+01	.0000E+01	.0000E+01
2226.32	.4791E+03	0.0000	0.00	.0000E+01	.0000E+01	.0000E+01	.0000E+01
2395.62	.4452E+03	0.0000	0.00	.0000E+01	.0000E+01	.0000E+01	.0000E+01
2567.45	.4154E+03	0.0000	0.00	.0000E+01	.0000E+01	.0000E+01	.0000E+01
2739.91	.3893E+03	0.0000	0.00	.0000E+01	.0000E+01	.0000E+01	.0000E+01
2912.99	.3662E+03	0.0000	0.00	.0000E+01	.0000E+01	.0000E+01	.0000E+01
3087.35	.3455E+03	0.0000	0.00	.0000E+01	.0000E+01	.0000E+01	.0000E+01

Appendix 5.1a (contd.)

[illegible]	.3272E+03	0.0000	0.00	.0000E+01	.0000E+01	.0000E+01	.0000E+01
[illegible]	.3112E+03	0.0000	0.00	.0000E+01	.0000E+01	.0000E+01	.0000E+01
[illegible]	.2960E+03	0.0000	0.00	.0000E+01	.0000E+01	.0000E+01	.0000E+01
[illegible]	.2837E+03	0.0000	0.00	.0000E+01	.0000E+01	.0000E+01	.0000E+01
[illegible]	.2719E+03	0.0000	0.00	.0000E+01	.0000E+01	.0000E+01	.0000E+01
[illegible]	.2610E+03	0.0000	0.00	.0000E+01	.0000E+01	.0000E+01	.0000E+01
[illegible]	.2511E+03	0.0000	0.00	.0000E+01	.0000E+01	.0000E+01	.0000E+01
[illegible]	.2415E+03	0.0000	0.00	.0000E+01	.0000E+01	.0000E+01	.0000E+01
[illegible]	.2222E+03	0.0000	0.00	.0000E+01	.0000E+01	.0000E+01	.0000E+01
[illegible]	.1964E+03	0.0000	0.00	.0000E+01	.0000E+01	.0000E+01	.0000E+01
[illegible]	.1759E+03	0.0000	0.00	.0000E+01	.0000E+01	.0000E+01	.0000E+01
[illegible]	.1593E+03	0.0000	0.00	.0000E+01	.0000E+01	.0000E+01	.0000E+01
[illegible]	.1456E+03	0.0000	0.00	.0000E+01	.0000E+01	.0000E+01	.0000E+01
[illegible]	.1340E+03	0.0000	0.00	.0000E+01	.0000E+01	.0000E+01	.0000E+01
[illegible]	.1242E+03	0.0000	0.00	.0000E+01	.0000E+01	.0000E+01	.0000E+01
[illegible]	.1157E+03	0.0000	0.00	.0000E+01	.0000E+01	.0000E+01	.0000E+01
[illegible]	.1082E+03	0.0000	0.00	.0000E+01	.0000E+01	.0000E+01	.0000E+01
[illegible]	.1016E+03	0.0000	0.00	.0000E+01	.0000E+01	.0000E+01	.0000E+01
[illegible]	.9581E+02	0.0000	0.00	.0000E+01	.0000E+01	.0000E+01	.0000E+01
[illegible]	.9063E+02	0.0000	0.00	.0000E+01	.0000E+01	.0000E+01	.0000E+01
[illegible]	.8601E+02	0.0000	0.00	.0000E+01	.0000E+01	.0000E+01	.0000E+01
[illegible]	.8181E+02	0.0000	0.00	.0000E+01	.0000E+01	.0000E+01	.0000E+01
[illegible]	.7803E+02	0.0000	0.00	.0000E+01	.0000E+01	.0000E+01	.0000E+01
[illegible]	.7453E+02	0.0000	0.00	.0000E+01	.0000E+01	.0000E+01	.0000E+01
[illegible]	.7135E+02	0.0000	0.00	.0000E+01	.0000E+01	.0000E+01	.0000E+01
[illegible]	.6846E+02	0.0000	0.00	.0000E+01	.0000E+01	.0000E+01	.0000E+01
16216.05	.6577E+02	0.0000	0.00	.2113E-06	.5169E-04	.1572E-01	.0000E+01
16848.56	.6331E+02	0.0000	0.00	.4064E-06	.1073E-03	.3391E-01	.7554E-01

Appendix 5.1a (contd.)

17425.43	.6077E+02	.0005	3.03	.6095E-06	.1736E-03	.5695E-01	.3077E+00
18132.20	.5883E+02	.0007	4.55	.4226E-06	.1294E-03	.4398E-01	.4694E+00
19768.96	.5683E+02	.0012	7.58	.2194E-06	.7198E-04	.2533E-01	.7202E+00
19400.68	.5498E+02	.0005	3.03	.0000E+01	.0000E+01	.0000E+01	.7202E+00
20032.39	.5325E+02	.0014	9.09	.6421E-06	.2400E-03	.9016E-01	.1075E+01
20679.26	.5158E+02	.0014	9.09	.4389E-06	.1749E-03	.6781E-01	.1260E+01
21321.00	.5003E+02	.0022	13.64	.6420E-06	.2720E-03	.1007E+00	.1641E+01
21957.85	.4850E+02	.0022	13.64	.0000E+01	.0000E+01	.0000E+01	.1641E+01
22599.67	.4720E+02	.0022	13.64	.7965E-06	.3792E-03	.1607E+00	.1843E+01
23241.48	.4589E+02	.0031	19.70	.1024E-05	.5158E-03	.2240E+00	.2259E+01
23878.20	.4468E+02	.0034	21.21	.0000E+01	.0000E+01	.0000E+01	.2363E+01
24520.07	.4350E+02	.0014	9.09	.0000E+01	.0000E+01	.0000E+01	.2363E+01
25151.78	.4241E+02	.0024	15.15	.2097E-05	.1237E-02	.5036E+00	.2972E+01
25700.55	.4136E+02	.0038	24.24	.1877E-05	.1165E-02	.5633E+00	.3494E+01
26430.37	.4036E+02	.0043	27.27	.0000E+01	.0000E+01	.0000E+01	.4227E+01
27072.19	.3940E+02	.0022	13.64	.0000E+01	.0000E+01	.0000E+01	.4421E+01
27701.95	.3849E+02	.0043	27.27	.2308E-05	.1654E-02	.8593E+00	.5586E+01
28350.77	.3762E+02	.0048	30.30	.0000E+01	.0000E+01	.0000E+01	.5738E+01
28992.59	.3679E+02	.0036	22.73	.2439E-07	.1914E-04	.1040E-01	.5906E+01
29624.30	.3601E+02	.0048	30.30	.1479E-05	.1212E-02	.6732E+00	.6830E+01
30266.12	.3524E+02	.0053	33.33	.6339E-06	.5421E-03	.3076E+00	.7100E+01
30907.94	.3451E+02	.0055	34.85	.2113E-06	.1885E-03	.1092E+00	.7375E+01
31549.76	.3381E+02	.0058	36.36	.2113E-06	.1964E-03	.1162E+00	.7510E+01
32096.74	.3312E+02	.0050	36.36	.0000E+01	.0000E+01	.0000E+01	.7510E+01
32843.51	.3248E+02	.0048	30.30	.3381E-05	.3406E-02	.2070E+01	.7962E+01

INTRUSION DISTRIBUTIONS

VOLUME
MODE = .3406E-02 C.C. / ANGSTROM AT A RADIUS OF .3248E+02 ANGSTROMS
MEAN PORE RADIUS = .4423E+02 ANGSTROMS
MEDIAN PORE RADIUS = .4241E+02 ANGSTROMS

SURFACE AREA
MODE = .2098E+01 SQ. M. / ANGSTROM AT A RADIUS OF .3248E+02 ANGSTROMS
MEAN PORE RADIUS = .4286E+02 ANGSTROMS
MEDIAN PORE RADIUS = .4136E+02 ANGSTROMS

Appendix 5.1b
Mean free paths of O_2, CO_2, CH_4 AND C_2H_4 at 1 atm. pressure and different temperatures

Molecule	Mean free path ($\lambda \times 10^3$) m.	
	423K	573K
O_2	110.2	150
CO_2	81.3	110
CH_4	89.0	120
C_2H_4	72.5	90

Appendix 5.2

Data on the linear gas velocity and moments for the diffusion of CH_4, C_2H_4, CO_2 and O_2 on silicon carbide pellets

System	Temp. (K)	v ($cm.s^{-1}$)	μ_1 (s)	μ_2	t_{OA} (s)
1	2	3	4	5	6
		1.34	137.3	185.5	3.31
		2.43	75.2	40.5	1.82
		4.70	39.7	10.3	0.94
	423	5.93	31.8	6.6	0.74
		7.29	26.0	4.9	0.60
		8.31	22.6	4.2	0.53
		9.21	20.3	3.6	0.48
		1.44	127.2	175.8	3.41
		2.64	70.2	36.3	1.86
		5.21	36.3	8.8	0.94
	473	6.63	28.7	6.1	0.74
		8.01	23.9	4.4	0.61
		9.28	20.9	3.7	0.52
		10.17	18.9	3.2	0.48
		1.48	126.6	185.8	3.55
		2.87	65.8	33.6	1.83
		5.66	33.8	7.7	0.93
$CH_4(N_2)$	508	7.17	27.0	5.0	0.73
		8.68	22.3	3.6	0.60
		9.84	19.7	3.3	0.53
		11.21	17.8	2.5	0.47
		1.65	112.2	137.5	3.41
		3.07	60.8	29.3	1.83
		5.99	31.9	6.4	0.94
	538	7.51	25.4	4.2	0.75
		9.19	20.5	3.1	0.61
		10.52	18.5	2.3	0.53
		11.66	16.80	2.2	0.48
		1.74	108.4	140.4	3.42
		3.15	60.3	28.5	1.89
		6.59	29.0	5.3	0.90
	573	7.80	25.3	4.5	0.76
		9.74	20.3	2.9	0.61
		11.20	17.5	2.3	0.53
		12.43	15.7	2.0	0.48

Appendix 5.2 Contd.

1	2	3	4	5	6
		1.18	149.8	491.1	3.69
		2.51	74.3	64.7	1.74
		4.68	41.2	12.7	0.93
	423	5.76	33.7	8.0	0.76
		6.95	27.7	5.0	0.63
		8.21	24.5	5.9	0.53
		9.52	21.2	3.0	0.46
		1.37	137.1	445.1	3.54
		2.67	71.0	93.4	1.82
		5.34	36.6	10.1	0.91
	473	6.68	30.3	3.2	0.73
		7.85	25.9	4.4	0.62
		9.24	22.2	4.4	0.53
		10.40	19.7	2.5	0.47
		1.37	125.9	411.0	3.85
		2.88	63.8	58.4	1.83
		5.70	33.5	9.6	0.92
O_2(He)	508	7.13	27.0	5.8	0.74
		8.62	23.0	8.7	0.61
		9.99	19.8	2.7	0.53
		11.24	17.8	2.0	0.47
		1.53	117.1	375.2	3.62
		2.96	63.1	55.8	1.87
		6.12	30.1	17.5	0.90
	538	7.38	26.2	5.9	0.75
		8.67	22.6	3.7	0.64
		10.51	18.7	2.6	0.53
		12.15	16.7	2.2	0.46
		1.59	131.6	771.8	3.71
		3.18	67.8	75.3	1.85
		6.52	34.3	10.7	0.91
	573	7.89	29.3	6.5	0.75
		9.61	24.0	4.4	0.61
		11.06	20.9	2.6	0.53
		12.77	18.1	2.2	0.46

Appendix 5.2 Contd.

1	2	3	4	5	6
		1.24	136.0	253.2	3.55
		2.31	72.9	61.3	1.90
		4.79	35.9	8.9	0.91
	423	5.94	29.3	10.2	0.74
		7.18	24.7	10.2	0.61
		8.27	21.2	6.5	0.53
		9.36	18.8	5.9	0.45
		1.35	125.4	197.5	3.62
		2.67	63.4	37.5	1.83
		5.49	31.2	10.1	0.89
	473	6.73	26.4	6.9	0.73
		7.98	22.7	6.1	0.61
		9.24	19.6	4.6	0.53
		10.40	17.1	3.7	0.47
		1.44	119.7	199.1	3.64
		2.31	61.9	43.7	1.87
		5.64	31.3	11.0	0.93
$CO_2(N_2)$	508	6.91	25.6	7.2	0.76
		8.77	20.8	5.1	0.60
		9.90	18.7	4.5	0.53
		11.06	16.2	3.9	0.47
		1.55	110.4	169.3	3.59
		3.06	57.2	32.6	1.82
		6.08	28.9	8.0	0.92
	538	7.34	24.4	6.9	0.76
		9.27	19.3	4.5	0.60
		10.45	17.8	4.2	0.53
		11.75	15.5	3.4	0.47
		1.65	108.0	101.9	3.58
		3.13	57.0	35.9	1.89
		6.20	29.3	8.9	0.95
	573	7.99	23.1	6.3	0.74
		9.69	19.3	4.6	0.62
		11.29	16.5	3.7	0.52
		12.56	14.6	2.4	0.47

Appendix 5.2 Contd.

1	2	3	4	5	6
		1.23	143.7	196.9	3.55
		2.33	78.3	38.3	1.88
		4.70	39.0	10.1	0.93
	423	5.75	32.6	8.2	0.76
		7.12	26.4	6.2	0.61
		8.14	23.2	5.0	0.54
		9.21	20.5	4.5	0.47
		1.37	134.4	153.9	3.55
		2.78	67.5	28.3	1.75
		5.13	36.4	8.0	0.95
	473	6.38	29.8	5.9	0.76
		7.89	24.5	4.4	0.62
		9.24	20.9	3.6	0.53
		10.26	18.6	3.5	0.47
		1.54	122.5	149.0	3.39
		2.79	67.9	29.6	1.87
		5.54	34.3	7.5	0.94
$C_2H_4(N_2)$	508	7.12	27.2	5.5	0.73
		8.42	28.5	3.5	0.62
		9.85	19.8	3.2	0.53
		10.93	17.8	3.1	0.48
		1.57	116.4	107.0	3.57
		3.02	61.2	19.7	1.86
		5.95	31.2	5.8	0.94
	538	7.67	25.2	3.7	0.73
		9.09	21.3	3.1	0.62
		10.71	17.8	2.3	0.52
		11.83	16.5	2.3	0.47
		1.69	111.0	114.4	3.51
		3.22	59.1	23.5	1.85
		6.40	30.0	5.3	0.93
	573	7.87	24.6	4.5	0.76
		9.85	19.9	2.9	0.60
		11.04	18.0	2.4	0.54
		12.48	15.8	2.1	0.48

Appendix 5.3

Calculation and results of moment analysis for the diffusion of CH_4, C_2H_4, CO_2 and O_2 on silicon carbide pellets

System	Temp. (K)	Slope S	$E_A \times 10$ ($cm^2.s^{-1}$)	Intercept	$D_e \times 10^2$ ($cm^2.s^{-1}$)	γ
$CH_4(N_2)$*	423	2.32	2.3	0.145	1.40	14.1
	473	2.57	2.5	0.140	1.40	16.9
	508	3.13	3.1	0.125	1.60	17.0
	538	3.42	3.4	0.105	1.90	15.7
	573	3.50	3.5	0.101	1.95	16.9
						(Av. 16.1)
$C_2H_4(N_2)$	423	2.30	2.3	0.187	1.10	13.2
	473	4.00	4.0	0.150	1.37	12.8
	508	4.40	4.4	0.145	1.40	14.1
	538	3.52	3.5	0.120	1.70	12.8
	573	5.56	5.5	0.115	1.80	13.8
						(Av. 13.3)
$CO_2(N_2)$	423	0.25	0.25	0.24	0.80	16.9
	473	0.215	0.21	0.215	0.91	18.7
	508	0.31	0.31	0.19	1.03	18.6
	538	0.29	0.29	0.17	1.15	18.5
	573	0.45	0.45	0.13	1.54	15.3
						(Av. 17.6)
O_2(He)	423	4.57	4.5	0.094	1.98	32.5
	473	5.15	5.1	0.078	2.38	32.6
	508	7.75	7.7	0.075	2.46	35.2
	538	8.57	8.5	0.070	2.64	36.3
	573	12.70	12.6	0.056	3.30	32.3
						(Av. 33.8)

* The carrier gas used is given in the bracket.

CHAPTER - 6

STEP-WISE THERMAL DESORPTION OF CARBON DIOXIDE ON SYNTHETIC ZEOLITES

6 STEP-WISE THERMAL DESORPTION OF CARBON DIOXIDE ON SYNTHETIC ZEOLITES

6.1 INTRODUCTION

Zeolites are used as adsorbents and as catalysts in heterogeneous reactions and the acidic and basic nature of their active sites are important in understanding their performance. Though a large amount of work has been done on the acidity of the zeolites, very little has been published on their basic properties and the use of basic zeolites in adsorption and catalysis [1-7]. It is accepted that Broensted acids and bases are conjugated and that weak acids have strong conjugate bases and strong acids have weak conjugate bases [8]. The existence of protons in zeolites can be associated with the basic sites. Barthomeuf and Mallmann [6] have estimated the basic strength of various zeolites using pyrrol and benzene adsorption. Also, the concepts of Broensted and Lewis basic sites have been proposed [7] based on the presence of basic OH groups and the framework oxygen atoms respectively.

Recently, Choudhary and Rane [9] have reported a new method, based on step-wise thermal desorption (STD) of carbon dioxide, for measuring the basicity of solid catalysts under operating conditions. Using this method, it is possible to measure quantitatively the basicity and base strength distribution on solid catalysts and adsorbents at the conditions close to their operation.

Zeolites are used for the adsorptive separation of gases containing CO_2 which is strongly adsorbed on them. In such

cases, the STD of CO_2 on these zeolites will also help in understanding the regenerability and temperature of regeneration of the particular zeolite adsorbent.

The objective of the present investigation is to study the chemisorption of CO_2 and STD of CO_2 for evaluating the basicity and base strength distribution on the zeolites and also to know the regenerability of the zeolite, if used in the adsorptive separation of gases containing carbon dioxide. A large number of synthetic zeolites viz. Na-H-ZSM-8, H-ZSM-8, MgO.H-ZSM-8, H-Na-ZSM-5, NaM, HM, NaY, CeNaY (Ce^{+3} exchange 33%), CeNaY (Ce^{+3}exchange 72%), deammoniated NH_4Y, NaX, KL, HKL, silicalite, $AlPO_4$-5 and SAPO-5 have been evaluated for their basicity by the step-wise thermal desorption of carbon dioxide on these zeolites .

6.2 EXPERIMENTAL

6.2.1 Gases

Helium : High purity (> 99.99%), obtained from Indian Oxygen Ltd., Bombay. It was passed over activated molecular sieves to remove traces of moisture.

Carbon dioxide : High purity (> 99.99%), obtained from Air-Liquid, France.

6.2.2 Zeolites

The Si/Al ratio, the degree of cation exchange and unit cell composition of the zeolites are given in Table 6.1.

Table 6.1

Chemical composition of the zeolites

Zeolite	Si/Al	Degree of NH_4^+-, H^+- or Ce^{+3}- exchange	Unit cell composition
Na-H-ZSM-5	17.2	0.61	$H_{3.22}Na_{2.06}(AlO_2)_{5.28}(SiO_2)_{44.3}\cdot nH_2O$
H-ZSM-8	29.6	0.96	$H_{3.01}Na_{0.13}(AlO_2)_{3.14}(SiO_2)_{92.86}\cdot nH_2O$
H-Na-ZSM-8	29.6	0.08	$H_{0.25}Na_{2.89}(AlO_2)_{3.14}(SiO_2)_{92.86}\cdot nH_2O$
HM	6.5	0.97	$H_{7.8}Na_{0.2}(AlO_2)_{8.0}(SiO_2)_{51.6}\cdot 26.3H_2O$
NaM	5.5	0.07	$H_{0.6}Na_{7.4}(AlO_2)_{8.0}(SiO_2)_{44.3}\cdot 23H_2O$
NH_4Y	2.4	0.92	$(NH_4)_{51.5}Na_{4.5}(AlO_2)_{56.0}(SiO_2)_{136}\cdot nH_2O$
NaY	2.4	-	$Na_{56}(AlO_2)_{56}(SiO_2)_{136}\cdot nH_2O$
CeNaY	2.4	0.33	$Ce_{6.2}Na_{37.4}(AlO_2)_{56}(SiO_2)_{136}\cdot nH_2O$
CeNaY	2.4	0.72	$Ce_{13.5}Na_{15.5}(AlO_2)_{56}(SiO_2)_{136}\cdot nH_2O$
KL	2.8	0.07	$K_{8.761}H_{0.624}(AlO_2)_{9.385}(SiO_2)_{26.6}\cdot nH_2O$
NaX	1.3	-	$Na_{83.12}(AlO_2)_{83.12}(SiO_2)_{108.88}\cdot nH_2O$

The synthesis and pre-treatment of the zeolites except MgO.H-ZSM-8 are discussed in Chapter 3 (Section 3.2.1).

MgO.H-ZSM-8

It was prepared by contacting H-ZSM-8 (H^+ exchange 0.96) zeolite (7.1 g) with 25 cm^3 of aqueous magnesium acetate (10%) solution at room temperature for two weeks, while shaking the flask containing the zeolite and the solution occasionally. The zeolite was then filtered using Gooch crucible and washed quickly with about 10 cm^3 of deionized water to remove the magnesium acetate impregnated on the external surface of the zeolite crystals. The zeolite was then dried in vacuum oven at 373 K for 12 h and calcined in air at 773 K for 12 h.

6.2.3 Measurement of Step-wise Thermal Desorption (STD) of Carbon Dioxide

About 1.0 g of the zeolite (particle size 0.3 mm) was packed in a quartz reactor (i.d.: 9 mm) between quartz wool plugs and introduced into the constant temperature zone of a vertical tubular furnace. The temperature of the furnace/reactor was controlled using an Aplab temperature controller and read on a Foronix digital temperature indicator.

The zeolite was treated *in situ* at its calcination temperature in a flow of moisture-free helium (flow rate: 20 $cm.^3min^{-1}$) for 2 h to remove adsorbed water and other impurities. A calcination temperature of 773 K was used for ZSM-5 and ZSM-8 type zeolites, mordenites, silicalite, $AlPO_4$-5 and SAPO-5. The remaining zeolites (X, Y, L) were calcined at 623 K. After calcination, the reactor was cooled to 323 K and the basic

sites of the zeolites saturated by passing pure CO_2 (20 $cm.^3min^{-1}$) for 30 min. The CO_2 physically adsorbed at this temperature was desorbed in a flow of helium (20 $cm.^3min^{-1}$) for 30 min.

The STD of CO_2 was carried out by desorbing CO_2 chemisorbed at 323 K on the zeolite in a flow of helium (20 $cm.^3min^{-1}$) by heating it from 323-1173 K in a number of temperature steps (323-473, 473-623, 623-773 and 773-1173 for ZSM-5, ZSM-8, mordenite, silicalite, $AlPO_4$-5 and SAPO-5; and 323-473, 473-623 and 623-1173 K for X, Y and L zeolites). The temperature in each step was raised at a heating rate of about 15 $K.min^{-1}$. After the maximum temperature of each step was attained, it was maintained for a period of 30 min to desorb the CO_2 reversibly adsorbed on the zeolite at that temperature. The amount of CO_2 desorbed in each step was determined gravimetrically by absorbing it completely in aqueous barium hydroxide solution in a series of two bubblers and filtering and drying the resulting barium carbonate until constant weight is obtained.

The amount of CO_2 desorbed during each temperature step is given by

$$[q_d]_{T_1}^{T_2} = 5.067(\text{weight of } BaCO_3)/W \qquad (6.1)$$

where $[q_d]_{T_1}^{T_2}$ is the amount of CO_2 desorbed on raising the temperature from T_1 to T_2 and W is the weight of the zeolite sample. The amount of CO_2 chemisorbed, q_T, at temperature T is estimated using the relation

$$q_T = [q_d]_T^{1173} \qquad (6.2)$$

where $[q_d]^{1173}$ is the amount of CO_2 desorbed when the temperature was raised from T to 1173 K.

The chemisorption data only upto calcination temperature of the zeolite are considered, and above the calcination temperature, the STD data was collected only to desorb completely the CO_2 chemisorbed. The chemisorption data collected above the calcination temperature do not reflect the zeolite property as, above the calcination temperature, not only the zeolite properties are changed, but also there is a possibility of structural collapse of the zeolites except the high silica ones.

In this study, chemisorption is considered as the amount of CO_2 retained by the pre-saturated zeolite after it was swept with pure helium for a period of 30 min. Further, it is assumed that CO_2 is chemisorbed only on the basic sites of the zeolites and that one molecule of CO_2 is adsorbed per site.

6.3 RESULTS AND DISCUSSION

6.3.1 STD of CO_2 on Zeolites

The base strength distribution is obtained from the STD of CO_2 (chemisorbed at 323 K) on the zeolites (Na-H-ZSM-8, H-ZSM-8, MgO.H-ZSM-8, H-Na-ZSM-5, NaM, HM, NaY, CeNaY (Ce^{+3} exchange 33%), CeNaY (Ce^{+3} exchange 72%), deammoniated NH_4Y, NaX, KL, HKL, silicalite, $AlPO_4$-5 and SAPO-5) from 323 to 1173 K in a number of temperature steps.

The STD data for the different zeolites have been presented in Table 6.2. Figures 6.1-6.3 show the base strength distribution on these zeolites. The columns show the energy

Table 6.2

Data on STD and chemisorption of carbon dioxide on different zeolites

STD Data		Chemisorption Data	
Temp. range (K)	Amt. desorbed q_d (μmol.g^{-1})	Temp. range (K)	Amt. chemisorbed q_i (μmol.g^{-1})
Na-H-ZSM-8			
323-473	110	323	162
473-623	12	473	52
623-773	12	623	40
773-1173	28	773	28
H-ZSM-8			
323-473	23.5	323	85.5
473-623	45	473	62
623-773	10	623	17
773-1173	7	773	7
MgO.H-ZSM-8			
323-473	26	323	113
473-623	33	473	87
623-773	26	623	54
773-1173	28	773	28
Na-ZSM-5			
323-473	111	323	351
473-623	100	473	240
623-773	89	623	140
773-1173	51	773	51
NaM			
323-473	1083	323	1197
473-623	33	473	114
623-773	32	623	81
773-1173	49	773	49

Table 6.2 (contd.)

STD Data		Chemisorption Data	
Temp. range (K)	Amt. desorbed q_d (μmol.g^{-1})	Temp. range (K)	Amt. chemisorbed q_i (μmol.g^{-1})
HM			
323-473	65	323	175
473-623	42	473	110
623-773	39	623	68
773-1173	29	773	29
NaY			
373-473	15	373	145
473-623	53	473	130
623-1173	77	623	77
CeNaY (Ce^{+3} exchange = 33%)			
323-473	83	323	172
473-623	32	473	89
623-1173	57	623	57
CeNaY (Ce^{+3} exchange = 72%)			
323-473	23	323	110
473-623	8	473	87
623-1173	79	623	79
Deammoniated NH_4 Y			
323-473	2	323	27
473-623	4	473	25
623-1173	21	623	21
NaX			
323-473	835	323	992
473-623	46	473	157
623-1173	111	623	111

Table 5.2 (contd.)

STD Data		Chemisorption Data	
Temp. range (K)	Amt. desorbed q_d (μmol.g^{-1})	Temp. range (K)	Amt. chemisorbed q_t (μmol.g^{-1})
XL			
323-473	60	323	178
473-623	20	473	118
623-1173	98	623	98
HXL			
323-473	30	323	134
473-623	35	473	104
623-1173	69	623	69
Silicalite-I			
323-473	0	323	59
473-623	26	473	59
623-773	9	623	33
773-1173	24	773	24
$AlPO_4$-5			
323-473	98	323	239
473-623	41	473	141
623-773	18	623	100
773-1173	82	773	82
SAPO-5			
323-473	26	323	84
473-623	19	473	58
623-773	8	623	39
773-1173	31	773	31

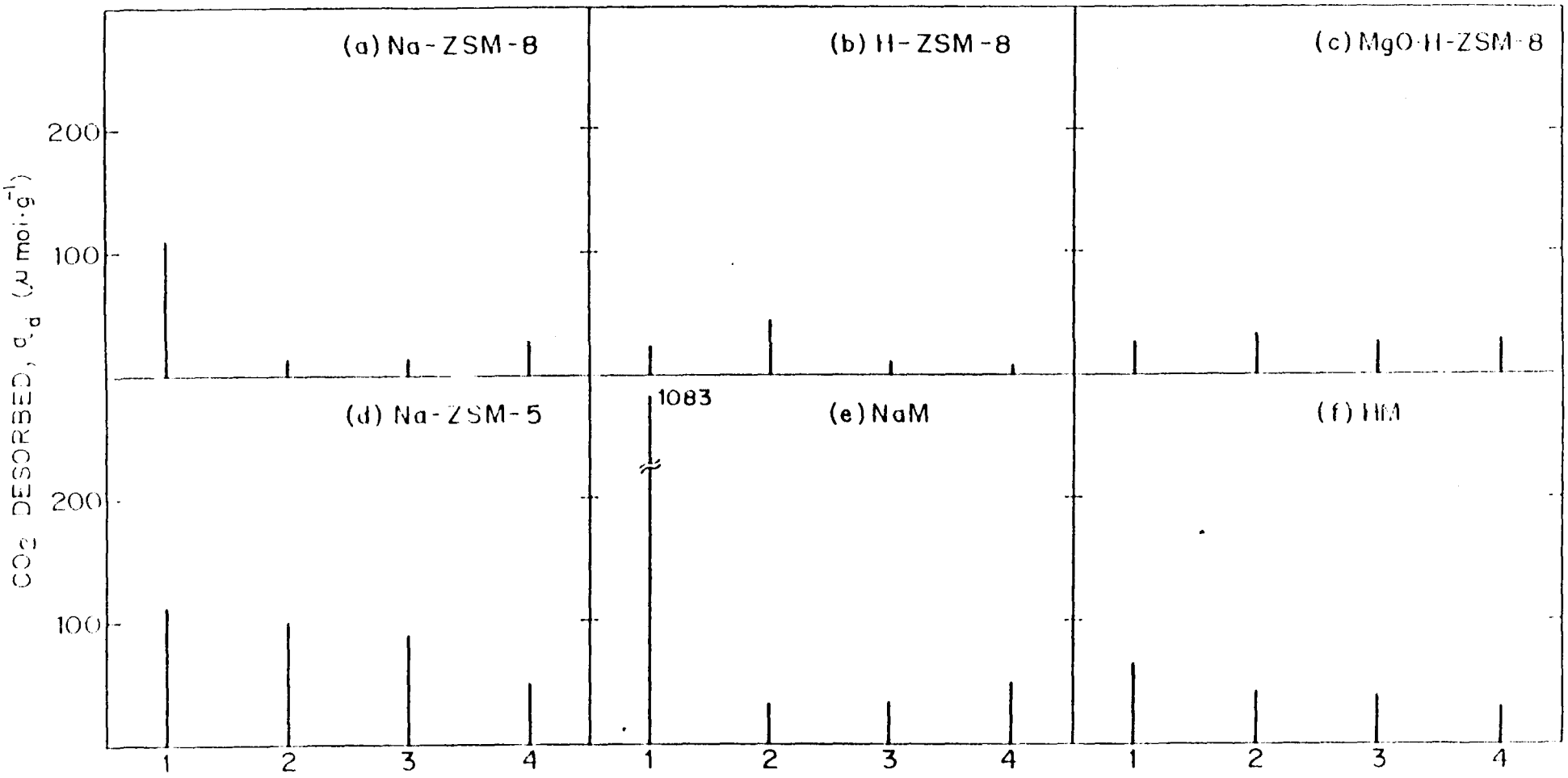

FIG.6-1: STEP-WISE THERMAL DESORPTION OF CARBONDIOXIDE ON HIGH SILICA ZEOLITES

1) $323K < T_d < 473K$ 2) $473K < T_d < 623K$ 3) $623K < T_d < 773K$ 4) $773K < T_d < 1173K$

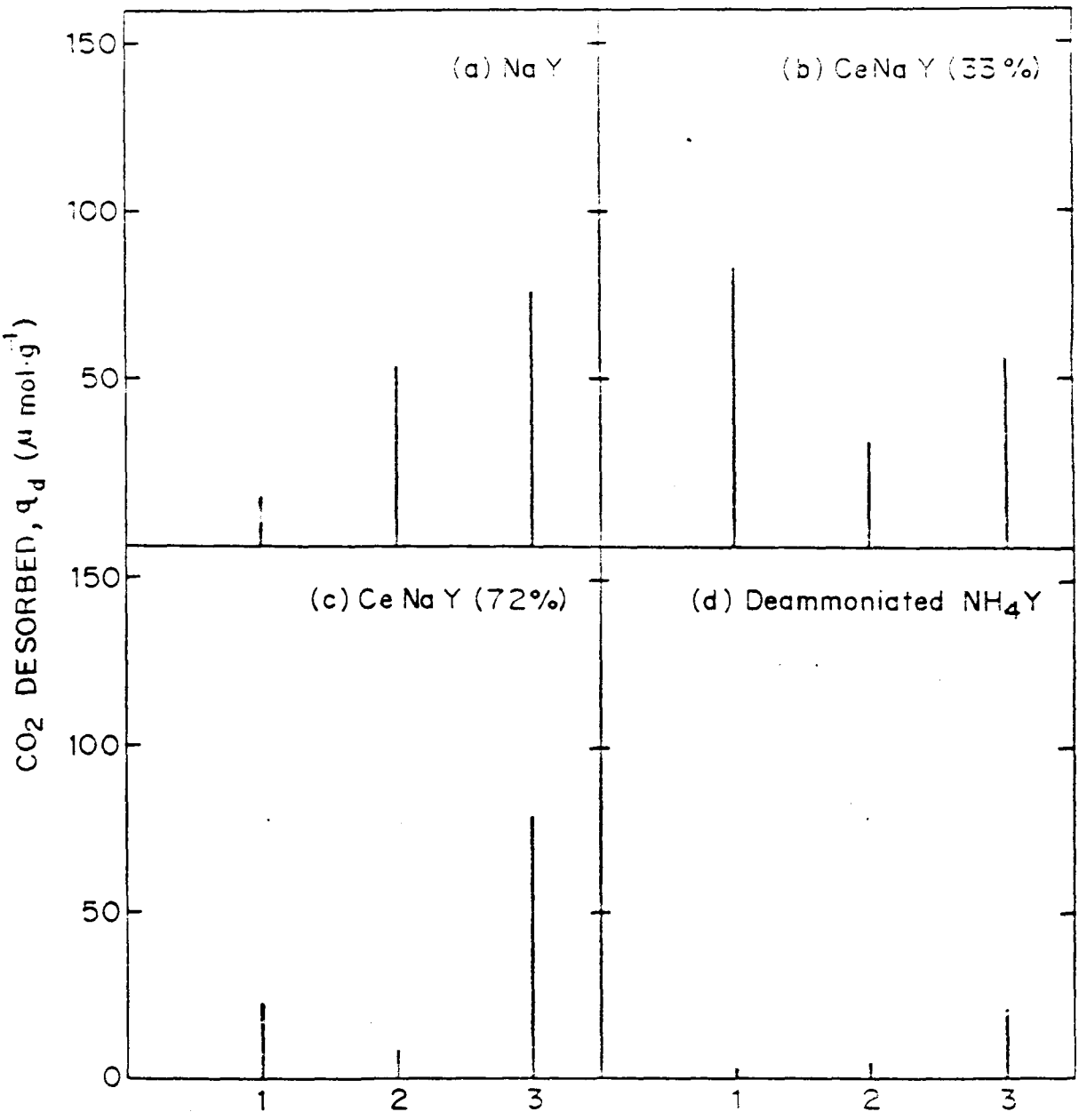

FIG. 6·2: STEP-WISE THERMAL DESORPTION OF CARBONDIOXIDE ON Y TYPE ZEOLITES

1)* $323\,K < T_d < 473\,K$ 2) $473\,K < T_d < 623\,K$ 3) $623\,K < T_d < 1173\,K$

[* FOR NaY 1) $373\,K < T_d < 473\,K$]

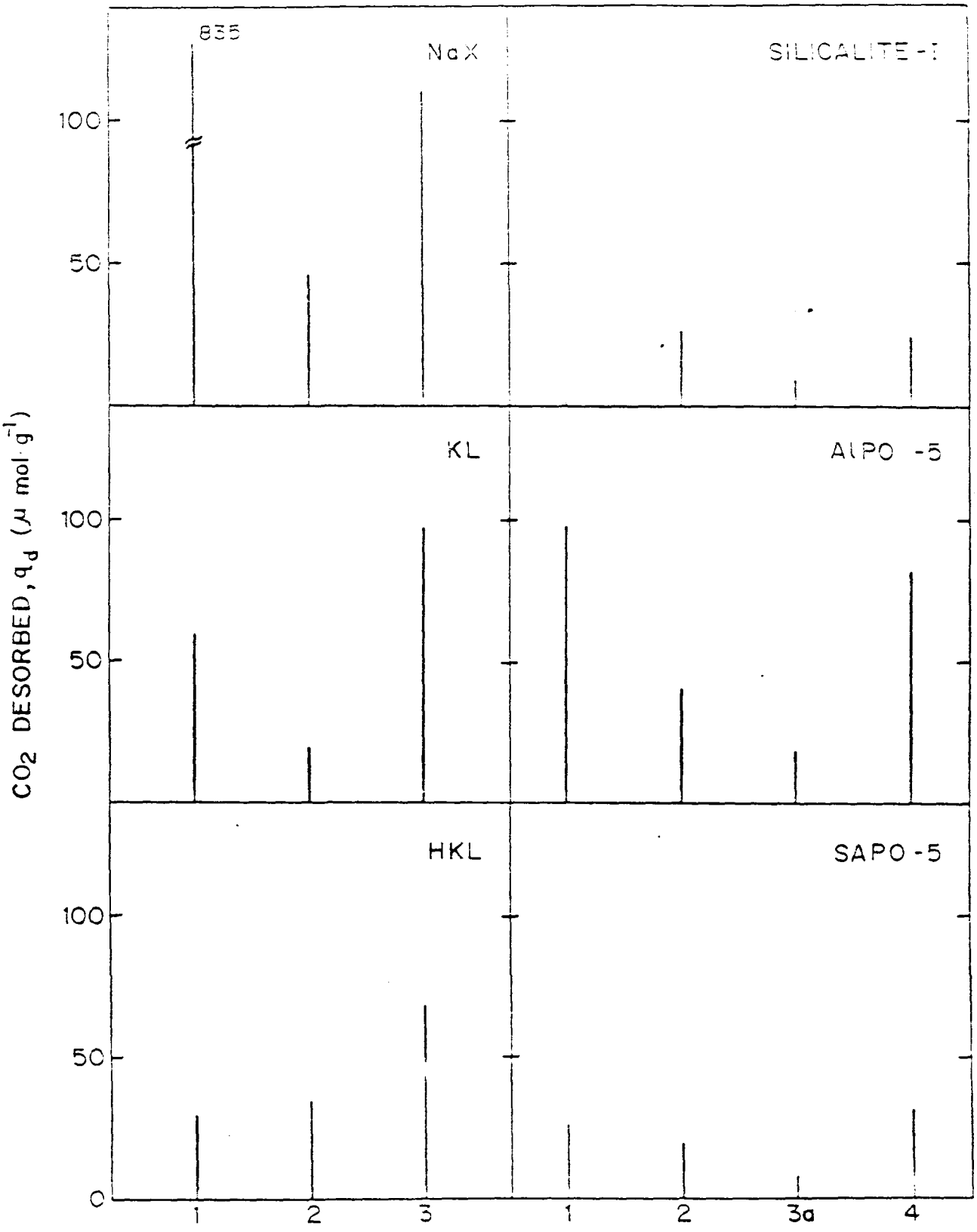

FIG.6·3: STEP-WISE THERMAL DESORPTION OF CARBONDICXIDE ON DIFFERENT ZEOLITES

1) $323K < T_d < 473K$ 2) $473K < T_d < 623K$ 3) $623K < T_d < 1173K$

3a) $623K < T_d < 773K$ 4) $773K < T_d < 1173K$

distribution of the sites involved in the chemisorption of CO_2 at the lowest temperature of STD, i.e. 323 K. Each column represents the number of sites measured in terms of CO_2 desorbed in the corresponding temperature step. The strength of these sites is expressed in terms of the desorption temperature of CO_2, T_d, which lies in the range in which the chemisorbed CO_2 is desorbed. The sites of strength $T_1 < T_d < T_2$ could be obtained from the amount of CO_2 which was initially chemisorbed at T_1 and subsequently desorbed when the temperature was increased from T_1 to T_2.

The STD results in Figs. 6.1-6.3 reveal that the base strength distribution on the zeolites is quite broad, it varies from zeolite to zeolite and depends strongly on the nature of the cation present in the zeolite and the degree of cation exchange.

6.3.2 Chemisorption of CO_2 in Zeolites

The data on the chemisorption of CO_2 in the zeolites at different temperatures (323-1173 K), obtained from the STD data, are included in Table 6.2. The temperature dependence of chemisorption on the zeolites is shown in Figs. 6.4-6.6. The chemisorption of CO_2 at higher temperature points to an involvement of stronger basic sites. The CO_2 chemisorption vs. temperature curves, therefore, present the type of site energy distribution in which the number of sites are expressed in terms of the amount of CO_2 chemisorbed as a function of chemisorption temperature.

Figures 6.4-6.6 indicate that the zeolites differ

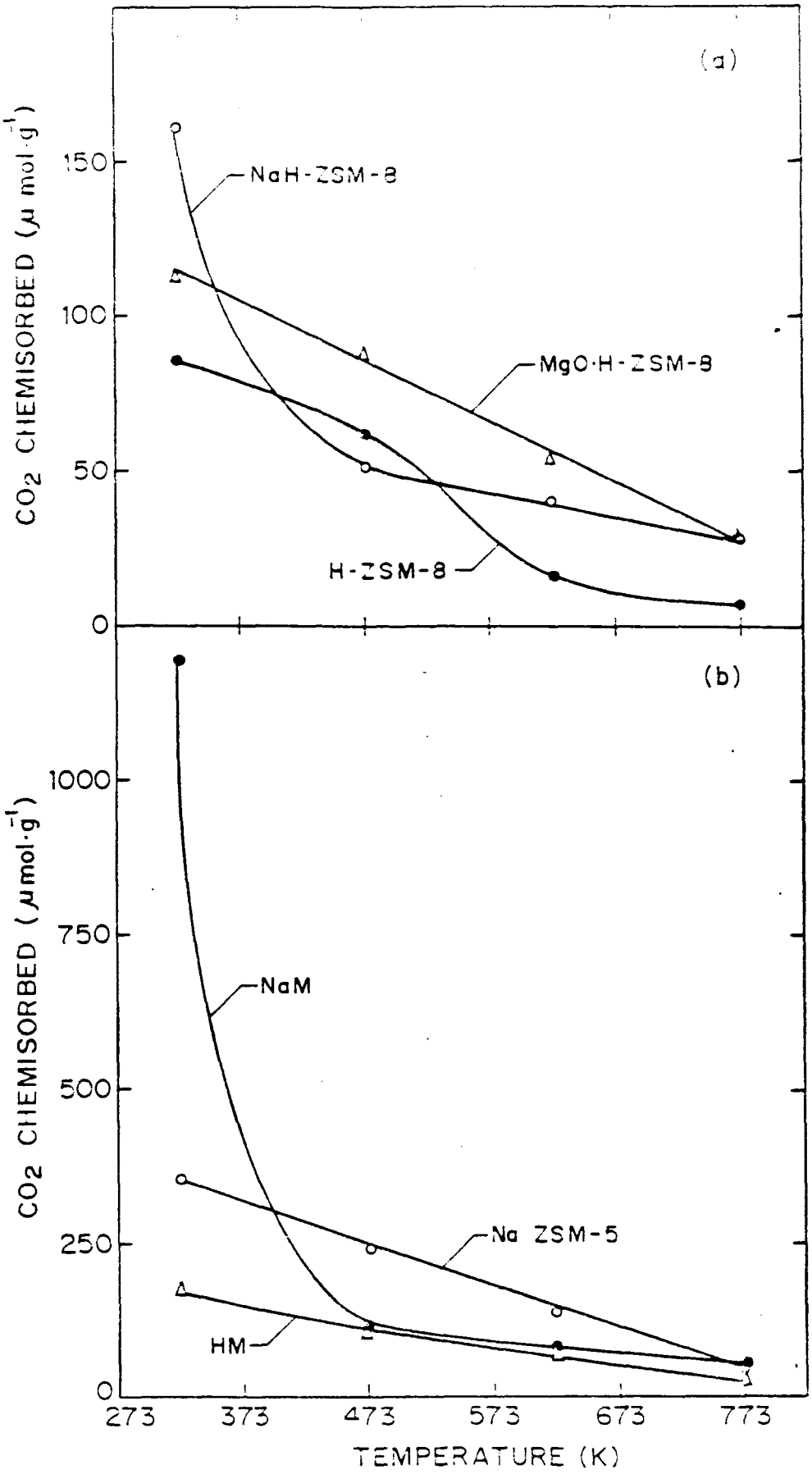

FIG. 6·4 : TEMPERATURE DEPENDENCE OF CHEMISORPTION OF CARBONDIOXIDE ON HIGH SILICA ZEOLITES

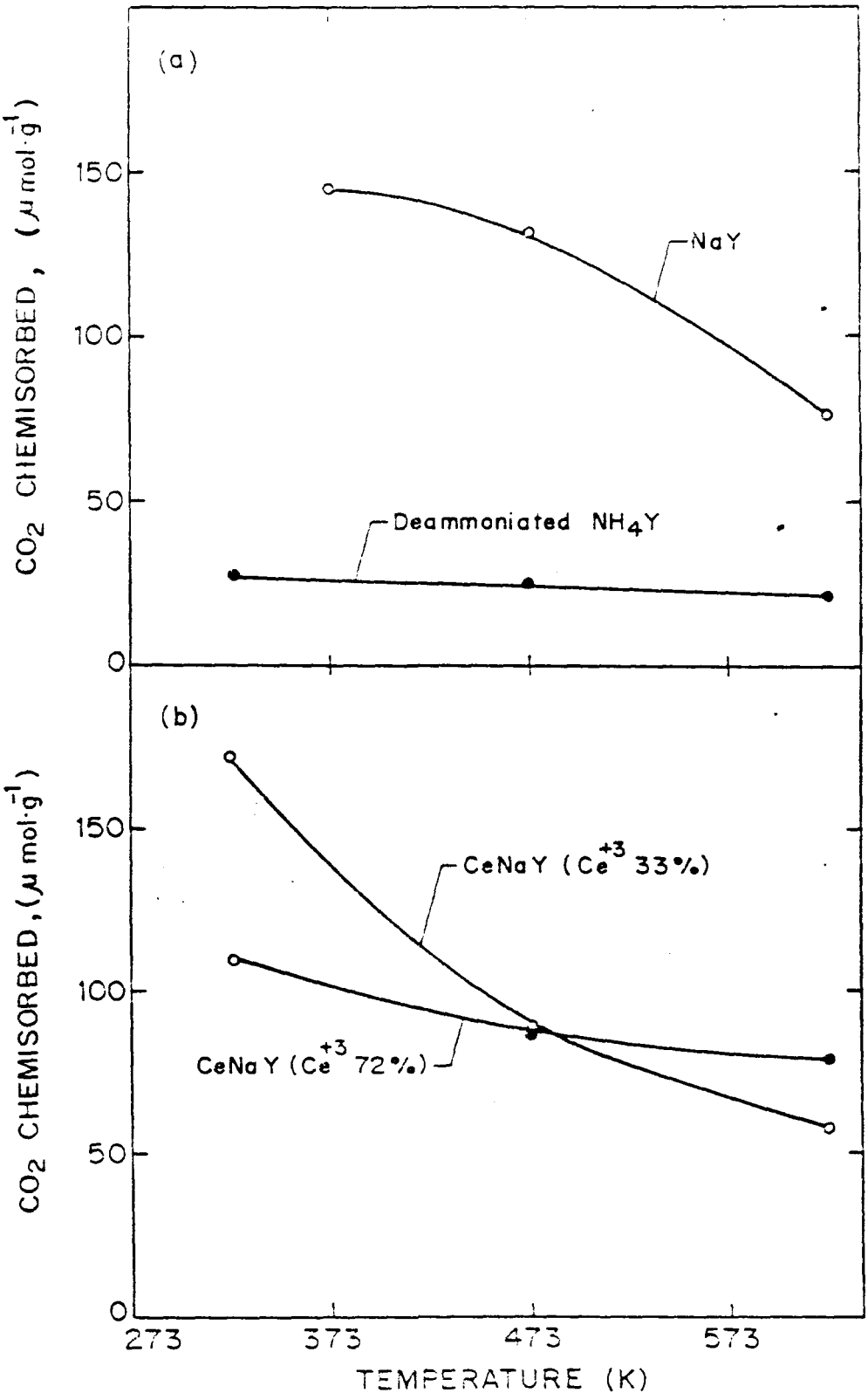

FIG. 6·5: TEMPERATURE DEPENDENCE OF CHEMISORPTION OF CARBONDIOXIDE ON Y-TYPE ZEOLITES

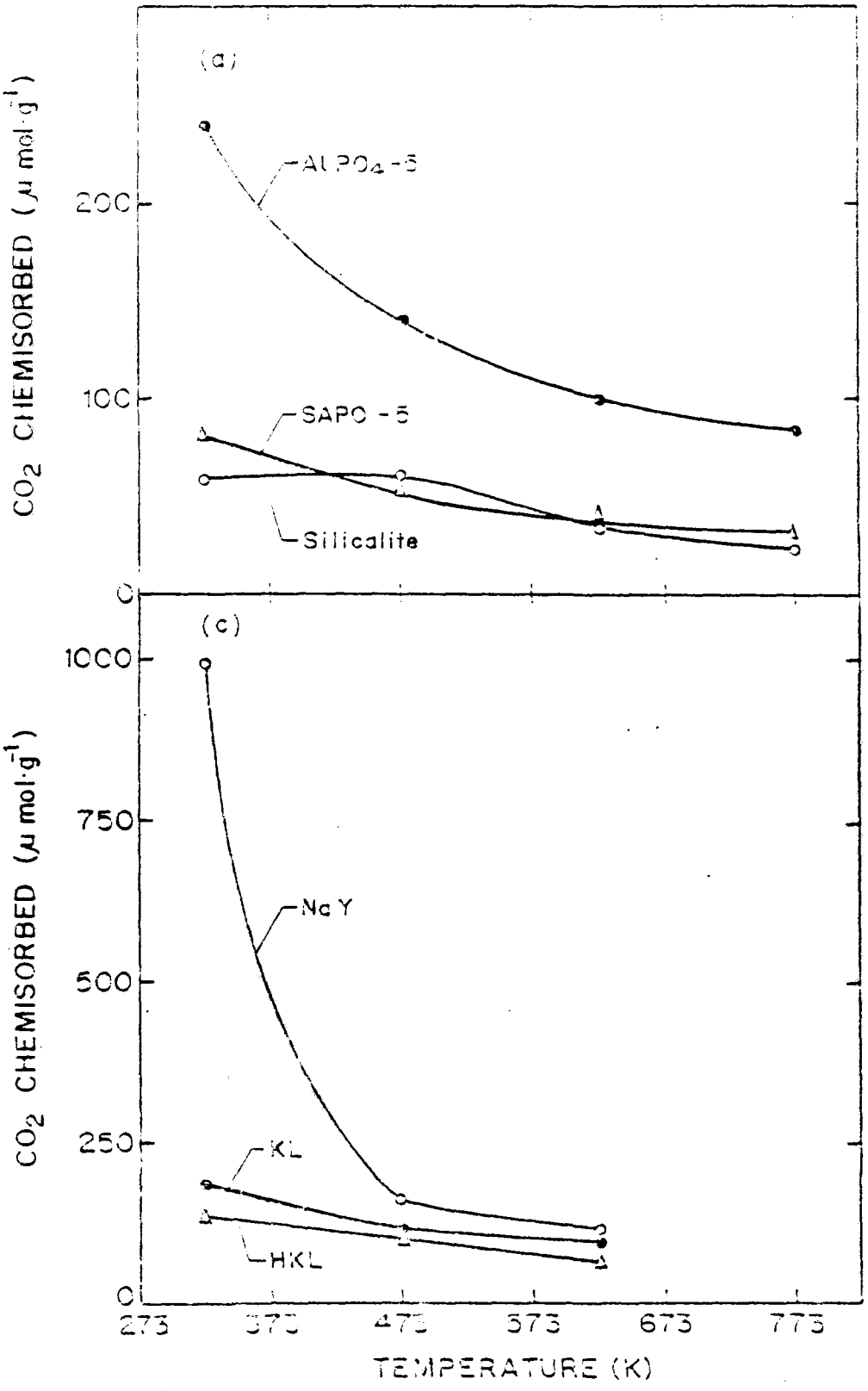

FIG. 6·6 : TEMPERATURE DEPENDENCE OF CHEMISORPTION OF CARBONDIOXIDE ON DIFFERENT ZEOLITES

widely from one another in their total basicity (measured in terms of the CO_2 chemisorbed at 323 K) and base strength distribution.

6.3.3 Basicity/Base Strength Distribution on Zeolites

The STD and chemisorption of CO_2 on zeolites (Figs. 6.1-6.6) show that the zeolites differ widely in their basicity. All the zeolites have broad base strength distribution and it is strongly influenced by Na or alkali metal content of the zeolite and also its Al content or the Si/Al ratio (Table 6.3).

The zeolites can be arranged in the decreasing order of their total basicity, measured in terms of the CO_2 chemisorbed at 323 K, as follows:

NaM > NaX > H-Na-ZSM-5 > $AlPO_4$-5 > KL > HM > CeNaY (Ce^{+3} exchange 33%) > Na-H-ZSM-8 > HKL > CeNaY (Ce^{+3} exchange 72%) > H-ZSM-8 = SAPO-5 > silicalite > HY.

The order of the zeolites for strong basic sites, measured in terms of the CO_2 chemisorbed at 623 K is as follows:

H-Na-ZSM-5 > NaX > $AlPO_4$-5 > KL > NaM > CeNaY (Ce^{+3} exchange 72%) > HKL > HM > CeNaY (Ce^{+3} exchange 33%) > Na-H-ZSM-8 > SAPO-5 > silicalite > HY > H-ZSM-8.

In general, the alkali metal and cerium cation exchanged form of the zeolite have more number of basic sites (as given by CO_2 chemisorption) compared to their H-form. However, the concentration of the cation in the zeolite do not have one to one correspondence to the total basicity or the number of stronger basic sites in the zeolites obtained from CO_2

Table 6.2

Comparison of zeolites for their base strength

Zeolite	Si/Al ratio	Conc. Al ($\mu mol.g^{-1}$)	Conc. Na ($\mu mol.g^{-1}$)	CO_2 chemisorbed at 323 K ($\mu mol.g^{-1}$)	CO_2 chemisorbed at 623 K ($\mu mol.g^{-1}$)
H-ZSM-8	29.6	545	23	85.5	17
Na-ZSM-8	29.6	539	496	162	40
Na-ZSM-5	17.2	1748	682	351	140
NaM	5.5	2153	1992	1197	81
HM	6.5	1973	49	175	68
CeNaY (Ce exchange 33%)	2.4	3165	2114	172	57
CeNaY (Ce exchange 72%)	2.4	3075	851	110	79
HY	-	3474	279	27	21
NaX	1.3	4591	4590	992	111
KL	2.8	3237	3033	178	98
HKL	-	-	-	134	69
$AlPO_4$-5	-	9180	-	239	100
SAPO-5	1.6	1318	-	84	39
Silicalite	-	-	-	59	33

chemisorption (Table 6.3). NaM, which gives the maximum CO_2 chemisorption is not the one that has the highest Al^{+3} or Na^{+} concentration. This clearly shows that not only the chemical environment, but also the structure plays a role in the basicity of the zeolite.

The STD of CO_2 gives quantitative information about the amount of CO_2 retained on the adsorbent at a particular desorption temperature. This data will be useful for knowing to what extent the zeolite could be regenerated.

The Na- exchanged forms of the zeolites can be arranged in the decreasing order of their basic sites (those involved in the chemisorption of CO_2 at 323 K) as follows:

NaM > NaX > H-Na-ZSM-5 > Na-H-ZSM-8.

Based on their stronger acid sites (those involved in the chemisorption of CO_2 at 623 K), they can be arranged in the following manner.

H-Na-ZSM-5 > NaX > NaM > NaY > Na-H-ZSM-8.

It has been observed [10] that in the base catalyzed ring transformation of -butyrolactone into -butyrothiolactone, NaX is more active than NaY and HY has no activity. Also, for side chain alkylation reactions, X-type zeolites are more active than Y-type zeolites. This indicates that NaX is more basic than NaY and HY has very few or no basic sites. Our observation based on CO_2 chemisorption on the zeolites (Table 6.3) is quite consistent with the above.

REFERENCES

1. Sidorenko, Y.N., Galich, P.N., Gutyrya, V.S., Il'In, V.G., Neimark, I.E., Dokl. Akad. Nauk. SSSR, 172, 132 (1967)
2. Yashima, T., Sato, K., Hayasaka, T., Hara, N., J. Catal., 26, 303 (1972)
3. Ono, Y., 'Catalysis by Zeolites' (Ed. B. Imelik et al.), Stud. Surf. Sci. Catal., Elsevier, Amsterdam, 5, 19 (1980)
4. Unland, M.L., Barker, G.E., 'Catalysis of organic reactions' (Ed. Moser, W.R.), Chemical industries series, 5, Dekker, N.Y. (1981)
5. Barthomeuf, D., Coudurier, G., Vedrine, J., Mat. Chem. Phys., 18, 553 (1988)
6. Barthomeuf, D. and De Mallmann, A., 'Innovations in Zeolite Material Science' (Ed. P.J. Grobet et al.), Stud. Surf. Sci. Catal., Elsevier, Amsterdam, 37, 365 (1988)
7. Barthomeuf, D., 'Acidity and Basicity in Zeolites', Paper presented in 'Zeccat 90', International symposium on zeolites, Leipzig, August 1990
8. Jensen, W.B., 'The Lewis Acid-base Concepts, an Overview', Wiley , 1980.
9. Choudhary, V.R. and Rane, V.H., Catal. Lett., 4, 101 (1990)
10. Tanabe, K., Misino, M., Ono, Y., Hattori, H., 'New Solid Acids and Bases', Stud. Surf. Sci. Catal., Elsevier, Amsterdam, 51, 159 (1989)